Chiral Self-Sorting of Atropo-Enantiomeric Perylene Bisimide Dyes

Dissertation zur Erlangung des
naturwissenschaftlichen Doktorgrades
der Julius-Maximilians-Universität Würzburg

vorgelegt von
Marina Montserrat Safont Sempere
aus Zaragoza

Würzburg 2010

Eingereicht am 17.12.2010
bei der Fakultät für Chemie und Pharmazie

1. Gutachter: Prof. Dr. Frank Würthner
2. Gutachter:
der Dissertation

1. Prüfer: Prof. Dr. Frank Würthner
2. Prüfer: Prof. Dr. Christoph Lambert
3. Prüfer: Prof. Dr. Ingo Fischer
des Öffentlichen Promotionskolloquiums

Tag des Öffentlichen Promotionskolloquiums: 25.02.2011

Doktorurkunde ausgehändigt am:

para mi familia

List of Abbreviations

AFM	atomic force microscopy
CD	circular dichroism
CV	cyclic voltammetry
COSY	correlated spectroscopy
CSI	cold spray ionization
CT	charge transfer
DCM	dichloromethane
DLS	dynamic light scattering
DMSO	dimethylsulfoxide
DPV	differential pulse voltammetry
DSC	differential scanning calorimetry
ee	enantiomeric excess
ESI-TOF	electrospray ionization time-of-flight
FAB	fast atom bombardment
FRET	fluorescence resonance energy-transfer
FTICR	Fourier transform cyclotron
HPLC	high performance liquid chromatography
HOPG	highly ordered pyrolytic graphite
HRMS	high resolution mass spectrometry
LC	liquid crystal / liquid crystalline
LD	linear dichroism
MALDI-TOF	matrix-assisted laser desorption injection time-of-flight
Me	methyl
MeOH	methanol
M.p.	melting point
NMR	nuclear magnetic resonance
NMP	*N*-methyl pyrrolidone
NOE	nuclear Overhauser effect
OEG	oligoethylene glycol
OFET	organic field effect transistor
OLED	organic light emitting diode
OPV	oligo(*p*-phenylenevinylene)

POM	polarized optical microscope
PBI	perylene bisimide
PFG	pulse field gradient
PET	photoinduced electron transfer
ppm	parts per million
RLS	resonance light scattering
ROESY	rotating-frame Overhauser enhancement spectroscopy
rt	room temperature
SEC	size exclusion chromatography
Tos	*p*-toluene sulfonate
THF	tetrahydrofurane
TMS	tetramethylsilane
UV/Vis	ultraviolet/visible

Table of Contents

Chapter 1

Introduction and Aim of this Thesis

Self-sorting, i.e., the ability of molecules to differentiate between self and non-self in complex mixtures,[1-5] is one of the most prominent prerequisites towards the development of life. Its importance is clearly illustrated by the DNA double helix (Figure 1), which can be considered the most sophisticated natural medium for data storage. The right base pairing in the DNA helix ensures the genetic information to be passed on correctly and thus, life to continue.[6,7] Inspired by this model we realize how important the understanding of the molecular codes involved in efficient self-sorting processes will be to mimic nature or improve its creations. In final instance this knowledge will enable the development of complex functional systems, and the prediction of their properties by the adequate election of the constitutional components.

a) b)

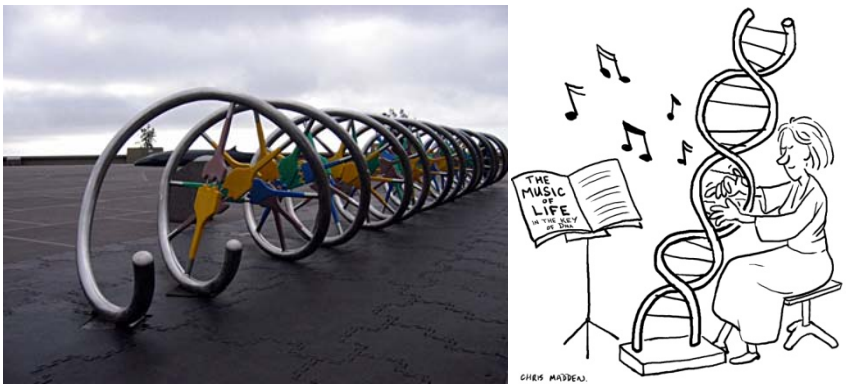

Figure 1. a) Model of a DNA double helix structure in Berkeley, California.[a] b) Cartoon entitled: The music of life (in the key of DNA).[b]

[a] www.chicagonow.com/blogs/doctors-next-door/DNA Double Helix Model

[b] License obtained from www.cartoonstock.com/newscartoons/cartoonists/cma/lowres/cman511

The understanding of chiral self-sorting, i.e., the ability of two enantiomers to recognize themselves or their chiral counterpart,[8-10] is also of paramount importance to answer the question of the origin of homochirality of life.[11-16] Accordingly, unraveling the molecular codes, which direct general and chiral self-sorting, should open countless possibilities for the development of new materials. To understand the basic keys directing self-sorting, a literature survey on this topic is given in **Chapter 2**. An exhaustive description and classification of the molecular codes (size and shape, complementarity of hydrogen bonded systems, steric effects, charge transfer and coordination sphere of metal ions) proven to drive efficient self-sorting processes in mixtures of interacting synthetic molecules is presented. Special emphasis is devoted to chiral self-sorting systems due to their great significance both in biological processes and organic synthesis.

In this thesis perylene bisimide (PBI) dyes have been chosen to explore their self-sorting abilities for two reasons. First, PBIs constitute a prominent class of chromophores widely used for the development of new functional organic materials[17-20] due to their optical and electrochemical properties.[21] Secondly, it has been demonstrated by X-ray diffraction of single crystal structures that the introduction of substituents in the bay area induces a twist of the naphthalene units providing PBIs with atropisomerism, which qualifies these dyes for chiral self-sorting studies.[22-29] However, first some problems had to be solved to make PBIs really suitable for such self-sorting studies. It is known that interconversion between the resultant *M* and *P* atropo-enantiomers occurs even for PBIs with four bulky bay substituents such as chloride.[26,28] Our group developed a strategy to avoid this interconversion by the introduction of two oligoethylene glycol (OEG) chains bridging the 1 and 7, and 6 and 12 bay positions and shielding both π-surfaces.[30-32] To enable the study and quantification of the self-sorting ability of such chiral conformationally stable PBIs by π–π-stacking one of the bridging units had to be removed in this thesis (Figure 2a).

The presence of only one bridging unit has several advantages: i) the interconversion between *M* and *P* enantiomers is still avoided and ii) π–π-stacking becomes possible through the free π-surface leading to the exclusive formation of dimers. Compared to earlier investigations on extended π-stacks of chiral PBIs[33] the restriction to monomeric and dimeric

species simplifies the system proper analysis of homo-and heterochiral aggregates. As imide substituent we have chosen 3,4,5-tridodecylphenyl because these groups provide solubility and mesogenic properties in the condensed state, thus allowing the exploration of the effect of core-chirality even in their condensed matter.

a)

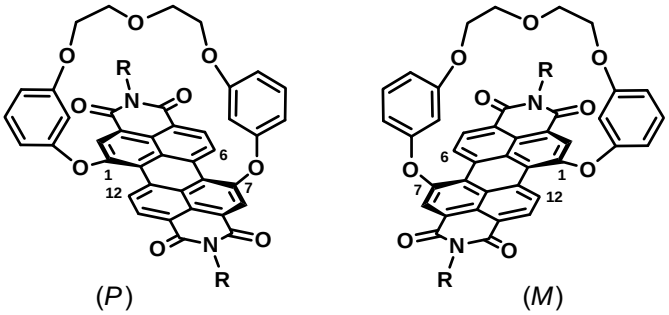

b)

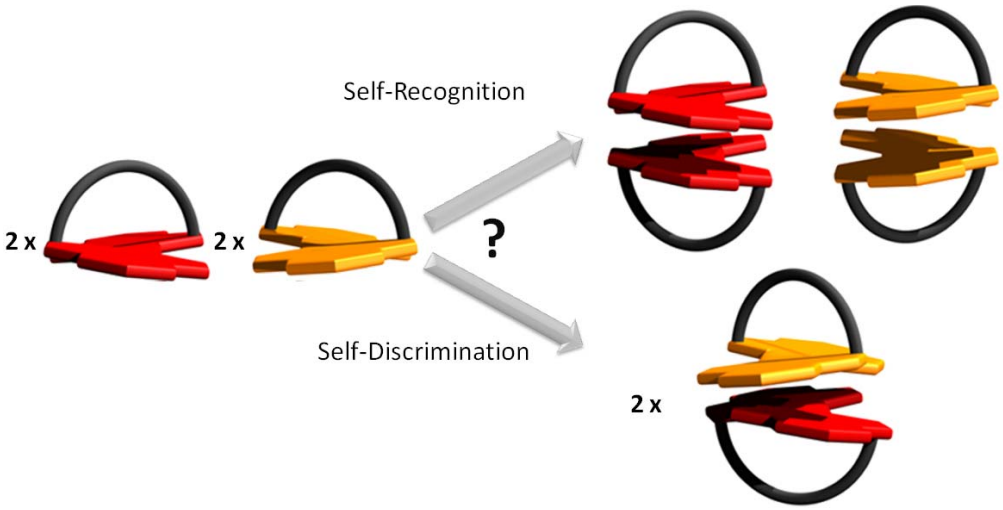

Figure 2. a) Chemical structure of new macrocyclic monobridged PBI target molecules. b) Schematic representation of the possible chiral self-recognition *vs.* self-discrimination processes in these novel macrocyclic PBIs.

In a racemic mixture of such chiral macrocyclic PBIs, both the formation of hetero or homochiral dimers in, respectively, a self-discrimination or a self-recognition event is possible (Figure 2b). Thus, the first aim of this thesis was the elucidation of the influence of conformational chirality on the self-assembly of PBIs, investigating the chiral self-sorting in racemic mixtures of novel chiral PBIs in solution, solid and condensed state. **Chapter 3** presents the successful synthesis of the first conformationally stable chiral PBIs by introducing a short OEG bridging unit shielding one π-surface of the PBI core which restricts the interconversion between *M* and *P* enantiomers and makes this PBI suitable for chiral self-

sorting studies. The achievement of such stable atropo-enantiomeric PBIs and their chiral resolution allowed comparative investigations on the self-assembly of the racemate and its pure enantiomers. Towards this goal mathematical models had to be established and various spectroscopic techniques (UV/Vis, NMR) had to be explored. **Chapter 4** shows a detailed study on the condensed state properties for the same molecules presented in Chapter 3 in order to reveal the influence of core chirality on the mesophase properties of such macrocyclic PBIs.

The next step in this PhD was the generalization of the work presented in Chapter 3 by modification of the bridge length of the PBI depicted in Figure 2a (Figure 3). The enlargement of the bridging units is expected to provide the PBI aromatic cores with increasing flexibility. We expect this increasing flexibility to have an impact on the self-recognition *vs.* self-discrimination ratio in racemic mixtures of these macrocyclic PBIs. In **Chapter 5** the successful synthesis and resolution of these different bridged macrocyclic PBIs is presented and the influence of increasing flexibility on molecular recognition in solution and in the condensed state is investigated.

A summary of our findings related to the presented topics is given in **Chapter 6** in English, German and Spanish.

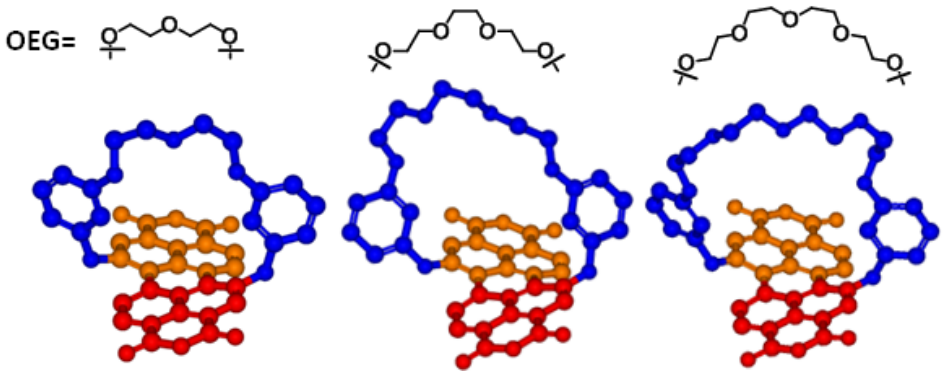

Figure 3. Energy minimized structures of macrocyclic monobridged PBIs with different sized bridging units using HyperChem, MM+. Imide substituents removed for clarity.

References

(1) Kramer, R.; Lehn, J. M.; Marquisrigault, A. *Proc. Nat. Acad. Sci. U.S.A.* **1993**, *90*, 5394.

(2) Taylor, P. N.; Anderson, H. L. *J. Am. Chem. Soc.* **1999**, *121*, 11538.

(3) Shivanyuk, A.; Rebek, J., Jr. *J. Am. Chem. Soc.* **2002**, *124*, 12074.

(4) Wu, A. X.; Isaacs, L. *J. Am. Chem. Soc.* **2003**, *125*, 4831.
(5) Mukhopadhyay, P.; Wu, A. X.; Isaacs, L. *J. Org. Chem.* **2004**, *69*, 6157.
(6) Watson, J. D.; Crick, F. H. C. *Nature* **1953**, *171*, 737.
(7) Lehninger, A. L.; Nelson, D. L.; Cox, M. M. *Lehninger Principles of Biochemistry*; 5th ed.; W. H. Freeman and Company: New York, 2008.
(8) Kühnle, A.; Linderoth, T. R.; Hammer, B.; Besenbacher, F. *Nature* **2002**, *415*, 891.
(9) Huang, W. H.; Zavalij, P. Y.; Isaacs, L. *Angew. Chem., Int. Ed.* **2007**, *46*, 7425.
(10) Zehnacker, A.; Suhm, M. A. *Angew. Chem., Int. Ed.* **2008**, *47*, 6970.
(11) Pasteur, L. C. R. *Hebd. Seanc. Acad. Sci.,* **1848**, *26*, 538.
(12) Kondepudi, D. K.; Kaufman, R. J.; Singh, N. *Science* **1990**, *250*, 975.
(13) Crusats, J.; Veintemillas-Verdaguer, S.; Ribó, J. M. *Chem. Eur. J.* **2006**, *12*, 7776.
(14) Fletcher, S. P.; Jagt, R. B. C.; Feringa, B. L. *Chem. Commun.* **2007**, 2578.
(15) Blackmond, D. G. *Chem. Eur. J.* **2007**, *13*, 3290.
(16) McBride, J. M.; Tully, J. C. *Nature* **2008**, *452*, 161.
(17) Schmidt, R.; Oh, J. H.; Sun, Y. S.; Deppisch, M.; Krause, A. M.; Radacki, K.; Braunschweig, H.; Konemann, M.; Erk, P.; Bao, Z. A.; Wurthner, F. *J. Am. Chem. Soc.* **2009**, *131*, 6215.
(18) Jaiser, F.; Neher, D.; Meisel, A.; Nothofer, H. G.; Miteva, T.; Herrmann, A.; Müllen, K.; Scherf, U. *J. Chem. Phys.* **2008**, *129*, 114901.
(19) Jones, B. A.; Facchetti, A.; Wasielewski, M. R.; Marks, T. J. *J. Am. Chem. Soc.* **2007**, *129*, 15259.
(20) Peumans, P.; Uchida, S.; Forrest, S. R. *Nature* **2003**, *425*, 158.
(21) Würthner, F. *Chem. Commun.* **2004**, 1564.
(22) Sautter, A.; Thalacker, C.; Würthner, F. *Angew. Chem., Int. Ed.* **2001**, *40*, 4425.
(23) Jones, B. A.; Ahrens, M. J.; Yoon, M. H.; Facchetti, A.; Marks, T. J.; Wasielewski, M. R. *Angew. Chem., Int. Ed.* **2004**, *43*, 6363.
(24) Chen, Z. J.; Debije, M. G.; Debaerdemaeker, T.; Osswald, P.; Würthner, F. *ChemPhysChem* **2004**, *5*, 137.
(25) Würthner, F.; Stepanenko, V.; Chen, Z. J.; Saha-Möller, C. R.; Kocher, N.; Stalke, D. *J. Org. Chem.* **2004**, *69*, 7933.
(26) Leroy-Lhez, S.; Baffreau, J.; Perrin, L.; Levillain, E.; Allain, M.; Blesa, M. J.; Hudhomme, P. *J. Org. Chem.* **2005**, *70*, 6313.
(27) Chao, C. C.; Leung, M. K.; Su, Y. O.; Chiu, K. Y.; Lin, T. H.; Shieh, S. J.; Lin, S. C. *J. Org. Chem.* **2005**, *70*, 4323.
(28) Gsänger, M.; Oh, J. H.; Könemann, M.; Hoffken, H. W.; Krause, A. M.; Bao, Z. N.; Würthner, F. *Angew. Chem., Int. Ed.*, *49*, 740.
(29) Würthner, F.; Osswald, P.; Schmidt, R.; Kaiser, T. E.; Mansikkamaki, H.; Könemann, M. *Org. Lett.* **2006**, *8*, 3765.
(30) Osswald, P.; Würthner, F. *J. Am. Chem. Soc.* **2007**, *129*, 14319.
(31) Osswald, P.; Reichert, M.; Bringmann, G.; Würthner, F. *J. Org. Chem.* **2007**, *72*, 3403.
(32) Osswald, P.; Würthner, F. *Chem. Eur. J.* **2007**, *13*, 7395.
(33) Dehm, V.; Chen, Z. J.; Baumeister, U.; Prins, P.; Siebbeles, L. D. A.; Würthner, F. *Org. Lett.* **2007**, *9*, 1085.

Chapter 2

State of Knowledge

Self-Sorting Phenomena in Complex Supramolecular Systems

Abstract: This chapter shows that artificial molecules —similarly to biological— can be successfully designed to exhibit high levels of selectivity in the molecular recognition or discrimination of surrounding species within complex mixtures. A description and classification of the molecular codes studied by different research groups (geometry, hydrogen-bonding complementarity, steric effects, charge transfer and coordination sphere of metal ions) to drive efficient self-sorting processes in mixtures of synthetic interacting molecules is given. In a second instance, special emphasis is devoted to chiral self-sorting systems due to their great significance both in biological processes and organic synthesis

2.1. Introduction

Nature successfully manages under extremely adverse conditions to accomplish intricate functions responsible for the regulation and control of the vast majority of biological processes that eventually sustain life on our planet.[1] Biological molecules are required to carry out selective functions whilst often being hindered by surrounding agents which are simultaneously competing to bind the same targets. This high degree of selectivity in nature ultimately depends on the "molecular instructions" encoded in the chemical structure of the interacting species responsible for every single recognition or discrimination event.[2] The formation of the DNA double helix, for instance, requires the base-pairing (sorting) of complementary nitrogenous bases (Adenine-Thymine (A-T) and Cytosine-Guanine (C-G)).[3,4] These high-fidelity recognition processes are crucial in the storage of genetic information used in the development and functioning of all known living organisms and some viruses. Other sophisticated superstructures such as microtubules,[5,6] are built upon polymerization of dimers of two different globular proteins (α- and β-globulin), giving rise to cylindrical micrometric arrangements.[7] The formation of heterodimers composed of two different proteins requires the self-discrimination of equals, and the simultaneous recognition of complementary units. In the final instance, the small molecules of life (e.g., sugars, amino acids and fatty acids) are able to assemble not only to form such above mentioned macromolecules, but also to self-sort in one of the most efficient and complex processes known in nature to build the functional basic unit of life: a cell.[8,9] In a cell, multiple levels of compartmentalization arising from the self-sorting of their molecular components allow the coexistence of different functional architectures acting independently. This exceptional selectivity in nature makes possible the existence of life on our planet.[10,11]

Unlike the high complexity of natural or biological architectures, the majority of artificial self-assembled systems reported in recent years have been investigated in isolation. This has been mainly due to the lack of suitable characterization methods and technical or economic constraints, which far exceed the resources of most research institutes. However, the remarkable development of analytical tools is increasingly enabling scientists to pinpoint intractable problems associated to multicomponent mixtures.[12] In this context, *Systems*

Chemistry has arisen in recent years as a new discipline that aims to investigate complex mixtures of interacting molecules.[13-17] These mixtures can give rise to outstanding emergent properties as a result of the interaction of the individual components and cannot be ascribed to any of their components acting in isolation. Although this emerging discipline is still in its infancy, ongoing research advances are enabling current (supramolecular) chemists to unravel the behavior of individual molecules in multicomponent mixtures and to anticipate the reasons that lead artificial molecules to bind or ignore a specific partner in a complex multicomponent environment.

In this literature survey, we will discuss the external variables and intrinsic factors (molecular codes) that influence the recognition or discrimination of supramolecularly interacting chemical species in solution.[18] The comprehension of this "molecular programming" in artificial systems will define the variables that control self-sorting processes, and may ultimately contribute to a better understanding of the self-assembly pathways in natural systems.[c]

2.2. Self-Sorting: Definition, Types and Influence of External Variables

2.2.1. Types of Self-Sorting

The behavior of individual synthetic molecules in complex systems was first investigated in mixtures of different helical metal complexes.[19] Lehn and co-workers studied the co-assembly of a mixture of two tris-bipyridine ligands (**1** and **2** in Scheme 1), previously demonstrated to self-assemble independently in the presence of Ni(II) and Cu(I) ions into well-defined triple and double helicates, respectively. When a mixture of 2 equivalents of **2**, 3 equivalents of **1**, 3 equivalents of Cu^{+} and 3 equivalents of Ni^{2+} was treated under appropriate conditions, precipitation of only the corresponding double and triple helicates in quantitative yields takes place. Fast atom bombardment (FAB) mass spectrometry and ^{1}H NMR experiments provided evidence supporting the recognition of the tetrahedrally coordinating copper ions by the

[c] By restricting ourselves to noncovalent bonds and self-sorting in solution we will not cover self-assembly processes on solid surfaces and self-sorting phenomena based on reversible covalent bonds.[19,20] However, excellent reviews have recently become available by De Feyter[18] and Otto,[13,14] which cover these topics.

tritopic ligand **2** and the octahedrally coordinating nickel ions by the ligand **1**, thereby ruling out the formation of crossover, mixed or undesired species. This singular observation was originally termed as *self-recognition* –or recognition of like from unlike and self from nonself–[19] to explain the preferential binding of like metal ions by like ligand strands, disregarding other species in solution.

Scheme 1.

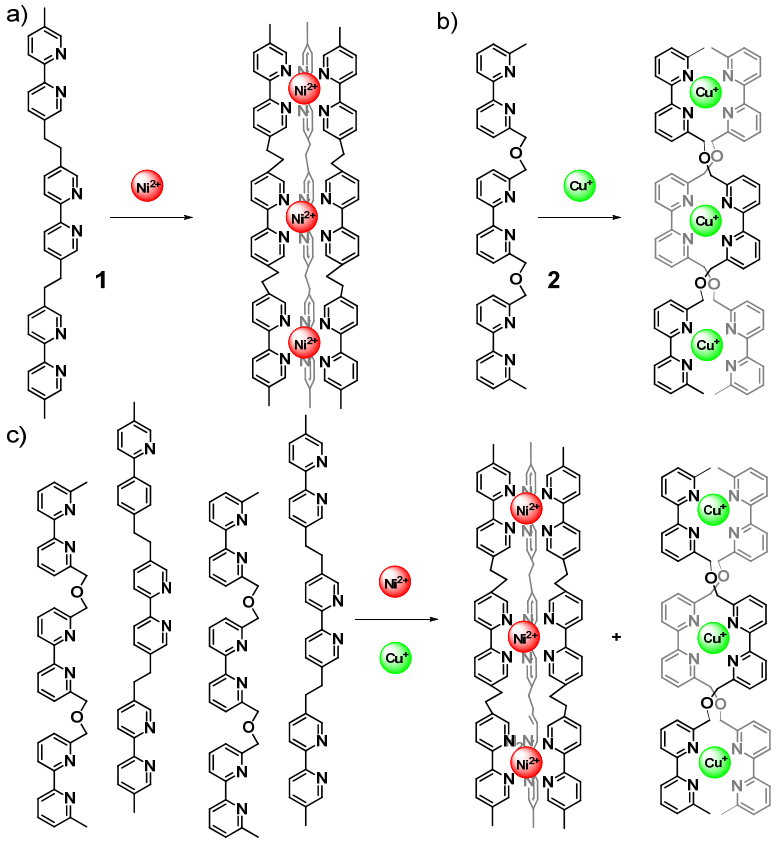

In recent years, this term has evolved to the current expression *self-sorting* suggested by Isaacs and co-workers[20,21] and nowadays largely accepted by the scientific community. *Self-sorting* can be defined as high fidelity recognition of self from non-self within complex mixtures.[20] If affinity for others is shown we will call this assembly process *self-discrimination* (*social self-sorting*),[22] and the affinity for itself will be called *self-recognition* (*narcissistic self-sorting*) (Figure 1).[23] Self-sorting systems can in turn be subdivided into those displaying *thermodynamic* or *kinetic* self-sorting: they have reached a thermodynamic equilibrium, or they can be considered as trapped species under kinetic control. The majority of the self-sorting systems described in literature operate under thermodynamic control. Recently, Schalley and co-workers have further classified self-sorting systems into *integrative*

or *nonintegrative*.[24] *Nonintegrative* self-sorting systems are characterized by the formation of a set of discrete complexes, each of them containing a single recognition center that is occupied by its complementary partner. In *integrative* systems, on the contrary, more than two species are bound in two or more recognition events with positional control and integrated into one global complex.

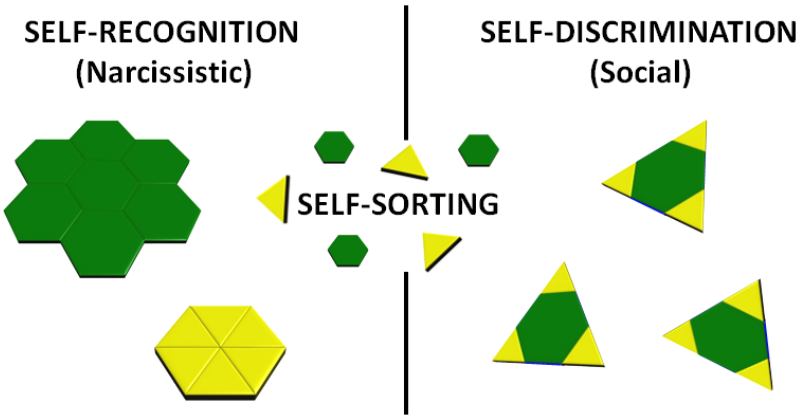

Figure 1. Schematic representation of the different types of self-sorting: self-recognition (narcissistic) vs. self-discrimination (social).

Regardless of the classification, self-sorting events are directed by the same intermolecular forces which govern any molecular recognition process, i.e., hydrogen bonds,[25-27] metal-ligand interactions[28-34] electrostatic interactions,[24] π–π-stacking,[35] and solvophobic effects,[36,37] and therefore, the factors that influence these recognition events will compromise the fidelity of the self-sorting processes.

2.2.2. External Variables Influencing the Outcome of a Self-Sorting Process

Similarly to any molecular recognition event or self-assembly process, several external variables (temperature, concentration, solvent, stoichiometry, pH, etc) can affect the outcome of a certain self-sorting process. The presence of water, for instance, prevents the stabilization of hydrogen-bonded assemblies[38] but, on the other hand, reinforces the interaction of nonpolar solutes by hydrophobic effect.[39,40] The effect of different external variables on individual binding events is widely applied to initiate self-assembly processes. However, their influence in complex mixtures of competing species, capable of self-recognizing or discriminating through intermolecular forces remains nearly unexplored. The understanding of these

variables in artificial self-sorting systems would undoubtedly pave the way for the comprehension of the sophisticated architectures in nature.

Isaacs and co-workers were the pioneers to study the impact of different external factors in mixtures of synthetic molecules containing hydrogen bonding groups, previously demonstrated to undergo self-assembly processes and give rise to well-defined supramolecular architectures (Chart 1).[20]

Chart 1.

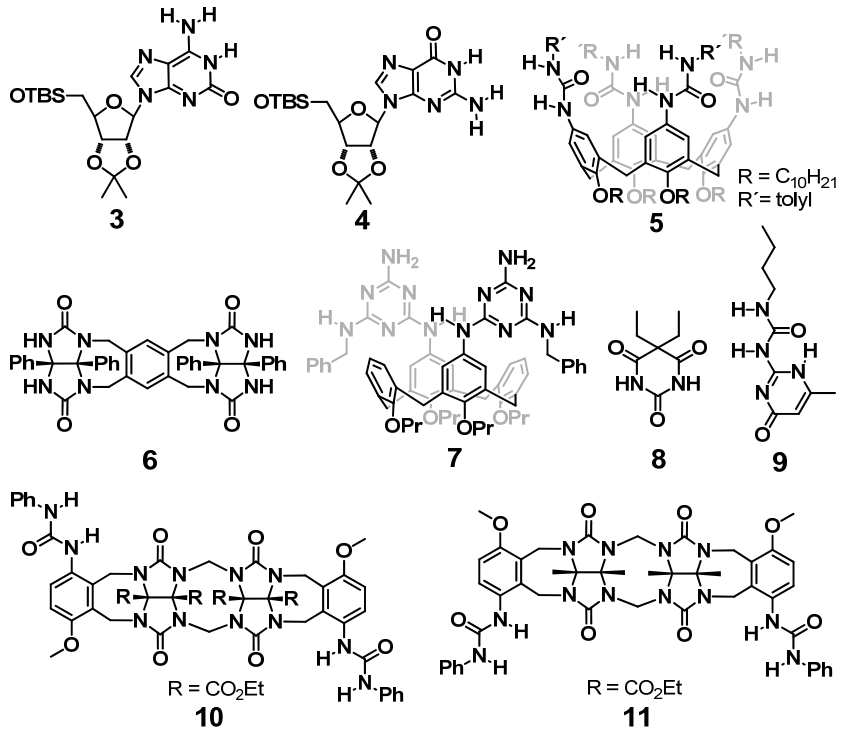

The authors selected two Davis´ ionophores **3** and **4** (capable of self-assembling in the presence of barium picrate into stacked decameric and octameric supramolecular architectures respectively from the corresponding pentameric and tetrameric rosettes), Rebek´s calixarene tetraurea **5** and molecular clip **6** (which have the ability to self-assemble into dimeric capsules and tennis-ball-like structures, respectively), Reinhoudt´s pyrimidine-based calixarene **7** (capable of self-assembling into rosettes in the presence of barbituric derivative **8**), Meijer´s ureidopyrimidinone **9** (which dimerizes via complementary hydrogen bonding) and two molecular clips **10** and **11** (able to form bimolecular tweezers) (Chart 1) and studied the behavior of this mixture in chloroform solution through ^{1}H NMR. On mixing **3**–**11** in the presence of barium picrate, the resulting ^{1}H NMR spectrum is nearly the superposition of the

^{1}H NMR spectra of the individual supramolecular architectures, along with small –hardly distinguishable– resonances that might correspond to small amounts of heteromeric crossover species. These results highlight that under these experimental conditions, the mixture of **3**–**11** and barium picrate clearly undergoes –almost in its entirety– self-recognition. In these studies, the authors also questioned to what extent some external variables (temperature, equilibrium constant, concentration and presence of hydrogen-bonding competitors) would compromise the self-recognition events.

a) *Temperature*: At high temperatures (323 K) the resonances of the rosette $\mathbf{7_3}$-$\mathbf{8_6}$ and ureidopyrimidinone $\mathbf{9_2}$ assemblies broaden dramatically, whereas the other resonances remain sharp, indicating their high stability. Interestingly, as the temperature is lowered back to 263 K, the majority of the resonances sharpen and new small resonances become noticeable, what the authors attributed to crossover species. Although self-recognition still prevails to a great extent in this system, temperature changes have been demonstrated to lead to an increased amount crossover associates in mixtures of these pure hydrogen-bonding assemblies.

b) *Equilibrium constants*: The authors performed simulations of a simple two component system comprising two monomers **A** and **B**, that can give rise to homodimers (**A**-**A** and **B**-**B**) and a heterodimer (**A**-**B**), whose equilibria are governed by three equilibrium constants (K_{AA}, K_{BB} and K_{AB}). According to these simulations, when the equilibrium constant of homomeric species is 100-fold or higher than that of heteromeric (K_{AB}), self-recognition products **A**-**A** and **B**-**B** represent more than 98% of the mixture. When this difference is reduced to only 10-fold, narcissistic self-sorting still prevails to a great extent over social self-sorting.

c) *Concentration*: Whilst the influence of concentration is already significant for self-assembly processes of individual species, it can be even more pronounced in complex mixtures. Assuming the two component system **A** and **B** outlined in the previous section and in the light of simulation experiments, when the concentration of one of the components (**A**) is remarkably smaller than that of the other (**B**), self-association of **A** is less likely than association with **B**, therefore favouring social self-sorting. However, when the concentration of **A** approaches that of **B**, narcissistic self-sorting dominates. These experiments represent a

rule-of-thumb for the construction of complex self-sorting systems: *self-recognition is most efficient when all components are present at the same concentration.*

d) *Competitive H-bonding species*: Self-sorting can be compromised in the presence of competitors for the hydrogen-bonding sites. When a self-sorted mixture of the corresponding assemblies of **3**, **4**, **6**, **9**, **10** and **11** was treated with increasing amounts of **8**, the assembly formed by **3** is disrupted, whereas the remaining supramolecular architectures of **4**, **6**, **9**, **10** and **11** barely underwent any appreciable change. These observations highlight that the presence of competitors in high concentration may provoke remarkable changes in some assemblies or, on the other hand, simply indifference. The match or mismatch of the hydrogen-bonding competitors with the members of the self-sorted mixture in this particular example plays a major role in the destabilization of pre-formed assemblies and the formation of new crossover species.

The external variables that compromise the self-sorting of mixtures of thermodynamically equilibrated H-bonding species, however, may not necessarily apply to self-sorted mixtures involving other, e.g. stronger noncovalent, interactions. In fact, recent studies have demonstrated that an increase of temperature can provoke quite distinct effects in multicomponent metal coordination-driven self-assembled polygons (Figure 12).[41] Stang and co-workers investigated the self-sorting ability of nine different metallosupramolecular architectures by simultaneous mixing of organoplatinum acceptors (molecular clips **12** and **16** in Figure 2) and a wide variety of pyridyl donors, well known to self-assemble in isolation into a wide variety of discrete supramolecular 2D rectangles, triangles and rhomboids and 3D triangular prisms or bipyramids. Each mixture was demonstrated to self-sort into multiple discrete supramolecular polygons, precluding the less stable disordered social assemblies.

Two different mixtures of compounds **12**–**15** on one hand (SS1) and **13**, **16**–**18** on the other hand (SS2) were subjected to temperature and solvent changes and their influence on the self-sorting phenomena was subsequently investigated. (Figure 2b).

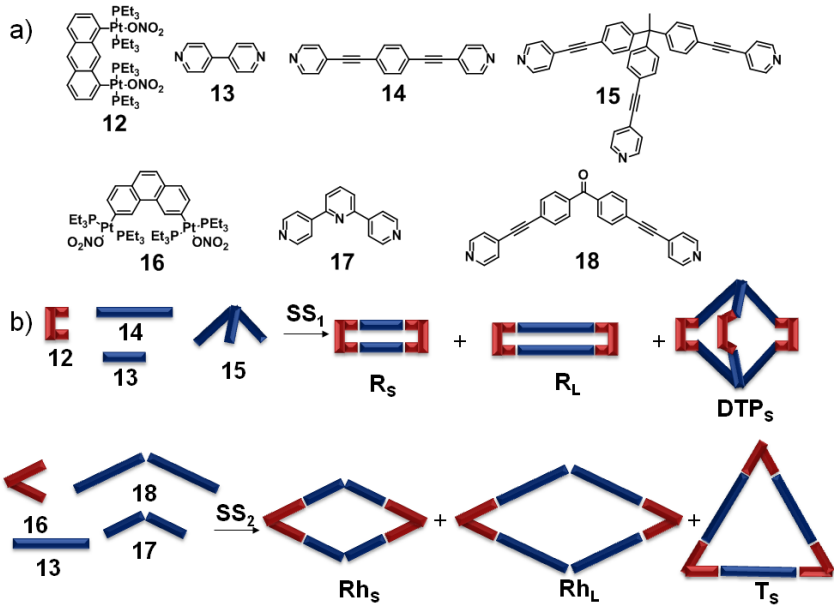

Figure 2. a) Chemical structure of the building blocks applied by Stang and co-workers in self-sorting experiments. b) Graphical representation of diverse coordination-driven self-assembled systems: small rectangle (R_S), large rectangle (R_L) and small distorted triangular prism (DTP_S) for SS1, and small rhomboid (Rh_S), large rhomboid (Rh_L) and small triangle (T_S) for SS2.

a) *Temperature*: At ambient conditions, disordered oligomeric structures are formed as major species by random combinations of the molecular subunits. These results reveal that the self-assembly process occurs extremely slowly at room temperature and the equilibrium is not reached even after 20 days. However, an increase of temperature to 65-70ºC for 24 hours causes a significant increase in the rate of the self-assembly process and the initially disordered species can be dynamically self-corrected to the thermodynamically preferred discrete supramolecular entities.[42] These findings are in sharp contrast with those observed by Isaacs in H-bonding self-sorted mixtures (Chart 1), where an increase of temperature provoked the destabilization of some of the individual pairs. This notable divergence arises, however, as a simple consequence of the different temperatures required in both systems to reach thermodynamic equilibrium: Isaacs´ hydrogen-bonded mixtures are able to reach thermodynamic equilibrium at ambient conditions, whereas the higher binding strength of metallosupramolecular interaction requires a higher thermal energy to self-correct kinetically trapped species towards the thermodynamically most favoured self-sorted architectures.

b) *Solvent*: Self-assembly processes are known to be highly sensitive to changes in solvent owing to the different thermodynamic stabilities of intermediate and final species formed in different media.[43] From among the two self-sorted mixtures investigated in these studies (Figure 2b), only the first one (SS1) formed from clip **12** underwent significant effects upon changing the solvent from d_6-acetone/D_2O (1:1) to either CD_2Cl_2 or d_6-acetone/D_2O (20:1) whereas the second (SS2) formed from clip **16** showed no appreciable changes. In the particular case of SS1, the initially organized structures R_S, R_L and DTP_S could be reversibly destructed or regenerated merely by changing the nature of the solvent. The choice of solvent has thus been proven to be critical to the efficiency of coordination-driven self-sorting systems.

In the light of these examples, it is evident that a certain external variable (solvent, temperature, etc) alters not only the stability of different noncovalent interactions but can even modify the composition of self-assembled objects formed by H-bonded or metallosupramolecular interactions within complex mixtures. However, the effect of these variables on complex mixtures of competing species in which several noncovalent interactions participate –as it occurs in nature– remains mostly unexplored.

Isaacs and co-workers investigated the influence of temperature, concentration, stoichiometry and pH in a sophisticated 12-component mixture in aqueous solution composed of different compounds, previously known to generate host-guest complexes through a wider variety of noncovalent forces (metal-coordination, ion-dipole, solvophobic forces, π–π-stacking and charge-transfer interactions).[21] As expected, pH changes cause dissociation or stabilization of some particular assemblies due to changes in protonation states. Interestingly, concentration changes did not appear to influence the recognition events even at micromolar scale. This fact is in contraposition with that observed in H-bonding self-sorting mixtures described above. The relative stoichiometry of some aggregates can also compromise the extent of self-sorting or ultimately generate new assemblies. On the basis of simulation experiments, the authors concluded that *social self-sorting systems may change partners over a relatively narrow concentration range*. This conclusion is in accordance with biological systems, in which self-organization regulates specific reactions, often at very dilute (nM)

concentrations while competing with a myriad of other possible reactants without physical barriers.[44,45]

Temperature variations, as expected, provoke substantial changes in the outcome of the social self-sorted mixture. At high temperatures, the ^{1}H NMR spectra become highly complex due to the appearance of new sets of resonances, most likely attributed to crossover species. In addition, the system undergoes an irreversible change when the temperature is lowered back to ambient conditions, as a result of crossover interactions between some of the members of the mixture.

In the light of these studies, it is not yet possible to derive a general rule how to apply external variables to direct self-sorting processes in complex mixtures of interacting species involving several noncovalent forces. Current research advances based on a larger variety of self-sorting systems, however, augur well for the near future. These will be discussed in the next section of this overview.

2.3. Molecular Codes for the Self-Sorting of Complex Mixtures

Disregarding the external factors that can influence the strength of different non-covalent interactions, in this section we wish to investigate the encoded information that makes a given molecule in a crowded environment behave the way it does. By *molecular codes* in the field of self-sorting, we refer to the intrinsic information coded in the molecular structure of a given interacting species that governs the strength of the intermolecular forces of the species with itself and with the rest of the members of the mixture. Molecules will tend to bind their ideal partner(s) by establishing the maximum possible number of intermolecular interactions, which can only take place when the interacting species have been suitably programmed with molecular codes.

There are different molecular codes that have been used in the literature by different research groups to efficiently direct self-sorting processes (Figure 3):

a) Geometrical complementarity by *size and shape* is unquestionably the most general molecular code that exhibits a strong impact on the strength of intermolecular interactions.[46] Size and shape rule recognition events, as illustrated by the lock-and-key-principle.[47] In

metal-coordination systems, for instance, ligands with different size, shape or rigidity can self-sort into distinct supramolecular architectures in the presence of a metal ion (Figure 2 and 3). Hydrogen-bonding, as well as charge-transfer interactions, between two given molecules require in the first instance a geometrical fit of the molecules involved to facilitate the approach of the donor and acceptor groups that ultimately will interact with one another and give rise to noncovalent bond formation.[48] Van der Waals forces and π–π stacking interactions[49] are maximized as the contact area between the interacting building blocks increases, which indeed depends on their size and shape.[50]

b) *Complementarity in hydrogen-bonded systems*: The match between the hydrogen-bonding donor and acceptor groups can decide the outcome of self-sorting events if the size and shape of the interacting species allows their approximation (Figure 3). Obviously, complementary hydrogen-bonding sites that are not geometrically well positioned will not give rise to bond formation.

c) *Steric effects*: The presence of bulky substituents in some of the building blocks can prevent their interactions with sterically hindered species or eventually facilitate the exclusive selection of unhindered components (Figure 3). This strategy is particularly suitable because a great number of possible structures can be ruled out just by controlling the bulkiness of the substituents of the interacting building blocks. However, the success of this approach is limited to molecules with a high similarity both in terms of size and shape.

d) *Coordination sphere in metal ligand interactions*: The ability of the metal ions to coordinate into different geometries upon coordination to ligands that can satisfy their coordination sphere is –although thus far scarcely investigated– a powerful tool to drive self-sorting processes. The coordination sphere and geometry of a metal ion depends fundamentally on its size, charge and electronic configuration and the availability of properly matched ligands. Different metal ions can coordinate alike ligands into diverse geometries (Figure 3) which might become an increasingly relevant molecular code in the pursuit of systems with high complexity.

e) *Charge-transfer*: Attractive interactions between species with opposing electron donating and accepting character can also direct self-sorting processes, primarily when their size and

shape is very similar. This molecular code is particularly attractive to create social assemblies by organization of the donor and acceptor molecules in an alternating fashion (Figure 3).

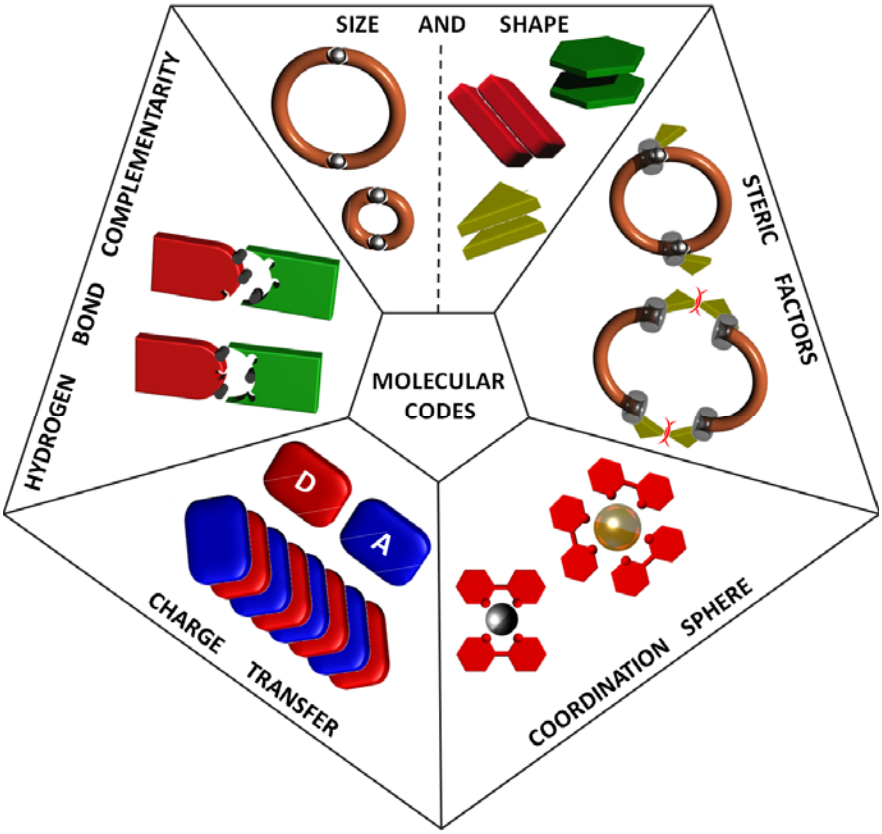

Figure 3. Schematic representation of the different molecular codes considered in this literature survey.

The final two molecular codes, coordination sphere in metal ligand interactions and charge transfer, are in essence closely related. In the case of the coordination sphere of metal ligand interactions, the spatial arrangement of the unoccupied orbitals of the metal ion (acceptor) directs the coordination of the occupied orbitals of the ligand (donor) for ligand-to-metal systems (the contrary for metal-to-ligand systems) in a determined manner.[51] Similarly in charge transfer interactions, the correct overlap between the HOMO and LUMO orbitals of the donor and acceptor π-systems participating in the assembly will govern the outcome of the self-sorting process. Although, these two molecular codes could be unified into donor-acceptor interactions, we will describe them separately owing to the dissimilarity of the respective supramolecular building blocks.

In the following sections we will explain in more detail the impact of these molecular codes in self-sorting events through different examples collected from the literature.

2.3.1. Size and Shape

As mentioned above, size and shape are undoubtedly the foremost variables that regulate the outcome of a self-sorting process, as demonstrated by significant number of examples based on hydrogen-bonding, π–π-stacking and metal ion coordination molecular recognition events. Regarding metal ion coordination-based self-sorting systems and shortly after the pioneering example described by Lehn,[19] Raymond and co-workers studied the self-sorting behavior of a mixture of three rigid bis(bidentate) catecholamide ligands (**19–21)** demonstrated in isolation to self-assemble into triple helicates of varying size in the presence of trivalent metal ions.[28]

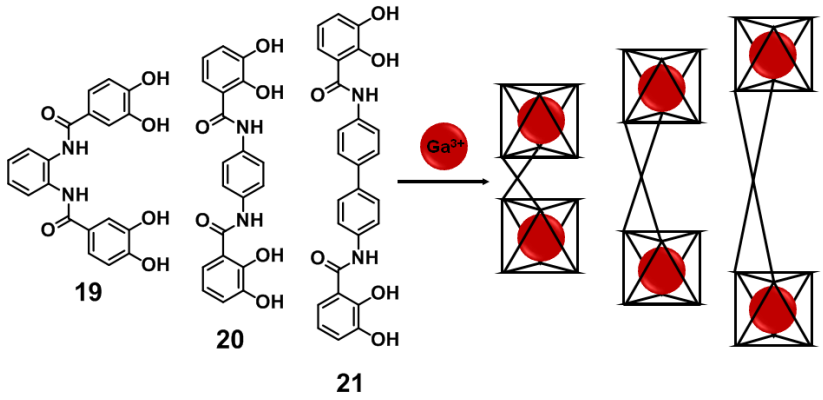

Figure 4. Chemical structure of ligands **19–21** and schematic representation of their self-recognition into triple helices upon treatment with gallium acetylacetonate (III).

The three ligands **19–21** were designed to increase the metal-metal distance systematically in the dinuclear helicates to probe the effect that size has on the ability of the helicates to form by self-assembly. Remarkably, when mixtures of any two or three of the ligands were reacted with Ga(III), only complexes containing one type of ligand were formed and no trace of mixed-ligand species could be observed in solution with ^{1}H NMR or electrospray ionization (ESI) mass spectrometry (Figure 4). Along with Lehn´s example, this revealed that self-recognition can be successfully achieved by controlling a geometrical variable, the distance between two metal coordination sites, i.e., size.

Stang and co-workers have extensively made use of rigid pyridyl-based donors and organoplatinum acceptors for the construction of a wide variety of coordination-driven 2D polygons and 3D cages (see Figure 2).[42,52-54] This approach is based mainly on the size and

shape that are encoded within the individual ligand building blocks, highlighting that structural information can efficiently drive the self-sorting processes. Similarly, Dalcanale and co-workers succeeded in the exclusive formation of self-recognizing nanoscale cavitand-based coordination cages (Scheme 2).[55]

Scheme 2.

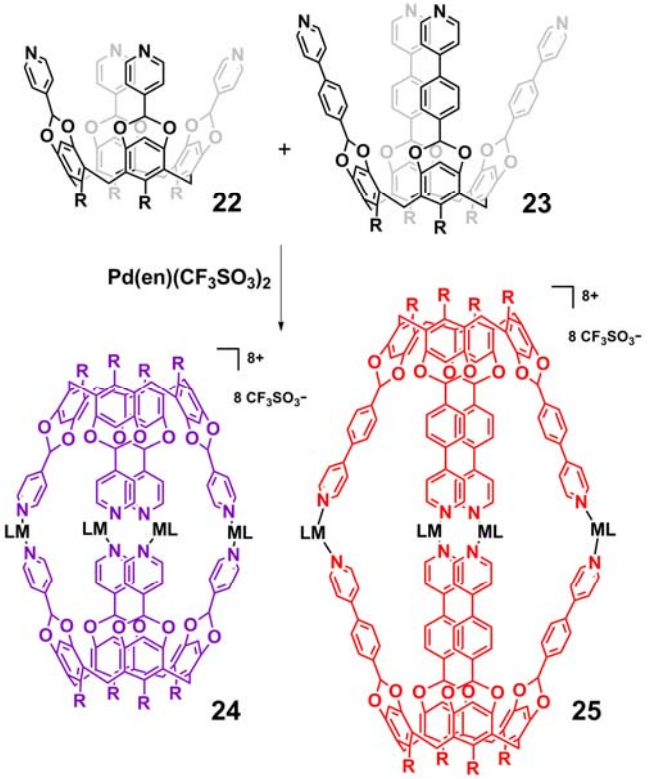

On treatment with Pd(II) or Pt(II) complexes, the cavitands self-assemble into dimeric capsules of varying depth, depending on the length of the pyridyl anchoring units. Interestingly, a competition experiment in which two cavitands of different length (**22** and **23**) were mixed with a stoichiometric amount of metal precursor was performed to verify whether a self-discrimination process takes place in this system or whether, as one might expect, a more likely self-recognition process is operative. ^{1}H NMR experiments of mixtures of **22**, **23** and Pd(ethylendiamine)$(CF_3SO_3)_2$ in acetone-d_6 showed the exclusive formation of signals belonging to homocages **24** and **25** (Scheme 2). The geometrical mismatch between the biting angles of two cavitand ligands disfavors heterocage formation during the self-assembly process. On the basis of these observations we can conclude that self-recognition is most efficient when the individual pairs are structurally most different from one another.

Aside from metal complexes which are ultimately based on metal-ligand point interactions, π–π-stacking interactions between aromatic scaffolds are also governed by the geometry of the interacting surfaces involved.[39,40] However, the surface area of intermolecular contact is in this case remarkably large, so dispersion forces and desolvation are particularly important.[56] Thus, a strong influence of the size and shape of the available surface area on the outcome of a self-sorting event is again anticipated for compounds bearing several aromatic building blocks.

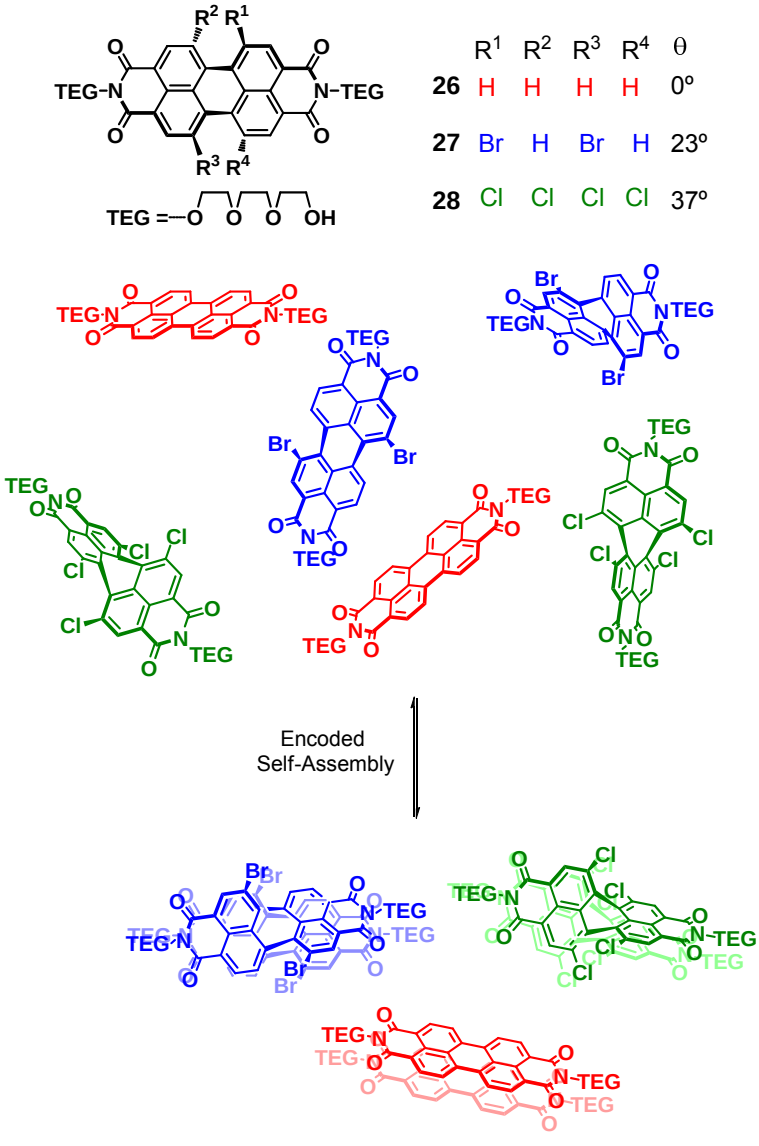

Figure 5. Self-recognition of perylene bisimides **26–28** via π–π-stacking governed by the contortion of the π-surface.

Li and co-workers have recently examined the self-sorting behavior of a mixture containing three bay-substituted perylene bisimide dyes **26–28** (Figure 5) that are characterized by a

different twist angle between the two naphthalimide subunits.[35] It is established that bulky bay substituents twist the perylene unit dihedrally out of the plane with angles from 0 to 37°,[57-59] thereby influencing the available contact surface area for π–π-stacking. Molecules with different twist angles were demonstrated through ^{1}H NMR and UV/Vis spectroscopy in chloroform to preferentially self-recognize into segregated nanostructures, even in the presence of other building blocks, thus revealing their unique molecular encryption (Figure 5). The outcome of this self-sorting process can easily be rationalized from available binding constants in methylcyclohexane at room temperature for the self-aggregation of perylene bisimides related to **26** ($K = 1.2 \times 10^5$ M^{-1}),[60] **27** ($K = 4.6 \times 10^3$ M^{-1}) and **28** ($K = 30$ M^{-1}).[61] The significantly larger binding constant for the perylene related to **26** is attributed to the fact that this is the only molecule in the given series that is perfectly flat. Accordingly, homo-aggregates of **26** take advantage of larger contact surfaces at the closest possible π–π-stacking of about 3.5 Å.[61] Twisting the perylene cores efficiently decreases the π–π-stacking forces and imprints a distinct molecular shape and a new self-assembly code.

The great majority of the examples described in literature involving narcissistic or social self-sorting systems are investigated in organic solvents. This fact is in sharp contrast with biological systems, which operate in aqueous media. Unlike conventional organic solvents, water molecules are arranged into a peculiar infinite network of hydrogen bonds with a localized structure,[62] which accounts for their extraordinary physical properties and also for the *hydrophobic effect*: water molecules are predisposed to form a cage around very non-polar solutes to minimize solvent-solute interactions.[40] Along with the molecular codes, this premise will thus condition to a great extent the outcome of a self-sorting process in aqueous media.

Cucurbit[n]urils (CB[n])[63-65] and cyclodextrins[66-68] are undoubtedly among the most deeply investigated building blocks within complex mixtures in aqueous media due to their ability to form stable host-guest complexes in water.

Harada and co-workers have devoted extensive studies to the investigation of cyclodextrin-based supramolecular architectures.[69-73] Recently, these authors have synthesized two isomers of cinammoyl cyclodextrins **29** and **30** and investigated their self-assembly separately in

aqueous solutions (Figure 6).[73] Cyclodextrin **29** was found to form a double threaded dimer **$(29)_2$**, as demonstrated by single crystal X-ray analysis and supported by pulse field gradient (PFG) NMR experiments. In contrast, cyclodextrin **30** formed extended supramolecular polymers **$(30)_n$** above a concentration of 32 mM. Interestingly, two dimensional (2D)-ROESY spectra of the mixture of both isomers did not show a correlation between the same species. Rather, correlation peaks between cyclodextrins **29** and **30** were observed, which account for the formation of an alternating supramolecular polymer **$(29•30)_n$** (Figure 6b) and not a self or random supramolecular complex. Although it is evident that solvophobic forces contribute to a great extent to this behavior, the difference in the substitution position on a glucopyranose unit –the shape– is far from being an innocent effect in the stabilization of these architectures.

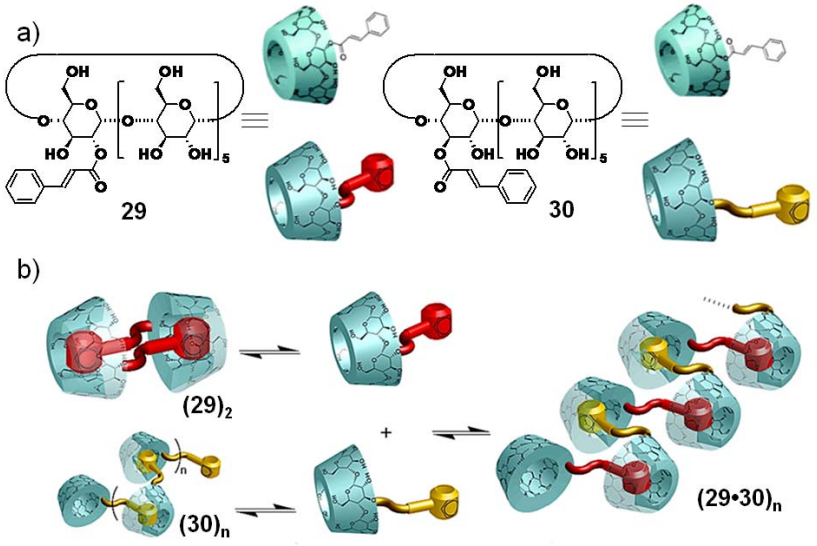

Figure 6. a) Chemical structures and cartoon representation of cyclodextrins **29** and **30**. b) Self-assembly of isolated and mixed cyclodextrins **29** and **30**. Reprinted with permission from ref. 73.

With regards to other systems investigated in water, CB[n] derivatives constitute prime components for the preparation of complex self-sorting systems primarily due to their high affinity and selectivity for a wide variety of inclusion guests.[74] CB[n]s are pumpkin-shaped macrocycles featuring a hydrophobic cavity and two identical hydrophilic carbonyl containing portals (Figure 7).[75-77] The hydrophobic cavity can be effectively exploited to host hydrophobic guests, whereas the hydrophilic portals benefit from interactions with positively charged groups through ion-dipole forces and H-bonding.[75] Although the hydrophobic effect

is a decisive factor in the interaction of CB[n]s with guests, the affinities are ultimately determined by the size of the hydrophobic pocket.

Isaacs and co-workers studied the binding ability of three members of the CB[n] family (CB[6], CB[7] and CB[8]) towards a set of up to 24 different guests with different chemical nature.[74] ^{1}H NMR competition experiments were used to measure the values of K_{rel} for CB[6], CB[7] and CB[8] towards a variety of guests referenced to an absolute K_a determined by UV/Vis studies. Remarkably, the authors observed a high level of selectivity and affinity of each member of the family and also high levels of selectivity exhibited by different members of the family for a common guest, which anticipates their utility in the investigation of more complex self-sorting systems. Several authors have subsequently proven the validity of CB[n]s as ideal building blocks for the preparation of functional biomimetic systems.[78-80] Interestingly, these studies reveal that upon careful optimization of experimental conditions, CB[n]s undergo dynamic behavior that can be thermodynamically or kinetically controlled.

Recently, Tuncel and co-workers have investigated the self-sorting ability of CB[n]-based pseudorotaxanes in aqueous media.[81] In a first step, the affinity of an axle **31** (Figure 7) equipped with two recognition sites –a central hydrophobic dodecyl chain and two diammonium triazoles– towards CB[6] (**32**), CB[7] (**33**) and CB[8] (**34**) was investigated independently through ^{1}H NMR titrations. Driven by size selectivity and reinforced by additional ion-dipole interactions, CB[6] prefers to bind the diaminotriazole sites, as triazole has an appropriate size to fill the cavity of CB[6]. In contrast and driven by solvophobic forces, CB[8] and CB[7] encapsulate the dodecyl protons but not the triazole units, since in this way the nonpolar spacer maximizes the interactions with the hydrophobic cavity, thereby finding refuge from the solvent (Figure 7a). Additionally, the authors examined what would occur when both CB[6] and CB[8] are available to bind with the axle (Figure 7b). Remarkably, ^{1}H NMR experiments revealed that the coexistence of both species does not influence each other´s ability to complex with the axle. These findings imply that CB[8] remains associated with the dodecyl spacer whereas CB[6] prefers to bind the ammonium triazoles, the analogous situation to that observed in isolation. After a certain time the reaction reaches an equilibrium resulting in two species: hetero[4]pseudorotaxane minor and

[3]pseudorotaxane major species (Figure 7b). These results are likely due to the blocking effect of the peripheral CB[6] units that prevents CB[8] from being threaded on to the dodecyl spacer.

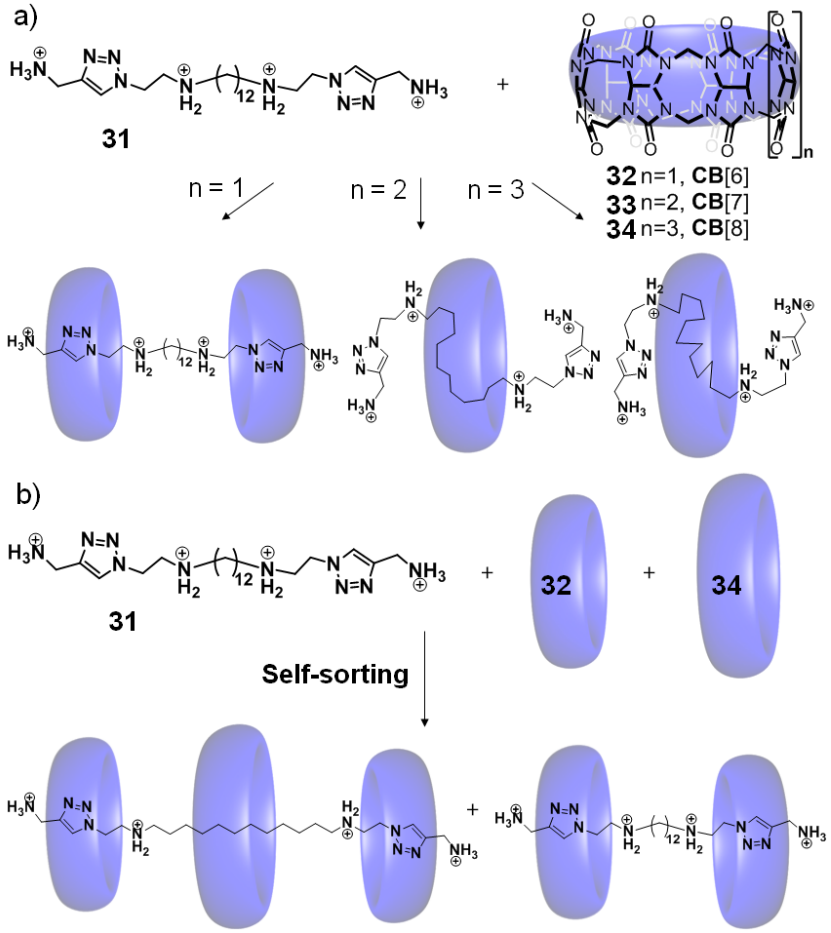

Figure 7. a) Chemical structure and self-assembly of axle **31** in the presence of CB[n]s **32**–**34**. b) Self-sorting of a mixture of axle **31** and CB[n]s **32** and **34**.

In addition to CB[n]s, successfully demonstrated to self-sort into various pseudorotaxanes in aqueous media, other authors have made use of this strategy to construct rotaxane-like supramolecular polymers in organic solvents. Huang and co-workers synthesized two **AB**-type heteroditopic monomers **39** and **40** and investigated their co-assembly into supramolecular copolymers.[82] Monomer **39** comprises a dibenzo-24-crown-8 (**36**) unit attached to a paraquat derivative (**38**), whereas monomer **40** features a bis(*p*-phenylene)-34-crown-10 (**35**) connected to a dibenzylammonium salt (**37**) (Figure 8). It is well-known that crown ethers **35** and **36** can effectively form 1:1 complexes with paraquat derivatives and dibenzylammonium salts, respectively.[83,84] Preliminary self-sorting experiments carried out on precursors **35**–**38** demonstrated that the complexation of crown ether **35** with paraquat

derivatives is much stronger that the complexation with dibenzylammonium salts, while the complexation of **36** with dibenzylammonium salts is stronger than that with paraquat derivatives. These control experiments anticipate that monomers **39** and **40** arrange into alternating supramolecular copolymers (Figure 8b). A thorough collection of experiments (concentration-dependent ^{1}H NMR, cyclic voltammetry (CV), viscosity, dynamic light scattering (DLS) and scanning electron microscopy (SEM)) demonstrated the formation of long high-molecular weight assemblies of alternating supramolecular copolymers. This remarkably high degree of selectivity is clearly driven by the different size of the crown ether moieties, and the complementarity of ion-dipole interactions between the macrocycles and the positively charged recognition elements. Recently, this strategy has been exploited to construct main-chain polyrotaxanes with supramolecular polymer backbones.[85]

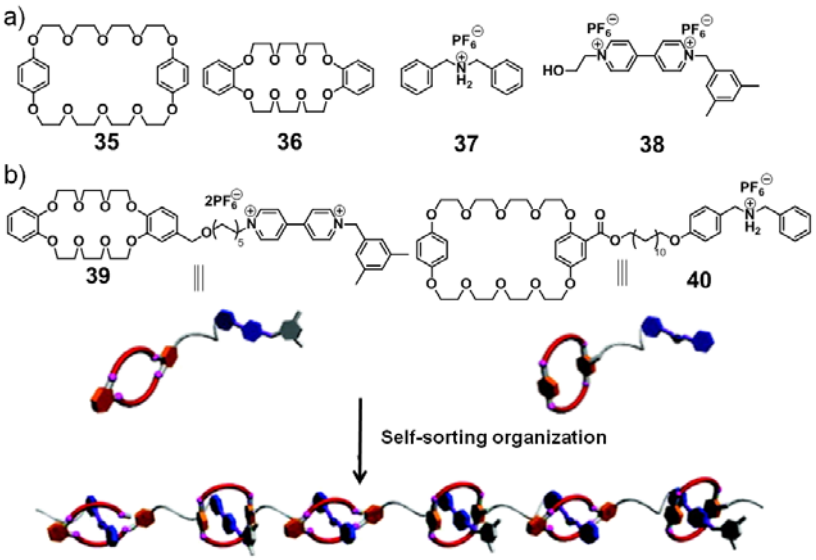

Figure 8. a) Chemical structure of precursors **35**–**38**. b) Chemical structure and cartoon representation of heteroditopic **39** and **40** and their self-sorting into alternating supramolecular polymers via integrative self-discrimination. Reprinted with permission from ref. 82.

2.3.2. Complementarity in Hydrogen-Bonded Systems

Complementarity plays a particularly important role in the stabilization of hydrogen-bonded assemblies,[86,87] to the point that it facilitates the approximation of the functional groups involved.[48] The pairing of nitrogenous bases (A-T and C-G) in the DNA double helix is undoubtedly one of the most obvious examples of complementary systems in nature.[88]

Although appropriate geometrical correspondence of the interacting groups is always a prerequisite, the match or mismatch between the pattern of hydrogen donors and acceptors ultimately decides the outcome of a recognition event, since in this way only the "right" pairs are allowed to form. In the stabilization of the DNA double helix, interactions among pyrimidines (C, T) are unfavored because the molecules are too far apart whereas purine-purine (A, G) pairings are too close, therefore leading to electrostatic repulsions. In the only other possible pairings (G-T and A-C) the pattern of hydrogen donors and acceptors do not correspond, which makes A-T and C-G the only remaining possibility in which base-pairing can take place, stabilized both in terms of hydrogen bond complementarity and geometrical fit. Thus, the importance of hydrogen-bonding complementarity in nature anticipates its significant role in the stabilization of artificial self-sorting systems as well.

Reinhoudt, Timmerman and co-workers investigated the self-sorting of hydrogen-bonding-based supramolecular systems for the first time in 1999.[25] Following their seminal work in which they studied the formation of a $\mathbf{(41)_3 \bullet (42)_6}$ box-like double rosette stabilized by 36 hydrogen bonds upon co-assembly of calixarene-based bismelamine derivative **41** and barbiturate **42**,[89] they wondered whether the introduction of an additional bismelamine unit would influence their behavior in the presence of barbiturate units (Figure 9). In a similar manner to bismelamine derivatives **41a-b**, tetramelamines **43a-b** were demonstrated by ^{1}H NMR to self-assemble into tetra(rosettes), although with a remarkably lower stability than bismelamine rosettes. When tetra(rosette) assembly $\mathbf{(43a)_3 \bullet (42)_{12}}$ was mixed with bismelamines **41a** or **41b**, the stability order was reversed, and assembly $\mathbf{(41)_3 \bullet (42)_6}$ was observed to form at the expense of $\mathbf{(43a)_3 \bullet (42)_{12}}$. The reduced stability of $\mathbf{(43a)_3 \bullet (42)_{12}}$ was attributed to the inward curvature of the two rosette planes that prevent the complete filling of the space between the two double rosettes. Finally, the self-sorting degree in mixtures of bis- and tetramelamines in the presence of **42** was examined. Mixtures of **41a** and **43a** or **43b** in a 2:1 ratio with a slight excess of **42** exclusively revealed the formation of homomeric assemblies $\mathbf{(41)_3 \bullet (42)_6}$ and $\mathbf{(43)_3 \bullet (42)_{12}}$ and no trace of heteroassemblies was detected (Figure 9b). However, when equal amounts of **43a** and **43b** were mixed with **42**, heteromeric assemblies were observed. These results are a clear consequence of the interplay of various

molecular codes, namely molecular shape and flexibility of the bis- or tetramelamine building blocks and hydrogen-bonding complementarity.

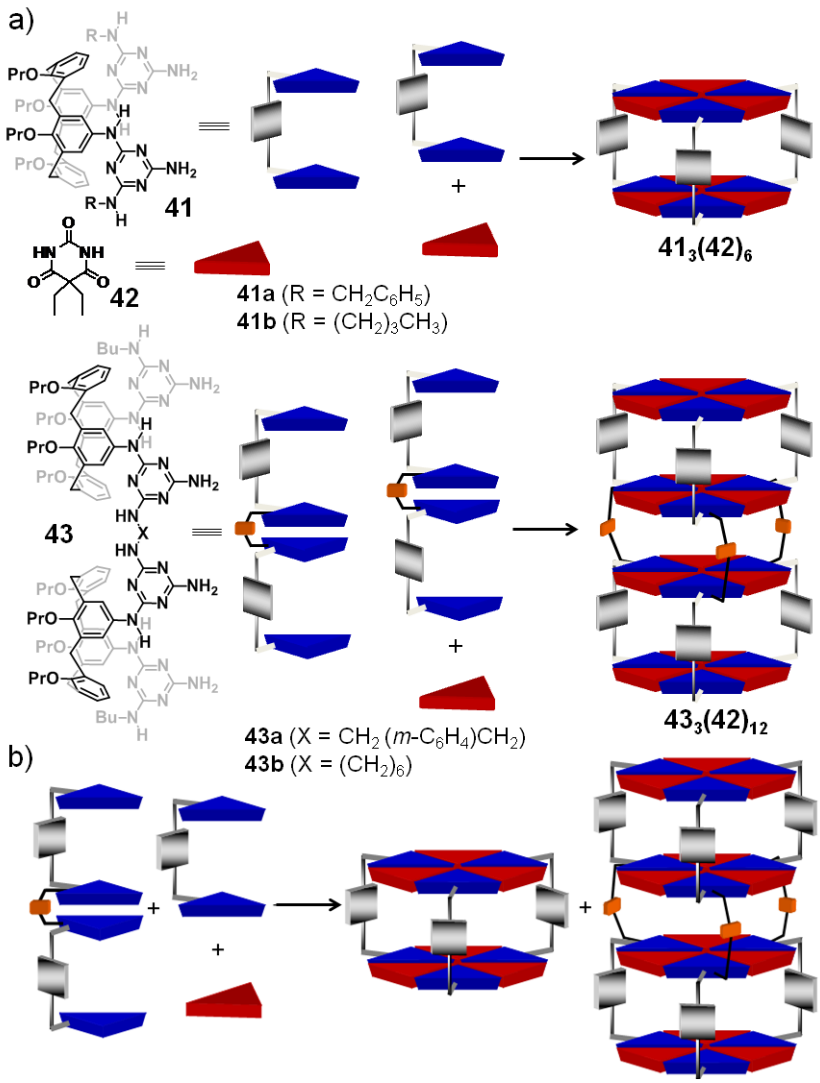

Figure 9. a) Chemical structure of derivatives **41**–**43** and their schematic representation. b) Self-recognition process in a mixture of **41**–**43**.

The role of hydrogen bond complementarity has also been widely explored in the field of supramolecular polymers.[90-93] Meijer, Sijbesma and co-workers reported the formation of supramolecular copolymers based on mixtures of 2-ureido-4[*1H*]-pyrimidinone **44** (Upy) and 2,7-diamido-1,8-naphthyridine **45** (Napy) building blocks (Figure 10).[94]

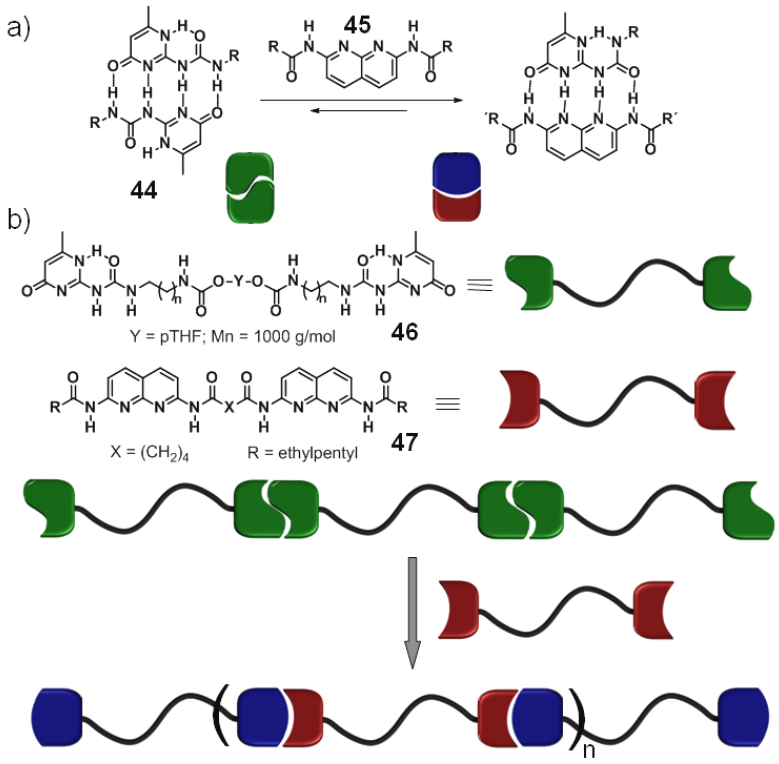

Figure 10. a) Chemical structures of precursors **44** (Upy) and **45** (Napy) and their self-assembly via hydrogen-bonding. b) Chemical structures of oligomeric **46** and **47** and cartoon representation of the self-discrimination process in a mixture of both.

Upy units were previously shown to yield self-complementary supramolecular polymers with high degrees of polymerization in the bulk as well as in solution with dimerization constants (K_{dim}) up to 6 x 10^7 M^{-1} in chloroform.[95-98] In an extension of this work, Li and co-workers have demonstrated that quadruple hydrogen bonds between the 6[*1H*] tautomeric form of **44** and Napy gives rise to complexes with binding constant of K_a ~ 5 x 10^6 M^{-1} (Figure 10a).[99] Despite of the lower value of this binding constant compared to the former, Upy dimers are disrupted in the presence of one equivalent of Napy in $CDCl_3$. This behavior can be rationalized by the fact that the hydrogen bonding pattern of **45** is not self-complementary. Accordingly, saturation of all hydrogen-bond donor and acceptor sites is only achieved in the heteroassembled stack that is also the one with the lowest total Gibbs energy. On the basis of these findings, a collection of Upy and Napy-based bifunctional monomers (**46**, **47**) were synthesized with the aim to study their self-assembly into supramolecular copolymers. In all cases, mixtures of linear polymers along with their cyclic homologues were observed, as indicated by ^{1}H NMR and viscosity experiments. Interestingly, upon titration of

bifunctional monomer **46** with **47**, almost insignificant amounts of cyclic products were observed. Instead, **47** was incorporated in the supramolecular polymer chain of **46** until an alternating copolymer is obtained at a 1:1 ratio of monomers (Figure 10b). If the ratio of monomer **47** exceeds that of 1:1, the excess of molecules of **47** act as end-cappers and the chain length of the polymer is reduced. The selectivity of the copolymerization process was also examined to be concentration dependent by ^{1}H NMR dilution and fluorescence spectroscopy experiments of Upy and Napy monomers. The combined techniques revealed a value of minimum concentration (5×10^{-5} M) above which the formation of heterodimers, i.e., self-discrimination, is favored. Shortly afterwards, Zimmerman and Park showed another beautiful example for the formation of alternating supramolecular multi-block copolymers based on a Napy bifunctional monomer in combination with the butylurea of guanosine.[100] The concentration and the ratio of the blocks in the mixture were demonstrated to strongly influence the degree of polymerization.

Rebek and co-workers as well as Atwood and co-workers have devoted extensive studies towards the investigation of hydrogen-bonded self-assembled capsules.[101,102] These are formed exclusively when, and only when suitable guests are present to fill the space inside. Thus, capsule formation is biased by a combination of geometry, hydrogen-bonding complementarity and the choice of a proper guest. For instance, six molecules of resorcinarene **48** (Figure 11) rearrange into a hexameric capsule in the presence of eight molecules of water, stabilized by 60 hydrogen bonds,[102] or with wet solvents[103,104] such as chloroform or benzene, or in the presence of large quaternary ammonium ions.[105,106] On the other hand, resorcinarene congener cavitand **49** self-assembles into a dimeric capsule through a seam of eight hydrogen bonds encapsulating three molecules of chloroform. Alternatively, on mixing the homomeric capsules $\mathbf{48_6}$ and $\mathbf{49_2}$ a hybrid structure **48•49** that coexists with the homomeric capsules immediately forms (Figure 11).[107] These results are attributed to the fact that both capsules share resorcinarene modules with comparable dimensions, symmetries, and hydrogen-bonding patterns. Accordingly, their codes are too similar to afford self-recognition.

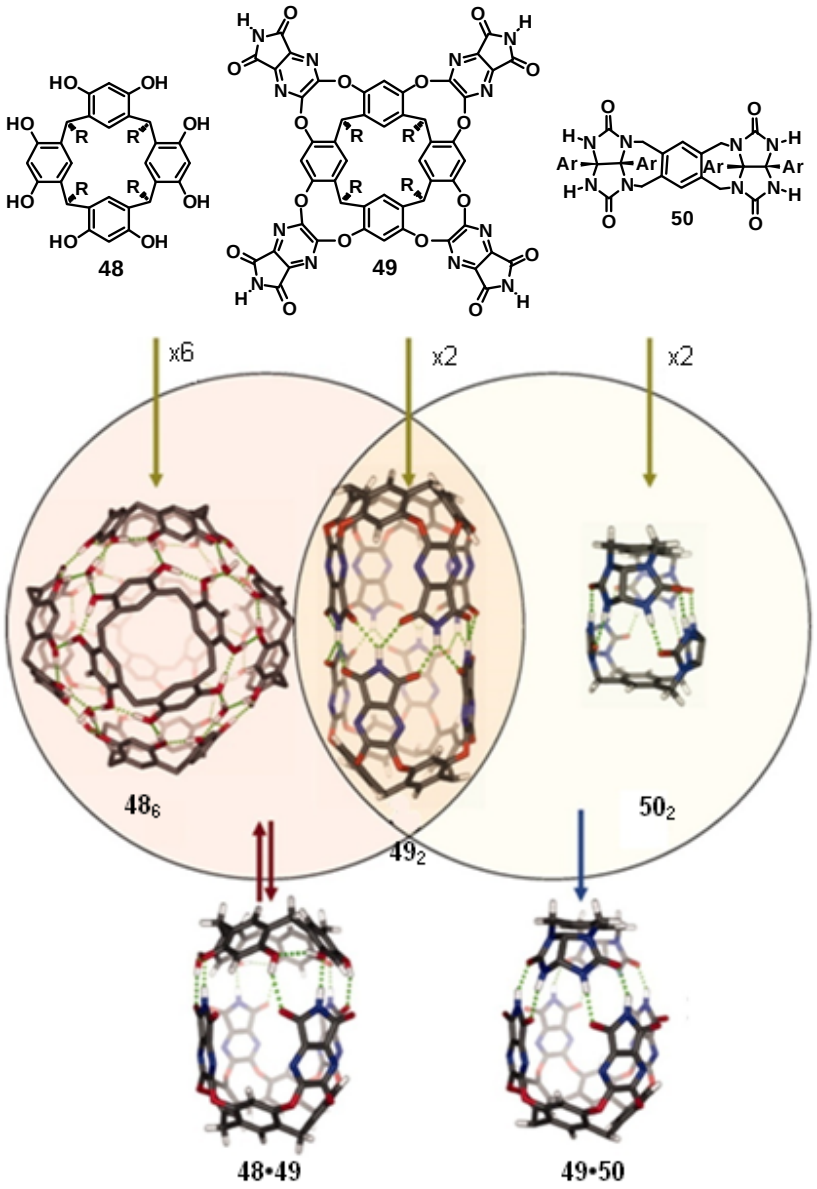

Figure 11. Chemical structures of derivatives **48**–**50** and energy-minimized structures of hexameric capsule $\mathbf{48_6}$, cylindrical capsule $\mathbf{49_2}$, hybrid capsule **48•49**, tennis ball $\mathbf{50_2}$ and hybrid capsule **49•50**. Peripheral alkyl and aryl groups (R = $C_{11}H_{23}$, Ar = p-C_6H_4-n-$(Bu)_2$) in the calculated structures have been removed for clarity. Reprinted with permission from ref. 109.

To explore the possibility to obtain high-fidelity social self-sorting capsule systems, the authors questioned whether the "tennis-ball" capsule $\mathbf{50_2}$,[108] previously known to dimerize in the presence of small guests such as methane, could give rise to hybrid capsules in the presence of cavitand **49**.[109] At first glance, this assumption appears unlikely, given the different sizes, symmetries and hydrogen-bonding patterns of $\mathbf{49_2}$ and $\mathbf{50_2}$. However, molecular modeling studies suggested that a slight torsion of the building blocks **49** and **50** can efficiently pair most of the hydrogen bond donor and acceptors, leaving only four imide

oxygens unsatisfied. To their surprise, ^{1}H NMR experiments proved the immediate and exclusive formation of a hybrid assembly **49•50** in $CDCl_3$, whereas no sign of homomeric capsules was observed. This social capsule was also demonstrated to form in the presence of solvent molecules other than chloroform such as tetrachloroethane, *p*-xylene and ethane to name a few. Although this high selectivity depends to a great extent on the hydrogen-bonding complementarity between the interacting capsules, the nature and size of the guest is also an influence. The template effect of guest molecules was also recognized to have a vital importance in the self-sorting behavior of metal-coordination-based cages.[110]

2.3.3. Steric Factors

Steric effects arise as a consequence of the spatial arrangement and bulkiness of atoms or substituents within a molecule. Accordingly, they are in essence geometrical codes related to shape. However, due to the increasing attention devoted by several research groups to the decisive effect of steric codes in self-sorting phenomena, we will regard them separately in an independent section. Their contribution, however, will only play a determinant role when the interacting building blocks are structurally similar in terms of geometry and/or hydrogen-bonding pattern.

In 2002 a decisive contribution of steric codes in self-sorting events was investigated by Zimmerman and co-workers in mixtures of hydrogen-bonded cyclic assemblies.[27] This work was based on earlier studies of the same group on hexameric self-assemblies of monomers **52** composed of complementary **ADD** and **DDA** hydrogen-bonding arrays in chloroform or even in more polar 15% aq. THF mixtures.[111] To elucidate self-sorting effects these authors examined the influence of the attachment of dendrons of different size (**51**, **52**) on their self-assembly (Figure 12).[27] ^{1}H NMR, size exclusion chromatography (SEC) and DLS experiments demonstrated the formation of cyclic hexameric aggregates $\mathbf{(51)_6}$ and $\mathbf{(52)_6}$ from the individual precursors **51** and **52**, respectively. Next, the authors questioned whether self-sorting in mixtures of third-(**51**) and first-(**52**) generation monomers would take place or, on the other hand, crossover species would form (Figure 12b).

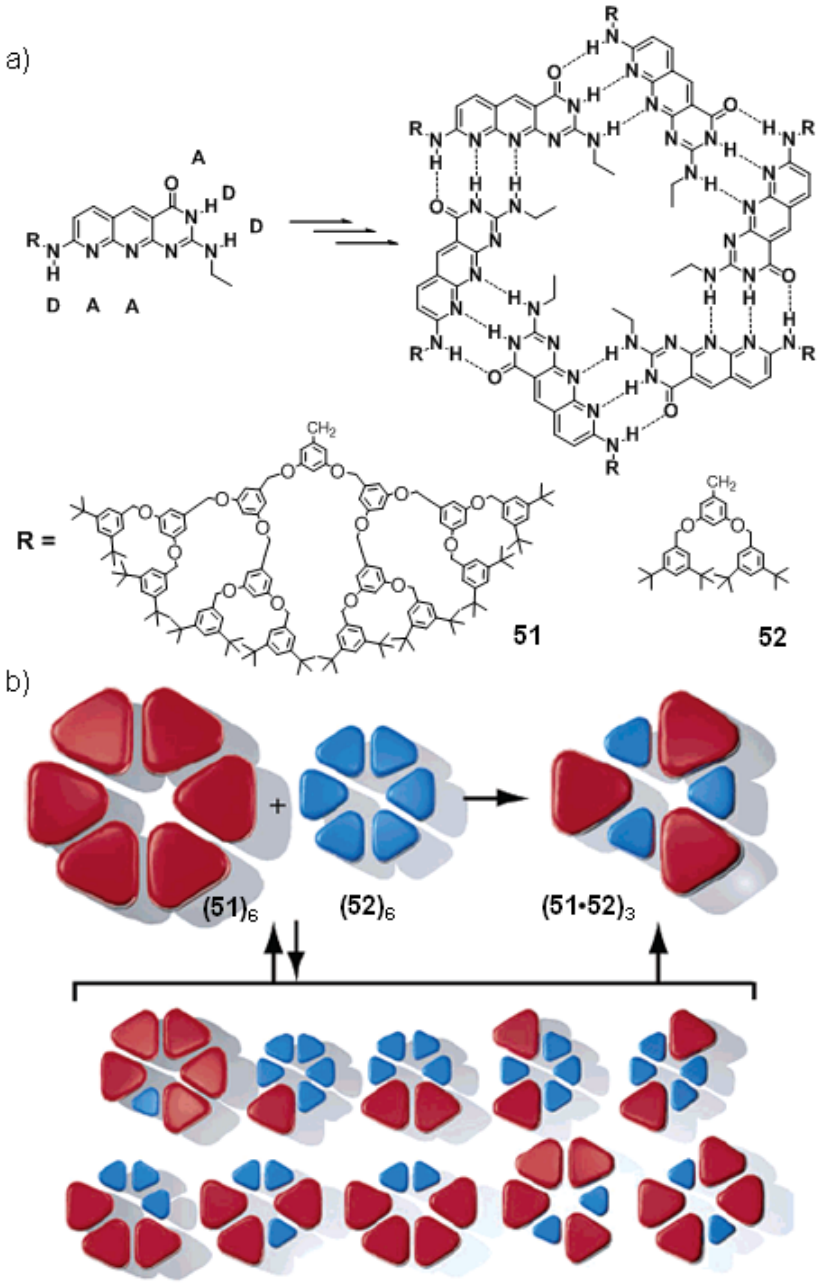

Figure 12. a) Chemical structures of third and first generation dendrons **51** and **52** respectively and cyclic assemblies formed thereof. b) Possible mixed aggregates formed from mixing of $\mathbf{(51)_6}$ and $\mathbf{(52)_6}$. Reprinted with permission from ref. 27.

Statistically, a mixture of up to 11 distinct hexameric aggregates is probable to form. Interestingly, the broadness of the SEC signal at intermediate mixing times suggests that many, if not all, of these possible aggregates coexist. However, after longer periods of time a progressive sharpening of the SEC peak takes place, suggesting that the initial mixture of aggregates convert to a discrete structure, different from $\mathbf{(52)_6}$ and $\mathbf{(51)_6}$. Given the low stability of the complex $\mathbf{(51)_6}$, mainly due to steric constraints, the authors hypothesized that

the destabilizing steric interactions between the peripheral dendrons can be minimized if the fully mixed and alternating **(51•52)$_3$** is formed. This hexamer would be particularly stabilized in terms of geometry, symmetry, hydrogen-bonding complementarity and ultimately biased by steric effects (Figure 12b).

More recently, the combination of steric and electronic codes has been applied for the self-sorting of metallosupramolecular squares by Stang and co-workers (Figure 13).[112]

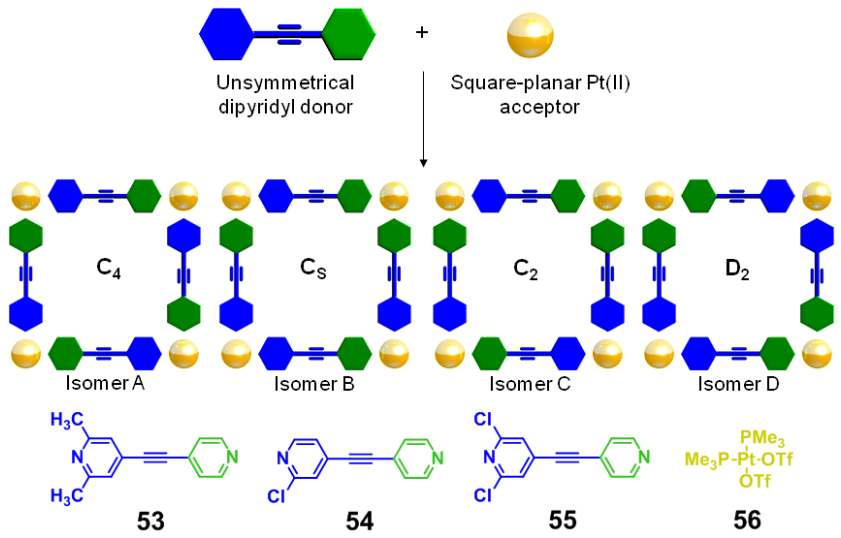

Figure 13. Chemical structure and schematic representation of the different metallosupramolecular squares that may form upon self-sorting of ligands **53**–**55** and Pt(II) acceptor **56**.

A set of unsymmetrical bis(4-pyridyl)acetylene ligands (**53**–**56**) was synthesized and their self-sorting behavior in the presence of Pt(II) building blocks investigated. All ligands are unsymmetrical, featuring one sterically hindered pyridyl ring connected to one or more substituents (depicted as navy blue hexagons in Figure 13) and one uncrowded pyridyl group (depicted as green). In the absence of any biasing interactions, there are four different isomers that may be formed upon self-assembly with a 90º Pt(II) acceptor unit (depicted as a golden sphere): isomer **A**, in which all unsymmetrical donors are oriented in an alternating fashion leading to identical coordination spheres at each Pt center (C_4 symmetry), isomer **D**, in which every acceptor is coordinated by two of the same pyridyl moieties leading to two distinct sets of Pt corners (D_2 symmetry) and the less symmetrical isomers **B** and **C** that contain three different types of Pt corners (symmetry C_S and C_2, respectively) (Figure 13). Whereas ligands **53** and **55** may, in theory, form four isomeric [4+4] assemblies when combined with acceptor

56, an even more complex set of isomeric cycles is possible for **54** depending on the relative orientations of the α-Cl atoms within each square (**A**-**D**). Interestingly, upon mixing **53** and **56** in a 1:1 ratio, only one of the possible squares (isomer **A**) is formed, as demonstrated by ^{1}H and ^{31}P NMR in CD_3NO_2. This high degree of self-sorting appears to arise solely as a result of interligand α-Me/α-Me steric interactions that prohibit the coordination of two of the bulky dimethyl pyridyl moieties to the same Pt(II) center as well as electronic effects associated to different electron-donating abilities. However, the efficiency of the self-sorting process diminishes drastically when the sterically bulky methyl groups are replaced by one (**54**) or two (**55**) Cl atoms in the presence of stoichiometric amounts of **56**. This has been mainly attributed to the decrease of the steric bulk of Cl atoms and the more similar electron-donating character of Cl-substituted and unsubstituted pyridyl moieties. These conclusions were supported by molecular modeling, which showed that the two chlorine atoms are too remote from the Pt-N coordination site to have any significant steric influence. These overall results highlight that unsymmetrical ditopic ligands can effectively direct self-sorting by steric and electronic effects, ruling out –due to identical size and shape– any geometrical bias.

A number of groups have recently made use of steric codes to direct the efficient self-sorting in mixtures of tetraurea calix[4]arenes[113-115] which are known to form dimeric capsules.[116,117] In a recent particularly appealing example, Böhmer and Schalley and co-workers studied the self-sorting behavior in a complex mixture comprising of up to eleven structurally related building blocks (Figure 14).[114] All calixarenes (**57**–**67**) are substituted by four urea groups on their wide rim and fixed in the cone conformation by four pentyl ether groups (Figure 14). They thus possess analogous size, shape and hydrogen-bonding patterns, thereby precluding any geometrical or complementarity bias. Their only difference concerns the nature –small or bulky– of the peripheral substituents attached to the urea groups. Whereas sterically less crowded calixarenes **57**–**62** are known to dimerize through a seam of 16 hydrogen bonds,[116,117] dimerization is obstructed when adjacent urea residues are covalently connected[118] through one or more loops, as is the case of calixarenes **63**–**67**. Nevertheless **63**–**67** still have a strong tendency to dimerize if a suitable partner (for instance "open chain" calixarenes **57**–**62**)[119,120] equipped with non-bulky groups is available, whose

urea substituents are small enough to penetrate the loops.[113] If, on the contrary, the substituents are too bulky, dimerization does not occur.

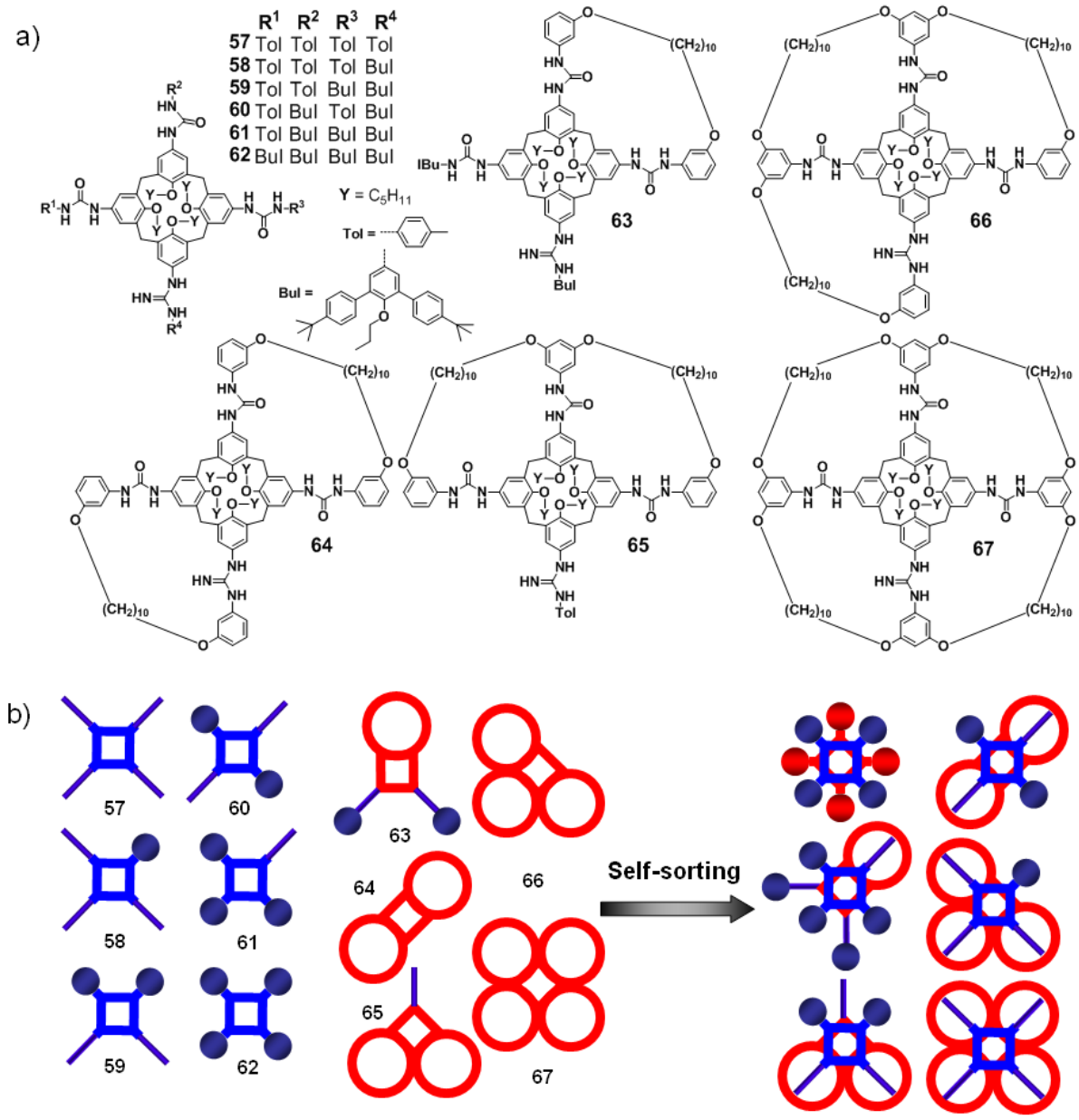

Figure 14. a) Chemical structures of calixarenes **57**–**67**. b) Cartoon representation of the self-sorting process in the mixture of eleven tetra-urea calix[4]arene derivatives **57**–**67** into their six allowed assemblies.

Statistically, the 11-component mixture can combine to form 66 different dimers. However, taking into account the abovementioned premises and by controlling the stoichiometry, an equimolar mixture of **57**–**67** should self-sort into only six different dimers: **57**-**67**, **58**-**66**, **59**-**65**, **60**-**64**, **61**-**63** and **62**-**62**.^{1}H NMR experiments in $CDCl_3$ were initially performed on a slightly less complex mixture comprising calixarenes **57**, **60**, **64**, **67** and **62** to evaluate the

self-sorting processes. As anticipated, only the pairs **57**-**67**, **60**-**64** and **62**-**62** were detected by NMR, in agreement with the rationales explained above. Unfortunately, more complex 10 or 11-component mixtures could not be properly analyzed by ^{1}H NMR. The authors therefore made use of electrospray ionization Fourier transform ion cyclotron (ESI-FTICR) mass spectrometry to analyze the mixtures. Initial control experiments performed on every independent pair demonstrated that the expected heterodimers **57**-**67**, **58**-**66**, **59**-**65**, **60**-**64**, **61**-**63** and **62**-**62** are by far the most abundant species. However, the spectrum of the mixture of all eleven monomers also showed the appearance of unexpected peaks. The authors attributed this observation to the liberation of monomers due to the low concentration regime in which these MS experiments were performed. By increasing the concentration of hindered compounds **63**–**67** in a 20% excess with respect to **57**–**62**, the equilibria could be successfully shifted back towards the exclusive formation of the expected capsules, thereby demonstrating that small external influences may significantly alter the behavior of a mixture.

Based on pseudorotaxane structures from Huang,[24,121] Stoddard and Williams[122,123] (see Scheme 3) a series of most illustrative examples on the utilization of sterical codes in self-sorting systems was introduced by Schalley and co-workers. Secondary dialkylammonium ions are able to thread through the cavity of benzo-21-crown-7 (C7) **71**, leading to pseudorotaxanes.[121] Phenyl groups can effectively suffice as stoppers in these systems to trap **71** on the axle. In contrast, dibenzo-24-crown-8 (C8) **70** units can form pseudorotaxanes with secondary dibenzylammonium ions, revealing that phenyl groups are not bulky enough to act as efficient stoppers for this larger macrocycle.[122,123] These premises were subsequently exploited to achieve efficient four component self-sorting systems composed of two crown ether units (C8 (**70**) and C7 (**71**)) and two ammonium salts (**68** and **69**).[24] Crown ether **71** is in principle too hindered to slip onto axle **68** due to the presence of sterically demanding benzyl and anthracenyl stoppers on both sides, whereas sterically less demanding axle **69** fits too loosely in the larger cavity of crown ether **70** (Scheme 3a). As anticipated by these prerequisites, the ESI mass spectrum of an equimolar mixture of all four compounds in dichloromethane revealed the presence of only two peaks corresponding to the complexes **72** and **73** which was further confirmed by ^{1}H NMR experiments. This type of self-sorting was

termed as *nonintegrative*, because it leads to a smaller than possible set of discrete complexes from subunits each equipped with just one binding site (Scheme 3a).

Scheme 3.

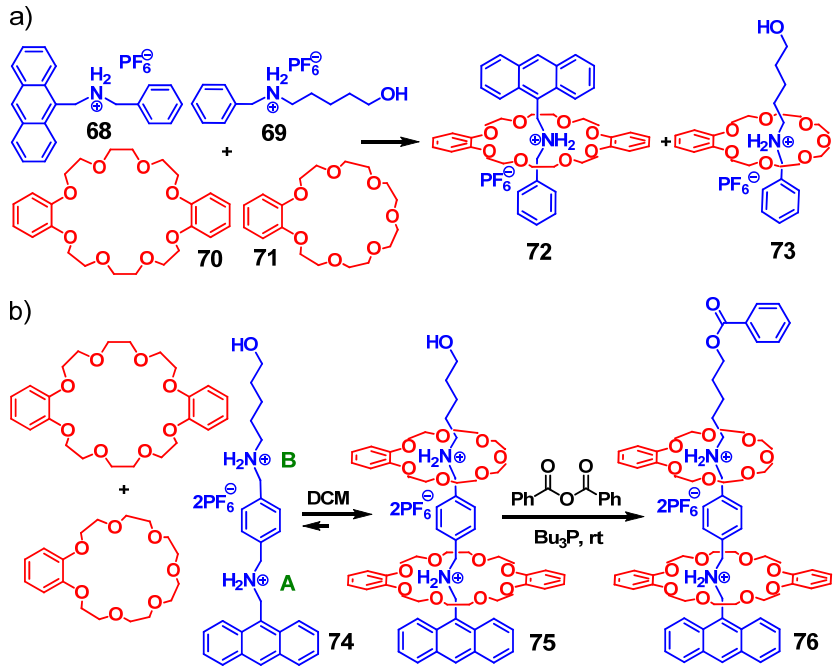

These investigations were later extended into *integrative* self-sorting systems, in which more than two different subunits are bound in two or more recognition events with positional control.[24,124] To this end, a divalent ammonium receptor axle **74** equipped with two binding sites **A** and **B** was synthesized, and its self-sorting in the presence of crown ethers C7 **71** and C8 **70** was investigated. ^{1}H NMR studies revealed that on mixing, crown ether **71** binds exclusively at site **B** of **74**. In contrast, the addition of 1 equivalent of C8 **70** provoked changes for the protons corresponding to both **A** and **B** sites, but the changes in **A** were more obvious, indicating that C8 **70** prefers to bind **A** once the mixture has reached the equilibrium. Accordingly, in the presence of both crown ethers **70** and **71**, **75** is the major component. Finally, this complex was subjected to an esterification reaction with benzoic anhydride to yield a "stopper cascade". In this rotaxane, the upper and middle phenyl ring of the axle prevent the slipping of the C7 **71** ring, whereas C8 **70** can still slip over the central phenyl group but not over C7 **71**, so that it is also trapped (Scheme 3b). Recently, the same authors have expanded this concept for the design of highly sophisticated rotaxane-based self-sorting systems comprising multiply threaded complexes.[124,125] ESI-FTICR mass spectrometry was

demonstrated to be a very useful tool to monitor the self-assembly intermediates, wrongly assembled structures as well as the final thermodynamic products of the self-sorted mixtures.

The examples described so far reveal that steric codes can significantly alter the self-sorting equilibria in either metallosupramolecular or hydrogen bonding-based assemblies. Their influence in systems assembled by means of other noncovalent forces remains, however, almost unexplored. In one distinct example, Würthner and co-workers studied hydrogen-bonding and π–π-stacking driven self-assembly, co-assembly and gelation ability of a series of perylene bisimide dyes functionalized with benzamide groups at the imide position and peripherally connected to different alkyl substituents (Figure 15).[126] Solvent and temperature-dependent UV/Vis and circular dichroism (CD) experiments demonstrated that perylene bisimide derivatives equipped with linear side chains (e.g. **77**) formed H-type aggregates (hypsochromically displaced major absorption band) giving rise to red gels,[127] whereas by introducing sterically demanding branched alkyl chains (e.g. **78**) the formation of J-type aggregates (bathochromically displaced major absorption band) yielding green gels was observed (Figure 15a).[128] This difference in self-assembly behavior was subsequently exploited to investigate the co-assembly of mixtures of perylene bisimides equipped with linear and branched chains. UV/Vis and CD studies performed on 80:20 mixtures of methylcyclohexane/tetrahydrofuran revealed that, when dye **78** was mixed with dye **77** at low **78**/**77** ratio, an exclusive formation of red H-type aggregates containing both chromophores was observed. However, the incorporation of the more bulky derivative **78** in these H-type π-stacks is limited to an amount of about 50%, (Figure 15). This ratio implies that **78** is incorporated in the mixed assembly with **77** in an alternate fashion, in which unfavorable steric constraints among two adjacent face-to-face π-stacked **78** are prevented. When the amount of **78** approaches 50% the system separates into H-type and J-type π-stacks and ultimately leads to a narcissistic self-sorting in which **77** and **78** form their respective independent assemblies. The latter situation is particularly favored at high ratios of **78** due to the energetic penalty associated with the packing of **77** into slipped J-aggregate stacks and the steric problems encountered upon incorporation of larger amounts of **78** into more compact H-type π-stacks (Figure 15b)

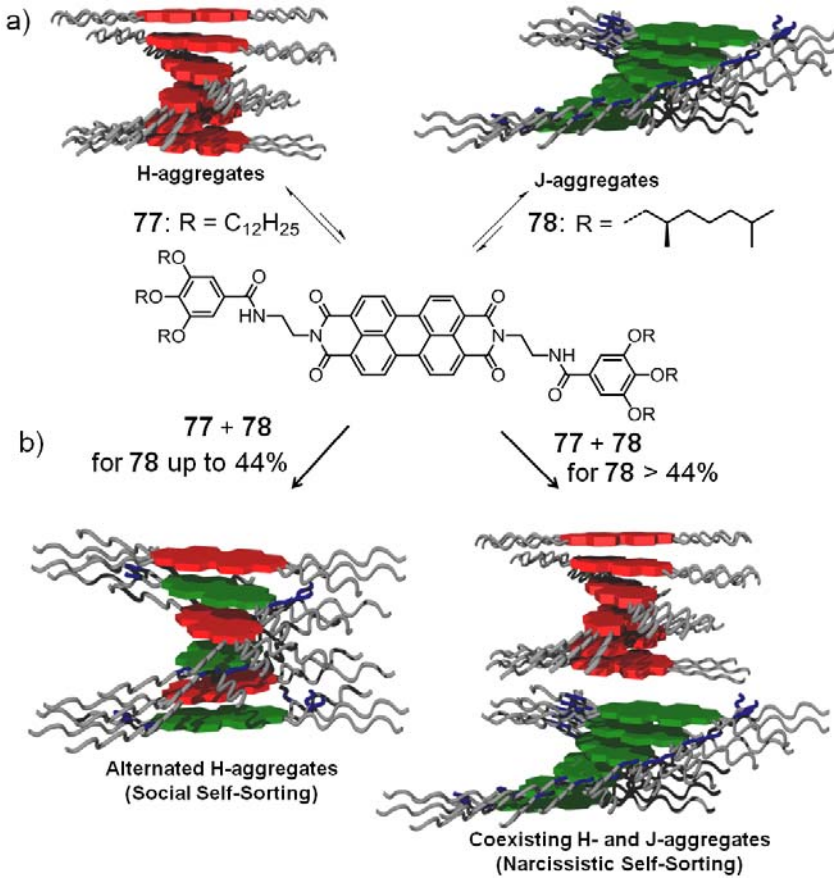

Figure 15. a) Chemical structures and independent self-assembly pathways for perylene bisimides **77** and **78**. b) Self-sorting processes in mixtures of perylene bisimides **77** and **78** depending on the relative concentration of the components in the mixture.

Recently, another example for the self-sorting capability of extended supramolecular networks was reported by Moffat and Smith.[129] These authors demonstrated a significant steric influence on the self-sorting ability of three different hydrogen-bonded organogelators. Two organogelators possess amide groups anchored to long alkyl surface groups whereas the remaining gelator features carbamate groups and lacks any additional chain. The joint effect of hydrogen bond complementarity and steric factors was proposed to control the self-sorting process, since only organogelators equipped with analogous hydrogen-bonding functionalities and steric restraints were demonstrated to socialize. Mixtures of the most structurally different gelators led, on the other hand, to complete self-recognition.

2.3.4. Coordination Sphere

As illustrated in previous chapters, metal ion-ligand interactions are most useful for the construction of supramolecular architectures. We have observed in chapter 3.1 that the size, shape and predefined geometry of organic ligands can serve as an efficient molecular code to direct self-sorting phenomena when combined with a metal ion (see for instance Figure 4 and Scheme 2). The high selectivity in these recognition processes is primarily of geometrical basis –for both systems all possible narcissistic or social assemblies involve the same metal ion-ligand point interactions– what rules out any intrinsic influence of the metal on the self-sorting phenomena. The situation, however, would be far more complex if two or more different metal ions are available to bind with one or more ligands. Under these conditions, a wide variety of combinations of metal complexes with numerous geometries is in theory possible to form. This diversity of complexes will largely depend on the *coordination sphere* in metal ion-ligand interactions,[130] which can be defined as the number of ligands attached to the metal ion. Three main factors govern the coordination sphere in a complex: a) the size, charge, hardness and polarizability of the metal atom,[131,132] b) the identity (and sterics) of the ligands and c) the electronic interactions between the ligands and the central atom or ion.[130] Ligands will follow the principle of "maximal site occupancy"[86,133,134] by realizing metal coordination at the maximum number of available sites, what is ultimately imprinted by the interactions between s and p molecular orbitals of the ligands and the d orbitals of the metal ions. Transition metals with vacant d-orbitals are known for their quite specific coordination modes which obviously constitute most appealing molecular codes to direct self-sorting phenomena.[19,133,135] In general, atoms of larger radii give rise to high coordination numbers, especially when the metal possesses a small number of valence electrons because that would mean that the metal can accept more electrons from Lewis bases, like for instance in $[Mo(CN)_8]^{4-}$. Small metals, on the other hand, lead to low coordination numbers particularly if the ions are rich in electrons, so that they are less able to accept electrons from any Lewis bases that are potential ligands, e.g. $[PtCl_4]^{2-}$. This high geometrical versatility when different metal ions and ligands are combined should place metal ion-coordination among the most relevant codes applicable for driving self-sorting processes in supramolecular systems.

Indeed, in the field of dynamic combinatorial libraries, the coordination geometry of the metal ion[136,137] and steric constraints[138] have been applied to drive the outcome of reversible chemical reactions. However, the influence of such metal ion coordination codes in mixtures of different metal ions and ligands has been to date nearly unexplored, what prevents us from drawing a realistic conclusion about their quantitative contribution.

In their seminal work Lehn and co-workers [19] took advantage of the tetrahedral coordination of Cu(I) ions and octahedral coordination of Ni(II) to accomplish self-recognition in mixtures of bipyridine-based ligands, yielding double and triple helicates respectively (see Scheme 1). This example highlights that the ability of the metal ions to coordinate into different geometries (along with the geometry of the ligands) can direct the self-recognition process. Nevertheless, since this early investigation little attention has been devoted to the study of systems comprising more than one metal ion in the presence of different ligands.

In an exciting example, Schmittel and co-workers have revealed a self-sorting process in mixtures of four different terpyridine or phenanthroline-based ligands (**79**–**82**) and two different metal ions (Zn(II) and Cu(I)).[139,140] Out of 20 possible combinations, the self-sorting library ended up with only two metal complexes: $[Cu(\mathbf{80})(\mathbf{82})]^{+}$ and $[Zn(\mathbf{79})(\mathbf{81})]^{2+}$ or $[Cu(\mathbf{79})(\mathbf{82})]^{+}$ and $[Zn(\mathbf{80})(\mathbf{81})]^{2+}$ depending on the relative stoichiometry chosen, as demonstrated by ^{1}H NMR, ESI-MS and differential pulse voltammetry (DPV). This high degree of self-sorting has been mainly attributed to geometrical, steric and electronic factors and, more importantly, to the extra stabilization gained from maximum site occupancy, that is, the difference in coordination number associated to Zn(II) and Cu(I). In a subsequent step these highly selective small building blocks were implemented into three polyfunctional ligands **83**–**85** whose integrative self-sorting in the presence of Cu(I) and Zn(II) led exclusively to the formation of a hitherto unknown supramolecular structure, a trapezoidal (**T**) metal-ligand assembly, whereas no trace of the other possible large ($\mathbf{R_L}$) or small ($\mathbf{R_S}$) rectangles could be observed (Figure 16). Recently**,** these authors have exploited their elegant concept for the fabrication of a five-component supramolecular triangle from structurally similar building blocks.[141]

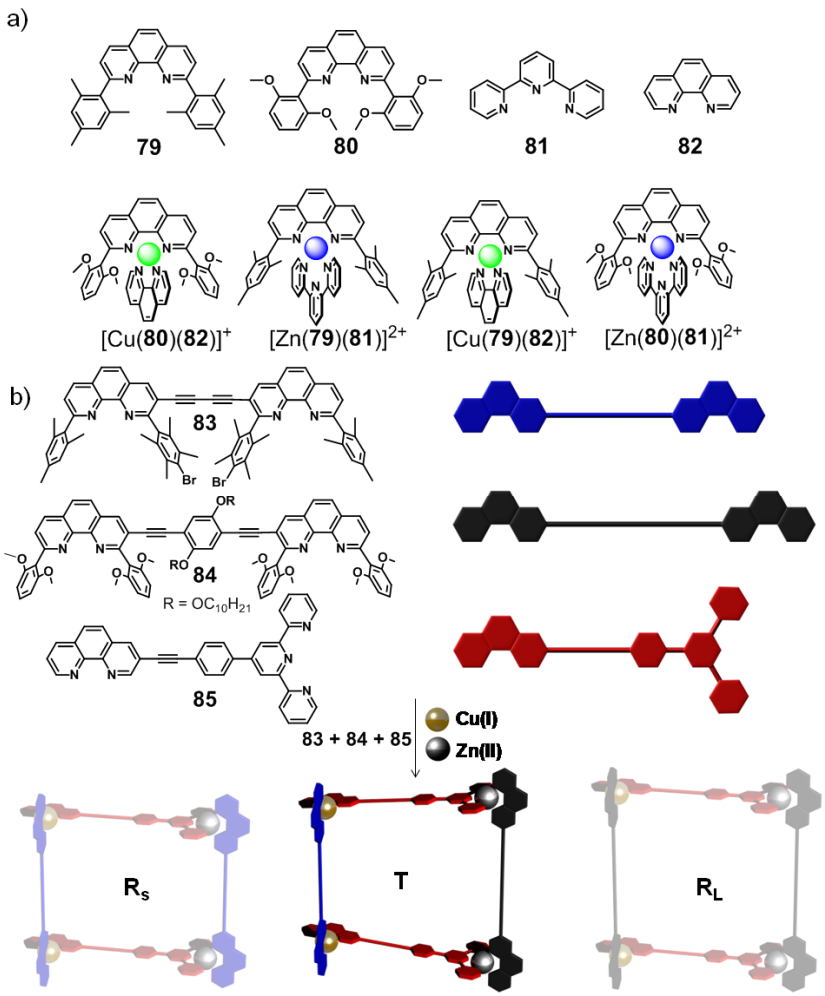

Figure 16. a) Molecular structure of ligands **79**–**82** and their respective non-integrative self-sorting. b) Chemical structure of polyfunctional ligands **83**–**85** and their integrative self-sorting in the presence of Cu^{+} and Zn^{2+}.

2.3.5. Charge Transfer

Electroactive molecular materials[142,143] have gained great attention in recent years for the fabrication of optoelectronic devices, such as organic field effect transistors[144-148] or photovoltaic devices.[149-152] An adequate control of the nanometer-scale morphology between electroactive molecules in such systems is a prerequisite for good performance.[153,154] In the particular case of bulk heterojunction organic solar cells, electron-donor and acceptor molecules must segregate into chemically homogeneous domains with typical sizes of the order of the exciton diffusion length (10–20 nm). This arrangement requires a good balance between self-recognition into nanometric domains and the interaction between donor and

acceptor molecules of different domains (social self-sorting) to ensure an efficient charge transfer process at the interface.

A charge transfer (or donor-acceptor) complex is formed when two or more molecules or different parts of a large molecule associate, so that a fraction of electronic charge is donated from D (donor) to A (acceptor) with weak covalent bond formation between the molecular entities.[39] In the valence bond model this attraction can be related to the mixing of the neutral state (AB) with a charge-separated state ($A^+ B^-$). Charge transfer complexes often manifest by the appearance of a weak electronic transition in the long-wavelength region of the absorption spectrum. These optical transitions are often referred to as *charge-transfer bands* (CT bands). Typical examples are mixtures of electron rich aromatic amines, i.e., aniline, and electron poor dinitrobenzenes (Figure 17a).[155,156]

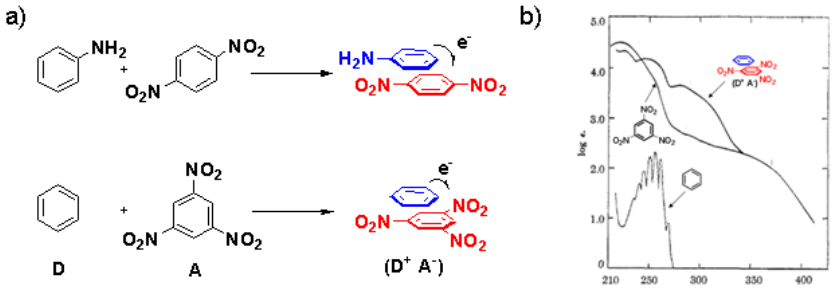

Figure 17. a) Formation of charge-transfer complexes in mixtures of aniline/1,4-dinitrobencene (top) and benzene/1,3,5-trinitrobenzene (bottom). b) Absorption spectra of benzene, 1,3,5-trinitrobenzene and benzene/1,3,5-trinitrobenzene molecular complex recorded in *n*-heptane. Reprinted with permission from ref. 156.

The UV/Vis spectra of aniline or dinitrobenzenes alone in chloroform solutions are characterized by the absence of any absorption in the visible region. Mixtures of aniline and either 1,3- or 1,4-dinitrobenzene, however, give rise to highly coloured solutions as a result of the emergence of a new charge-transfer band centred at ~480 nm.[155] The presence of an intermolecular charge-transfer transition at ~300 nm indicates the formation of a molecular complex between benzene and 1,3,5-trinitrobenzene (Figure 17b).[156] The low value of binding constant in this system (4.09 M^{-1}, *n*-heptane) clearly reflects that charge-transfer interactions make a very small contribution to the stability of the ground state of π-stacked molecular complexes.[39,157] In contrast, by simply replacing the nitro groups of 1,3,5-trinitrobenzene by

alkylamide substituents, the resulting discotic triamides are able to self-assemble into one-dimensional rod-like associates of several micrometers by hydrogen-bonding and π-stacking, affording binding constants of ~ 5×10^8 M^{-1} in heptane.[158-160]

These findings highlight that charge-transfer interactions have a remarkably smaller weight in comparison with similar systems assembled by stronger non-covalent interactions such as hydrogen bonds, which allows us to hypothesize that charge-transfer contributions should have only a modest influence on the outcome of a self-sorting mixture.[157] Nevertheless, when the structural similarities and the type and number of participating noncovalent forces among the interacting molecules reach a maximum, geometrical complementarity is obviously less relevant and molecular codes that apparently have a small weight ─such as charge transfer events─ become important to the point that they can bias the molecular recognition events. This strategy has been applied successfully in several examples of π-conjugated self-sorting systems published in the literature.[161-163]

Torres and co-workers reported a convincing example in which similar geometry of the involved molecules in the self-sorting process allows electronic charge transfer interactions to be the chief driving force for the social self-sorting event.[163] They reported a dimeric system composed of two phthalocyanines covalently connected by a [2,2]paracyclophane unit (**86**) (Figure 18).

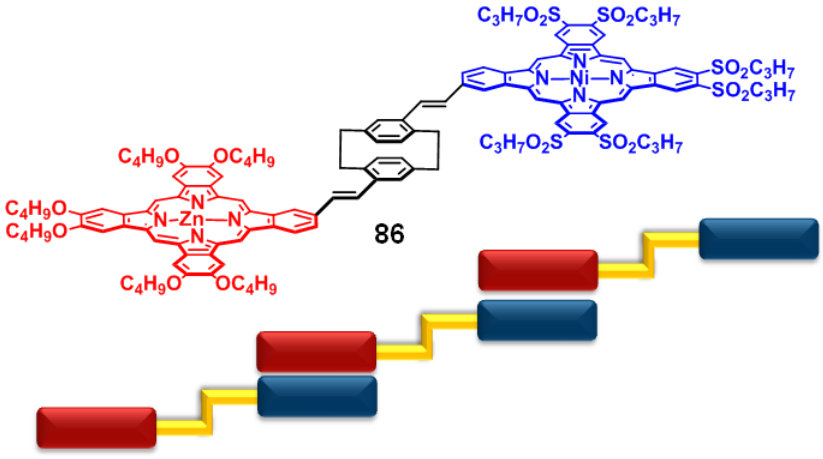

Figure 18. Chemical structure of phthalocyanine **86** and schematic representation of the self-discrimination process within supramolecular aggregates.

Each of these covalently linked phthalocyanines possesses a different electronic character due to the presence of electron donating alkoxy or electron withdrawing alkylsulfonyl

substituents. The presence of a charge-transfer (CT) band in UV/Vis absorption spectra in chloroform demonstrated that the molecules self-sort in a self-discriminating manner driven by their complementary electronic character (Figure 18).

In another example Fujita and co-workers masterly captured the simultaneous influence of geometrical as well as charge transfer codes for an efficient self-sorting process in coordination cages.[164-167] They recently reported the interaction of cage **87** –formed by two large organic panels with electron acceptor properties and D_{3h} geometry, three rod like pillars and six metal hinges– with naphthalenediimide acceptor **89** and three different donors (triphenylene (**88**), perylene and pyrene) (Figure 19).[167] As shown by a series of experiments, if the number of stacked guest molecules *n* in the cavity (this can be controlled simply by adjusting the length of the organic pillar sets) is odd, alternating donor-acceptor (**D-A**) arrays, e.g. **A-D-A-D-A**, are favored, leading to self-discrimination driven by the electronic nature of the molecules.[164] On the other hand, when *n* is even, such preferred alternating **D-A** arrays are excluded (Figure 19), which makes the prediction of the preferred stack structure less trivial. **A-A** interactions were apparently better tolerated than **D-D** interactions, which turns cage **87** into a good candidate for exchange studies. The formation of the **A-D-D-A** complex **87•(88)$_2$** was achieved by treatment of cage **87** with pure donor **88**. Next, ^{1}H NMR studies demonstrated that after addition of acceptor **89** to the former assembly **87•(88)$_2$**, substitution of one donor unit **88** by one acceptor **89** unit takes place, whereas **A-A-A-A** stacking **87•(89)$_2$**, was not obtained. Moreover, cold spray ionization mass spectrometry (CSI-MS), ^{1}H NMR spectroscopy and X-ray diffraction experiments clearly supported the formation of the **A-D-A-A** inclusion complex **87•(88•89)** from a 1:1 mixture of donor **88** and acceptor **89** (Figure 19c). These results suggest that charge-transfer contributions are relevant for the final arrangement of the guests inside the cage. The importance of the donor geometry could be made evident by the calculated energy barriers for the exchange process between different donors (triphenylene (**88**), perylene and pyrene) and acceptor **89** from temperature dependent ^{1}H NMR data. Here, the highest energy barrier was observed for the exchange of the donor triphenylene (C_3 symmetry) which is geometrically most related to the cage panel unit. Since

dispersion and charge transfer interactions both depend on the area of the π–π contact surface this is a very reasonable result.

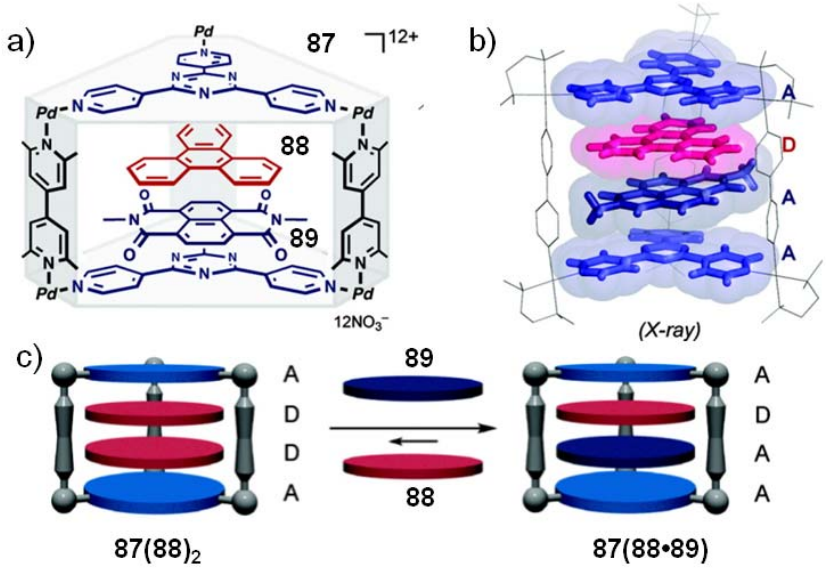

Figure 19. a) Chemical structure of cage **87**, and guests **88** and **89**. b) Structure of the resulting self-assembly of inclusion complex **87**•(**88**•**89**) in single crystals. c) Guest exchange between complexes **87**•(**88**)$_2$ and **87**•(**88**•**89**). Reprinted with permission from ref. 167.

The success in the socialization of different molecules possessing opposite electronic nature, is therefore, strongly dependent on a good geometrical complementarity. When, on the other hand, the structural fit is reduced, the weak charge transfer forces between the interacting molecules can not overcome the penalty associated to the loss of dispersion interactions that are in general larger between identical molecules owing to identical size of the contact surface. As a consequence, the equilibrium will shift from self-discrimination towards self-recognition. In this regard, an example from Shinkai and co-workers is quite illustrative as it describes the self-sorting of electron rich quaterthiophene **90** and electron poor perylene bisimide **91** organogelators(Figure 20).[168] UV/Vis, CD and SEM studies revealed an independent formation of oligothiophene and perylene bisimide nanofibers from a 1:1 mixture of both molecules, respectively, which are in contact only in some nodes (Figure 20). Two main reasons have been identified by the authors why self-recognition dominates the self-assembly of these molecules: i) the formation of four hydrogen bonds is possible between two quaterthiophene **90** molecules whereas only two are formed between two perylene bisimides **91**, and ii) a much larger overlap of the π-surfaces can occur if equal

molecules are stacked, i.e., similar geometry of the molecules favors π-stacking in a self-recognition manner. These two joint effects account for the higher binding constant of **90** (>10^5 M^{-1} in chloroform) compared to that of **91** (1.3 × 10^3 M^{-1} in chloroform) Such substantial difference (>100-fold) between the association constants of both components suggests –as discussed by Isaacs and co-workers–[20] an efficient self-recognition process if no additional interactions come into play. Obviously, charge transfer interactions between oligothiophenes and perylene bisimides are too weak to bias the system towards self-discrimination.

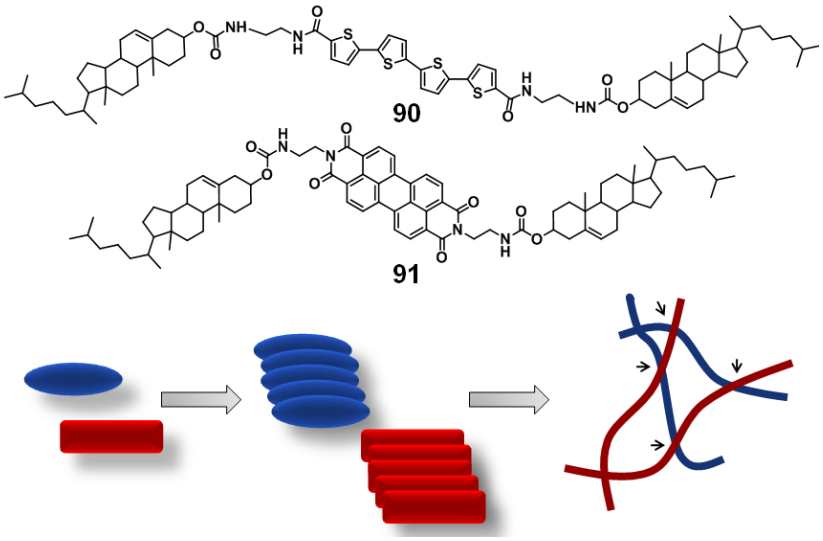

Figure 20. Chemical structure of **90** and **91** and representation of their "orthogonal" self-assembly into independent fibers of electron rich oligothiophene and electron poor perylene bisimide stacks with only few p- n- heterojunction nodes (black arrows).

Particularly illustrative examples in this regard are bulk heterojunction solar cell materials composed of poly(3-hexylthiophene) and C_{60} or derivatives, e.g. PCBM ([6,6]phenyl-C_{61}-butyric acid methyl ester)[149,169] or merocyanine HB194 and fullerene derivatives (Figure 21).[154,170] Both materials afford excellent power conversion efficiencies of about 5% owing to the excellent segregation of the two constituent molecules in the bulk heterojunction active layer. The rationale behind these self-recognition phenomena on the macroscopic scale appears to be of geometrical origin: the denser and better packed solid-state material is formed upon segregation of the globular fullerenes from the planar π-conjugated polythiophene or merocyanine molecules. Thus, obviously van der Waals interactions

outweigh in these examples the energy gain from charge-transfer interactions between electron-rich and electron-poor π-conjugated molecules. For the case of merocyanine dyes the segregation has been also attributed to a pronounced propensity of these dipolar dyes for self-recognition arising from substantial dipole-dipole interactions.[171,172]

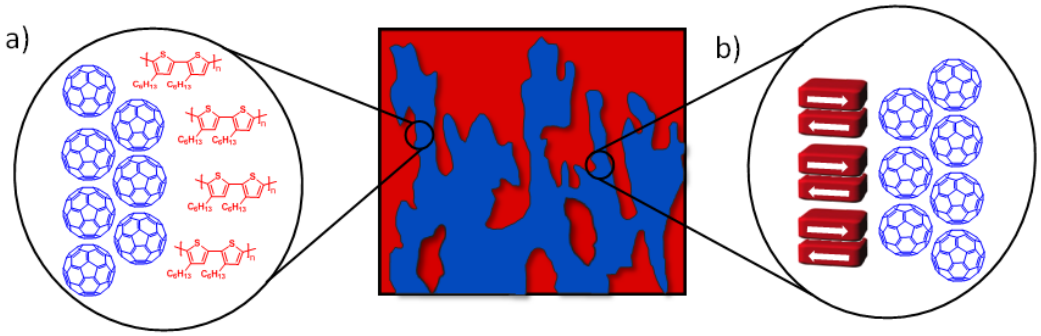

Figure 21. Nanosegregated domains in bulk heterojunction solar cells arising from self-recognition phenomena. a) Poly(3-hexylthiophene) and [60]fullerene. b) Merocyanine dyes and [60]fullerene materials.

On the basis of these observations one might anticipate that only members of a mixture featuring nearly identical geometry and suitable complementarity of additional noncovalent forces would allow electronic charge-transfer effects to determine the outcome of the self-sorting process. For more complex aggregate systems, however, this is not necessarily the case which can be illustrated by a series of studies on the co-assembly of oligophenylenevinylenes (OPVs) and perylene bisimides.[173-176] Thus, an example for an integrative co-assembly of structurally rather dissimilar molecules is given by the OPVs **92** and the electron poor perylene bisimides **93** (Figure 22).[173,175] OPV derivative **92** features, besides a relatively large aromatic π–π-surface, a self-complementary ureidopyrimidinone (Upy) unit on one side and long alkyl chains on the opposite side to increase solubility in nonpolar media. The joint contribution of π–π-stacking, quadruple hydrogen-bonding and additional peripheral van der Waals contacts between alkyl chains leads to the formation of H-type helical π-stacks upon self-assembly in heptane. Perylene bisimide **93**, on the other hand, self-assembles in nonpolar solvents via π–π-interactions and van der Waals forces among peripheral alkyl chains into slipped stacks.[61] Mixing **92** and **93** in a 1:1 ratio in hexane,

however, results in the appearance of a weak charge transfer (CT) band in UV/Vis studies, which points to the formation of a mixed assembly of **92** and **93** (Figure 22a).[175]

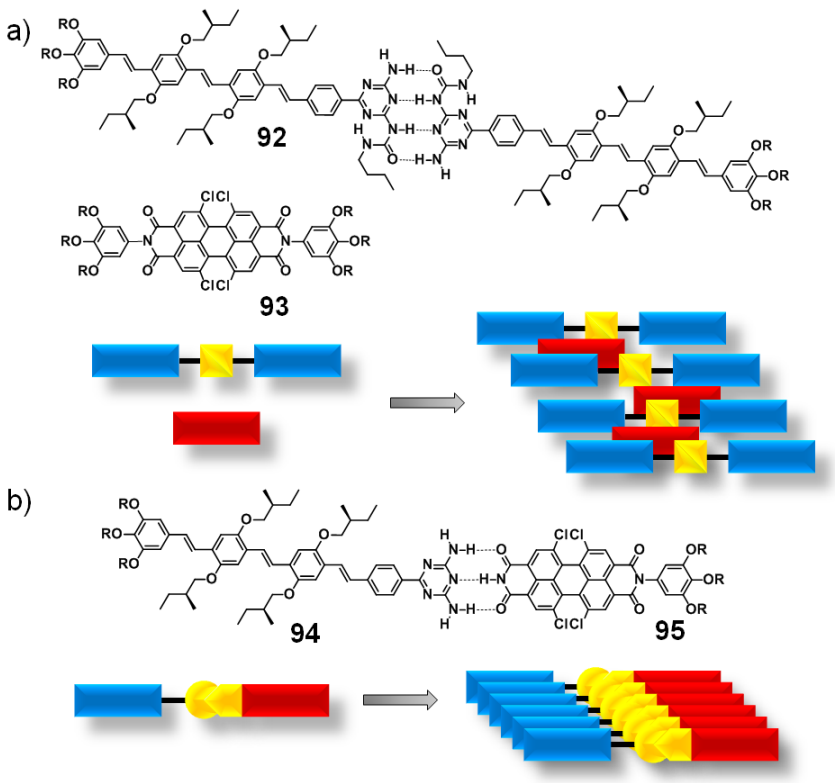

Figure 22. a) Chemical structure of studied OPV **92** and perylene bisimide **93** and cartoon representation of the social co-assembly process. b) Chemical structure of modified OPV **94** and perylene bisimide **95** and schematic representation of their self-assembly into p- and n-type stacks.

Obviously, the opposite electronic character of **92** and **93** governs the co-assembly including self-discrimination features that are favored by the attractive charge transfer interaction between OPV donors and perylene bisimide acceptors. This effect appears to be particularly pronounced for chlorinated perylene bisimides due to their strong electron acceptor character.[177] Further investigations addressed the question whether the opposite self-sorting behavior could take place in mixtures of structurally different OPV **94** and perylene bisimide **95**, which are designed to form a hydrogen-bonded complex with each other (Figure 22b). UV/Vis studies in heptane revealed the appearance of a red shifted perylene bisimide band. However, this band was a slipped π-stack of cofacially aggregated dyes **94** and **95**.[175] In this mixture hydrogen-bonding and geometrical factors are clearly the most relevant codes

that govern the desired narcissistic self-sorting of these functional dyes into supramolecular p-n-heterojunction π-stacks.[174,176]

To summarize, charge transfer interactions between donor and acceptor π-systems in solution are very weak, and only play an important role when other premises have been fulfilled. It is also noteworthy to point out that charge transfer complexes are not always easy to detect as the charge transfer bands are hidden beneath other absorption bands due to their low intensity.

2.4. Chiral Self-Sorting

In the previous sections we have discussed the molecular codes that can independently or jointly direct efficient self-sorting processes in artificial systems. Although it must be underlined that the molecular codes directing chiral self-sorting are not distinct from those discussed above for "general" self-sorting, due to the relevant implications of chiral recognition in natural systems we will draw special attention to chiral self-sorting systems and, as such, will regard them separately.

Chiral recognition,[178-180] i.e., the ability of a chiral molecule to differentiate between two enantiomers, is of great significance both in biological processes and organic synthesis as demonstrated in asymmetric catalysis[181-183] or enantioselective recognition by enzymes and protein receptor sites.[184,185] Nevertheless, the origin of homochirality of important natural building blocks (e.g., L-amino acids and D-sugars and the biopolymers derived thereof) still remains a fundamental question despite the great efforts invested in the last decades to elucidate this matter.[186-191] A better understanding of chiral recognition is thus a key for a more rational catalyst design for asymmetric synthesis, new materials with intriguing chiral properties and may contribute to a better understanding of the origin of homochirality in biological molecules.

In accordance with the definition of self-sorting, chiral recognition between enantiomeric pairs can lead to self-recognition or self-discrimination, depending on whether an enantiomer preferentially recognizes itself or its mirror image, to generate homo- or heterochiral self-assemblies respectively. However, an important consideration has to be taken into account

regarding chiral systems, i.e., pairs of enantiomers, in contrast to the previously described self-sorting systems, to which we will refer as "general": in chiral self-sorting the physical properties of the interacting monomers (enantiomers) are –except for their interaction with polarized light– equal and hence, they exhibit identical spectroscopic features. These can only be differentiated when both enantiomers interact with themselves or their mirror images to afford homo- or heterochiral aggregates, which in turn possess diastereomeric nature and thus display different spectroscopic properties. This constraint makes the analysis of chiral self-sorting mixtures more challenging in comparison with "general" self sorting systems. Consequently, the control of the molecular codes directing chiral self-sorting is a demanding task.

As discussed previously in the chapter on "general" self-sorting, size and shape are undoubtedly the most relevant molecular codes that make a particular pair of molecules recognize (or discriminate) each other. In chiral self-sorting systems this molecular code has a lower weight, as pairs of enantiomers possess identical size and shape and differ only in the relative spatial orientation derived from their opposite chirality (i.e., mirror-image shape). This suggests that geometrical factors will not exhibit such an overwhelming preponderance as occurred in conventional self-sorting systems. Although in the past the greatest attention has been devoted to the study of chiral self-sorting upon crystallization,[34,192,193] we will focus exclusively on those investigations carried out in solution to ensure that derived molecular codes are of thermodynamic origin.

Extended twisted π-surfaces appear to be most suitable targets for such investigations because they combine sufficiently large van der Waals contact areas –as required for self-assembly in dilute solution– and pronounced chirality. However, most of the published examples on chiral self-sorting take advantage from stronger intermolecular forces, such as recognition by multiple hydrogen bonds or metallosupramolecular intermolecular forces. In this regard, Aida and co-workers synthesized a racemic "S" shaped xylylene-bridged bis(cyclic dipeptide) **96** which posses L and D chirality (Figure 23).[194]

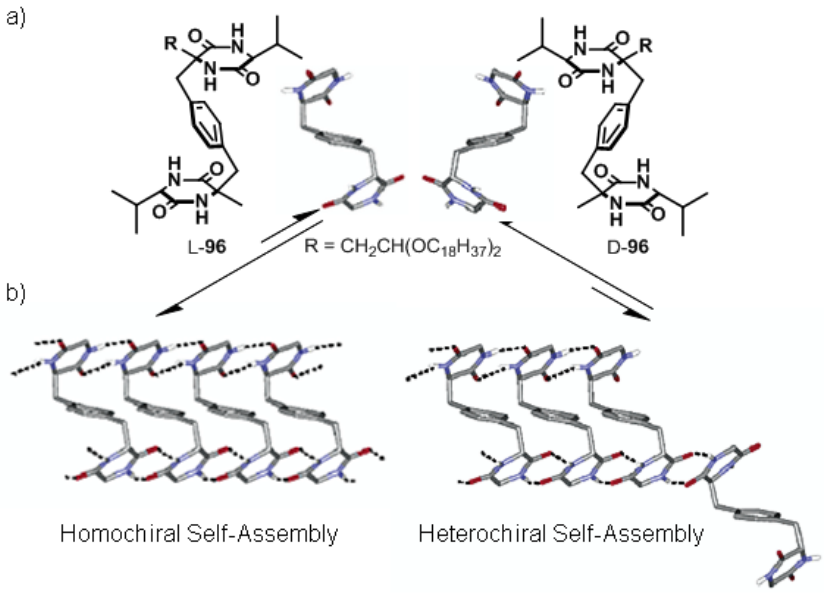

Figure 23. Chemical structure of "S" shaped xylylene-bridged bis(cyclic dipeptide) **96** and schematic representation of its supramolecular polymerization in a self-recognition process. Reprinted with permission from ref. 194.

The "S" shape of their molecules could be proven by the single crystal X-ray analysis of a derivative of molecule **96**. By means of SEC they could determine that these molecules form a supramolecular polymer capable of self-associating with a high degree of enantioselectivity (self-recognition). The reason for the exclusive formation of homochiral assemblies is the shape complementarity derived from the "S" shaped molecules. In the case of homochiral supramolecular polymerization, participation of the two diketopiperadine units in the formation of four simultaneous hydrogen bonds via complementary H-bonding takes place. This is not possible for a heterochiral assembly, in which only one diketopiperadine is allowed to participate in the hydrogen-bonding formation due to the possible mismatch of the hydrogen donor-acceptor arrays (Figure 23b).

Isaacs and co-workers investigated the self-recognition behavior in a series of chiral molecular clips assembled by the accumulation of different intermolecular forces.[12,195] They described the synthesis and characterization of C-shaped methylene-bridged glycoluril dimers bearing H-bonding groups attached at their aromatic rings (**97a,b**), which enables self-assembly via hydrogen-bonding in combination with π–π-stacking (Figure 24).

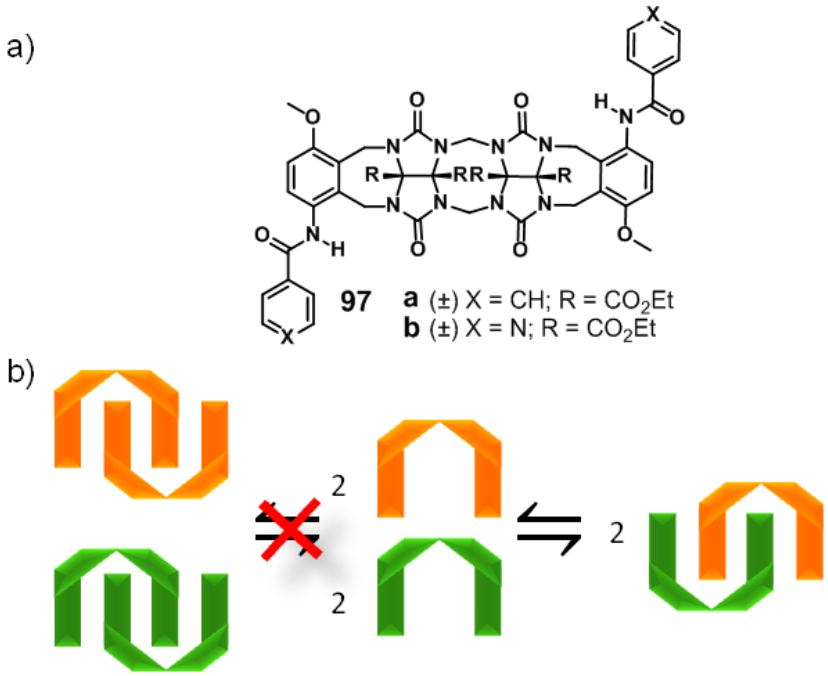

Figure 24. a) Chemical structure of chiral clips **97a**,**b**. b) Cartoon of their self-sorting process.

^{1}H NMR in $CDCl_3$ and X-ray analysis of the crystalline structure obtained for **97b** revealed that these aggregates display high levels of chiral discrimination giving rise to heterochiral dimers. The preference in the formation of heterochiral over homochiral dimers was attributed to the possibility of simultaneous formation of π–π-interactions and two hydrogen bonds, whereas the hypothetical homochiral dimer can only be stabilized by π–π-interactions and one hydrogen bond. Accordingly, the spatial orientation of the H-bonding groups controls the self-sorting process by favoring aggregates with the highest accumulation of intermolecular contacts.

Osuka, Shinokubo and co-workers reported the synthesis of a racemic porphyrin **98** and the resolution of its enantiomers by chiral HPLC (Figure 25a).[196] The binding constant of the pure enantiomers and the racemate for the formation of homo- and heterochiral dimers could be determined by concentration dependent fluorescence spectra in chloroform as K_{homo} = 1.2 × 10^7 M^{-1} and K_{rac} = 1.8 × 10^8 M^{-1}, respectively. Using these binding constants given by the authors the heterodimerization binding constant can be calculated as $K_{D(hetero)}$ = 7 × 10^8 M^{-1}.[197,198] Accordingly, a racemic mixture contains 3% homo vs. 97% heterochiral dimers, i.e., chiral self-discrimination takes place. Additional proof was provided by ^{1}H NMR spectra for solutions of the pure enantiomers and the racemic mixture, which revealed the presence of

different assemblies. Single crystal X-ray analysis of the homochiral dimers obtained from the solution of the pure enantiomers and that of the heterochiral dimers obtained from the racemic mixture provided structural details to rationalize the preference for the formation of heterochiral dimer aggregates. Whereas in the heterodimer the porphyrins are arranged in a centrosymmetric fashion, homochiral dimers require the screwing of the porphyrin planes to realize both metal-ligand contacts. As pointed out by the authors the former assembly is electrostatically favored owing to the cancellation of the dipole moments (Figure 25b,c). Additionally, minor structural differences observed between the crystal structures of the hetero and homochiral dimers –small variations in the intermolecular distances and relative position of the structures, distortion of the molecules in the case of the homochiral dimer to enable the Zn-N coordinative bond– may influence the self-sorting process.

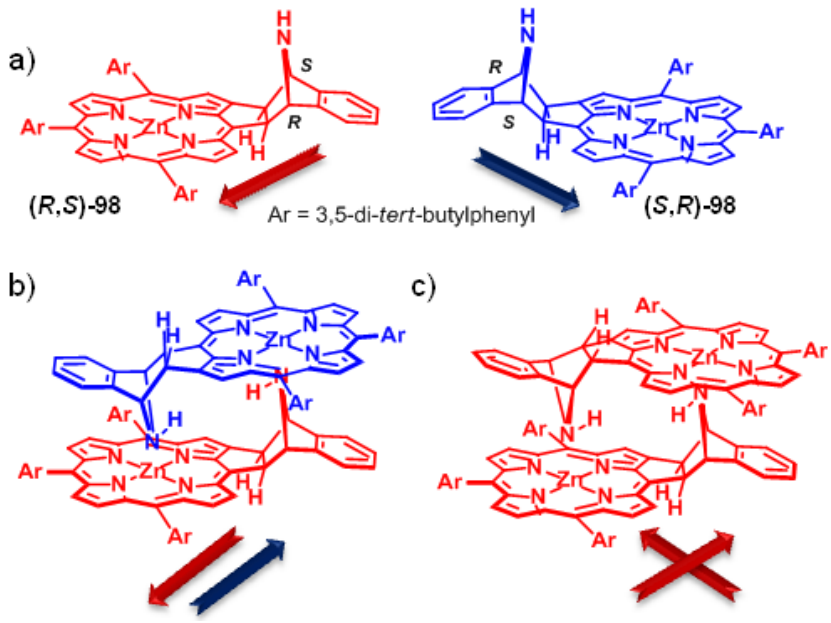

Figure 25. a) Structures of enantiomeric (*R*,*S*)-**98** and (*S*,*R*)-**98**. Schematic representation of b) hetero- and c) homochiral dimer aggregates derived thereof. The arrows represent an approximation of the orientation of the dipole moments.

In addition to geometry and complementarity of intermolecular forces, steric factors have been demonstrated to be rather useful molecular codes to achieve high-fidelity chiral self-sorting.[199-202] Verlhac and co-workers reported a family of atropisomeric bidentate ligands with a dissymmetric benzimidazole-pyridine binding site (**99–101**).[203] Naphthyl (**99**), tolyl

(**100**) and cumyl (**101**) substituents were introduced to study the steric impact in the fidelity of chiral self-sorting after copper complexation (Figure 26).

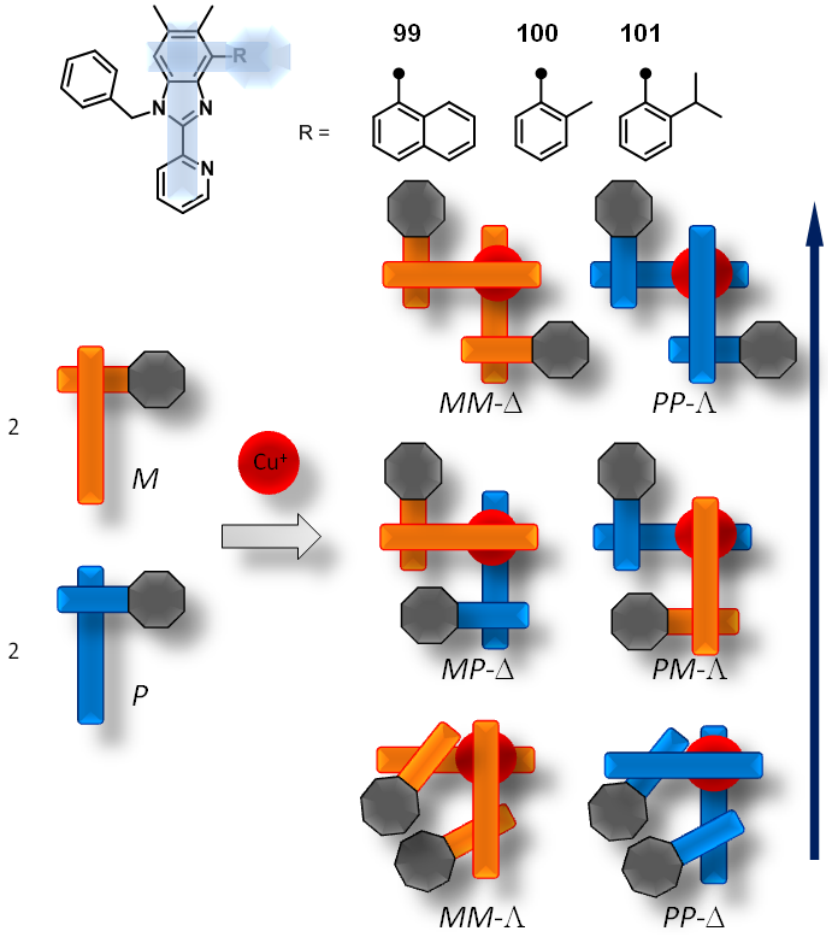

Figure 26. Chemical structure of ligands **99-101** and schematic representation of the possible isomers formed upon complexation of ligands **99-101** with Cu^{+}.

When two equivalents of **101** were treated with one equivalent of $[Cu^{I}(MeCN)_4]^{+}$ in CD_2Cl_2, a single symmetric C_2 metal species could be observed through ^1H NMR in 95% yield, which corresponds to the homochiral assembly pair *MM*Δ/*PP*Λ (Figure 26). Minor traces (5%) of more sterically hindered *MP*Δ/*PM*Λ were also found, whereas no sign of the most sterically hindered isomers *MM*Λ/*PP*Δ was observed. ^1H NMR experiments revealed that the decrease in the bulkiness of the substituents in **99** (naphthyl) and **100** (tolyl) leads to larger amounts of *MP*Δ/*PM*Λ and even traces of *MM*Λ/*PP*Δ species, although in all cases the major species remained the homochiral *MM*Δ/*PP*Λ assemblies. Figure 26 illustrates the key structural features responsible for the metal ion directed self-recognition process. It is evident that in the homochiral complexes *MM*Δ/*PP*Λ the bulky substituents are pointing in opposite directions. The bulkiness of the substituents will determine to what extent the more sterically

demanding heterochiral complexes *MP*Δ/*PM*Λ are formed, while the most hindered homochiral *MM*Λ/*PP*Δ species in which both substituents are pointing in the same direction are impeded. It can be realized from this study how the adequate selection of substituents with different steric requirements can lead to highly efficient chiral self-sorting.

Bozec, Maury, Lacour and co-workers took advantage of the electrostatic nature of ionic metal-ligand complexes to induce chiral-self-sorting in diastereomeric cation-anion propeller pairs (Figure 27).[204-208]

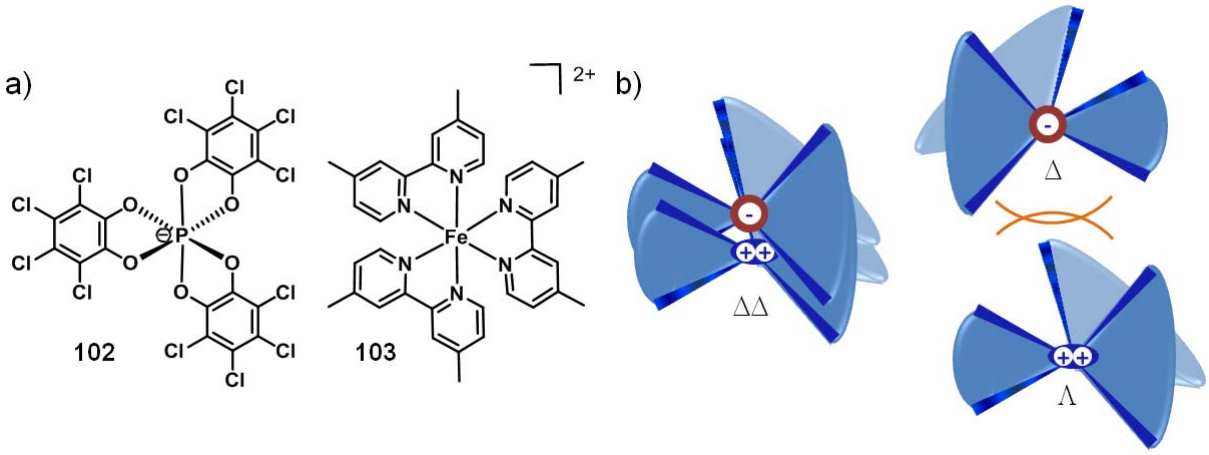

Figure 27. a) Chemical structure of enantiopure TRISPHAT anion **102** and racemic $[Fe(4,4'.Me_2bpy)_3]^{2+}$ (bpy = 2,2'-bipyridine) **103**. b) Schematic representation of the formed homochiral assemblies (left) and the unfavorable heterochiral assembly.

When enantiopure counterions are combined with chiral ions, two different diastereomeric ion pairs which possess different chemical and physical properties and, consequently, interaction energies can be formed. As a consequence, high levels of asymmetric recognition between chiral cations and anions can be achieved.[204-208] The authors rationalize the high fidelity recognition to an optimization of the electrostatic interactions between cation and anion propellers, as demonstrated for the TRISPHAT anion **102** and the $[Fe(4,4'.Me_2bpy)_3]^{2+}$ (bpy = 2,2'-bipiridine) cation **103**.[204] As sketched in Figure 27, the anion/cation distance can be reduced much more in the homochiral association than in the heterochiral to stabilize the ionic pair.

The use of cation templates has been successfully exploited by Davis and co-workers to program chiral self-sorting (Figure 28).[209,210] Firstly, they probed the self-assembly of chiral guanosine units (D,L)-**104** and (D,L)-**105** in the presence of K^+ and Cs^+, respectively (Figure

28a,b).[209] ^{1}H NMR in CD_3CN and single crystal X-ray diffraction experiments, both in the presence of templating cations, evidenced the formation of a defined decameric complex (assembled by Cs^+-templated stacking of two pentameric hydrogen-bonded cycles for **104**), and an octameric complex (assembled by K^+-templated stacking of two tetrameric hydrogen-bonded cycles for **105**) for the enantiopure starting materials (Figure 28a,b). While in assemblies of **104** sugar-base hydrogen bonds can be formed, this is not possible for **105**. This makes **104** an excellent candidate for chiral self-recognition. Indeed, a racemic mixture of guanosine **105** in the presence of K^+ showed more than ten separate signals in the ^{1}H NMR spectra, unlike the simple set of signals observed for the pure enantiomers, pointing to the formation of a diastereomeric mixture of the racemate. In contrast, the racemic mixture of guanosine **104** in the presence of Cs^+ showed only one major set of signals. These signals were different to those corresponding to the enantiomeric decamers, indicating the predominance of a new species. After X-ray analysis of the supramolecular structure of (D,L)-**104** in the crystalline state it was confirmed that (D,L)-**104** undergoes chiral self-sorting in the presence of Cs^+ giving rise to a meso-decamer by stacking of a (D)-**104** pentamer and (L)-**104** pentamer. Similar experiments for guanosine (D,L)-**104** with differently sized alkali cations (Li^+, Na^+, K^+ or Rb^+) did not provide convincing evidence for such a self-sorting. Thus, the size of the templating cation plays a major role. In further work, the authors showed that not only can the size of the cation direct self-sorting, but the charge is also important.[210] ^{1}H NMR in CD_2Cl_2 and X-ray studies revealed that guanosine **105** self-assembles into homochiral quadruplex stacks in the presence of Ba^{2+}, whereas a mixture of heterochiral quadruplex stacks was obtained in the presence of K^+ (Figure 28c). Since the size of Ba^{2+} and K^+ is very similar, the cation's charge has been recognized as the driving force directing self-sorting. The unfavorable entropy associated to the self-recognition of eight enantiomers can be overcome by enthalpic stabilization derived from cation-dipole interactions, G-quartet hydrogen bonds and G-quadruplex-picrate (counter-anion) interactions through the divalent cation.

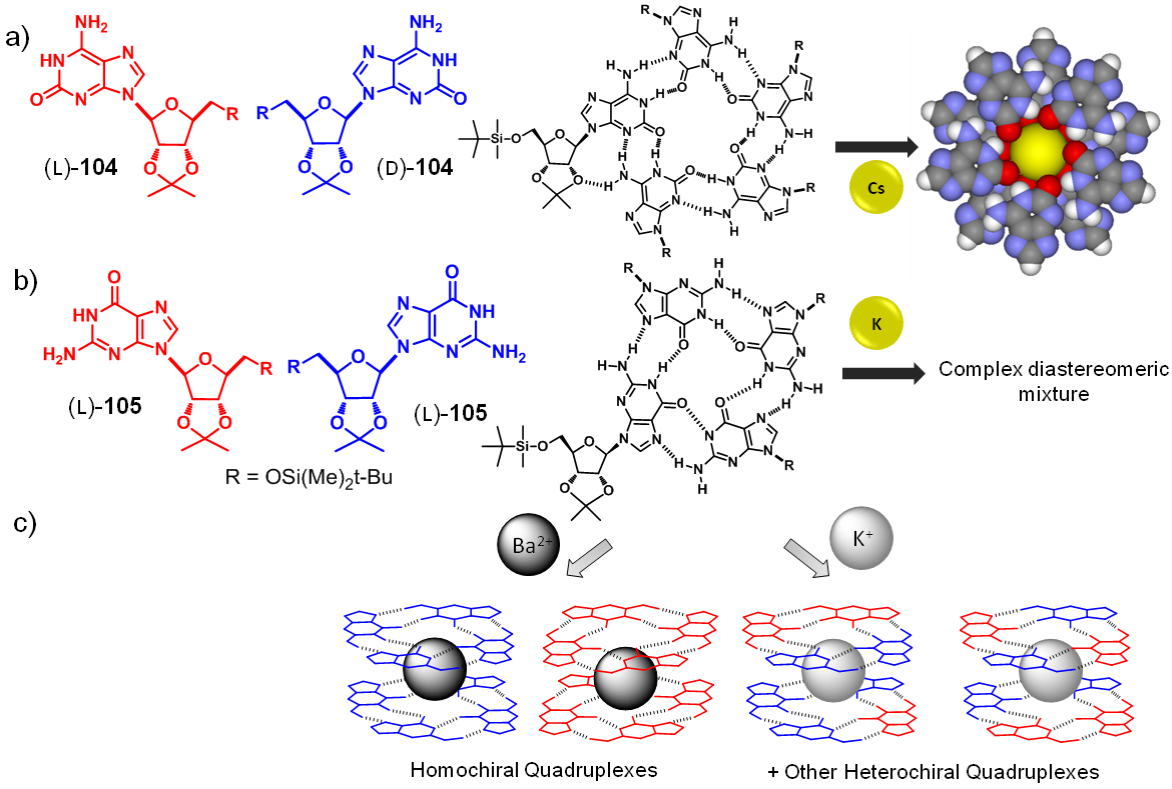

Figure 28. Chemical structures of guanosine derivative **104** and hydrogen-bonded quintuplet (a) and guanosine derivative **105** and corresponding hydrogen-bonded quadruplex (b) and chiral self-sorting processes in the presence of alkali ions (a,b). c) Homochiral and heterochiral quadruplexes formed by **105** in the presence of Ba^{2+} and K^{+}. Reprinted with permission from ref. 209.

A final, particularly elegant example of a self-sorting process was reported by Osuka, Kim and co-workers,[211-213] based on meso-meso linked-pyridine-appended zinc(II) porphyrins **106a–c** possessing axial chirality leading to non-interconvertible *P* and *M* enantiomers (Figure 29).[211] In non-coordinating solvents such as CH_2Cl_2, dimeric porphyrins **106a–c** self-assemble into three-dimensional porphyrin boxes **107a–c** (Figure 29), as evidenced by ^1H NMR studies and X-ray diffraction of their crystalline structures. These porphyrin boxes form from racemic solutions with extraordinarily large binding constants through simultaneous eight-point metallosupramolecular coordination. Boxes formed from **106a–c** could be demonstrated to be chiral by CD spectroscopy after resolution of their enantiomers using chiral HPLC. As expected after chiral resolution, mirror image CD spectra were obtained. The formation of these chiral boxes was attributed to a rather specific self-recognition process of the dimeric porphyrins which can only form such boxes from identical, i.e., single enantiomer, building blocks. Otherwise, upon co-assembly of both enantiomers polymeric

structures would form. This last example is most illustrative for a predefined self-assembly pathway that has been properly encoded in the molecular building blocks to direct a sequence of self-recognition processes. The interplay between enthalpic and entropic contributions obviously directs a high fidelity self-sorting process under the given experimental conditions.

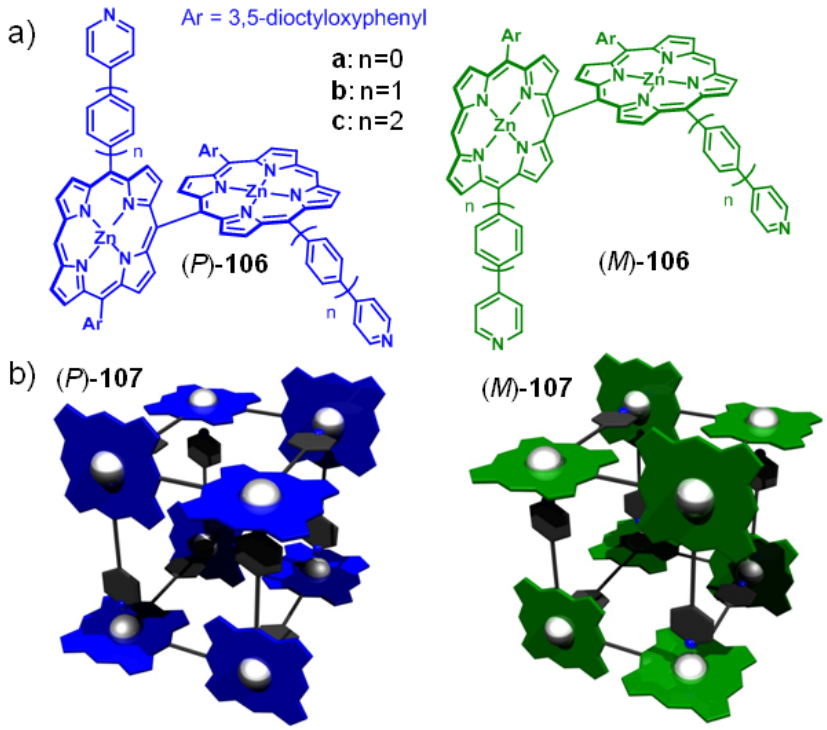

Figure 29. a) Chemical structures of chiral porphyrins **106a–c**. b) Homochiral boxes **107a–c** derived thereof.

2.5. Conclusions

In this literature survey we have collected the first decade of research on artificial molecules that were shown to exhibit high levels of selectivity in the molecular recognition or discrimination of surrounding species within complex mixtures. We have discussed the *molecular codes* (size and shape, complementarity in hydrogen-bonded systems, sterics, coordination sphere of metal ions and charge transfer) that lead synthetic molecules in a crowded environment to bind only to their ideal partner(s). We have shown that the geometrical parameters *size* and *shape* play the most prominent role among these molecular codes. Once this criterion is satisfied, other molecular codes can come into play and eventually direct the self-sorting processes. *Complementarity in hydrogen-bonded systems* for instance, requires an appropriate geometrical correspondence between the interacting arrays

for the match or mismatch between the pattern of hydrogen donors and acceptors to take place. This molecular code is most strikingly demonstrated in double strand DNA and has been successfully exploited to direct social or narcissistic self-sorting in mixtures of hydrogen-bonded assemblies.

In metallosupramolecular systems, the geometry and rigidity of the ligands as well as the *coordination sphere in metal-ligand interactions* determine to a great extent the outcome of a self-sorting mixture. Different ligands can coordinate into varying geometries, what has already been exploited to construct unprecedented supramolecular architectures of amazing size and shape. Several research groups have also elucidated *steric* and *charge transfer effects* to direct high-fidelity self-assembly processes within complex mixtures. However, their weight is quantitatively smaller in comparison with the abovementioned codes and can only provide sufficient bias when the interacting building blocks are structurally most similar in terms of size and shape, hydrogen-bonding pattern or coordination ability.

Due to the importance of chiral recognition in nature, we have dedicated an independent section to chiral self-sorting systems. The high similarity of the molecules involved in chiral self-sorting –pairs of enantiomers have equal size and shape, differing only in their mirror image spatial orientation– makes their investigation particularly demanding. The examples collected in this literature survey include those showing self-discrimination and those showing self-recognition, however, mostly with rather modest bias.

It is not only intrinsic molecular codes which are important in the fidelity of self-sorting events. Self-sorting processes depend to a great extent on the external variables (solvent, temperature, concentration, pH, etc) that can influence differently the equilibrium and/or the stability of independent recognition processes involving different non-covalent interactions. To date we are still far from deriving a general rule that can predict how a complex mixture involving different non-covalent forces would behave upon variation of a given external variable.

However, the achievements to date in the field of supramolecular chemistry allow us to be optimistic in the years to come. We currently know how to make use of the principles of self-assembly to create supramolecular architectures of remarkable complexity with well defined

size and shape by proper design of their small constitutive building blocks. Highly organized structures such as vesicular assemblies –which are in essence small membrane-enclosed containers that can transport substances– are nowadays already routinely constructed by different research groups upon self-assembly of artificial amphiphilic molecules and used for catalytic or transporting purposes.[214] The construction of superstructures that can resemble nature´s creations require, therefore, advances in this direction, and self-sorting is undoubtedly one of the indispensable means. Recently, synthetic amphiphilic molecules have been successfully programmed to self-sort, so that distinct types of molecules self-assemble into different domains or compartments in aqueous media.[215] Compartmentalization is one of the prerequisites for the emergence of life. The cell membrane, for instance, protects the inner components from an adverse environment[216] and multi-compartmentalization is essential for the achievement of simultaneous functions in isolated environments within cellular organisms. The marriage between self-assembly and self-sorting will certainly open up ground-breaking possibilities for the creation of sophisticated synchronous multifunctional systems. We could envisage in a not too distant future the construction of artificial systems that can resemble the intricacy of a cell. Whether or not this approach is a chimera, still remains to be seen. But one issue is clear: self-sorting is one of the means towards this goal.

2.6. Notes and References

(1) Campbell, N. A.; Reece, J. B.; Taylor, M. R.; Simon, E. J.; Dickey, J. L. *Biology: Concepts and Connections*; 6th ed.; CA: Benjamin/Cummings Publishing Company, San Francisco, 2008.
(2) Oshovsky, G. V.; Reinhoudt, D. N.; Verboom, W. *Angew. Chem., Int. Ed.* **2007**, *46*, 2366.
(3) Watson, J. D.; Crick, F. H. C. *Nature* **1953**, *171*, 737.
(4) Lehninger, A. L.; Nelson, D. L.; Cox, M. M. *Lehninger Principles of Biochemistry*; 5th ed.; W. H. Freeman and Company: New York, 2008.
(5) Amos, L. A.; Baker, T. S. *Nature* **1979**, *279*, 607.
(6) Desai, A.; Mitchison, T. J. *Annu. Rev. Cell Dev. Biol.* **1997**, *13*, 83.
(7) Weisenberg, R. C. *Science* **1972**, *177*, 1104.
(8) Alberts, B.; Johnson, A.; Lewis, J.; Raff, M.; Roberts, K.; Walter, P. *Molecular Biology of the Cell*; 4th ed.; Garland Science: New York, 2002.

(9) Lodish, H.; Berk, A.; Matsudaira, P.; Kaiser, C. A.; Krieger, M.; Scott, M. P.; Zipurksy, S. L.; Darnell, J. *Molecular Cell Biology*; 5th ed.; WH Freeman: New York, 2004.
(10) Jaeger, K.-E.; Eggert, T. *Curr. Opin. Biotechnol.* **2004**, *15*, 305.
(11) Hough, D. W.; Danson, M. J. *Curr. Opin. Chem. Biol.* **1999**, *3*, 39.
(12) Ghosh, S.; Wu, A. X.; Fettinger, J. C.; Zavalij, P. Y.; Isaacs, L. *J. Org. Chem.* **2008**, *73*, 5915.
(13) Corbett, P. T.; Sanders, J. K. M.; Otto, S. *Angew. Chem., Int. Ed.* **2007**, *46*, 8858.
(14) Ludlow, R. F.; Otto, S. *Chem. Soc. Rev.* **2008**, *37*, 101.
(15) Peyralans, J. J. P.; Otto, S. *Curr. Opin. Chem. Biol.* **2009**, *13*, 705.
(16) Nitschke, J. R. *Nature* **2009**, *462*, 736.
(17) Wagner, N.; Ashkenasy, G. *J. Chem. Phys.* **2009**, 16907 (1).
(18) Elemans, J.; Lei, S. B.; De Feyter, S. *Angew. Chem., Int. Ed.* **2009**, *48*, 7298.
(19) Kramer, R.; Lehn, J. M.; Marquisrigault, A. *Proc. Nat. Acad. Sci. U.S.A.* **1993**, *90*, 5394.
(20) Wu, A. X.; Isaacs, L. *J. Am. Chem. Soc.* **2003**, *125*, 4831.
(21) Mukhopadhyay, P.; Wu, A. X.; Isaacs, L. *J. Org. Chem.* **2004**, *69*, 6157.
(22) Shivanyuk, A.; Rebek, J., Jr. *J. Am. Chem. Soc.* **2002**, *124*, 12074.
(23) Taylor, P. N.; Anderson, H. L. *J. Am. Chem. Soc.* **1999**, *121*, 11538.
(24) Jiang, W.; Winkler, H. D. F.; Schalley, C. A. *J. Am. Chem. Soc.* **2008**, *130*, 13852.
(25) Jolliffe, K. A.; Timmerman, P.; Reinhoudt, D. N. *Angew. Chem., Int. Ed.* **1999**, *38*, 933.
(26) Corbin, P. S.; Lawless, L. J.; Li, Z. T.; Ma, Y. G.; Witmer, M. J.; Zimmerman, S. C. *Proc. Nat. Acad. Sci. U.S.A.* **2002**, *99*, 5099.
(27) Ma, Y. G.; Kolotuchin, S. V.; Zimmerman, S. C. *J. Am. Chem. Soc.* **2002**, *124*, 13757.
(28) Caulder, D. L.; Raymond, K. N. *Angew. Chem., Int. Ed.* **1997**, *36*, 1440.
(29) Enemark, E. J.; Stack, T. D. P. *Angew. Chem., Int. Ed.* **1998**, *37*, 932.
(30) Stiller, R.; Lehn, J.-M. *Eur. J. Inorg. Chem.* **1998**, 977.
(31) Albrecht, M.; Schneider, M.; Röttele, H. *Angew. Chem., Int. Ed.* **1999**, *38*, 557.
(32) Schultz, D.; Nitschke, J. R. *Angew. Chem., Int. Ed.* **2006**, *45*, 2453.
(33) Legrand, Y. M.; van der Lee, A.; Barboiu, M. *Inorg. Chem.* **2007**, *46*, 9540.
(34) Barboiu, M.; Dumitru, F.; Legrand, Y. M.; Petit, E.; van der Lee, A. *Chem. Commun.* **2009**, 2192.
(35) Shaller, A. D.; Wang, W.; Gan, H. Y.; Li, A. D. Q. *Angew. Chem., Int. Ed.* **2008**, *47*, 7705.
(36) Bilgiçer, B.; Xing, X.; Kumar, K. *J. Am. Chem. Soc.* **2001**, *123*, 11815.
(37) Schnarr, N. A.; Kennan, A. J. *J. Am. Chem. Soc.* **2003**, *125*, 667.
(38) Rehm, T.; Schmuck, C. *Chem. Commun.* **2008**, 801.
(39) Hunter, C. A.; Lawson, K. R.; Perkins, J.; Urch, C. J. *J. Chem. Soc., Perkin Trans. 2* **2001**, 651.
(40) Hunter, C. A. *Angew. Chem., Int. Ed.* **2004**, *43*, 5310.
(41) Zheng, Y. R.; Yang, H. B.; Ghosh, K.; Zhao, L.; Stang, P. J. *Chem. Eur. J.* **2009**, *15*, 7203.
(42) Addicott, C.; Das, N.; Stang, P. J. *Inorg. Chem.* **2004**, *43*, 5335.

(43) Kuehl, C. J.; Huang, S. D.; Stang, P. J. *J. Am. Chem. Soc.* **2001**, *123*, 9634.
(44) Whitesides, G. M.; Mathias, J. P.; Seto, C. T. *Science* **1991**, *254*, 1312.
(45) Misteli, T. *J. Cell Biol.* **2001**, *155*, 181.
(46) Eliseev, A. V.; Nelen, M. I. *J. Am. Chem. Soc.* **1997**, *119*, 1147.
(47) Fischer, E. *Ber. Dtsch. Chem. Ges.* **1894**, *27*, 2985.
(48) Pérez, E. M.; Martín, N. *Chem. Soc. Rev.* **2008**, *37*, 1512.
(49) Grimme, S. *Angew. Chem., Int. Ed.* **2008**, *47*, 3430.
(50) Israelachvili, J. *Intermolecular and Surface Forces*; 2nd ed.; Academic Press: San Diego, CA, 1991.
(51) Atkins, P. W.; Overton, T.; Rourke, J.; Weller, M.; Armstrong, F. *Shriver and Atkins inorganic chemistry*; 4th ed.; Oxford University Press, 2006.
(52) Chi, K. W.; Addicott, C.; Arif, A. M.; Stang, P. J. *J. Am. Chem. Soc.* **2004**, *126*, 16569.
(53) Yang, H. B.; Ghosh, K.; Northrop, B. H.; Stang, P. J. *Org. Lett.* **2007**, *9*, 1561.
(54) Zheng, Y. R.; Yang, H. B.; Northrop, B. H.; Ghosh, K.; Stang, P. J. *Inorg. Chem.* **2008**, *47*, 4706.
(55) Pinalli, R.; Cristini, V.; Sottili, V.; Geremia, S.; Campagnolo, M.; Caneschi, A.; Dalcanale, E. *J. Am. Chem. Soc.* **2004**, *126*, 6516.
(56) Chen, Z. J.; Lohr, A.; Saha-Möller, C. R.; Würthner, F. *Chem. Soc. Rev.* **2009**, *38*, 564.
(57) Würthner, F. *Chem. Commun.* **2004**, 1564.
(58) Osswald, P.; Würthner, F. *J. Am. Chem. Soc.* **2007**, *129*, 14319.
(59) Wang, W.; Bain, A. D.; Wang, L. Q.; Exarhos, G. J.; Li, A. D. Q. *J. Phys. Chem. A* **2008**, *112*, 3094.
(60) Würthner, F.; Chen, Z.; Dehm, V.; Stepanenko, V. *Chem. Commun.* **2006**, 1188.
(61) Chen, Z. J.; Baumeister, U.; Tschierske, C.; Würthner, F. *Chem. Eur. J.* **2007**, *13*, 450.
(62) Ludwig, R. *Angew. Chem., Int. Ed.* **2001**, *40*, 1808.
(63) Lagona, J.; Mukhopadhyay, P.; Chakrabarti, S.; Isaacs, L. *Angew. Chem., Int. Ed.* **2005**, *44*, 4844.
(64) Kim, K.; Selvapalam, N.; Ko, Y. H.; Park, K. M.; Kim, D.; Kim, J. *Chem. Soc. Rev.* **2007**, *36*, 267.
(65) Huang, W. H.; Zavalij, P. Y.; Isaacs, L. *J. Am. Chem. Soc.* **2008**, *130*, 8446.
(66) Harada, A.; Takashima, Y.; Yamaguchi, H. *Chem. Soc. Rev.* **2009**, *38*, 875.
(67) Harada, A.; Hashidzume, A.; Yamaguchi, H.; Takashima, Y. *Chem. Rev.* **2009**, *109*, 5974.
(68) Chen, Y.; Liu, Y. *Chem. Soc. Rev.* **2010**, *39*, 495.
(69) Miyauchi, M.; Harada, A. *J. Am. Chem. Soc.* **2004**, *126*, 11418.
(70) Miyauchi, M.; Takashima, Y.; Yamaguchi, H.; Harada, A. *J. Am. Chem. Soc.* **2005**, *127*, 2984.
(71) Kuad, P.; Miyawaki, A.; Takashima, Y.; Yamaguchi, H.; Harada, A. *J. Am. Chem. Soc.* **2007**, *129*, 12630.
(72) Yamauchi, K.; Takashima, Y.; Hashidzume, A.; Yamaguchi, H.; Harada, A. *J. Am. Chem. Soc.* **2008**, *130*, 5024.

(73) Tomimasu, N.; Kanaya, A.; Takashima, Y.; Yamaguchi, H.; Harada, A. *J. Am. Chem. Soc.* **2009**, *131*, 12339.
(74) Liu, S. M.; Ruspic, C.; Mukhopadhyay, P.; Chakrabarti, S.; Zavalij, P. Y.; Isaacs, L. *J. Am. Chem. Soc.* **2005**, *127*, 15959.
(75) Freeman, W. A.; Mock, W. L.; Shih, N. Y. *J. Am. Chem. Soc.* **1981**, *103*, 7367.
(76) Mock, W. L. *Comprehensive Supramolecular Chemistry*; Pergamon Press: Oxford, 1996.
(77) Rekharsky, M. V.; Mori, T.; Yang, C.; Ko, Y. H.; Selvapalam, N.; Kim, H.; Sobransingh, D.; Kaifer, A. E.; Liu, S. M.; Isaacs, L.; Chen, W.; Moghaddam, S.; Gilson, M. K.; Kim, K. M.; Inoue, Y. *Proc. Nat. Acad. Sci. U.S.A.* **2007**, *104*, 20737.
(78) Mukhopadhyay, P.; Zavalij, P. Y.; Isaacs, L. *J. Am. Chem. Soc.* **2006**, *128*, 14093.
(79) Rekharsky, M. V.; Yamamura, H.; Ko, Y. H.; Selvapalam, N.; Kim, K.; Inoue, Y. *Chem. Commun.* **2008**, 2236.
(80) Masson, E.; Lu, X. Y.; Ling, X. X.; Patchell, D. L. *Org. Lett.* **2009**, *11*, 3798.
(81) Celtek, G.; Artar, M.; Scherman, O. A.; Tuncel, D. *Chem. Eur. J.* **2009**, *15*, 10360.
(82) Wang, F.; Han, C. Y.; He, C. L.; Zhou, Q. Z.; Zhang, J. Q.; Wang, C.; Li, N.; Huang, F. H. *J. Am. Chem. Soc.* **2008**, *130*, 11254.
(83) Ashton, P. R.; Philp, D.; Reddington, M. V.; Slawin, A. M. Z.; Spencer, N.; Stoddart, J. F.; Williams, D. J. *Chem. Commun.* **1991**, 1680.
(84) Ashton, P. R.; Chrystal, E. J. T.; Glink, P. T.; Menzer, S.; Schiavo, C.; Spencer, N.; Stoddart, J. F.; Tasker, P. A.; White, A. J. P.; Williams, D. J. *Chem. Eur. J.* **1996**, *2*, 709.
(85) Wang, F.; Zheng, B.; Zhu, K. L.; Zhou, Q. Z.; Zhai, C. X.; Li, S. J.; Li, N.; Huang, F. H. *Chem. Commun.* **2009**, 4375.
(86) Lehn, J. M. *Supramolecular Chemistry: Concepts and Perspectives*; VCH: Weinheim, Germany, 1995.
(87) De Greef, T. F. A.; Smulders, M. M. J.; Wolffs, M.; Schenning, A. P. H. J.; Sijbesma, R. P.; Meijer, E. W. *Chem. Rev.* **2009**, *109*, 5687.
(88) Yakovchuk, P.; Protozanova, E.; Frank-Kamenetskii, M. D. *Nucleic Acids Res.* **2006**, *34*, 564.
(89) Timmerman, P.; Vreekamp, R. H.; Hulst, R.; Verboom, W.; Reinhoudt, D. N.; Rissanen, K.; Udachin, K. A.; Ripmeester, J. *Chem. Eur. J.* **1997**, *3*, 1823.
(90) Fouquey, C.; Lehn, J. M.; Levelut, A.-M. *Adv. Mater.* **1990**, *2*, 254.
(91) Brunsveld, L.; Folmer, B. J. B.; Meijer, E. W.; Sijbesma, R. P. *Chem. Rev.* **2001**, *101*, 4071.
(92) Mock, W. L. *Supramolecular Polymers*; 2nd ed.; Taylor francis: New York, 2005.
(93) Fox, J. D.; Rowan, S. J. *Macromolecules* **2009**, *42*, 6823.
(94) Ligthart, G.; Ohkawa, H.; Sijbesma, R. P.; Meijer, E. W. *J. Am. Chem. Soc.* **2005**, *127*, 810.
(95) Sijbesma, R. P.; Beijer, F. H.; Brunsveld, L.; Folmer, B. J. B.; Hirschberg, J.; Lange, R. F. M.; Lowe, J. K. L.; Meijer, E. W. *Science* **1997**, *278*, 1601.
(96) Hirschberg, J.; Beijer, F. H.; van Aert, H. A.; Magusim, P.; Sijbesma, R. P.; Meijer, E. W. *Macromolecules* **1999**, *32*, 2696.

(97) Folmer, B. J. B.; Sijbesma, R. P.; Versteegen, R. M.; van der Rijt, J. A. J.; Meijer, E. W. *Adv. Mater.* **2000**, *12*, 874.
(98) Söntjens, S. H. M.; Sijbesma, R. P.; van Genderen, M. H. P.; Meijer, E. W. *J. Am. Chem. Soc.* **2000**, *122*, 7487.
(99) Zhao, X.; Wang, X. Z.; Jiang, X. K.; Chen, Y. Q.; Li, Z. T.; Chen, G. J. *J. Am. Chem. Soc.* **2003**, *125*, 15128.
(100) Park, T.; Zimmerman, S. C. *J. Am. Chem. Soc.* **2006**, *128*, 13986.
(101) Conn, M. M.; Rebek, J., Jr. *Chem. Rev.* **1997**, *97*, 1647.
(102) MacGillivray, L. R.; Atwood, J. L. *Nature* **1997**, *389*, 469.
(103) Avram, L.; Cohen, Y. *J. Am. Chem. Soc.* **2002**, *124*, 15148.
(104) Shivanyuk, A.; Rebek, J., Jr. *J. Am. Chem. Soc.* **2003**, *125*, 3432.
(105) Shivanyuk, A.; Rebek, J., Jr. *Proc. Nat. Acad. Sci. U.S.A.* **2001**, *98*, 7662.
(106) Shivanyuk, A.; Rebek, J., Jr. *Chem. Commun.* **2001**, 2424.
(107) Ajami, D.; Schramm, M. P.; Volonterio, A.; Rebek, J., Jr. *Angew. Chem., Int. Ed.* **2007**, *46*, 242.
(108) Wyler, R.; de Mendoza, J.; Rebek, J., Jr. *Angew. Chem., Int. Ed. Eng.* **1993**, *32*, 1699.
(109) Ajami, D.; Hou, J. L.; Dale, T. J.; Barrett, E.; Rebek, J., Jr. *Proc. Nat. Acad. Sci. U.S.A.* **2009**, *106*, 10430.
(110) Kubota, Y.; Sakamoto, S.; Yamaguchi, K.; Fujita, M. *Proc. Nat. Acad. Sci. U.S.A.* **2002**, *99*, 4854.
(111) Kolotuchin, S. V.; Zimmerman, S. C. *J. Am. Chem. Soc.* **1998**, *120*, 9092.
(112) Zhao, L.; Northrop, B. H.; Zheng, Y. R.; Yang, H. B.; Lee, H. J.; Lee, Y. M.; Park, J. Y.; Chi, K. W.; Stang, P. J. *J. Org. Chem.* **2008**, *73*, 6580.
(113) Braekers, D.; Peters, C.; Bogdan, A.; Rudzevich, Y.; Böhmer, V.; Desreux, J. F. *J. Org. Chem.* **2008**, *73*, 701.
(114) Rudzevich, Y.; Rudzevich, V.; Klautzsch, F.; Schalley, C. A.; Böhmer, V. *Angew. Chem., Int. Ed.* **2009**, *48*, 3867.
(115) Rudzevich, Y.; Rudzevich, V.; Böhmer, V. *Chem. Eur. J.* **2010**, *16*, 4541.
(116) Mogck, O.; Paulus, E. F.; Böhmer, V.; Thondorf, I.; Vogt, W. *Chem. Commun.* **1996**, 2533.
(117) Schalley, C. A.; Castellano, R. K.; Brody, M. S.; Rudkevich, D. M.; Siuzdak, G.; Rebek, J., Jr. *J. Am. Chem. Soc.* **1999**, *121*, 4568.
(118) Pop, A.; Vysotsky, M. O.; Saadioui, M.; Böhmer, V. *Chem. Commun.* **2003**, 1124.
(119) Molokanova, O.; Bogdan, A.; Vysotsky, M. O.; Bolte, M.; Ikai, T.; Okamoto, Y.; Böhmer, V. *Chem. Eur. J.* **2007**, *13*, 6157.
(120) Wang, L. Y.; Vysotsky, M. O.; Bogdan, A.; Bolte, M.; Böhmer, V. *Science* **2004**, *304*, 1312.
(121) Zhang, C. J.; Li, S. J.; Zhang, J. Q.; Zhu, K. L.; Li, N.; Huang, F. H. *Org. Lett.* **2007**, *9*, 5553.
(122) Ashton, P. R.; Claessens, C. G.; Hayes, W.; Menzer, S.; Stoddart, J. F.; White, A. J. P.; Williams, D. J. *Angew. Chem., Int. Ed.* **1995**, *34*, 1862.
(123) Ashton, P. R.; Ballardini, R.; Balzani, V.; Gomez-Lopez, M.; Lawrence, S. E.; Martinez-Diaz, M. V.; Montalti, M.; Piersanti, A.; Prodi, L.; Stoddart, J. F.; Williams, D. J. *J. Am. Chem. Soc.* **1997**, *119*, 10641.

(124) Jiang, W.; Schalley, C. A. *Proc. Nat. Acad. Sci. U.S.A.* **2009**, *106*, 10425.
(125) Jiang, W.; Schafer, A.; Mohr, P. C.; Schalley, C. A. *J. Am. Chem. Soc.* **2010**, *132*, 2309.
(126) Ghosh, S.; Li, X. Q.; Stepanenko, V.; Würthner, F. *Chem. Eur. J.* **2008**, *14*, 11343.
(127) Li, X.-Q.; Stepanenko, V.; Chen, Z.; Prins, P.; Siebbeles, L. D. A.; Würthner, F. *Chem. Commun.* **2006**, 3871.
(128) Würthner, F.; Bauer, C.; Stepanenko, V.; Yagai, S. *Adv. Mater.* **2008**, *20*, 1695.
(129) Moffat, J. R.; Smith, D. K. *Chem. Commun.* **2009**, 316.
(130) Atkins, P. W.; Overton, T. L.; Rourke, J. P.; Weller, M. T.; Armstrong, F. A. *Inorganic Chemistry, 5th Ed.*; Oxford University Press, 2010.
(131) Irving, H.; Williams, R. J. P. *J. Chem. Soc.* **1953**, 3192.
(132) Cotton, F. A.; Wilkinson, G.; Murillo, C. A.; Bochmann, M. *Advanced Inorganic Chemistry*; 6th ed.; John Wiley & Sons: New York, 1999.
(133) Lehn, J. M.; Eliseev, A. V. *Science* **2001**, *291*, 2331.
(134) Langner, A.; Tait, S. L.; Lin, N.; Rajadurai, C.; Ruben, M.; Kern, K. *Proc. Nat. Acad. Sci. U.S.A.* **2007**, *104*, 17927.
(135) Stiller, R.; Lehn, J. M. *Eur. J. Inorg. Chem.* **1998**, 977.
(136) Ulrich, S.; Lehn, J. M. *Chem. Eur. J.* **2009**, *15*, 5640.
(137) Ulrich, S.; Lehn, J. M. *J. Am. Chem. Soc.* **2009**, *131*, 5546.
(138) Saur, I.; Scopelliti, R.; Severin, K. *Chem. Eur. J.* **2006**, *12*, 1058.
(139) Schmittel, M.; Kalsani, V.; Fenske, D.; Wiegrefe, A. *Chem. Commun.* **2004**, 490.
(140) Mahata, K.; Schmittel, M. *J. Am. Chem. Soc.* **2009**, *131*, 16544.
(141) Mahata, K.; Schmittel, M. *Chem. Commun.* **2010**, 4163.
(142) Pron, A.; Gawrys, P.; Zagorska, M.; Djurado, D.; Demadrille, R. *Chem. Soc. Rev.* **2010**, *39*, 2577.
(143) Grimsdale, A. C.; Müllen, K. *Macromol. Rapid Commun.* **2007**, *28*, 1676.
(144) Katz, H. E.; Bao, Z. N.; Gilat, S. L. *Acc. Chem. Res.* **2001**, *34*, 359.
(145) Würthner, F. *Angew. Chem., Int. Ed.* **2001**, *40*, 1037.
(146) Anthony, J. E. *Chem. Rev.* **2006**, *106*, 5028.
(147) Ponce Ortiz, R.; Facchetti, A.; Marks, T. J. *Chem. Rev.* **2010**, *110*, 205.
(148) Wu, W.; Liu, Y.; Zhu, D. *Chem. Soc. Rev.* **2010**, *39*, 1489.
(149) Gunes, S.; Neugebauer, H.; Sariciftci, N. S. *Chem. Rev.* **2007**, *107*, 1324.
(150) Roncali, J. *Acc. Chem. Res.* **2009**, *42*, 1719.
(151) Bredas, J. L.; Durrant, J. R. *Acc. Chem. Res.* **2009**, *42*, 1689.
(152) Thompson, B. C.; Fréchet, J. M. J. *Angew. Chem., Int. Ed.* **2008**, *47*, 58.
(153) Otero, R.; Ecija, D.; Fernández, G.; Gallego, J. M.; Sánchez, L.; Martín, N.; Miranda, R. *Nano Lett.* **2007**, *7*, 2602.
(154) Würthner, F.; Meerholz, K. *Chem. Eur. J.* **2010**, *16*, 9366.
(155) Landauer, J.; McConnell, H. *J. Am. Chem. Soc.* **1952**, *74*, 1221.
(156) Lawrey, D. M. G.; McConnell, H. *J. Am. Chem. Soc.* **1952**, *74*, 6175.
(157) Briegleb, G. B. *Elektronen-Donator-Acceptor-Komplexe*; Sprinter: Berlin, 1961.
(158) Smulders, M. M. J.; Schenning, A.; Meijer, E. W. *J. Am. Chem. Soc.* **2008**, *130*, 606.
(159) de Greef, T. F. A.; Nieuwenhuizen, M. M. L.; Stals, P. J. M.; Fitie, C. F. C.; Palmans, A. R. A.; Sijbesma, R. P.; Meijer, E. W. *Chem. Commun.* **2008**, 4306.

(160) Brunsveld, L.; Schenning, A.; Broeren, M. A. C.; Janssen, H. M.; Vekemans, J.; Meijer, E. W. *Chem. Lett.* **2000**, 292.
(161) Tahara, K.; Fujita, T.; Sonoda, M.; Shiro, M.; Tobe, Y. *J. Am. Chem. Soc.* **2008**, *130*, 14339.
(162) Ajayaghosh, A.; Vijayakumar, C.; Praveen, V. K.; Babu, S. S.; Varghese, R. *J. Am. Chem. Soc.* **2006**, *128*, 7174.
(163) de la Escosura, A.; Martínez-Díaz, M. V.; Thordarson, P.; Rowan, A. E.; Nolte, R. J. M.; Torres, T. *J. Am. Chem. Soc.* **2003**, *125*, 12300.
(164) Yoshizawa, M.; Nakagawa, J.; Kurnazawa, K.; Nagao, M.; Kawano, M.; Ozeki, T.; Fujita, M. *Angew. Chem., Int. Ed.* **2005**, *44*, 1810.
(165) Klosterman, J. K.; Yamauchi, Y.; Fujita, M. *Chem. Soc. Rev.* **2009**, *38*, 1714.
(166) Yamauchi, Y.; Yoshizawa, M.; Akita, M.; Fujita, M. *J. Am. Chem. Soc.* **2010**, *132*, 960.
(167) Murase, T.; Horiuchi, S.; Fujita, M. *J. Am. Chem. Soc.* **2010**, 7864.
(168) Sugiyasu, K.; Kawano, S. I.; Fujita, N.; Shinkai, S. *Chem. Mater.* **2008**, *20*, 2863.
(169) Hummelen, J. C.; Knight, B. W.; Lepeq, F.; Wudl, F.; Yao, J.; Wilkins, C. L. *J. Org. Chem.* **1995**, *60*, 532.
(170) Bürckstümmer, H.; Kronenberg, N. M.; Gsänger, M.; Stolte, M.; Meerholz, K.; Würthner, F. *J. Mater. Chem.* **2010**, *20*, 240.
(171) Würthner, F.; Yao, S. *Angew. Chem., Int. Ed.* **2000**, *39*, 1978.
(172) Würthner, F.; Yao, S.; Debaerdemaeker, T.; Wortmann, R. *J. Am. Chem. Soc.* **2002**, *124*, 9431.
(173) van Herrikhuyzen, J.; Syamakumari, A.; Schenning, A.; Meijer, E. W. *J. Am. Chem. Soc.* **2004**, *126*, 10021.
(174) Würthner, F.; Chen, Z.; Hoeben, F. J. M.; Osswald, P.; You, C.-C.; Jonkheijm, P.; Herrikhuyzen, J. v.; Schenning, A. P. H. J.; van der Schoot, P. P. A. M.; Meijer, E. W.; Beckers, E. H. A.; Meskers, S. C. J.; Janssen, R. A. J. *J. Am. Chem. Soc.* **2004**, *126*, 10611.
(175) Jonkheijm, P.; Stutzmann, N.; Chen, Z. J.; de Leeuw, D. M.; Meijer, E. W.; Schenning, A.; Würthner, F. *J. Am. Chem. Soc.* **2006**, *128*, 9535.
(176) Beckers, E. H. A.; Chen, Z.; Meskers, S. C. J.; Jonkheijm, P.; Schenning, A. P. H. J.; Li, X.-Q.; Osswald, P.; Würthner, F.; Janssen, R. A. J. *J. Phys. Chem. B.* **2006**, *110*, 16967.
(177) Sadrai, M.; Bird, G. R.; Potenza, J. A.; Schugar, H. J. *Acta Cryst. Sec. C* **1990**, *46*, 637.
(178) Kühnle, A.; Linderoth, T. R.; Hammer, B.; Besenbacher, F. *Nature* **2002**, *415*, 891.
(179) Huang, W. H.; Zavalij, P. Y.; Isaacs, L. *Angew. Chem., Int. Ed.* **2007**, *46*, 7425.
(180) Zehnacker, A.; Suhm, M. A. *Angew. Chem., Int. Ed.* **2008**, *47*, 6970.
(181) Mohr, J. T.; Krout, M. R.; Stoltz, B. M. *Nature* **2008**, *455*, 323.
(182) Lacour, J.; Linder, D. *Science* **2007**, *317*, 462.
(183) List, B.; Yang, J. W. *Science* **2006**, *313*, 1584.
(184) Reetz, M. T. *Proc. Nat. Acad. Sci. U.S.A.* **2004**, *101*, 5716.
(185) Thomas, C. M.; Ward, T. R. *Chem. Soc. Rev.* **2005**, *34*, 337.
(186) Pasteur, L. C. R. *Hebd. Seanc. Acad. Sci.,* **1848**, *26*, 538.

(187) Kondepudi, D. K.; Kaufman, R. J.; Singh, N. *Science* **1990**, *250*, 975.
(188) Crusats, J.; Veintemillas-Verdaguer, S.; Ribó, J. M. *Chem. Eur. J.* **2006**, *12*, 7776.
(189) Fletcher, S. P.; Jagt, R. B. C.; Feringa, B. L. *Chem. Commun.* **2007**, 2578.
(190) Blackmond, D. G. *Chem. Eur. J.* **2007**, *13*, 3290.
(191) McBride, J. M.; Tully, J. C. *Nature* **2008**, *452*, 161.
(192) Hutin, M.; Cramer, C. J.; Gagliardi, L.; Shahi, A. R. M.; Bernardinelli, G.; Cerny, R.; Nitschke, J. R. *J. Am. Chem. Soc.* **2007**, *129*, 8774.
(193) Dumitru, F.; Legrand, Y. M.; Van der Lee, A.; Barboiu, M. *Chem. Commun.* **2009**, 2667.
(194) Ishida, Y.; Aida, T. *J. Am. Chem. Soc.* **2002**, *124*, 14017.
(195) Isaacs, L.; Witt, D. *Angew. Chem., Int. Ed.* **2002**, *41*, 1905.
(196) Mizumura, M.; Shinokubo, H.; Osuka, A. *Angew. Chem., Int. Ed.* **2008**, *47*, 5378.
(197) Safont-Sempere, M. M.; Osswald, P.; Radacki, K.; Würthner, F. *Chem. Eur. J.* **2010**, *16*, 9366.
(198) Gut, D.; Rudi, A.; Kopilov, J.; Goldberg, I.; Kol, M. *J. Am. Chem. Soc.* **2002**, *124*, 5449.
(199) Takacs, J. M.; Hrvatin, P. M.; Atkins, J. M.; Reddy, D. S.; Clark, J. L. *New J. Chem.* **2005**, *29*, 263.
(200) Kim, T. W.; Lah, M. S.; Hong, J. I. *Chem. Commun.* **2001**, 743.
(201) Rang, A.; Nieger, M.; Engeser, M.; Lützen, A.; Schalley, C. A. *Chem. Commun.* **2008**, 4789.
(202) Chas, M.; Gil-Ramírez, G.; Escudero-Adán, E. C.; Benet-Buchholz, J.; Ballester, P. *Org. Lett.* **2010**, *12*, 1740.
(203) Vincent, J. M.; Philouze, C.; Pianet, I.; Verlhac, J. B. *Chem. Eur. J.* **2000**, *6*, 3595.
(204) Lacour, J.; Jodry, J. J.; Ginglinger, C.; Torche-Haldimann, S. *Angew. Chem., Int. Ed.* **1998**, *37*, 2379.
(205) Maury, O.; Lacour, J.; Le Bozec, H. *Eur. J. Inorg. Chem.* **2001**, 201.
(206) Jodry, J. J.; Frantz, R.; Lacour, J. *Inorg. Chem.* **2004**, *43*, 3329.
(207) Bergman, S. D.; Frantz, R.; Gut, D.; Kol, M.; Lacour, J. *Chem. Commun.* **2006**, 850.
(208) Lacour, J.; Goujon-Ginglinger, C.; Torche-Haldimann, S.; Jodry, J. J. *Angew. Chem., Int. Ed.* **2000**, *39*, 3695.
(209) Shi, X. D.; Fettinger, J. C.; Cai, M. M.; Davis, J. T. *Angew. Chem., Int. Ed.* **2000**, *39*, 3124.
(210) Shi, X. D.; Fettinger, J. C.; Davis, J. T. *J. Am. Chem. Soc.* **2001**, *123*, 6738.
(211) Hwang, I. W.; Kamada, T.; Ahn, T. K.; Ko, D. M.; Nakamura, T.; Tsuda, A.; Osuka, A.; Kim, D. *J. Am. Chem. Soc.* **2004**, *126*, 16187.
(212) Kamada, T.; Aratani, N.; Ikeda, T.; Shibata, N.; Higuchi, Y.; Wakamiya, A.; Yamaguchi, S.; Kim, K. S.; Yoon, Z. S.; Kim, D.; Osuka, A. *J. Am. Chem. Soc.* **2006**, *128*, 7670.
(213) Maeda, C.; Kamada, T.; Aratani, N.; Sasamori, T.; Tokitoh, N.; Osuka, A. *Chem. Eur. J.* **2009**, *15*, 9681.
(214) Ryu, J. H.; Hong, D. J.; Lee, M. *Chem. Commun.* **2008**, 1043.
(215) Pal, A.; Karthikeyan, S.; Sijbesma, R. P. *J. Am. Chem. Soc.* **2010**, *132*, 7842.
(216) van Esch, J. H. *Nature* **2010**, *466*, 193.

Chapter 3

Chiral Self-Recognition and Self-Discrimination of Strapped Perylene Bisimides by π-Stacking Dimerization

Abstract: We present the successful synthesis of a conformationally stable chiral perylene bisimide (PBI) by introduction of a bridging unit on one π-face of the PBI core which restricts the interconversion between *M* and *P* enantiomers, making such PBI suitable for chiral self-sorting studies. Our detailed self-assembly studies with these hitherto unknown chiral PBI revealed that self-recognition prevails over self-discrimination in the chiral self-sorting of PBIs. The results presented in this work construct the fundament for future studies to develop controlled PBI chiral assemblies with new properties and may initiate activities on chiral recognition of other π-conjugated dyes towards a better understanding of self-sorting phenomena.

3.1. Introduction

The importance of self-assembly and self-organization for the creation of higher order functional structures is evident in natural systems.[1,2] Both in biological processes and in organic synthesis, chiral recognition,[3-5] i.e., the ability of a chiral molecule to differentiate between two enantiomers, is of great significance as demonstrated in asymmetric catalysis[6-8] and enantioselective recognition by enzymes and protein receptor sites.[9,10] Chiral recognition between enantiomeric pairs can lead to self-recognition[11-14] or self-discrimination,[15-22] depending on whether an enantiomer preferentially recognizes itself or its mirror image to generate homochiral or heterochiral self-assemblies, respectively. Such stereoselective recognition events may have intriguing consequences like the formation of homochiral compounds from racemates in autocatalytic reactions.[23-25] Accordingly, a better understanding of chiral recognition phenomena will ultimately enable a more rational catalyst design for asymmetric synthesis and may even contribute to a better understanding of the origin of homochirality in biological molecules (e.g., L-amino acids and D-sugars and the biopolymers derived thereof). Despite such important prospects, little attention has been paid to the elucidation of self-recognition versus self-discrimination phenomena of chiral compounds in supramolecular systems. Most of the known examples for chiral recognition are based on the rather strong "inorganic" metal-ligand[11-13,15-20] and cation-anion interactions,[26-29] whereas examples based on weak "organic" interactions like hydrogen bonding and π–π-interactions remain relatively rare.[13,14,21,22]

Perylene bisimide (PBI) dyes have attracted considerable attention during the past years as fluorophores and organic semiconductor materials due to their unique optical and electrochemical properties.[30] Moreover, the concurrence of a large π-surface and a pronounced quadrupole moment of PBIs enables exceptionally strong π–π-stacking interactions between these dyes.[31] PBIs containing substituents in the bay positions (1, 6, 7, 12-positions) are of particular interest as they possess conformational chirality due to the twisting of the perylene core, leading to atropo-enantiomers (*P* and *M* enantiomers).[32-34]

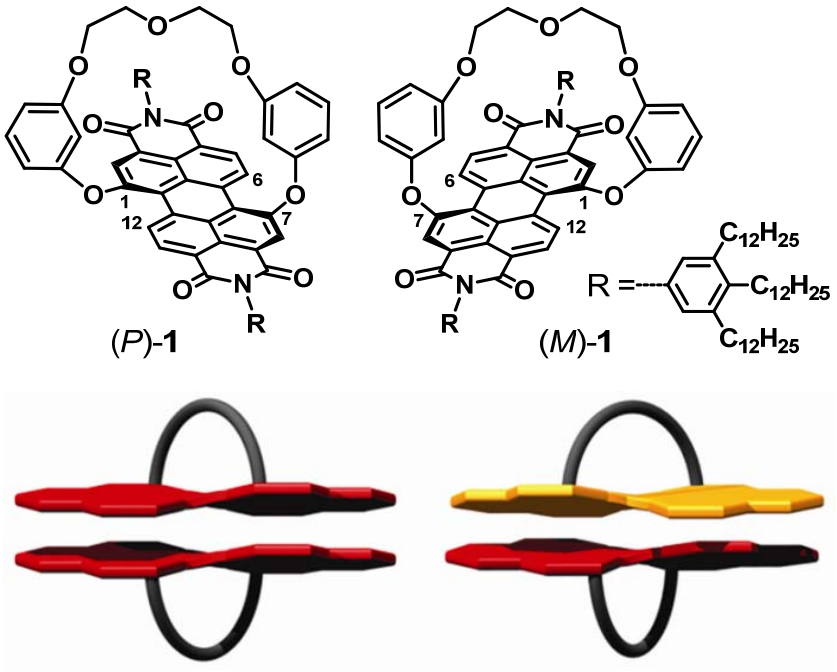

Figure 1. Structures of atropo-enantiomeric (*P*)-**1** and (*M*)-**1** and schematic representation of homo- and heterochiral dimeric aggregates derived thereof.

Very recently, Li and co-workers have elegantly explored the influence of core-twisting on dynamic self-assembly (DSA) of conformationally flexible PBIs and their covalent cyclodimerization.[35,36] However, for the investigation of chiral recognition properties of this important class of functional dyes, conformationally stable enantiopure PBIs are required. Due to the fast interconversion process between atropo-enantiomers of PBIs, such enantiopure derivatives are rather scarce.[32] Recently, we could accomplish epimerically pure tetra-aryloxy-substituted PBIs by restricting the interconversion of atropisomers through bridging the aryloxy bay-substituents.[33] However, these chiral PBIs are not suitable for self-assembly studies to explore the chiral recognition properties since both π-faces of the perylene core are blocked by bridging units. Therefore, to enable such studies, we have synthesized the chiral, at bay position 1,7-disubstituted macrocyclic PBI **1** and resolved the atropo-enantiomers (*P*)-**1** and (*M*)-**1** (Figure 1). The bridging unit on one π-face of these strapped PBIs **1** allows only dimerization by interaction of free π-faces and restricts the interconversion between *M* and *P* enantiomers. Self-assembly studies with these new chiral PBIs revealed that self-recognition, i.e., formation of homochiral dimers, prevails over self-discrimination, i.e., formation of heterochiral dimers, by π–π-stacking. One unexpected finding of our present studies is that the formation of minor amounts of heterochiral dimers enables the determination of *P*/*M*

enantiomeric ratios of chiral PBIs by ^{1}H NMR spectroscopy without using any extern chiral auxiliary.[37]

3.2. Results and Discussion

3.2.1. Synthesis

The strapped PBI **1** was synthesized by macrocyclization of the corresponding 1,7-di(3-hydroxyphenoxy)-substituted PBIs **2** through etherification with di(ethylene glycol) ditosylate in the presence of cesium carbonate in THF (Scheme 1).[33,34] For the investigation of chiral recognition process of these PBIs in solution, PBI **1** containing six long alkyl chains in imide substituents was used. This derivative is soluble in nonpolar solvents like *n*-hexane or *n*-heptane, in which aggregation of PBIs can be observed at rather low concentrations.[38] The starting compound *N,N′*-dicyclohexyl-1,7-dibromoperylene- 3,4:9,10-tetracarboxylic acid bisimide **3** was synthesized according to literature procedures.[39,40] Compound **4** was obtained by nucleophilic substitution of the two bromine atoms of PBI **3** with 3-methoxyphenol following Seybold′s strategy[41] using NMP as solvent and potassium carbonate as base. After saponification of **4**, the insoluble perylene bisanhydride **5** could be obtained in nearly quantitative yield. Perylene bisanhydride **5** was condensed with 3,4,5-tridodecylphenylamine, which was synthesized according to literature procedures,[42] to afford PBI **6**. The cleavage of the ether groups of **4** was achieved with boron tribromide in dry dichloromethane to obtain 3-hydroxyphenoxy-substituted PBI **2**.[43] The free OH groups of the phenoxy substituents are now available for the two-fold Williamson etherification (used also for the synthesis of similar PBI macrocycles)[44] to give the desired PBIs **1** (Scheme 1) as racemate. The atropo-enantiomers (*P* and *M*) of PBI **1** were resolved by semi-preparative HPLC on a chiral column (Trentec, Reprosil 100 chiral-NR) using a mixture of dichloromethane and *n*-hexane as eluent. The stereochemical assignment of the isolated enantiomers was achieved by comparison of their circular dichroism (CD) spectra with those of the previously reported structurally similar epimerically pure *P*- and *M*-configured macrocyclic PBIs.[33]

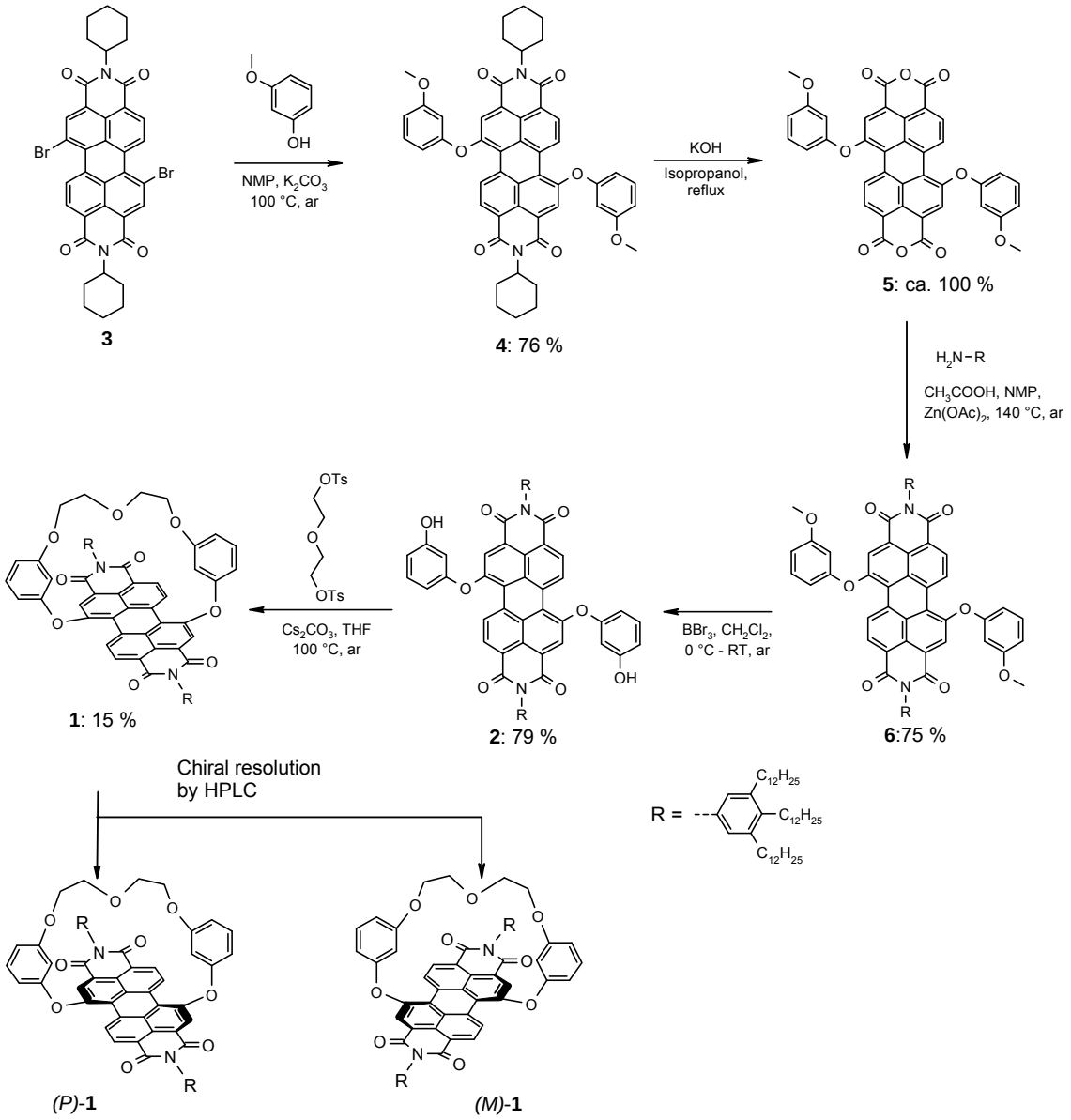

Scheme 1. Detailed synthesis of strapped PBIs **1**. The racemate was resolved by semi-preparative HPLC on a chiral normal phase column (Trentec, Reprosil 100 chiral-NR) with a dichloromethane and *n*-hexane mixture.

3.2.2. Circular Dichroism (CD) Studies

The CD spectra of monomeric (*P*)-**1** and (*M*)-**1** enantiomers in dichloromethane ($c = 5 \times 10^{-6}$ M) show monosignated spectra in the visible region (400–600 nm) in a mirror image relation (Figure 2, top panel, blue lines) due to intrinsic molecular chirality.[33] In nonpolar *n*-hexane a bisignate Cotton effect (zero crossing at 542 nm) is observed for both enantiomers at a concentration of 5×10^{-4} M (Figure 2, upper panel, red lines), which can be attributed to chiral excitonic coupling[45,46] of the transition dipole moments of the chromophores and thus

the formation of dimeric aggregates in a helical π–π-stacking arrangement. The negative sign of the exciton couplet (at 555 nm) for (*P*)-**1** indicates a left-handed helicity (the opposite for (*M*)-**1**) of the respective dimeric aggregate according to exciton chirality method.[45-47]

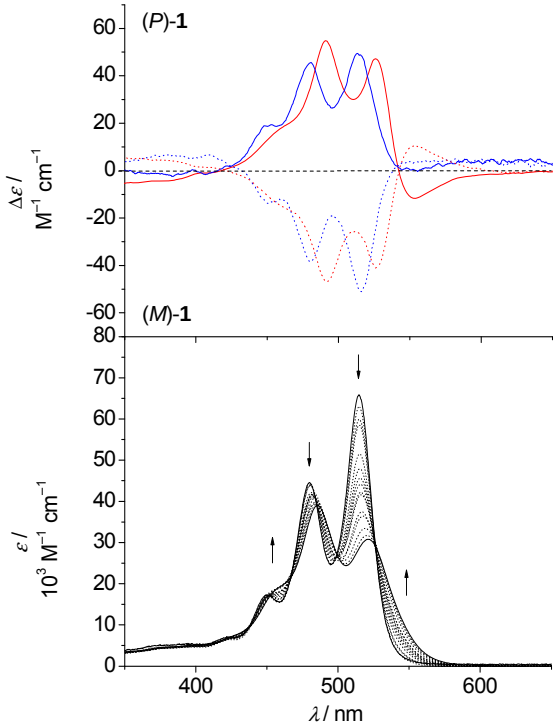

Figure 2. Top panel: CD spectra of (*P*)-**1** (solid lines) and (*M*)-**1** (dashed lines) in CH_2Cl_2 (5×10^{-6} M) (blue lines) and in *n*-hexane (5×10^{-4} M) (red lines) at 298 K. Bottom panel: concentration-dependent UV/Vis absorption spectra of (*rac*)-**1** in *n*-heptane at 331 K; arrows indicate spectral changes with increasing concentration from 5×10^{-6} M to 1×10^{-3} M.

3.2.3. Concentration-Dependent UV/Vis Absorption Studies and Quantification of the Ratio of Homo and Heterochiral Dimers

The binding constants K_D for dimerization of (*rac*)-**1**, (*P*)-**1** and (*M*)-**1** were determined by concentration-dependent UV/Vis absorption studies at 331 K in *n*-heptane. The concentration-dependent UV/Vis absorption spectra (all experiments were repeated twice) of these three samples are virtually identical, indicating similar aggregation behavior (see Figures 3–5). In all cases, isosbestic points are observed at 526 and 466 nm, suggesting the presence of a thermodynamic equilibrium between two species.[48] The experimental data obtained from the concentration-dependent UV/Vis absorption studies can be adequately fitted by nonlinear regression analysis using the dimerization model (see Figures 3–5).[49,50] In the dimerization

model an exclusive equilibrium between monomer (M) and dimer (D) is assumed (Eq. (1))[31]

$$\mathrm{M} \quad + \quad \mathrm{M} \quad \rightleftarrows \quad \mathrm{D} \qquad\qquad K_{\mathrm{D}} = \frac{[\mathrm{D}]}{[\mathrm{M}]^2}$$

(1)

The molar fraction of monomer species present in the solution is defined as $\alpha_{\mathrm{mon}} = [\mathrm{M}]/[\mathrm{M}]_0$, where $[\mathrm{M}]_0$ is the total dye concentration of the molecules. Furthermore, the fraction of aggregated molecules can be written as $\alpha_{\mathrm{agg}} = 1 - \alpha_{\mathrm{mon}}$. By considering $[\mathrm{M}]_0 = 2[\mathrm{D}] + [\mathrm{M}]$ and Eq. (1), the monomer concentration [M] and molar fraction of monomers (α_{mon}) can be given in dependence of the dimerization constant and total dye concentration (Eqs (2),(3)).

$$[\mathrm{M}] = \frac{-1+\sqrt{8K_{\mathrm{D}}[\mathrm{M}]_0+1}}{4K_{\mathrm{D}}}$$

(2)

$$\alpha_{\mathrm{mon}} = \frac{-1+\sqrt{8K_{\mathrm{D}}[\mathrm{M}]_0+1}}{4K_{\mathrm{D}}[\mathrm{M}]_0}$$

(3)

In order to relate Eqs (1)–(3) to experimental data, the apparent molar absorptivity $\bar{\varepsilon}$ of the dye in solution can be expressed as

$$\bar{\varepsilon} = \varepsilon_{\mathrm{M}}\alpha_{\mathrm{mon}} + (1-\alpha_{\mathrm{mon}})\varepsilon_{\mathrm{D}}$$

(4)

where ε_{M} and ε_{D} are the molar absorptivities of the monomer and the dimer species, respectively. By combining Esq. (1)–(4), we obtain

$$\bar{\varepsilon} = \frac{\sqrt{8K_{\mathrm{D}}[\mathrm{M}]_0+1}-1}{4K_{\mathrm{D}}[\mathrm{M}]_0}(\varepsilon_{\mathrm{M}}-\varepsilon_{\mathrm{D}})+\varepsilon_{\mathrm{D}}$$

(5)

Nonlinear regression analysis applying the dimerization model (Eq. (5)) was performed at the selected wavelengths wavelengths 506, 512, 516, 521 and 541 nm to yield K_D and ε_D. The respective fraction of monomeric species (α_{mon}) (see Figures 3b–5b) was then calculated for each data point according to Eq. (6).

$$\alpha_{mon} = \frac{\bar{\varepsilon} - \varepsilon_D}{\varepsilon_M - \varepsilon_D} \qquad (6)$$

However, the optimal approach for the determination of K_D from concentration-dependent UV/Vis absorption data is to take into account the complete spectral range through multiwavelength analysis of the data set. Such an analysis was made possible by a custom-made program[51] in which a numeric stable fit-routine based on an exact physical model (dimerization model presented above) is introduced. Such analysis allows not only a more accurate calculation of the binding constants due to the larger amount of data included in the fit, but also an exact deconvolution of the experimental absorption data into pure monomer and dimer spectra and derived spectra for each experimental concentration. The results of this multilinear fitting procedure are shown in Figures 3c–5c.

First (left) and second (right) sets of concentration-dependent UV/Vis absorption studies for (*P*)-**1**.

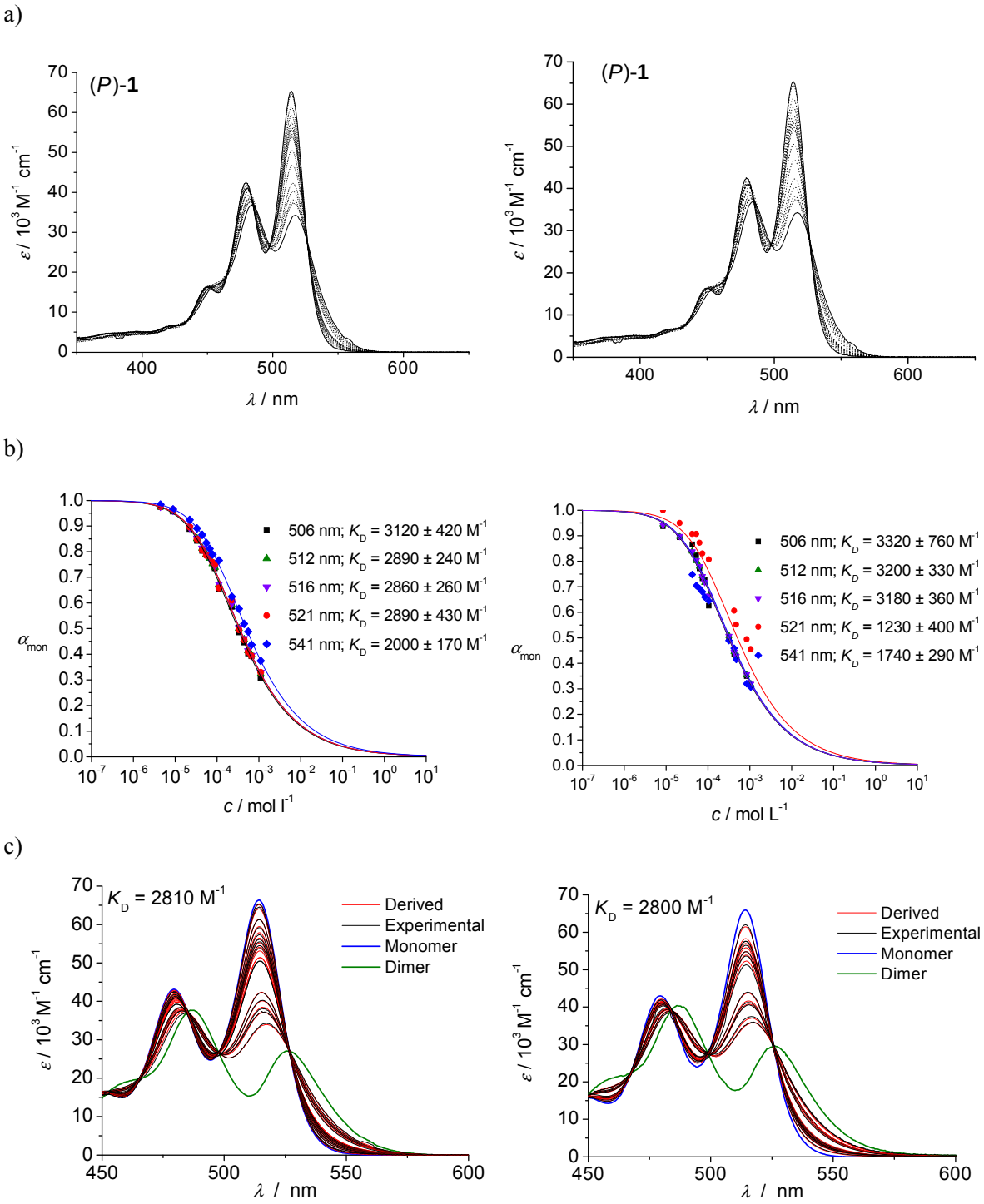

Figure 3. a) Concentration-dependent UV/Vis absorption spectra of (*P*)-**1** in *n*-heptane at 331 K ($[M]_0$ = 4 × 10^{-6} M to 1 × 10^{-3} M), b) molar fraction of monomer species and dimerization constants obtained from nonlinear regression analysis at selected wavelengths indicated in the inset, and c) results from the multilinear fit routine showing the comparison of experimental (black) and derived (red) spectra at respective concentrations as well as derived pure monomer (blue) and dimer (green) spectra.

First (left) and second (right) sets of concentration-dependent UV/Vis absorption studies for (*M*)-**1**

a)

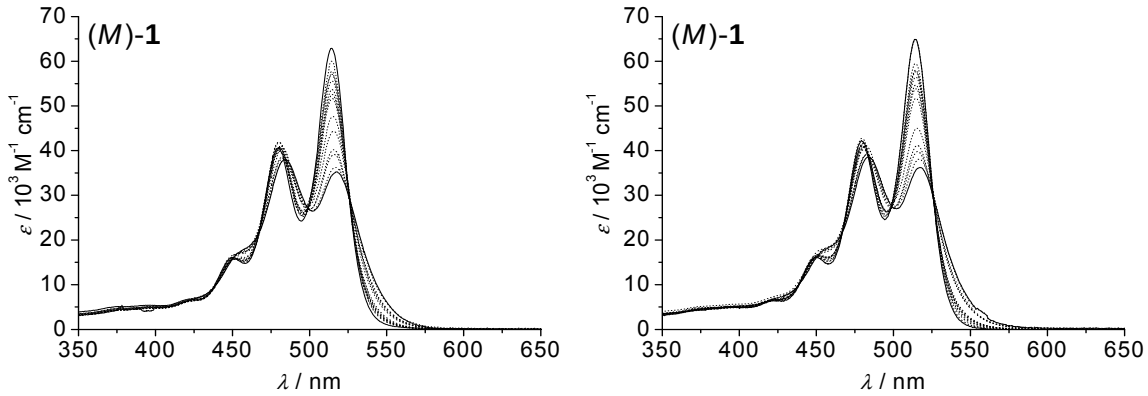

b)

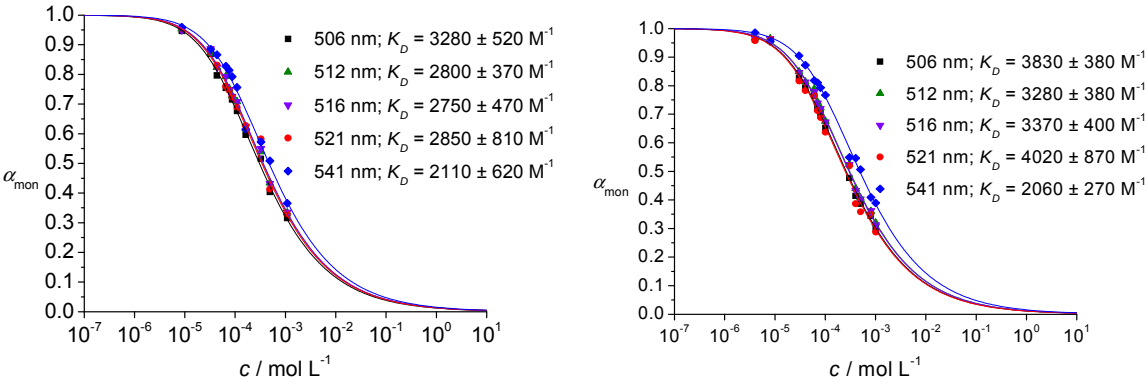

c)

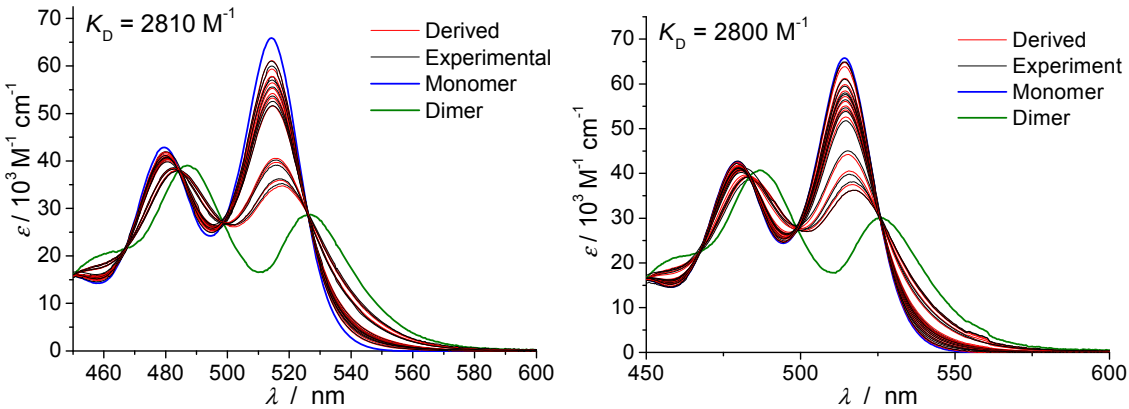

Figure 4. a) Concentration-dependent UV/Vis absorption spectra of (*M*)-**1** in *n*-heptane at 331 K ($[M]_0$ = 4 × 10^{-6} M to 1 × 10^{-3} M), b) molar fraction of monomer species and dimerization constants obtained from nonlinear regression analysis at selected wavelengths indicated in the inset, and c) results from the multilinear fit routine showing the comparison of experimental (black) and derived (red) spectra at respective concentrations as well as derived pure monomer (blue) and dimer (green) spectra.

First (left) and second (right) sets of concentration-dependent UV/Vis absorption studies for (*rac*)-**1**

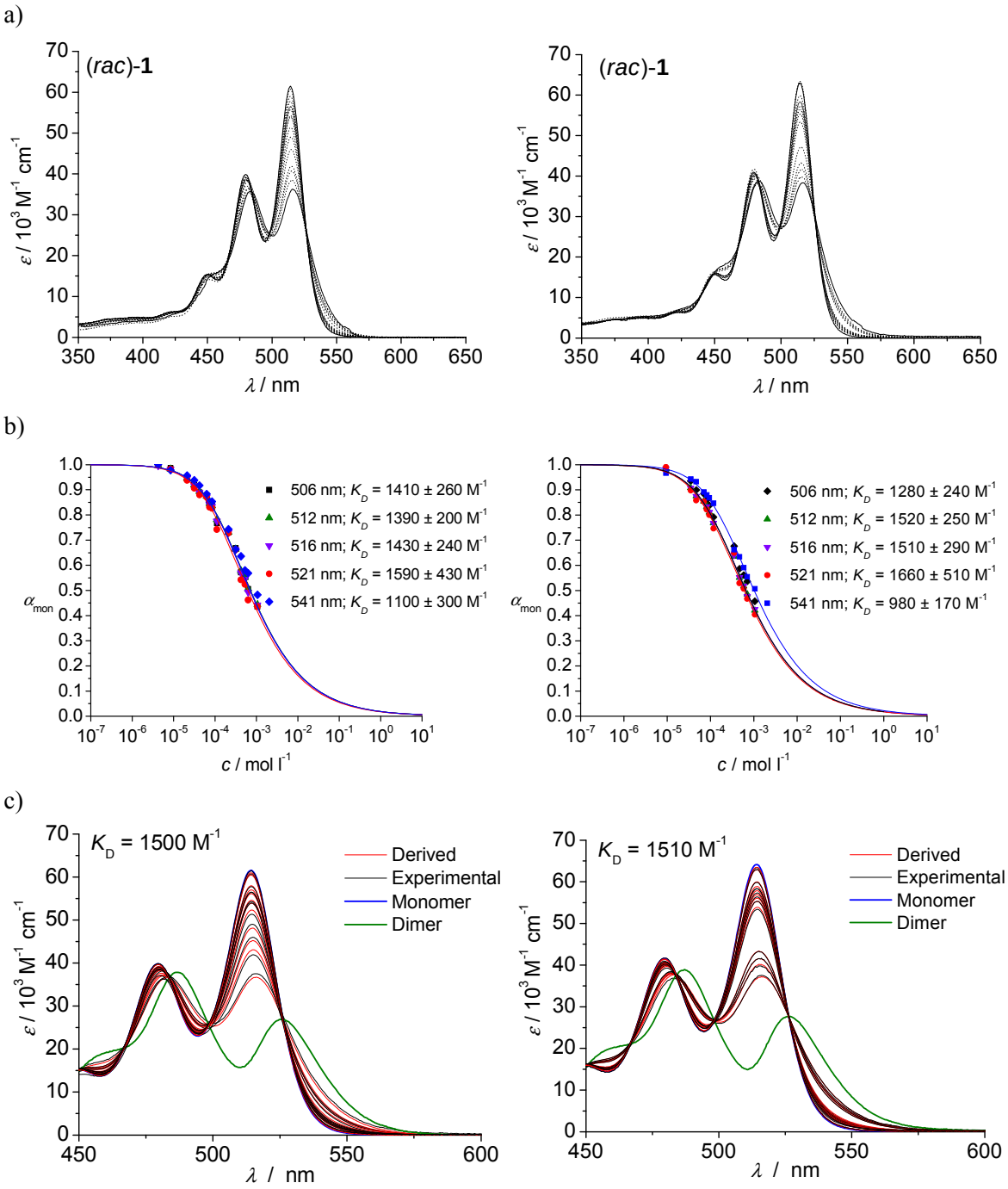

Figure 5. a) Concentration-dependent UV/Vis absorption spectra of (*rac*)-**1** in *n*-heptane at 331 K ($[M]_0 = 4 \times 10^{-6}$ M to 1×10^{-3} M), b) molar fraction of monomer species and dimerization constants obtained from nonlinear regression analysis at selected wavelengths indicated in the inset, and c) results from the multilinear fit routine showing the comparison of experimental (black) and derived (red) spectra at respective concentrations as well as derived pure monomer (blue) and dimer (green) spectra.

The comparison of the binding constants obtained from analysis at selected wavelengths with those obtained by the multilinear fit procedure reveals slight deviations (Table 1). However, since the amount of data introduced in the multilinear fit is much larger compared to that of the analysis at selected wavelengths, the results from multilinear analysis are more reliable. Here, nearly the same binding constant values are found for all dilution studies involving pure enantiomer solutions, and also for the racemate reproducible values were obtained. Notably, the derived spectra at given concentrations are in very good accordance with the experimental ones, which additionally indicates the reliability of the multilinear analysis method.

Table 1. Dimerization binding constants K_D of racemate and pure enantiomers of PBI **1** as obtained from two independent studies by nonlinear regression analysis at selected wavelengths and multilinear fit of the data, respectively.

Sample	K_D [M^{-1}]					
	506 nm	512 nm	516 nm	521 nm	541 nm	Multilinear fit (error ± 15 %)
(*rac*)-**1**	1410 ± 260	1390 ± 200	1430 ± 240	1590 ± 430	1100 ± 300	1500
	1280 ± 240	1520 ± 250	1510 ± 290	1660 ± 510	980 ± 170	1510
(*M*)-**1**	3280 ± 520	2800 ± 370	2750 ± 470	2850 ± 810	2110 ± 620	2810
	3830 ± 380	3280 ± 380	3370 ± 400	4020 ± 870	2060 ± 270	2800
(*P*)-**1**	3120 ± 420	2890 ± 240	2860 ± 260	2890 ± 430	2000 ± 170	2810
	3320 ± 760	3200 ± 330	3180 ± 360	1230 ± 400	1740 ± 290	2800

The considered dimerization constants K_D of (*rac*)-**1** and enantiomers (*P*)-**1** and (*M*)-**1** at 331 K calculated from the values obtained with the multilinear fit are collected in Table 2. It is remarkable that the K_D values determined for the pure enantiomers are significantly larger than that for the racemate, implying that the formation of homochiral dimers is thermodynamically more favored.

Table 2. Dimerization constants K_D determined for (*rac*)-**1**, (*P*)-**1** and (*M*)-**1** in *n*-heptane at 331 K by multilinear fit of the concentration-dependent UV/Vis absorption data to the dimerization model.

Sample	(*P*)-**1**	(*M*)-**1**	(*rac*)-**1**
K_D [M^{-1}]	2800	2800	1500

Quantitative information about the ratio of homochiral and heterochiral dimers can be obtained from the K_D values of PBI **1**. The K_D value obtained for enantiopure (*P*)-**1** (or (*M*)-**1**) is obviously related to the formation of homochiral dimers (i.e., $K_D = K_{D(homo)}$), while in the case of the racemate (*rac*)-**1** the obtained $K_{D(rac)}$ is the average value of homo- and hetero-dimerization processes. According to Kol and co-workers,[52] for racemates the binding constant can be expressed as

$$K_{D(rac)} = \frac{[D]}{[M]^2} \tag{7}$$

and

$$K_{D(rac)} = \frac{K_{D(hetero)} + 2K_{D(homo)}}{4} \tag{8}$$

where [D] is the total dimer concentration (homo- and heterochiral dimers) and [M] is the free monomer concentration. By applying the respective K_D values obtained for the enantiopure ($K_{D(homo)}$) and racemic ($K_{D(rac)}$) PBI samples to Eq. (8), $K_{D(hetero)}$ can be calculated as 400 M^{-1}.

The concentration ratio of homo- and heterodimers can be expressed as shown in Eq. (9).

$$\frac{[\text{Homodimer}]}{[\text{Heterodimer}]} = \frac{[MM]+[PP]}{[MP]} \tag{9}$$

For dimerization processes between *M* and *P* enantiomers, the following equilibria and corresponding equilibrium constants have to be considered (Eqs (10)–(12)).

$$P + P \rightleftarrows PP \qquad K_{PP} = \frac{[PP]}{[P]^2} \tag{10}$$

$$M + M \rightleftarrows MM \qquad K_{MM} = \frac{[MM]}{[M]^2} \tag{11}$$

$$P + M \rightleftarrows MP \qquad K_{MP} = \frac{[MP]}{[P][M]} \tag{12}$$

where $K_{MM} = K_{PP} = K_{D(homo)}$ and $K_{MP} = K_{PM} = K_{D(hetero)}$. By applying Eqs (10)–(12) in (9) one obtains Eq. (13).

$$\frac{[\text{Homodimer}]}{[\text{Heterodimer}]} = \frac{K_{D(homo)}[M]^2 + K_{D(homo)}[P]^2}{K_{D(hetero)}[M][P]} \tag{13}$$

In the case of the racemate it applies further that $[M] = [P]$, thus, Eq. (13) can be written in this case as

$$\frac{[\text{Homodimer}]}{[\text{Heterodimer}]} = \frac{K_{D(homo)}[M]^2 + K_{D(homo)}[M]^2}{K_{D(hetero)}[M][M]} = \frac{2K_{D(homo)}[M]^2}{K_{D(hetero)}[M]^2} = \frac{2K_{D(homo)}}{K_{D(hetero)}} \tag{14}$$

Finally, by applying the values for $K_{D(homo)} = 2800\ M^{-1}$ and $K_{D(hetero)} = 400\ M^{-1}$ in Eq. (14) we obtain [Homodimer]/[Heterodimer] = 14, which corresponds to 93.4 % homodimers and 6.6 % heterodimers in the racemic solution. This result confirms the prevalence of chiral self-recognition (homodimerization) over self-discrimination (heterodimerization) of these PBIs by π-stacking dimerization.

3.2.4. Deduction of the Equilibrium Constant *K′* for the Formation of Heterodimers from Homodimers

Once obtained the values of $K_{D(homo)}$ and $K_{D(hetero)}$ the equilibrium constant (K') and related Gibbs energy ($\Delta G'$) for the formation of heterodimers from a racemic mixture of homodimers can be calculated. For the equilibrium between homo- and heterodimers, the equilibrium constant is given as

$$PP + MM \rightleftarrows 2MP \qquad 4K' = \frac{[MP]^2}{[PP][MM]} \tag{15}$$

For this equilibrium, by substituting Eqs (10)–(12) in Eq. (15) one obtains Eq. (16) taking

into account a statistical factor of 4.

$$4K' = \frac{K^2_{\mathrm{D(hetero)}}[M]^2[P]^2}{K^2_{\mathrm{D(homo)}}[M]^2[P]^2} = \frac{K^2_{\mathrm{D(hetero)}}}{K^2_{\mathrm{D(homo)}}} \quad (16)$$

From the values for $K_{\mathrm{D(homo)}}$ = 2800 M^{-1} and $K_{\mathrm{D(hetero)}}$ = 400 M^{-1} follows K' = 5 × 10^{-3}, which corresponds to a Gibbs energy of 14.5 kJ mol^{-1} according to $\Delta G' = -RT \ln K'$ (where R is the ideal gas constant and T is the temperature in Kelvin) for the formation of heterodimers from the racemic mixture of homodimeric species. Note that the obtained Gibbs energy has a positive sign as the formation of heterodimers from homodimers is an energetically disfavored process.

3.2.5. ^{1}H NMR Spectroscopy

To get more insights into the chiral recognition behaviour of PBI **1**, ^{1}H NMR investigations in deuterated *n*-hexane at 331 K were performed. As expected, identical NMR spectra were obtained for (*P*)-**1** and (*M*)-**1** enantiomers (c = 10^{-3} M). However, significant differences were observed in spectra of (*rac*)-**1** (c = 2 × 10^{-3} M).[53] As can be seen in Figure 6a, the superposed spectra of racemate (*rac*)-**1** and enantiopure (*P*)-**1** (or (*M*)-**1**) show significant differences in chemical shift, particularly of the protons in the aromatic region. For the concentration and temperature used in the ^{1}H NMR experiments, at least 60 % of dimeric species should be present as estimated from UV/Vis studies (Figures 3–5). Thus, the observed differences between the spectra of (*rac*)-**1** and enantiopure (*P*)-**1** (or (*M*)-**1**) should be related to the contemporaneous presence of homo- and heterochiral dimers in the case of racemate. In order to clarify the observed differences in chemical shifts of racemate and pure enantiomers, a series of solutions in [D_{14}] *n*-hexane with varying enantiomeric excess (*ee*) ranging from 18 to 90 % *ee* at c = 1 × 10^{-3} M were investigated by ^{1}H NMR. The spectra in Figure 6b show two sets of signals for the aromatic protons of perylene core (denoted as H^a,$H^{a'}$, H^b,$H^{b'}$ and H^c,$H^{c'}$) in solutions with *ee* not equal to 0 or 100 %. The relative intensities of the respective signal pairs are directly proportional to the % *ee* applied (Table 3).

Table 3. Comparison of the experimental *ee* values with those calculated from integral ratios of signal pairs of H^a,$H^{a'}$, H^b,$H^{b'}$ and H^c,$H^{c'}$.

% *ee* experimental	% *ee* calculated		
	H^a,$H^{a'}$	H^b,$H^{b'}$	H^c,$H^{c'}$
84	86	[a]	[a]
76	79	[a]	[a]
72	76	74	[a]
62	66	62	64
52	56	56	56
42	46	46	42
30	34	[a]	33

[a] As the signals of H^b,$H^{b'}$ and H^c,$H^{c'}$ are superimposed, no accurate calculation of the % *ee* is possible.

To understand the meaning of the split signals under fast exchange conditions, we have to take into account that three equilibria are present in solution (Eqs (10)–(12)) if *ee* is not equal to 100 %. In this case two set of signals for perylene protons are observed due to NMR non-equivalence, which correspond to a weighted average of the three signals standing for [*M*], [*MM*] and [*MP*] for δ_M, and for [*P*], [*PP*] and [*MP*] for δ_P. Accordingly, the relative intensities of the signals in the mixture reflect the relative amounts of [*M*] and [*P*] in the sample. For [*P*] > [*M*] we obtain Eqs (17)–(19) according to references [54-57].

$$I_M = \alpha([M]+2[MM]+[MP]) \tag{17}$$

$$I_P = \alpha([P]+2[PP]+[MP]) \tag{18}$$

$$ee = \frac{(c_P - c_M)}{(c_P + c_M)} = \frac{(I_P - I_M)}{(I_P + I_M)} \tag{19}$$

where I = intensity of NMR signal, c = concentration and α = constant.

This observation can be explained in terms of the different fractions of time spend by the two parent (*M*) and (*P*) enantiomers in the monomeric, homodimeric and heterodimeric state under fast-exchange conditions, giving rise to different averaged diastereotopic environments. Obviously, this situation is given under the premise that the composition of enantiomers is not racemic (cp. Figure 6), a sufficient amount of heterochiral dimer is present, and the homo- and heterochiral dimers which are in diastereomeric relationship feature different chemical

environments for the H^x and $H^{x'}$ protons (x = a, b or c) leading to magnetic non-equivalence of those protons.[55-58] We conjecture that the unexpected separation of the perylene H^x and $H^{x'}$ proton signals arises from pronounced differences in the aromatic shielding of these protons in homo- and heterodimers present in the equilibrium, and thus provoke signal split.

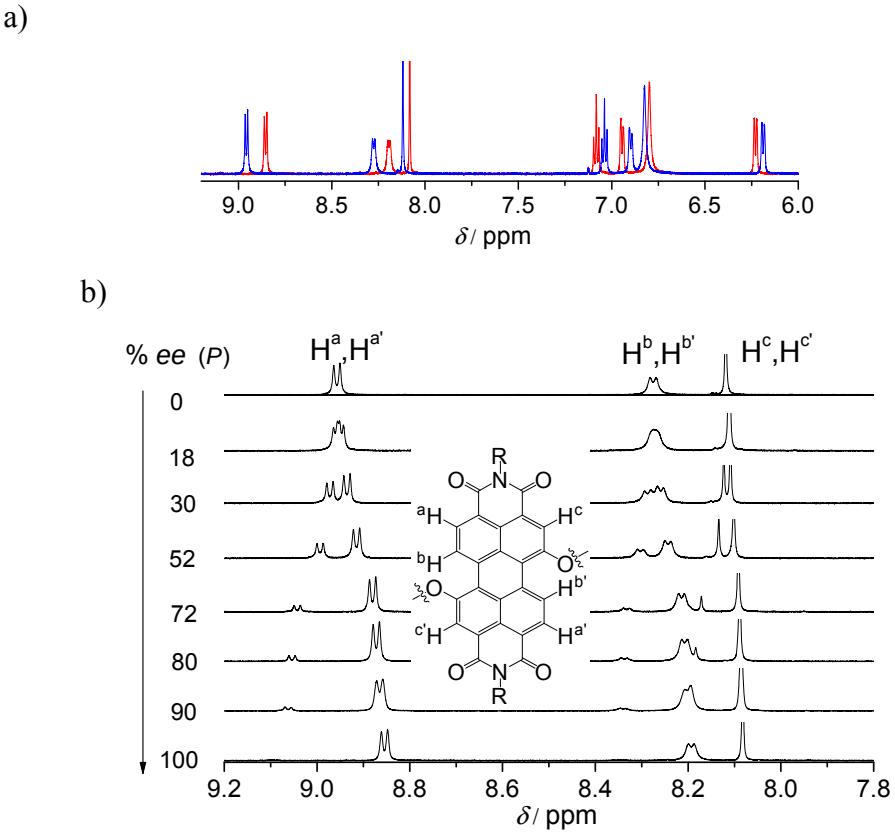

Figure 6. a) 600 MHz ^{1}H NMR spectra (aromatic region is shown) of (*P*)-**1** (or (*M*)-**1**) ($c = 1 \times 10^{-3}$ M) (red spectrum) and (*rac*)-**1** ($c = 2 \times 10^{-3}$ M) (blue spectrum). b) 600 MHz ^{1}H NMR spectra (region of PBI core protons) of solutions with different *ee* (%) referred to (*P*) enantiomer ($c = 1 \times 10^{-3}$ M). All spectra were measured in [D_{14}] *n*-hexane at 331 K.

3.3. Conclusions

To conclude, we have successfully synthesized conformationally restricted chiral 1,7-diaryloxy-substituted PBIs and resolved their atropo-enantiomers. The new chiral compounds are adequately characterized by ^{1}H NMR and high resolution mass spectrometry (HRMS). Based on our spectroscopic studies of racemic and enantiopure PBI dyes, we could show for the first time that self-recognition prevails over self-discrimination in π-stacking dimerization of PBIs. The formation of minor amounts of heterochiral dimers allows the direct

determination of the *ee* of chiral PBIs by ^{1}H NMR without using any extern chiral auxiliaries. Our findings may initiate activities on π-stacking dimerization of other chiral dyes towards a better understanding of self-sorting phenomena, which is of general interest.

3.4. Experimental Section

Cesium carbonate (99 %), boron tribromide (≥ 99 %), 3-methoxyphenol (97 %), potassium carbonate (≥ 99 %), dichloromethane and *N*-methyl pyrrolidone (NMP) (99.5 %) were obtained from commercial suppliers. All chemicals and reagents were used as received, unless otherwise stated. NMP was fractionally distilled prior to use, dichloromethane was distilled under nitrogen from calcium hydride, and potassium carbonate was dried *in vacuo* at 100 °C for 24 h. Diethylene glycol ditosylate[59] and *N,N'*-dicyclohexyl-1,7-dibromoperylene- 3,4:9,10-tetracarboxylic acid bisimide **3** were prepared according to literature procedures.[39,40] The two regioisomers of dibromoperylene bisimide **3** (1,6- and 1,7-disubstituted) were not separated[60] and **3** was applied in the next step as a regioisomeric mixture. As monitored by high field ^{1}H NMR spectroscopy (600 MHz), **3** contained about 5–10 % of the respective 1,6-isomers. Flash column chromatography was performed using silica gel (Si60, mesh size 40–63 μm) from Merck. ^{1}H NMR spectra were recorded with a Bruker Avance 400 MHz and a Brucker Advance DMX 600 MHz instruments. Chemical shifts are given in parts per million (ppm) and are referred to TMS as internal standard. ^{1}H coupling constants *J* are given in Hertz (Hz). MALDI-TOF mass spectra were recorded on an Autoflex II from Bruker Daltonics and HRMS were recorded on a MicrOTOF Focus from Bruker Daltonics. Analytical HPLC was carried out on a JASCO system (PU 2080 PLUS) with a diode array detector (MD 2015), equipped with a ternary gradient unit (DG-2080-533) and inline-degasser (LG 2080-02). Semi-preparative HPLC was performed on a JASCO system (PU 2080 PLUS) with an UV/Vis detector (UV 2077 PLUS). Vapor pressure osmometry (VPO) measurements were performed on a KNAUER osmometer with a universal temperature measurement unit. Benzil was used as standard and a calibration curve in terms of *R* (ohm) vs. molal osmotic concentration (moles per kg *n*-hexane) was accomplished up to 0.016 molal.

UV/Vis Absorption and Circular Dichroism (CD): For all spectroscopic measurements, spectroscopic grade solvents (Uvasol®) from Merck were used. UV/Vis spectra were recorded with a Perkin Elmer PE 950 equipped with a PTP-1 peltier element. CD spectra were measured with a JASCO J-810 spectrometer equipped with a CDF-242 peltier element.

Detailed synthesis of PBIs 1:

***N,N′*-Dicyclohexyl-1,7-di(3-methoxyphenoxy)perylene-3,4:9,10-tetracarboxylic acid bisimide (4):** *N,N′*-Dicyclohexyl-1,7-dibromoperylene-3,4:9,10-tetracarboxylic acid bisimide **3** (500 mg, 0.70 mmol), 3-methoxyphenol (757 mg, 6.10 mmol) and potassium carbonate (303 mg, 3.50 mmol) were dissolved in NMP (30 mL) and stirred for 1 h at 120 °C under argon atmosphere. The reaction mixture was cooled to RT and added dropwise to 1 M hydrochloric acid (50 mL) under stirring. The precipitate was collected by filtration and dried *in vacuo*. Purification of the crude product was carried out by column chromatography (silica gel, CH_2Cl_2/*n*-hexane 4:1) and yielded 370 mg (0.46 mmol, 76 %) red solid in sufficient purity for further reaction: m.p. 317–320 °C; ^{1}H NMR (400 MHz, $CDCl_3$, 25 °C, TMS): δ = 9.56 (d, J = 8.5 Hz, 2H), 8.58 (d, J = 8.3 Hz), 8.32 (s, 2H), 7.33 (t, J = 8.5 Hz, 2H), 6.80 (ddd, J = 8.2, 1.6 Hz, 2H), 6.72 (m, 4H), 4.99 (m, 2H), 2.51 (m, 4H), 1.88 (m, 4H), 1.73 (m, 6H), 1.45–1.26 ppm (m, 6H); MS (MALDI TOF, pos. mode, DCTB): *m/z*: calcd for $C_{50}H_{42}N_2O_8$ 798.3 $[M]^+$; found: 798.3; elemental analysis calcd for $C_{50}H_{42}N_2O_8$: C 75.17, H 5.30, N 3.51; found: C 75.28, H 5.39, N 3.46; UV/Vis (CH_2Cl_2): λ_{max} (ε_{max}) = 537 nm (49300 $M^{-1}cm^{-1}$); fluorescence (CH_2Cl_2): λ_{max} = 566 nm, Φ_{fl} = 0.90.

Synthesis of 1,7-di(3-methoxyphenoxy)perylene-3,4:9,10-tetracarboxylic acid bisanhydride (5) and *N,N*-di(3,4,5-tridodecylphenyl)-1,7-di(3-methoxyphenoxy) perylene-3,4:9,10-tetracarboxylic acid bisimide (6): *N,N′*-Dicyclohexyl-1,7-di(3-methoxyphenoxy)perylene-3,4:9,10-tetracarboxylic acid bisimide **4** (690 mg, 0.86 mmol) and KOH (3.45 g, 86.25 mmol) were dissolved in 35 mL isopropanol. The solution was stirred for 2 h under reflux. Subsequently, the mixture was added dropwise to 60 mL of acetic acid. The precipitate was separated by filtration and washed with 50 mL water and 50 mL of a saturated solution of $NaHCO_3$. The product could be neither purified nor characterized by NMR due its

insolubility in common solvents. The crude product **5** was used directly for the imidization with 3,4,5-tridodecylphenylamine.

A portion of 300 mg (0.47 mmol) of 1,7-di(3-methoxyphenoxy)perylene- 3,4:9,10-tetracarboxylic acid bisanhydride **5** (crude product), 3,4,5-tridodecylphenylamine (400 mg, 0.67 mmol), acetic acid (0.5 mL) and zinc acetate (30 mg, 0.16 mmol) were dissolved in 7 mL NMP. The mixture was stirred at 140 °C under argon for 16 h. Afterwards the reaction mixture was added dropwise into an aqueous HCl (15 %) solution. The resulting precipitate was separated by filtration. The pure product **6** was obtained after column chromatography (silica gel, *n*-hexane/CH_2Cl_2 4:6). Yield: 450 mg (0.25 mmol, 75 % refered to the amine). Red amorphous solid: m.p. 205–212 °C; ^{1}H NMR (400 MHz, $CDCl_3$, 25 °C, TMS): δ = 9.63 (d, *J* = 8.5 Hz, 2H), 8.67 (d, *J* = 8.5 Hz, 2H), 8.40 (s, 2H), 7.32 (t, *J* = 8.4 Hz, 2H), 6.85 (s, 4H), 6.78 (m, 2H), 6.74 (m, 2H), 6.72 (m, 2H), 3.82 (s, 6H), 2.63 (t, *J* = 8.2 Hz), 12H), 1.61 (m, 12H), 1.39–1.19 (m, 108H), 0.91–0.81 ppm (m, 18H); HRMS (ESI, pos. mode, acetonitrile/chloroform 1:1): *m/z* calcd for $C_{122}H_{175}N_2O_8$ $[M+H]^+$: 1796.3304; found: 1796.3343.

***N,N′*-Di(3,4,5-tridodecylphenyl)-1,7-di(3-hydroxyphenoxy)perylene-3,4:9,10-tetracarboxylic acid bisimide (2):**

N,N′-Di(3,4,5-tridodecylphenyl)-1,7-di(3-methoxyphenoxy)perylene-3,4:9,10- tetracarboxylic acid bisimide **6** (214 mg, 0.12 mmol) was dissolved in 20 mL dry dichloromethane under argon atmosphere. The mixture was cooled to 0 ºC and pure BBr_3 (0.08 mL, 0.91 mmol) was added directly to the solution. The reaction mixture was stirred for 1 h at 0 °C and for additional 3 h at RT. Afterwards, the solvent was removed by distillation and 20 mL water/methanol (1:4) were added to the residue and treated for 45 min in ultrasound bath. The solid crude product was separated by filtration. The purification was carried out by column chromatography (dichloromethane/*n*-hexane 4:1). Yield: 160 mg (0.09 mmol, 79 %). Violet solid: m.p. 168–170 °C; ^{1}H NMR (400 MHz, $CDCl_3$, 25 °C, TMS): δ = 9.41 (d, *J*= 8.6 Hz, 2H), 8.59 (d, *J* = 8.6 Hz, 2H), 8.28 (s, 2H), 7.24 (t, *J* = 8.3 Hz, 2H), 6.90 (s, 4H), 6.69 (m, *J* = 7.1 Hz, 2H), 6.63 (m, 2H), 6.60 (m, 2H), 5.70 (s, 1H, -OH), 2.60 (t, 12H), 1.60–1.53 (m, 12H), 1.37–1.19 (m, 108H), 0.91–0.84 ppm (m, 18H); HRMS (ESI, pos. mode,

acetonitrile/chloroform 1:1): *m/z* calcd for $C_{120}H_{171}N_2O_8$ $[M+H]^+$: 1768.2991; found: 1768.3030.

Macrocycle 1:

N,N'-Di(3,4,5-tridodecylphenyl)-1,7-di(3-hydroxyphenoxy)perylene-3,4:9,10- tetracarboxylic acid bisimide **2** (150 mg, 0.08 mmol), diethylene glycol ditosylate (68 mg, 0.17 mmol), and Cs_2CO_3 (221 mg, 0.68 mmol) were dissolved in 250 mL dry THF. The mixture was stirred under argon atmosphere at reflux during 24 h. The solvent was evaporated and the residue was extracted three times with dichloromethane/water (1:1). The organic layer was separated and the solvent was removed under reduced pressure. The purification was carried out by column chromatography (silica gel, dichloromethane/*n*-hexane 45:55). Yield: 23 mg (11.43 μmol, 15 %). Orange amorphous solid: m.p. 245–248 °C; ^{1}H NMR (400 MHz, $CDCl_3$, TMS): δ = 9.32 (d, *J* = 8.2 Hz, 2H), 8.61 (d, *J* = 8.2 Hz, 2H), 8.42 (s, 2H), 7.27 (t, *J* = 8.2 Hz, 2H), 6.69 (dd, *J* = 7.2 Hz, 2H) , 6.86 (s, 4H) , 6.43 (dd, *J* = 8.2 Hz, 2H), 5.63 (t, *J* = 2.0 Hz), 3.75–3.47 (m, 8H), 2.64 (t, *J* = 8.0 Hz, 12H), 1.59–1.55 (m, 12H), 1.32–1.18 (m, 108H), 0.83–0.78 ppm (m, 18H); HRMS (ESI, pos. mode, acetonitrile/chloroform 1:1): *m/z* calcd for $C_{124}H_{177}N_2O_9$ $[M+H]^+$: 1838.3448; found: 1838.3485; UV/Vis (CH_2Cl_2): λ_{max} (ε_{max}): 528 nm (64900 $M^{-1}cm^{-1}$); UV/Vis (*n*-hexane)**:** λ_{max} (ε_{max}) = 517 nm (60000 $M^{-1}cm^{-1}$); fluorescence (CH_2Cl_2): λ_{max} = 545 nm, Φ_{fl} = 0.09; fluorescence (*n*-hexane): λ_{max} = 527 nm, Φ_{fl} = 0.88.

Resolution of enantiomers *P*-(+)-1 and *M*-(–)-1 by HPLC: Resolution of the enantiomers was achieved on a semi-preparative chiral column (Trentec Reprosil 100 chiral-NR) in normal phase with dichloromethane/*n*-hexane (25:75) as eluent. The flow rate used was 8 mL/min. 11.5 mg of each enantiomer were isolated with *ee* ≥ 99 %. m.p. 106–114 °C.

M-(–)-**1**: Retention time (Trentec, Reprosil 100 chiral-NR, dichloromethane/*n*-hexane (25:75), flow: 1.0 mL/min; Ø = 0.8 cm): 11.0 min; λ_{max} ($\Delta\varepsilon$): 527 nm (– 44 $M^{-1}cm^{-1}$).

P-(+)-**1**: Retention time (Trentec, Reprosil 100 chiral-NR, dichloromethane/*n*-hexane (25:75), flow: 1.0 mL/min; Ø = 0.8 cm): 11.8 min; λ_{max} ($\Delta\varepsilon$): 527 nm (+ 41 $M^{-1}cm^{-1}$).

The stereochemical assignment of the isolated enantiomers was achieved by comparison of their circular CD spectra with those of the previously reported, structurally similar, epimerically pure *P*- and *M*-configured macrocyclic PBIs.[34]

3.5. Notes and References

(1) Lehn, J.-M. *Supramolecular Chemistry: Concepts and Perspectives*; VCH: Weinheim, **1995**.
(2) Whitesides, G. M.; Grzybowski, B. *Science* **2002**, *295*, 2418.
(3) Kühnle, A.; Linderoth, T. R.; Hammer, B.; Besenbacher, F. *Nature* **2002**, *415*, 891.
(4) Huang, W. H.; Zavalij, P. Y.; Isaacs, L. *Angew. Chem., Int. Ed.* **2007**, *46*, 7425.
(5) Zehnacker, A.; Suhm, M. A. *Angew. Chem., Int. Ed.* **2008**, *47*, 6970.
(6) Mohr, J. T.; Krout, M. R.; Stoltz, B. M. *Nature* **2008**, *455*, 323.
(7) Lacour, J.; Linder, D. *Science* **2007**, *317*, 462.
(8) List, B.; Yang, J. W. *Science* **2006**, *313*, 1584.
(9) Reetz, M. T. *Proc. Natl. Acad. Sci. U. S. A.* **2004**, *101*, 5716.
(10) Thomas, C. M.; Ward, T. R. *Chem. Soc. Rev.* **2005**, *34*, 337.
(11) Trzaska, S. T.; Hsu, H. F.; Swager, T. M. *J. Am. Chem. Soc.* **1999**, *121*, 4518.
(12) Vincent, J. M.; Philouze, C.; Pianet, I.; Verlhac, J. B. *Chem. Eur. J.* **2000**, *6*, 3595.
(13) Kamada, T.; Aratani, N.; Ikeda, T.; Shibata, N.; Higuchi, Y.; Wakamiya, A.; Yamaguchi, S.; Kim, K. S.; Yoon, Z. S.; Kim, D.; Osuka, A. *J. Am. Chem. Soc.* **2006**, *128*, 7670.
(14) Ghosh, S.; Wu, A. X.; Fettinger, J. C.; Zavalij, P. Y.; Isaacs, L. *J. Org. Chem.* **2008**, *73*, 5915.
(15) Kim, T. W.; Lah, M. S.; Hong, J. I. *Chem. Commun.* **2001**, 743.
(16) Takacs, J. M.; Hrvatin, P. M.; Atkins, J. M.; Reddy, D. S.; Clark, J. L. *New J. Chem.* **2005**, *29*, 263.
(17) Claessens, C. G.; Torres, T. *J. Am. Chem. Soc.* **2002**, *124*, 14522.
(18) Mizumura, M.; Shinokubo, H.; Osuka, A. *Angew. Chem., Int. Ed.* **2008**, *47*, 5378.
(19) Burchell, T. J.; Puddephatt, R. J. *Inorg. Chem.* **2006**, *45*, 650.
(20) Weilandt, T.; Kiehne, U.; Schnakenburg, G.; Lützen, A. *Chem. Commun.* **2009**, 2320.
(21) Alkorta, I.; Elguero, J. *J. Am. Chem. Soc.* **2002**, *124*, 1488.
(22) Bergman, S. D.; Kol, M. *Inorg. Chem.* **2005**, *44*, 1647.
(23) Soai, K.; Shibata, T.; Morioka, H.; Choji, K. *Nature* **1995**, *378*, 767.
(24) Blackmond, D. G. *Proc. Natl. Acad. Sci. U. S. A.* **2004**, *101*, 5732.
(25) Noorduin, W. L.; Vlieg, E.; Kellogg, R. M.; Kaptein, B. *Angew. Chem., Int. Ed.* **2009**, *48*, 9600.
(26) Maury, O.; Lacour, J.; Le Bozec, H. *Eur. J. Inorg. Chem.* **2001**, 201.
(27) Bergman, S. D.; Frantz, R.; Gut, D.; Kol, M.; Lacour, J. *Chem. Commun.* **2006**, 850.
(28) Jodry, J. J.; Frantz, R.; Lacour, J. *Inorg. Chem.* **2004**, *43*, 3329.
(29) Govindaswamy, P.; Linder, D.; Lacour, J.; Suss-Fink, G.; Therrien, B. *Chem. Commun.* **2006**, 4691.
(30) Würthner, F. *Chem. Commun.* **2004**, 1564.
(31) Chen, Z. J.; Lohr, A.; Saha-Möller, C. R.; Würthner, F. *Chem. Soc. Rev.* **2009**, *38*, 564.
(32) Osswald, P.; Würthner, F. *J. Am. Chem. Soc.* **2007**, *129*, 14319.
(33) Osswald, P.; Reichert, M.; Bringmann, G.; Würthner, F. *J. Org. Chem.* **2007**, *72*, 3403.
(34) Osswald, P.; Würthner, F. *Chem. Eur. J.* **2007**, *13*, 7395.
(35) Wang, W.; Shaller, A. D.; Li, A. D. Q. *J. Am. Chem. Soc.* **2008**, *130*, 8271.

(36) Shaller, A. D.; Wang, W.; Gan, H. Y.; Li, A. D. Q. *Angew. Chem., Int. Ed.* **2008**, *47*, 7705.
(37) Wenzel, T. J. *Discrimination of Chiral Compounds Using NMR Spectroscopy*; John Wiley & Sons: Hoboken, 2007.
(38) Chen, Z. J.; Stepanenko, V.; Dehm, V.; Prins, P.; Siebbeles, L. D. A.; Seibt, J.; Marquetand, P.; Engel, V.; Würthner, F. *Chem. Eur. J.* **2007**, *13*, 436.
(39) Böhm, A.; Arms, H.; Henning, G.; Blaschka, P.; AG), B., 1997; Vol. DE19547209 A1.
(40) Böhm, A.; Arms, H.; Henning, G.; Blaschka, P.; AG), B., 1997; Vol. DE19547210 A1.
(41) Seybold, G.; Wagenblast, G. *Dyes and Pigments* **1989**, *11*, 303.
(42) Würthner, F.; Chen, Z. J.; Dehm, V.; Stepanenko, V. *Chem. Commun.* **2006**, 1188.
(43) Sautter, A.; Thalacker, C.; Würthner, F. *Angew. Chem., Int. Ed.* **2001**, *40*, 4425.
(44) Osswald, P.; Leusser, D.; Stalke, D.; Würthner, F. *Angew. Chem., Int. Ed.* **2005**, *44*, 250.
(45) Berova, N.; Nakanishi, K. *Circular Dichroism: Principles and Applications*; Wiley-VCH: New York, 2000.
(46) Berova, N.; Di Bari, L.; Pescitelli, G. *Chem. Soc. Rev.* **2007**, *36*, 914.
(47) Note that, ideally, the positive and negative signals of bisignate CD couplets should be of similar intensity.[45,46] However, this situation holds only true if achiral dyes are stacked in a helical fashion. Here, the different amplitudes of the positive and negative parts of the bisignated CD couplets might arise from the intrinsic molecular chirality of these twisted PBIs (see: V. Buß, C. Reichardt, *Chem. Commun.* **1992**, 1636).
(48) Evidently, in the case of (*rac*)-**1** more than two species are involved due to the possibility of homo- and heterochiral dimers formation. Thus, the dimerization process is either highly stereoselective or both dimers exhibit (almost) identical UV/Vis absorption spectra.
(49) Connors, K. A. *Binding Constants: The Measurement of Molecular Complex Stability*; Wiley: New York, 1987.
(50) Additionally, we have performed vapor pressure osmometry (VPO) measurements at 10^{-2} M concentration in *n*-hexane. On the basis of the measured colligative concentrations, aggregation numbers *N* of 2.5 and 2.3 are estimated for (*rac*)-**1** and (*P*)-**1**, respectively. These data again corroborate the formation of dimers in self-assemblyof PBIs **1**.
(51) Wortmann, R.; Rösch, U.; Redi-Abshiro, M.; Würthner, F. *Angew. Chem., Int. Ed.* **2003**, *42*, 2080.
(52) Gut, D.; Rudi, A.; Kopilov, J.; Goldberg, I.; Kol, M. *J. Am. Chem. Soc.* **2002**, *124*, 5449.
(53) To exclude concentration effects as a possible reason for the different chemical shifts of the aromatic protons of (*rac*)-**1** and (*P*)-**1** (or (*M*)-**1**), a double-concentrated solution of (*rac*)-**1** was measured relative to that of (*P*)-**1** (or (*M*)-**1**).
(54) Luchinat, C.; Roelens, S. *J. Am. Chem. Soc.* **1986**, *108*, 4873.
(55) Giordano, C.; Restelli, A.; Villa, M.; Annunziata, R. *J. Org. Chem.* **1991**, *56*, 2270.
(56) Harger, M. J. P. *J. Chem. Soc., Perkin Trans. 2* **1977**, 1882.
(57) Dobashi, A.; Saito, N.; Motoyama, Y.; Hara, S. *J. Am. Chem. Soc.* **1986**, *108*, 307.
(58) Williams, T.; Pitcher, R. G.; Bommer, P.; Gutzwill.J; Uskokovi.M *J. Am. Chem. Soc.*

1969, *91*, 1871.

(59) Marquis, D.; Desvergne, J. P.; Bouaslaurent, H. *J. Org. Chem.* **1995**, *60*, 7984.

(60) Würthner, F.; Stepanenko, V.; Chen, Z. J.; Saha-Möller, C. R.; Kocher, N.; Stalke, D. *J. Org. Chem.* **2004**, *69*, 7933.

Chapter 4

Impact of Core Chirality on Mesophase Properties of Atropo-Enantiomeric Perylene Bisimides

Abstract: The three dimensional organization of a racemic core-twisted perylene bisimide (PBI) **1** and its pure atropo-enantiomers ((*P*)-**1** and (*M*)-**1**) are compared in the condensed state to elucidate the impact of core chirality in such materials. Our studies revealed distinctive differences in the condensed state properties of the racemic and enantiopure PBIs. While the racemic material forms a soft crystalline phase, the pure enantiomers (*P*)-**1** and (*M*)-**1** exhibit a smectic liquid crystalline mesophase of much lower viscosity as evidenced by differential scanning calorimetry (DSC), polarization optical microscopy (POM), X-ray diffraction of extruded samples and atomic force microscopy (AFM) investigations. Two different packing models for the condensed state of the racemate and its pure enantiomers have been proposed based on the observed mesophase properties and force field calculations.

4.1. Introduction

Highly organized self-assembled nanomaterials are of great importance for optoelectronic devices,[1-4] catalysis,[5,6] sensing[7-9] and chiral recognition.[10-12] Liquid crystals[13-16] and, in particular, columnar mesophases[17-20] have attracted considerable interest in the past years due to their intriguing electronic and optical properties.[21-23] Their self-organization, self-healing of structural defects and the facile low-temperature processing of oriented thin films make liquid crystals highly attractive for the development of novel, highly organized materials.[24-26] The introduction of chirality in liquid crystals[27-32] may endow such materials with some specific functionalities such as polar order[33-36] and second order nonlinear optical properties,[37,38] and selective reflection or full color thermal imaging.[39-41] Chiral discotic liquid crystalline molecules can be achieved mainly through two different approaches: i) by attaching chiral side chains to the central aromatic core,[42-45] and ii) inducing chirality in the aromatic core.[46,47] The former approach has been widely applied to introduce helicity in columnar phases. However, only few examples of core chiral nonracemic discotic liquid crystals have been reported so far. Among them, helicenes[46] and binaphthyl derivatives[47] revealed helical self-organization in columnar phases owing to the presence of chiral aromatic cores.

Helicenes (and helicene-like derivatives),[48-54] binaphthyl[55-59] and biphenyl[60-62] derivatives are the most prominent examples of chiral aromatic compounds with stable inherent chirality. For larger polycyclic aromatic hydrocarbons inherent chiral aromatic cores are accessible by the twisting of the extended π-systems by attaching sterically demanding substituents in the bay area.[63-69] This strategy has been successfully applied in a large number of π-conjugated organic semiconductor systems such as triphenylenes,[63,64] acenes[65-67] and perylene bisimide (PBI) dyes.[70,71]

The outstanding optical and electronic properties of PBI dyes[72] have been proved to be of great advantage for a variety of applications, e.g., light emitting diodes (LEDs),[26,73,74] organic field effect transistors (OFETs)[75-78] and solar cells.[20,79,80] Moreover, in our recent studies, we could demonstrate high charge carrier mobilities not only for planar[81-83] but also for core-twisted PBIs.[84] The twisting of the PBI core affords the desired core

chirality, and the proper choice of the bay substituents allows the chiral resolution to enantiopure bay-substituted PBIs. However, it has been demonstrated that even for bulky substituents such as bromine in bay-positions (1,6,7,12-positions), racemization of the atropo-enantiomers (*M* and *P* enantiomers) occurs at ambient temperature.[71] Recently, epimerically pure tetra-aryloxy-substituted PBIs could be obtained by restricting the interconversion of their atropisomers through bridging the aryloxy bay substituents.[85,86] However, their intrinsic rigidity and both sterically hindered π-surfaces prevent their aggregation through π–π interactions. To overcome this drawback, we recently synthesized the chiral macrocyclic PBI **1** bearing a bridging unit at 1,7 positions and hence suitable for self-assembly, and its atropo-enantiomers ((*P*)-**1** and (*M*)-**1**, see Figure 1a) were resolved as reported elsewhere (Chapter 3).[70] The formation of chiral dimeric aggregates was demonstrated in solution and the predominance of homochiral self-assemblies over the heterochiral ones was evidenced, with a difference of 14.5 kJ mol^{-1} in the Gibbs energy for the formation of heterodimers from a racemic mixture of homodimers.[70] Thus, preferential formation of excitonically coupled homochiral dimers is anticipated also in the condensed state of PBIs **1** owing to this considerable thermodynamic bias.

Liquid crystallinity of PBI derivatives was observed in materials with multiple long flexible alkyl chains attached at the imide positions. This strategy has been previously successfully applied in planar[87-89] as well as in core-twisted PBIs.[69] As the macrocyclic PBIs **1** possess long flexible alkyl chains at the imide positions and a large chiral aromatic core, liquid crystallinity of the configurationally fixed core chiral PBIs **1** is expected. Although liquid crystals based on chiral carbohydrate cores have been appreciably studied,[27,29] and the effect of chirality in metallomesogens has been investigated by using racemates and their respective enantiomers,[31,32] to our knowledge, there are only few reports on comparative studies of racemic and enantiopure core chiral atropo-enantiomeric mesogens.

The set of racemic and enantiopure PBIs **1** now offers the unique opportunity to explore the effect of core chirality on the condensed state properties of such mesogens. Here we

report that the PBIs **1** with twisted chiral core exhibit thermotropic phases. More interestingly, our comparative studies with the racemic and enantiomerically pure (*P*)-**1** and (*M*)-**1** have revealed that the racemate possesses a soft *columnar* crystalline phase, while the enantiomerically pure PBIs organize in *lamellar* smectic liquid crystalline phase. Such distinctive condensed state properties of racemic and the respective pure enantiomers are unprecedented for aromatic core chiral molecules. This novel chirality effect is rationalized on the basis of the efficient alternate packing of *MM* and *PP* homochiral dimers in racemic PBI **1** which is triggered by favorable non-bonding interactions of the molecular bridges (Figure 1b), while for the enantiomerically pure PBIs such a packing is unfavorable for steric reasons (Figure 1c).

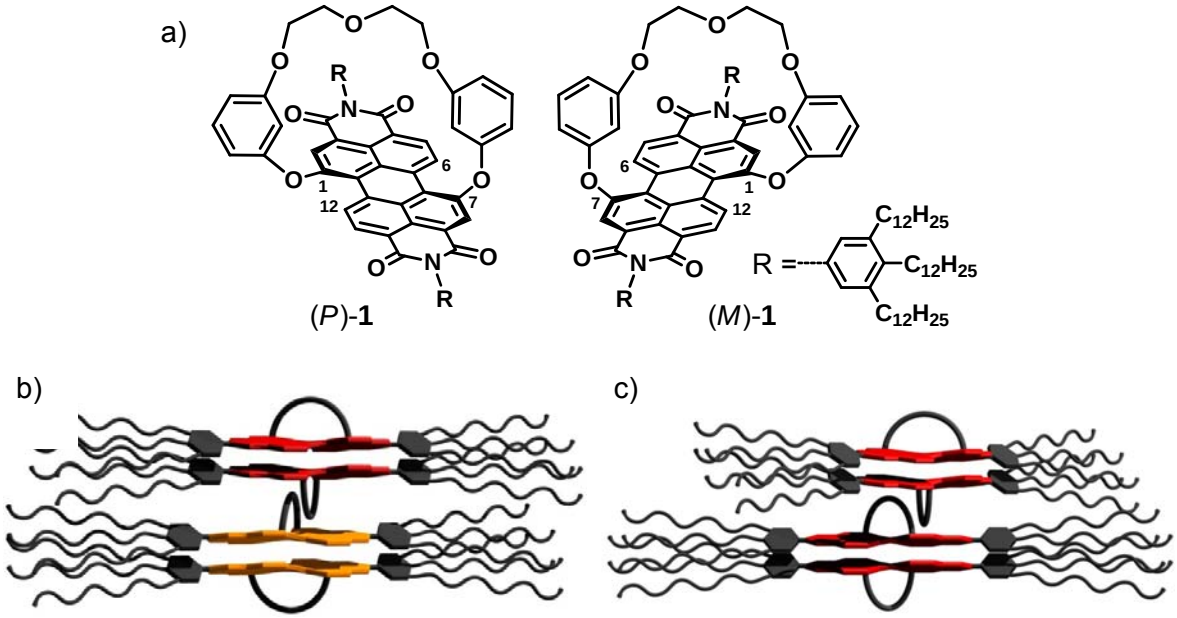

Figure 1. a) Structure of atropo-enantiomeric PBIs (*P*)-**1** and (*M*)-**1**, b) schematic representation of the stacking through the bridging unit of two different *MM* (red) and *PP* (yellow) and c) two equal *MM* (red) homochiral dimers.

4.2. Results and Discussion

4.2.1. Thermotropic Behavior

The thermotropic properties of PBIs (*rac*)-**1**, (*M*)-**1** and (*P*)-**1** were characterized by differential scanning calorimetry (DSC), polarized optical microscope (POM) and X-ray diffraction.

DSC thermograms for the second heating and cooling cycles are depicted in Figure 2

and the obtained thermodynamic properties are summarized in Table 1.

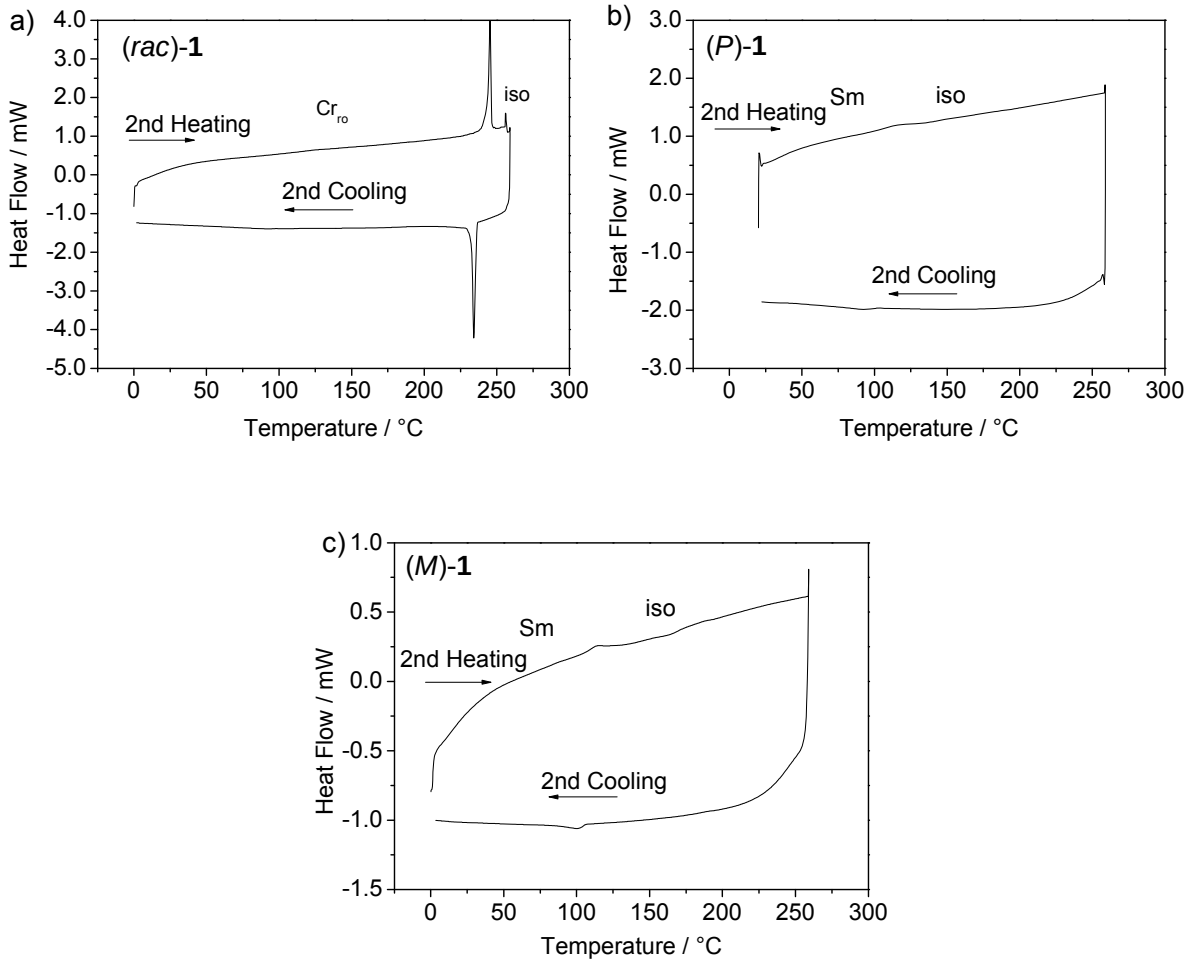

Figure 2. DSC thermograms (heating and cooling runs at a scanning rate of 10 °C min^{-1}) of a) (*rac*)-**1**, b) (*P*)-**1** and c) (*M*)-**1**; second cycle is shown. Cr_{ro} is indicative of a soft crystalline rectangular phase, whilst Sm represents a smectic phase.

All compounds (*rac*)-**1**, (*M*)-**1** and (*P*)-**1** revealed only one transition from a birefringent to an isotropic phase in the studied temperature range from 0 to 250 °C. For compound (*rac*)-**1** an endothermic transition at 245 ºC was observed with a relatively high transition enthalpy of 32.2 kJ mol^{-1} (Figure 2a). In contrast, the pure enantiomeric (*M*)-**1** and (*P*)-**1** showed a transition temperature at 115 ºC with a transition enthalpy of 4 kJ mol^{-1}. No significant differences between (*M*)-**1** and (*P*)-**1** are observed, which is actually expected for a pair of enantiomers (Figure 2b,c). It is noteworthy that the clearing temperature and transition enthalpy of (*rac*)-**1** are significantly higher than for pure enantiomers (*M*)-**1** and (*P*)-**1**, indicating higher thermodynamic stability of the packing of the racemate with

regard to that of the pure enantiomers (Table 1). The high transition enthalpy and transition entropy of (*rac*)-**1** point to a transition from a highly ordered crystalline structure to an isotropic phase, while the relatively low values for (*M*)-**1** (or (*P*)-**1**) are in proper agreement with a liquid crystal phase transition. Large differences in the isotropization temperature between the racemate and pure enantiomers have been previously reported for crystalline compounds,[90,91] however, such studies are scarce for liquid crystalline materials.[31,32,92]

Table 1. Thermodynamic data obtained from DSC studies of (*rac*)-**1**, (*P*)-**1** and (*M*)-**1**.

	T (°C)	ΔH (kJ mol^{-1})	ΔS (J mol^{-1} K^{-1})
(*rac*)-**1**	245	32.2	62.2
(*P*)-**1**	117	4.3	10.3
(*M*)-**1**	117	4.1	10.2

POM studies revealed that (*rac*)-**1** does not exhibit any typical texture for liquid crystals, instead, birefringent, fibrous-like structures were growing very fast at 240 ºC (cooling rate 0.1 ºC min^{-1}) (Figure 3a). Such a texture is not characteristic for a classical liquid crystalline phase but rather reminiscent of a growing crystal. However, the material could still be sheared, pointing to their soft nature.

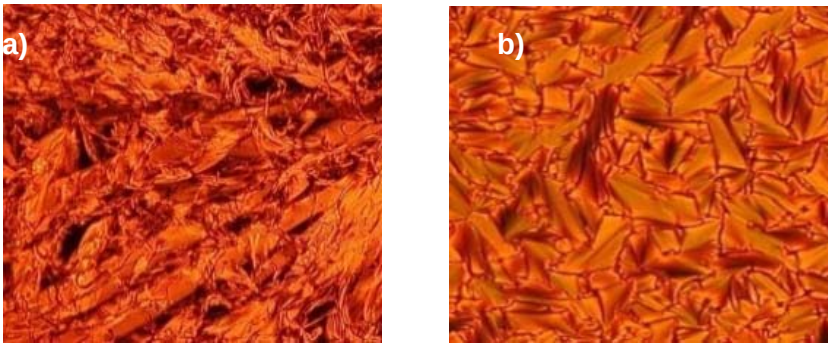

Figure 3. Textures observed for a) (*rac*)-**1** and b) (*M*)-**1** (or (*P*)-**1**) under POM.

In contrast, well defined fan-shaped textures typical for a lamellar phase[93,94] were observed for (*M*)-**1** and (*P*)-**1** (Figure 3b) after cooling down from the isotropic phase (cooling rate 0.1 ºC min^{-1}). The low viscosity of this mesophase could be demonstrated by shearing, which produced a homeotropic alignment of the sample between two glass slides

(Figure 4). In combination with the typical fan-shaped texture, these results are indicative of a lamellar liquid crystal phase of SmA type for the enantiomerically pure materials.

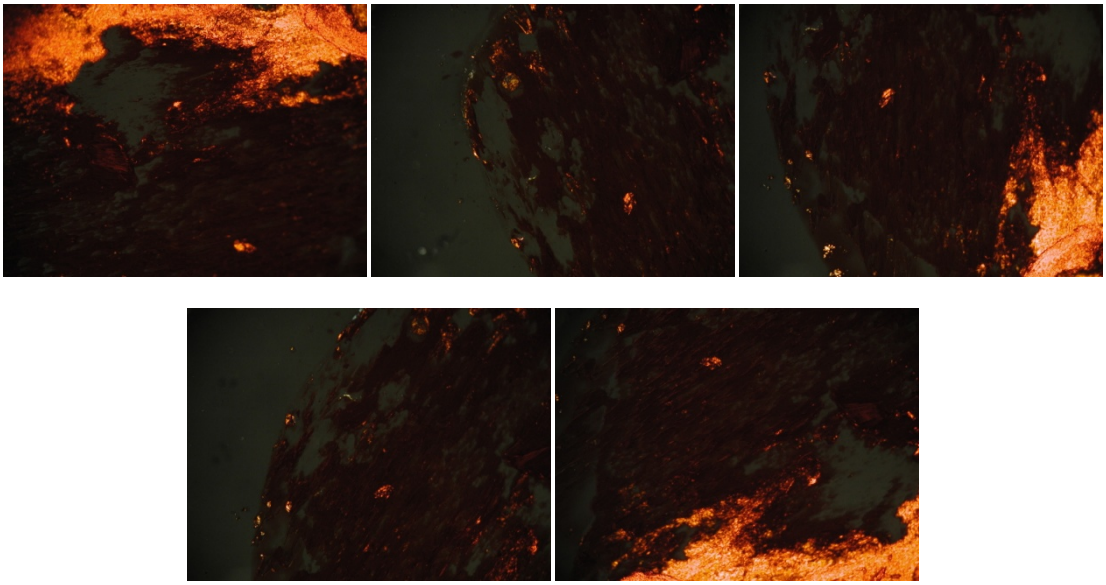

Figure 4. Pictures of a (*M*)-**1** sheared sample at different rotation angles respective to the light beam in the polarization microscope with the polarizator in perpendicular mode.

The data for the thermotropic behavior of (*rac*)-**1** and (*M*)-**1** (or (*P*)-**1**) suggest significantly different supramolecular organizations of the mesophases of racemic and enantiopure materials that could be illustrated by a contact zone experiment (Figure 5).

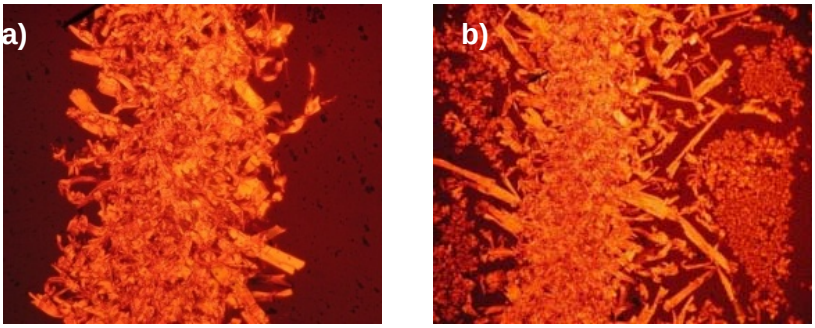

Figure 5. POM pictures of the contact zone between (*M*)-**1** (right) and (*P*)-**1** (left) after cooling from 250 °C to 240 °C (a) and 80 °C (b) at a cooling rate of 0.1 °C min^{-1}.

In this experiment, the enantiomers (*M*)-**1** and (*P*)-**1** were placed between two glass slides creating a contact zone in which an enantiomeric excess gradient was expected. The probe was first melted at 120 °C and further heated to 250 °C, the transition temperature of the racemate. A texture identical to the one previously observed for (*rac*)-**1** could be revealed in the contact zone of both enantiomers at 240 °C upon cooling at a rate of 0.1 °C

min^{-1} (Figure 5a). The areas left and right to the contact zone remained isotropic until the phase transition temperature for the enantiomerically pure samples was reached (Figure 5b). These results indicate that only the almost exact 1:1 mixture and the neat enantiomeric compounds are able to form anisotropic mesophases with a large gap of mixing in between. This implies that (*rac*)-**1** builds one distinct more stable phase with a significantly different supramolecular organization and physical properties compared to those of the pure enantiomers. Similar observations were reported previously for mixtures of donor and acceptor discotic mesogens.[95-98]

Structural investigations of the observed phases were performed by WAXS and MAXS on aligned samples after extrusion of the material to fibers at about 30 to 50 °C below the transition temperature to the isotropic phase.[d] Compound (*rac*)-**1** exhibits a typical fiber pattern consisting of equatorial and meridional reflections reminiscent of a columnar self-organization (Figure 6a).

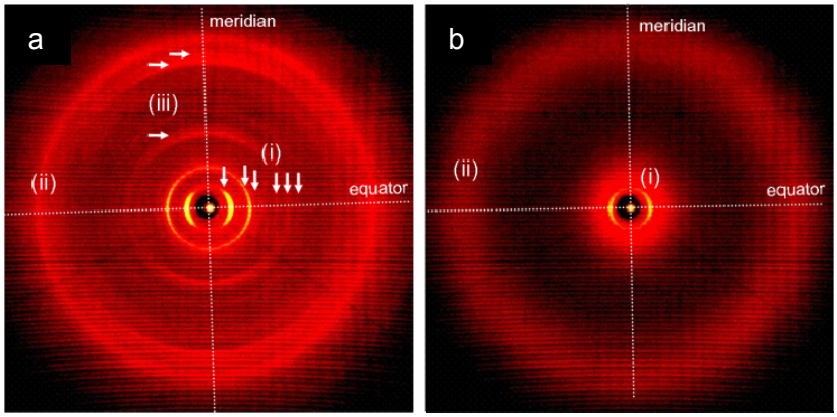

Figure 6. Diffraction pattern corresponding to (a) (*rac*)-**1** at 149 °C and (b) (*M*)-**1** at 80 °C.

The observed six equatorial reflections (i) (indicated by arrows in Figure 6a) point to a two-dimensional order of columns (Table 2). The best least square fit was obtained assuming a centered rectangular order with lattice parameters a = 65.1 Å and b = 18.2 Å (see Figure 8a). The large arcs of the reflections indicate a poor alignment or a considerable degree of disorder of the columnar material. The reflections are relatively sharp compared to liquid crystalline materials but too broad for genuine crystals, indicating a soft crystalline nature of the phase. A

[d] Studies performed in collaboration with Prof. Matthias Lehmann.

diffuse, broad halo (ii) at 4.6 Å observed for (*rac*)-**1** can typically be attributed to disordered liquid-like aliphatic chains. The diffuse part of the halo, however, is superposed by a second halo at 4.5 Å with a much smaller, unusual half-width corresponding to 45 correlated CH_2 units. This may indicate that there is a portion of highly ordered aliphatic components. Two of the three reflections (iii) on the meridian corresponding to 9.6 Å and 4.9 Å can be indexed as 002 and 004. The third reflection at 5.1 Å is not positioned at an expected layer line, and thus point to only short range intracolumnar order attributed to the aromatic cores separated by the bridge of the PBI that partitions the aromatic cores along the column (see Figure 7).

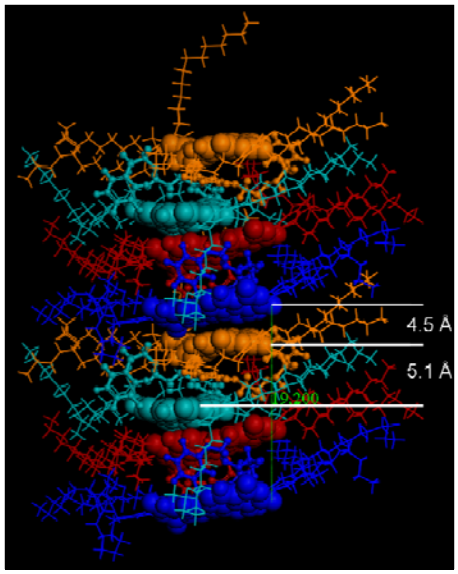

Figure 7. Columnar stack showing the 5.1 Å distance, which presumably has its origin in two aromatic entities separated by the bridges.

The height of a columnar unit, and thus that of the three-dimensional orthorhombic unit cell, amounts to 19.2 Å. It is highly remarkable that PBIs sterically blocked at one π-face by the bridging unit are still able to stack in columnar aggregates. The dimer formation by the free π-face of the chiral molecules can proceed through π-stacking which is highly favorable in *MM* or *PP* dimer aggregates, and these are indeed the predominant species in solution as previously shown in Chapter 3. These dimers can then generate columnar stacks by a centrosymmetric packing of bridging units. Only when *PP* and *MM* dimers alternate, the long axes of the PBI chromophores point almost to the same direction which allows such an efficient centrosymmetric packing and nanosegregation of the polar centers from the nonpolar flexible chains (Figures 1b and 8b), and that is the driving force towards the columnar

structure. Consequently, the unit cell must contain a *PPMM* sequence along the *c*-direction, which is in agreement with the mixing experiment revealing the columnar soft crystalline phase only in the vicinity of the contact zone between *P* and *M* enantiomer.

Table 2. Experimental and calculated *d*-values of (*rac*)-**1** at 149 °C in its orthorhombic soft crystalline phase with parameters: a = 65.1 Å, b = 18.2 Å and c = 19.2 Å.

hkl	*d* (measured) / Å	*d* (calculated) / Å	Correlation length / Å
200	32.6	32.6	468 (≈ 14 columns)
110	17.5	17.5	
310	14.1	14.0	
510	10.5	10.6	
020	9.0	9.1	
220	9.0	8.8	
420	8.0	8.0	
002	9.6		
-	5.1		
004	4.9	4.8	
halo	4.6 (4.5)		(202)

Based on these results, the packing in soft crystalline material of (*rac*)-**1** with orthorhombic three-dimensional order and eight PBI molecules in the unit cell (two columns with two dimers each) was modeled with the program Package Materials Studio and geometry minimized by the force field module Forcite Plus (COMPASS) (Figure 8).[e] First, a single stack of four PBI mesogens *MPPM* was assembled in a perfectly aligned fashion, placed in a large orthorhombic cell and the cell parameters *a/2* and *c* were slowly adjusted to the experimental values, while optimizing the geometry of the assembly. During this procedure, the PBIs which are slightly rotated to each other in the π-stack remained at their positions and mainly the bridges and dodecyl chains were optimized for

[e] Calculations carried out in collaboration with Prof. Matthias Lehmann.

packing and space filling. Subsequently, the cell was enlarged by the factor of two from *a*/2 to *a* and the value for parameter *b* was selected that a second *MPPM* stack did not experience any steric interaction with the first, when the assemblies were positioned at x = *a*/4 and y = *b*/4 for the first and x = 3*a*/4 and y = 3*b*/4 for the second column. Before *b* was now stepwise reduced, two lateral aliphatic chains were folded back from each molecule to fill the space along the long axis of the PBIs. Thus, in total 16 of 48 chains are folded in that way in order to reduce the steric interaction and hence to maintain a high order of the aliphatic chains when the cell size is reduced.

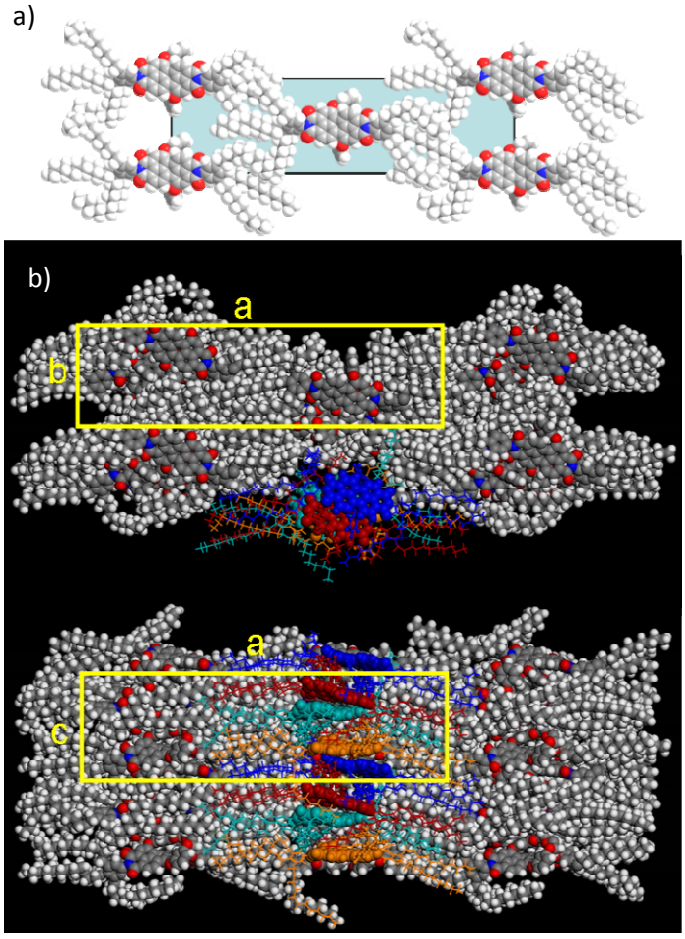

Figure 8. a) Simplified model of the centered rectangular columnar order of (*rac*)-**1**. b) Model of the columnar phase of (*rac*)-**1** minimized by the force field COMPASS (Forcite Plus module). Top view (TOP) and side view (BOTTOM) of the proposed orthorhombic unit cell. For the highlighted column, chains are visualized by line representations, bridging units by the ball stick model and PBIs by the CPK model.

The parameter *b* was then stepwise reduced by 2 Å and in each step the cell was geometry optimized (500 iterations). The stacks were positioned in order to maintain the centered

rectangular order, before *b* was reduced again until the experimental value was obtained. The final cell was geometry optimized until a minimum was reached. Subsequently, a supercell (2*a*, 2*b*, *c*) containing four unit cells was formed and exposed to five annealing cycles between 300 K and 700 K for a total of 50ps. The structure was again geometry minimized until the calculation did converge. Figure 8b depicts a top and a side view. It is interesting to note that, although the modeling starts from perfectly stacked PBIs, the minimization in the proposed unit cell results always in a slight translation of the PBI cores thereby optimizing the overall non-bonding interactions. The densely packed structure appears to be a compromise between packing of rigid cores, flexible bridging units and aliphatic chains.

The calculated density based on the X-ray results amounts to 1,07 g cm^{-3} at 149 °C, a typical and reasonable value for organic materials and especially for materials with a large portion of aliphatic chains.[99] For an ideal columnar model assuming perfect nanosegregation of aliphatic chains and aromatic PBI cores, calculation of the cross-section of the columnar core (A_{core}) (Table 3) may confirm a non-tilted disposition of PBI units. The calculation starts with the volume occupied by the aliphatic chains V_{chains} of one molecule which can be estimated using temperature-dependent data published by B. Donnio et al.[100] Subtraction of NV_{chain} (N being the number of molecules present in a unit cell) from the cell volume V_{cell} gives the core volume, which divided by the parameter c affords the cross-section of two columnar cores. A_{core} amounts to 138 cm^2 and is thus slightly larger than the rhombohedral surface calculated for the cross-section of a PBI (Table 3),[101] indicating that the dense packing of aliphatic chains leaves enough space for columns of non-tilted PBI cores.

Table 3. Calculation of the PBI core surface taking into account the model depicted in Figure 8a.

T/ °C	V_{chains} / Å^3	V_{cell} / Å^3	N	A_{core} / Å^2	[a]$A_{rhombohedral}$ / Å^2
149	2186	22784	8	138	133

[a]Calculated

Interestingly, the *a* parameter of the unit cell reveal a very small temperature dependence with 64.6 Å at 149 °C, 65.4 Å at 80 °C and 65.8 Å at 30 °C. Generally, the distance between columns for discotic mesogens increases upon cooling with simultaneous decrease of the intracolumnar distance. This process can be rationalized in

terms of a decreasing of the π–π-distance accompanied by a larger fraction of s-*trans* conformation of the aliphatic chains. In the case of (*rac*)-**1** the bridging units prevent a strong compression along the columns by increasing π–π-interactions, and thus a strong temperature-dependence of the columnar diameter and intracolumnar distances was not expected. Indeed, the *c* parameter decreases form 19.2 Å at 149 °C to 18.8 Å at 30 °C, i.e. a decrease of only 2%.

The WAXS diffraction pattern of enantiopure (*M*)-**1** (Figure 6b) shows significantly broader reflections than observed for (*rac*)-**1**. Only one refelxion at the equator and a halo at the meridian are monitored for (*M*)-**1**. The single reflection at the equator corresponds to a distance of 35.3 Å at 80 °C and 35.4 Å at 30 °C. These values reveal a larger separation of the perylene chromophores along the molecular long axes compared with the separation of molecules in the soft crystalline (*rac*)-**1** (Figure 9b).

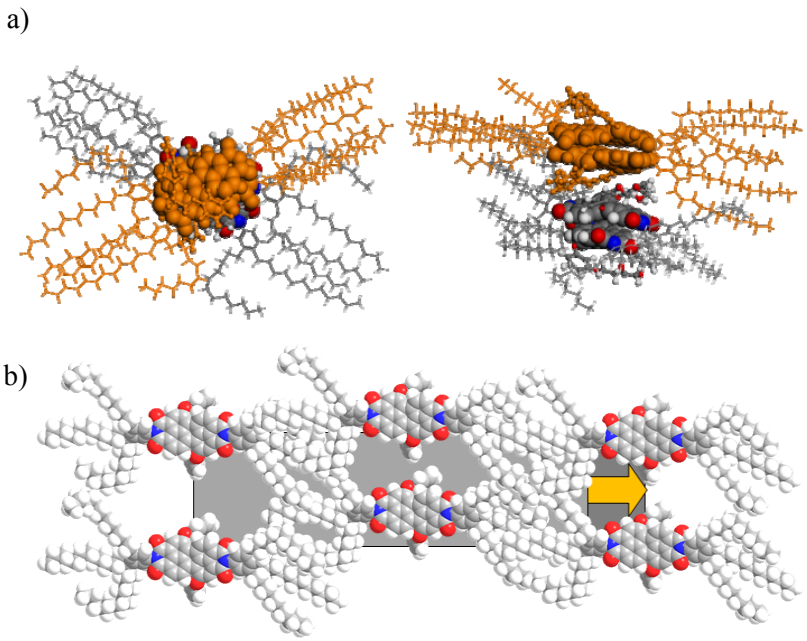

Figure 9. a) Trial to stack homochiral dimers into columnar stacks. Rotation of the dimers does not favor a dense packing. Dimers (orange) can be regarded as calamitic mesogens. b) Model developed for a lamellar phase of the homochiral dimers.

The absence of any meridional reflections excludes the presence of columnar order. The halo observed with a maximum at 4.4 Å might originate from overlapping signals of the average separation of aliphatic chains and dimers of PBI (*M*)-**1**. It becomes evident that the bridging units in enantiomerically pure molecules do not allow for nanosegregation

and efficient stacking along a column. The steric constraints imposed by the bridging units prevent further aggregation between *MM* (or *PP*) dimers into extended one-dimensional columnar entities (Figure 9a). The dimeric unit, however, can be regarded as a calamitic mesogen with a rather rigid dimeric core and nonpolar long, flexible alkyl chains at the two extremities. Nanosegregation of the rigid, polar core and the nonpolar chains being then the driving force for the formation of a lamellar structure, which can be easily rationalized starting from the rectangular order of dimers in the orthorhombic soft crystal by the extension of the cell along the *a*-direction (Figure 9b, yellow arrow). The two-dimensional positional information between the dimers will be lost with the increase of parameter *a* and only information on the distance between lamellae will remain available. The less favorable contact surfaces between *MM* (or *PP*) equally homochiral dimers as a consequence of the steric shielding of the bridging units may even allow the molecules to displace translationally and rotate in a layer. This model describes a smectic A (SmA) phase and is in agreement with POM studies, showing a characteristic SmA texture (Figure 4b).

The different mode of self-assembly for (*rac*)-**1** and (*M*)-**1** (or (*P*)-**1**) is clearly a consequence of the molecular chirality of these PBIs and predominant chiral self-recognition, leading to the formation of homochiral dimeric building blocks. The subsequent self-assembly of these dimer aggregates into soft materials is then controlled by the nanosegregation of the different molecular subunits, and thus by the optimization of weaker non-bonding interactions with particular importance of the sterical constraints imposed by the bridging units. The conditions for threedimensional ordering are better fulfilled when *MM* and *PP* dimers can alternate along a column, which is possible in the case of the racemate, but not for enantiomerically pure PBIs. Thus, the condensed phase of pure enantiomers possesses a much higher fluidity and lower order.

4.2.2. Thin Film CD and UV/Vis Studies

The self-assembly of (*rac*)-**1**, (*M*)-**1** and (*P*)-**1** in *n*-hexane at a concentration of 10^{-3} M has recently been investigated and the formation of π–π-stacking dimers has been proved

(Chapter 3). All performed CD experiments were tested to rule out possible linear dichroism (LD) effects (Figure 10).

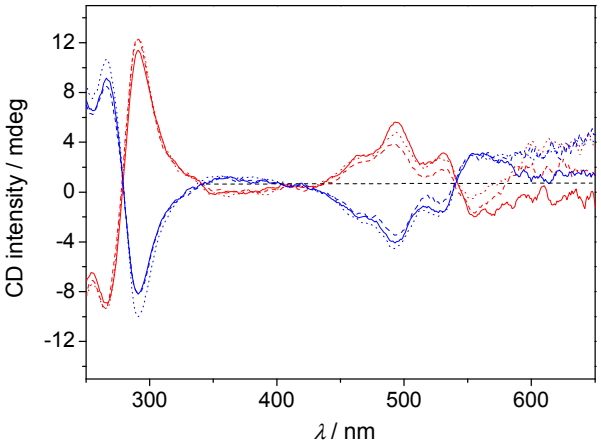

Figure 10. CD spectra of thin films of (*P*)-**1** (red line) and (*M*)-**1** (blue line) measured perpendicular to the light beam at three different angles: 0° (solid line), 45° (dashed line) and 90° (dotted line).

In Figure 11, the CD and UV/Vis spectra of highly concentrated solutions and thin films of (*P*)-**1** and (*M*)-**1** are presented for comparison.

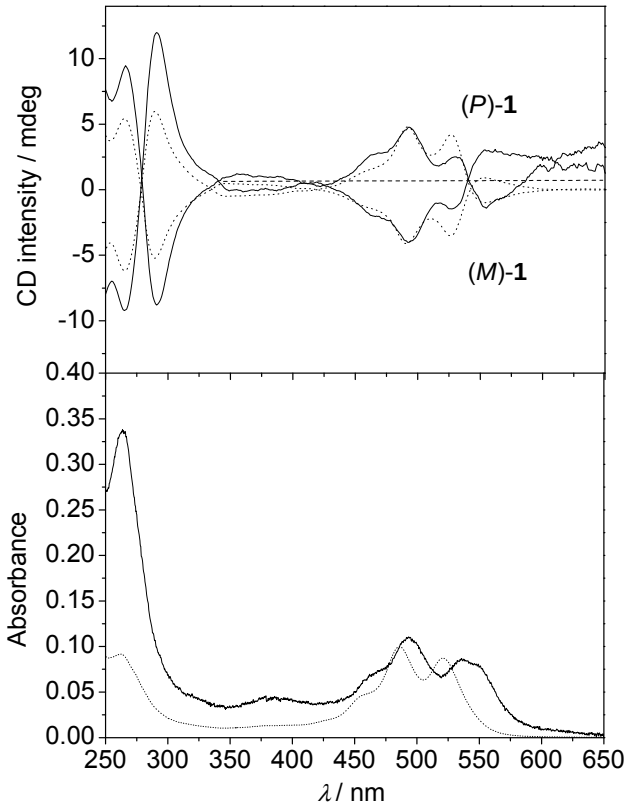

Figure 11. Top panel: CD spectra of (*P*)-**1** and (*M*)-**1** in thin films (solid lines) and *n*-hexane solution (c = 10^{-3} M) (dotted lines), at RT. Bottom panel: UV/Vis absorption spectra[105] in thin

film (solid line) and *n*-hexane solution ($c = 10^{-3}$ M) (dotted line) at RT. For better comparison, the solution spectra are normalized to the maxima of the thin film spectra.

As it can be realized, for both solution and thin film similar spectral patterns are observed. The CD spectra of (*M*)-**1** and (*P*)-**1** thin films and solution are shown ((*rac*)-**1** has no CD signal) and, as expected for an enantiomeric pair, they are mirror images (Figure 11, top panel). Small differences observed in the intensity of the CD signals of (*M*)-**1** and (*P*)-**1** in thin films are due to the fact that their thickness was not rigorously controlled. Bisignate Cotton effect is observed in solution and thin film spectra, which is a result of chiral excitonic coupling between the chromophores. It is to note that the positive and negative areas of the couplet do not match the additivity rule.[102,103] However, it should be emphasized that this rule is only valid for helical aggregates formed from inherently achiral building blocks, and thus not truly applicable to the present system.[104] The presence of bisignate Cotton effect in the films confirms the supramolecular chiral nature of the dimers present in the liquid crystalline phase, being (*P*)-helical dimers formed by (*M*)-**1** and (*M*)-helical supramolecular dimers formed by (*P*)-**1** according to exciton chirality method. [102,103]

4.2.3. Surface Morphology

The surface morphologies of the thin films of (*rac*)-**1** and (*M*)-**1**[106] were investigated by AFM on a glass surface in air using taping-mode. For (*rac*)-**1**, a homogeneous distribution of multilayer structures can be recognized by AFM (Figure 12a), while for (*M*)-**1** regular multilayer structures with layer-height up to 20 nm irregularly dispersed on the surface are observed (Figure 13a,b). In order to obtain a better orientation on the surface, thin films of (*rac*)-**1** and (*M*)-**1** were heated to the isotropic phase, slowly cooled down and annealed at 200 °C for (*rac*)-**1** and at 80 °C for (*M*)-**1**. The surface morphology of these annealed samples measured at room temperature shows significant differences between (*rac*)-**1** and (*M*)-**1** and in comparison with the untreated samples shown in Figure 12a and 13a,b. Organization into multilayers with a regular layer height of 4.0 ± 0.5 nm stacked up to five layers (Figure 13c) can be visualized for (*M*)-**1**. These data are in accordance with an edge-on orientation of PBI molecules on the glass surface (aromatic core perpendicular to

the glass surface). The layer height of 4.0 ± 0.5 nm found for (*M*)-**1** thin film is in perfect accordance with the X-ray diffraction data. For (*rac*)-**1** a lower height of the layers of 3.0 ± 0.4 nm is estimated in agreement with X-ray results for the homogenously aligned columns. Moreover, the packing of (*rac*)-**1** seems much tighter than for (*M*)-**1**.

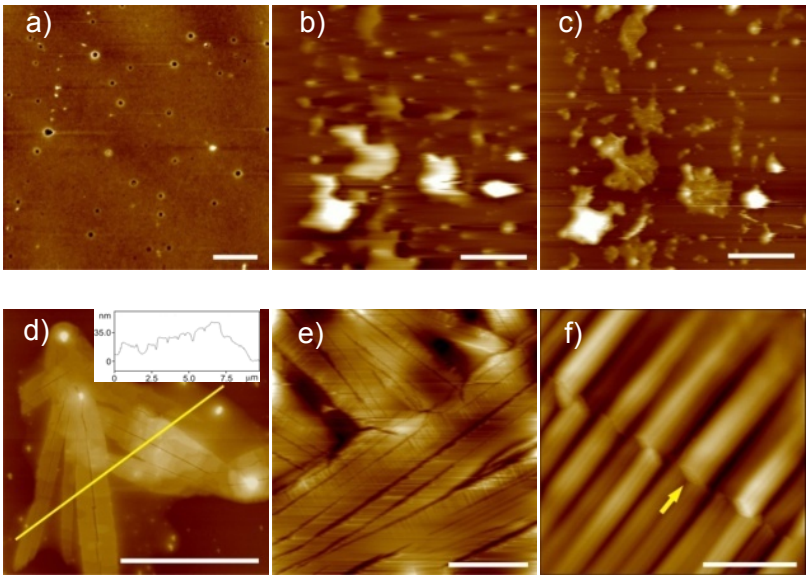

Figure 12. AFM height images of (*rac*)-**1** measured during a heating-cooling cycle on glass surface: a) at RT after evaporation of the solvent of the drop-casted *n*-hexane solution (c = 10^{-3} M); b) melting drops at 235 °C; c) first nanocrystals formed at 200 °C; d) close view of nanocrystal after cooling down from 235 °C to RT, insert shows cross-section profile along the yellow line; e) nanocrystal at RT; f) magnification of image (e) showing details of the layers (yellow arrow). The scale bar is 5 µm (a–d), 30 µm (e), and 1.5 µm (f). The z scale is 30 nm (a), 100 nm (b–e), and 80 nm (f).

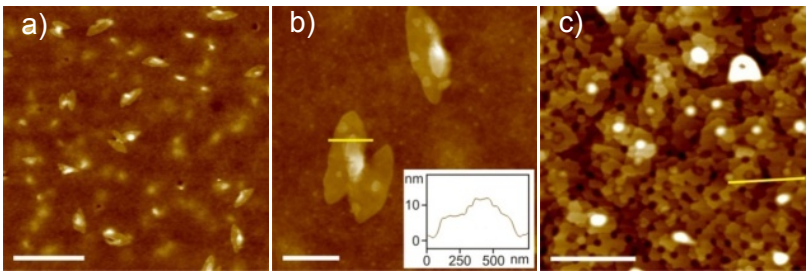

Figure 13. AFM height images of (*M*)-**1** measured during a heating-cooling cycle on glass surface: a) thin film at RT prepared by drop-casting of *n*-hexane solution (c = 10^{-3} M); b) enlargement of image (a) showing additionally the cross-section profile along the yellow line; c) thin film resulted from cooling down from the isotropic phase. The scale bar is 4 µm (a,c) and 1 µm (b). The z scale is 50 nm (a,b) and 40 nm (c).

To verify the higher viscosity of the racemate, measurements of the elasticity module

were carried out for both, racemate and pure enantiomer.[107] For (*M*)-**1**, it was not possible to obtain an elasticity module value due to the liquid crystalline, fluid nature of the film on the glass surface. A value of 0.052 MPa was obtained for the film of (*rac*)-**1** confirming its higher viscosity compared with the enantiomerically pure material, and thus consistent with the soft crystalline nature of this mesophase (Figure 14).

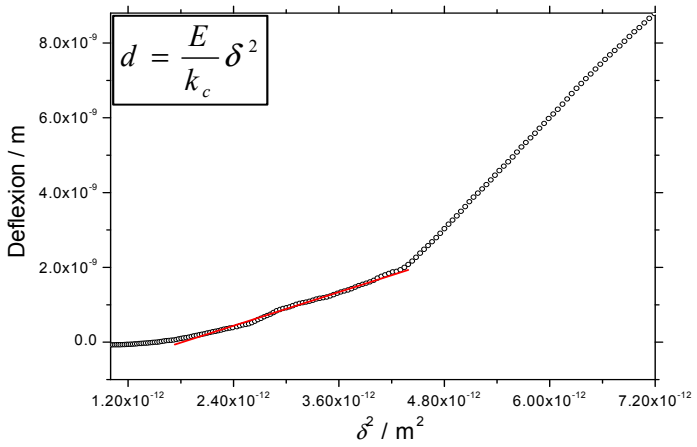

Figure 14. Deflection of the AFM tip as a function of the square of the indentation depth for (*rac*)-**1** and corresponding applied equation for obtaining the elasticity module, where d is the vertical displacement of the cantilever, k_C is the stiffness of the cantilever, δ is the indentation depth and E is the elasticity module.

4.3. Conclusions

With our careful examination of the thermal properties and the packing of chiral PBIs **1** in the condensed state we have been able to elucidate molecular codes of relevance for self-assembled soft materials. We have demonstrated here for the first time the impact of chirality induced by the twisting of the aromatic core for the condensed state properties of PBIs. The simultaneous presence of equal amounts of each enantiomers in (*rac*)-**1** allows this material to self-organize in a soft columnar crystalline phase of higher thermodynamic stability in comparison to the enantiopure (*M*)-**1** (or (*P*)-**1**), which organizes in lamellar liquid crystalline phase. In the light of experimental data supported by force field calculations of the condensed state packing, and taking into account the preference for the formation of π–π-stacked homochiral dimers for (*rac*)-**1** and (*M*)-**1** or (*P*)-**1** as demonstrated previously in solution, our results indicate that nanosegregation and interaction between the bridging units are the crucial parameters for the difference in their

condensed state properties. Alternation of *MM* and *PP* homochiral dimers in the condensed phase of (*rac*)-**1** allows for excellent nanosegregation and dense packing of the dimeric supramolecular building blocks in columns. In contrast, for enantiomerically pure (*M*)-**1** (or (*P*)-**1**) the bridging units can be regarded as sterically shielding entities preventing nanosegregation into columns, leading consequently to a lamellar organization of the chromophores and a highly fluid mesophase. The realization of mesophases of low viscosity which are very uncommon for such large polycyclic aromatic hydrocarbons might be of considerable interest for other groups that are interested in alignment of organic semiconductors by simple techniques such as shearing.

4.4. Experimental Section

Materials and Methods

Macrocyclic PBIs **1** were synthesized according to the procedure reported recently.[70]

Instruments

For all spectroscopic measurements, spectroscopic grade solvents (Uvasol®) were used. UV/Vis spectra were measured on Perkin Elmer PE 950 under ambient conditions. Circular dichroism (CD) spectra were measured with a JASCO J-810 spectrometer equipped with a CDF-242 peltier element. Differential scanning calorimetry (DSC) measurements were carried out using a TA Q1000 calorimeter with a heating/cooling rate of 10 °C min^{-1}. At least two heating–cooling cycles were performed for each compound. Optical textures of the liquid crystal phases at crossed polarizer were acquired with an Olympus BX-41 polarization microscope equipped with a Linkam THMS 600 hot stage and a temperature controller unit.

UV/Vis and CD Measurements

CD and UV/Vis experiments of (*rac*)-**1**, (*M*)-**1** and (*P*)-**1** thin films were performed and compared with previous studies in solution (*n*-hexane, $c = 10^{-3}$ M). Thin films were prepared by spin-coating of a 5×10^{-3} M solution in chloroform on a quartz surface in two steps, first at 1500 rpm and after 5 seconds at 3000 rpm for additional 10 seconds, in order

to obtain a good dispensing of the liquid at low speeds and homogenization at higher speed.

X-ray Diffraction

X-ray diffraction measurements were performed on extruded samples in glass capillaries of 1.5 mm diameter. The wide angle X-ray scattering (WAXS) measurements were carried out using a standard copper anode (2.2 kW) source with pinhole collimation equipped with an X-ray mirror (Osmic type CMF15-sCu6) and a Bruker detector (Highstar) with 1024 × 1024 pixels. The diffraction data were calibrated by using silver behenate as a calibration standard.[108] The X-ray patterns were analyzed with the datasqueeze software (http://www.data squeezesoftware.com/).

Modeling

The modeling of the columnar structure was performed using the program package Materials Studio from Accelrys. The structures were geometry minimized and annealed by employing the force field COMPASS in the module Forcite Plus.

Atomic Force Microscopy (AFM)

The AFM images were recorded on Nanoscope IV controller Veeco Multi Mode by using an E-scanner with a maximum scan area of 15 × 15 mm. Silicon cantilevers with a nominal spring constant of 34.0–71.0 N m^{-1} and with resonant frequency of 300 kHz, and a typical tip radius of 7 nm (OMCLAC160TS, Olympus) were employed. Solution of PBI **1** in *n*-hexane ($c = 4 \times 10^{-3}$ M) was spin-coated onto a glass surface under 7000 rpm.

4.5. References and Notes

(1) Puigmartí-Luis, J.; Laukhin, V.; del Pino, A. P.; Vidal-Gancedo, J.; Rovira, C.; Laukhina, E.; Amabilino, D. B. *Angew. Chem., Int. Ed.* **2007**, *46*, 238.
(2) Yamamoto, Y.; Fukushima, T.; Suna, Y.; Ishii, N.; Saeki, A.; Seki, S.; Tagawa, S.; Taniguchi, M.; Kawai, T.; Aida, T. *Science* **2006**, *314*, 1761.
(3) Hill, J. P.; Jin, W. S.; Kosaka, A.; Fukushima, T.; Ichihara, H.; Shimomura, T.; Ito, K.; Hashizume, T.; Ishii, N.; Aida, T. *Science* **2004**, *304*, 1481.
(4) van der Boom, T.; Hayes, R. T.; Zhao, Y. Y.; Bushard, P. J.; Weiss, E. A.; Wasielewski, M. R. *J. Am. Chem. Soc.* **2002**, *124*, 9582.
(5) Bell, A. T. *Science* **2003**, *299*, 1688.

(6) Wessig, P. *Angew. Chem., Int. Ed.* **2006**, *45*, 2168.
(7) Zhang, X.; Rehm, S.; Safont-Sempere, M. M.; Würthner, F. *Nature Chem.* **2009**, *1*, 623-629.
(8) Hatchett, D. W.; Josowicz, M. *Chem. Rev.* **2008**, *108*, 746.
(9) Bell, T. W.; Hext, N. M. *Chem Soc Rev* **2004**, *33*, 589.
(10) Kitaev, V. *J. Mater. Chem.* **2008**, *18*, 4745.
(11) Hu, X. B.; An, Q.; Li, G. T.; Tao, S. Y.; Liu, B. *Angew. Chem., Int. Ed.* **2006**, *45*, 8145.
(12) Pu, L. *Chem. Rev.* **2004**, *104*, 1687.
(13) Kato, T.; Hirai, Y.; Nakaso, S.; Moriyama, M. *Chem. Soc. Rev.* **2007**, *36*, 1857.
(14) Goodby, J. W.; Gortz, V.; Cowling, S. J.; Mackenzie, G.; Martin, P.; Plusquellec, D.; Benvegnu, T.; Boullanger, P.; Lafont, D.; Queneau, Y.; Chambert, S.; Fitremann, J. *Chem. Soc. Rev.* **2007**, *36*, 1971.
(15) Kato, T.; Mizoshita, N.; Kishimoto, K. *Angew. Chem., Int. Ed.* **2006**, *45*, 38.
(16) Goodby, J. W. *Chem. Soc. Rev.* **2007**, *36*, 1855.
(17) Kato, T.; Yasuda, T.; Kamikawa, Y.; Yoshio, M. *Chem. Commun.* **2009**, 729.
(18) Laschat, S.; Baro, A.; Steinke, N.; Giesselmann, F.; Högele, C.; Scalia, G.; Judele, R.; Kapatsina, E.; Sauer, S.; Schreivogel, A.; Tosoni, M. *Angew. Chem., Int. Ed.* **2007**, *46*, 4832.
(19) Pisula, W.; Kastler, M.; Wasserfallen, D.; Robertson, J. W. F.; Nolde, F.; Kohl, C.; Müllen, K. *Angew. Chem., Int. Ed.* **2006**, *45*, 819.
(20) Schmidt-Mende, L.; Fechtenkötter, A.; Müllen, K.; Moons, E.; Friend, R. H.; MacKenzie, J. D. *Science* **2001**, *293*, 1119.
(21) Sergeyev, S.; Pisula, W.; Geerts, Y. H. *Chem. Soc. Rev.* **2007**, *36*, 1902.
(22) Crispin, X.; Cornil, A.; Friedlein, R.; Okudaira, K. K.; Lemaur, V.; Crispin, A.; Kestemont, G.; Lehmann, M.; Fahlman, M.; Lazzaroni, R.; Geerts, Y.; Wendin, G.; Ueno, N.; Bredas, J. L.; Salaneck, W. R. *J. Am. Chem. Soc.* **2004**, *126*, 11889.
(23) Nelson, J. *Science* **2001**, *293*, 1059.
(24) Simpson, C. D.; Wu, J. S.; Watson, M. D.; Müllen, K. *J. Mater. Chem.* **2004**, *14*, 494.
(25) Hoeben, F. J. M.; Jonkheijm, P.; Meijer, E. W.; Schenning, A. *Chem. Rev.* **2005**, *105*, 1491.
(26) Ego, C.; Marsitzky, D.; Becker, S.; Zhang, J. Y.; Grimsdale, A. C.; Müllen, K.; MacKenzie, J. D.; Silva, C.; Friend, R. H. *J. Am. Chem. Soc.* **2003**, *125*, 437.
(27) Belaissaoui, A.; Cowling, S. J.; Saez, I. M.; Goodby, J. W. *Soft Matter* **2010**, *6*, 1958.
(28) Hough, L. E.; Spannuth, M.; Nakata, M.; Coleman, D. A.; Jones, C. D.; Dantlgraber, G.; Tschierske, C.; Watanabe, J.; Körblova, E.; Walba, D. M.; Maclennan, J. E.; Glaser, M. A.; Clark, N. A. *Science* **2009**, *325*, 452.
(29) Goodby, J. W.; Saez, I. M.; Cowling, S. J.; Görtz, V.; Draper, M.; Hall, A. W.; Sia, S.; Cosquer, G.; Lee, S. E.; Raynes, E. P. *Angew. Chem., Int. Ed.* **2008**, *47*, 2754.
(30) Tejedor, R. M.; Oriol, L.; Serrano, J. L.; Sierra, T. *J. Mater. Chem.* **2008**, *18*, 2899.
(31) Barberá, J.; Cavero, E.; Lehmann, M.; Serrano, J. L.; Sierra, T.; Vázquez, J. T. *J. Am. Chem. Soc.* **2003**, *125*, 4527.

(32) Okamoto, K.; Matsuoka, Y.; Wakabayashi, N.; Yamagishi, A.; Hoshino, N. *Chem. Commun.* **2002**, 282.
(33) Walba, D. M.; Körblova, E.; Shao, R.; Maclennan, J. E.; Link, D. R.; Glaser, M. A.; Clark, N. A. *Science* **2000**, *288*, 2181.
(34) Barberá, J.; Iglesias, R.; Serrano, J. L.; Sierra, T.; de la Fuente, M. R.; Palacios, B.; Pérez-Jubindo, M. A.; Vázquez, J. T. *J. Am. Chem. Soc.* **1998**, *120*, 2908.
(35) Bock, H.; Helfrich, W. *Liq. Cryst.* **1995**, *18*, 707.
(36) Scherowsky, G.; Chen, X. H. *Liq. Cryst.* **1994**, *17*, 803.
(37) Gubler, U.; Bosshard, C. *Nature Materials* **2002**, *1*, 209.
(38) Verbiest, T.; Van Elshocht, S.; Kauranen, M.; Hellemans, L.; Snauwaert, J.; Nuckolls, C.; Katz, T. J.; Persoons, A. *Science* **1998**, *282*, 913.
(39) Brettar, J.; Bürgi, T.; Donnio, B.; Guillon, D.; Klappert, R.; Scharf, T.; Deschenaux, R. *Adv. Funct. Mater.* **2006**, *16*, 260.
(40) Abraham, S.; Paul, S.; Narayan, G.; Prasad, S. K.; Rao, D. S. S.; Jayaraman, N.; Das, S. *Adv. Funct. Mater.* **2005**, *15*, 1579.
(41) Tamaoki, N. *Adv. Mater.* **2001**, *13*, 1135.
(42) Huang, Y. W.; Yan, Y.; Smarsly, B. M.; Wei, Z. X.; Faul, C. F. J. *J. Mater. Chem.* **2009**, *19*, 2356.
(43) Dehm, V.; Chen, Z. J.; Baumeister, U.; Prins, P.; Siebbeles, L. D. A.; Würthner, F. *Org. Lett.* **2007**, *9*, 1085.
(44) Percec, V.; Dulcey, A. E.; Balagurusamy, V. S. K.; Miura, Y.; Smidrkal, J.; Peterca, M.; Nummelin, S.; Edlund, U.; Hudson, S. D.; Heiney, P. A.; Hu, D. A.; Magonov, S. N.; Vinogradov, S. A. *Nature* **2004**, *430*, 764.
(45) Bushey, M. L.; Hwang, A.; Stephens, P. W.; Nuckolls, C. *Angew. Chem., Int. Ed.* **2002**, *41*, 2828.
(46) Nuckolls, C.; Katz, T. J. *J. Am. Chem. Soc.* **1998**, *120*, 9541.
(47) Yang, C. W.; Hsia, T. H.; Chen, C. C.; Lai, C. K.; Liu, R. S. *Org. Lett.* **2008**, *10*, 4069.
(48) Fasel, R.; Parschau, M.; Ernst, K. H. *Nature* **2006**, *439*, 449.
(49) Wigglesworth, T. J.; Sud, D.; Norsten, T. B.; Lekhi, V. S.; Branda, N. R. *J. Am. Chem. Soc.* **2005**, *127*, 7272.
(50) Rajca, A.; Miyasaka, M.; Pink, M.; Wang, H.; Rajca, S. *J. Am. Chem. Soc.* **2004**, *126*, 15211.
(51) Phillips, K. E. S.; Katz, T. J.; Jockusch, S.; Lovinger, A. J.; Turro, N. J. *J. Am. Chem. Soc.* **2001**, *123*, 11899.
(52) Amemiya, R.; Yamaguchi, M. *Org. Biomol. Chem.* **2008**, *6*, 26.
(53) Schmuck, C. *Angew. Chem., Int. Ed.* **2003**, *42*, 2448.
(54) Grimme, S.; Harren, J.; Sobanski, A.; Vogtle, F. *Eur. J. Org. Chem.* **1998**, 1491.
(55) Zhou, Y. C.; Zhang, D. Q.; Zhang, Y. Z.; Tang, Y. L.; Zhu, D. B. *J. Org. Chem.* **2005**, *70*, 6164.
(56) van Delden, R. A.; Mecca, T.; Rosini, C.; Feringa, B. L. *Chem. Eur. J.* **2004**, *10*, 61.
(57) Terada, M. *Chem. Commun.* **2008**, 4097.
(58) Tsubaki, K. *Org. Biomol. Chem.* **2007**, *5*, 2179.

(59) Pu, L. *Chem. Rev.* **1998**, *98*, 2405.
(60) Ceccacci, F.; Mancini, G.; Sferrazza, A.; Villani, C. *J. Am. Chem. Soc.* **2005**, *127*, 13762.
(61) Ceccacci, F.; Diociaiuti, M.; Galantini, L.; Mancini, G.; Mencarelli, P.; Scipioni, A.; Villani, C. *Org. Lett.* **2004**, *6*, 1565.
(62) Bringmann, G.; Mortimer, A. J. P.; Keller, P. A.; Gresser, M. J.; Garner, J.; Breuning, M. *Angew. Chem., Int. Ed.* **2005**, *44*, 5384.
(63) Hilton, C. L.; Crowfoot, J. M.; Rempala, P.; King, B. T. *J. Am. Chem. Soc.* **2008**, *130*, 13392.
(64) Pérez, D.; Guitián, E. *Chem. Soc. Rev.* **2004**, *33*, 274.
(65) Walters, R. S.; Kraml, C. M.; Byrne, N.; Ho, D. M.; Qin, Q.; Coughlin, F. J.; Bernhard, S.; Pascal, R. A. *J. Am. Chem. Soc.* **2008**, *130*, 16435.
(66) Lu, J.; Ho, D. M.; Vogelaar, N. J.; Kraml, C. M.; Pascal, R. A. *J. Am. Chem. Soc.* **2004**, *126*, 11168.
(67) Pascal, R. A. *Chem. Rev.* **2006**, *106*, 4809.
(68) Chen, Z. J.; Lohr, A.; Saha-Möller, C. R.; Würthner, F. *Chem. Soc. Rev.* **2009**, *38*, 564.
(69) Chen, Z. J.; Baumeister, U.; Tschierske, C.; Würthner, F. *Chem. Eur. J.* **2007**, *13*, 450.
(70) Safont-Sempere, M. M.; Stepanenko, V.; Lehmann, M.; Würthner, F. *Chem. Eur. J.* **2010**, *16*, 7376.
(71) Osswald, P.; Würthner, F. *J. Am. Chem. Soc.* **2007**, *129*, 14319.
(72) Würthner, F. *Chem. Commun.* **2004**, 1564.
(73) Jaiser, F.; Neher, D.; Meisel, A.; Nothofer, H. G.; Miteva, T.; Herrmann, A.; Müllen, K.; Scherf, U. *J. Chem. Phys.* **2008**, *129*, 114901.
(74) Pandey, A. K.; Nunzi, J. M. *Appl. Phys. Lett.* **2007**, *90*, 263508.
(75) Schmidt, R.; Oh, J. H.; Sun, Y. S.; Deppisch, M.; Krause, A. M.; Radacki, K.; Braunschweig, H.; Könemann, M.; Erk, P.; Bao, Z. A.; Würthner, F. *J. Am. Chem. Soc.* **2009**, *131*, 6215.
(76) Weitz, R. T.; Amsharov, K.; Zschieschang, U.; Villas, E. B.; Goswami, D. K.; Burghard, M.; Dosch, H.; Jansen, M.; Kern, K.; Klauk, H. *J. Am. Chem. Soc.* **2008**, *130*, 4637.
(77) Jones, B. A.; Facchetti, A.; Wasielewski, M. R.; Marks, T. J. *Adv. Funct. Mater.* **2008**, *18*, 1329.
(78) Jones, B. A.; Facchetti, A.; Wasielewski, M. R.; Marks, T. J. *J. Am. Chem. Soc.* **2007**, *129*, 15259.
(79) Lindner, S. M.; Huttner, S.; Chiche, A.; Thelakkat, M.; Krausch, G. *Angew. Chem., Int. Ed.* **2006**, *45*, 3364.
(80) Peumans, P.; Uchida, S.; Forrest, S. R. *Nature* **2003**, *425*, 158.
(81) Debije, M. G.; Chen, Z. J.; Piris, J.; Neder, R. B.; Watson, M. M.; Müllen, K.; Würthner, F. *J. Mater. Chem.* **2005**, *15*, 1270.
(82) An, Z. S.; Yu, J. S.; Jones, S. C.; Barlow, S.; Yoo, S.; Domercq, B.; Prins, P.; Siebbeles, L. D. A.; Kippelen, B.; Marder, S. R. *Adv. Mater.* **2005**, *17*, 2580.
(83) Chen, Z. J.; Stepanenko, V.; Dehm, V.; Prins, P.; Siebbeles, L. D. A.; Seibt, J.;

Marquetand, P.; Engel, V.; Würthner, F. *Chem. Eur. J.* **2007**, *13*, 436.
(84) Gsänger, M.; Oh, J. H.; Könemann, M.; Höffken, H. W.; Krause, A. M.; Bao, Z. N.; Würthner, F. *Angew. Chem., Int. Ed.* **2010**, *49*, 740.
(85) Osswald, P.; Reichert, M.; Bringmann, G.; Würthner, F. *J. Org. Chem.* **2007**, *72*, 3403.
(86) Osswald, P.; Würthner, F. *Chem. Eur. J.* **2007**, *13*, 7395.
(87) Wicklein, A.; Lang, A.; Muth, M.; Thelakkat, M. *J. Am. Chem. Soc.* **2009**, *131*, 14442.
(88) Hansen, M. R.; Schnitzler, T.; Pisula, W.; Graf, R.; Müllen, K.; Spiess, H. W. *Angew. Chem., Int. Ed.* **2009**, *48*, 4621.
(89) Würthner, F.; Chen, Z. J.; Dehm, V.; Stepanenko, V. *Chem. Commun.* **2006**, 1188.
(90) Jacques, J.; Collet, A.; Wilen, S. H. *Enantiomers, Racemates, and Resolutions*; Wiley: New York, 1981.
(91) Brock, C. P.; Schweizer, W. B.; Dunitz, J. D. *J. Am. Chem. Soc.* **1991**, *113*, 9811.
(92) Bahr, C.; Heppke, G.; Sabaschus, B. *Liq. Cryst.* **1991**, *9*, 31.
(93) Dierking, I. *Textures of Liquid Crystals*; Wiley-VCH: Weinheim, 2003.
(94) Collings, P. J.; Hird, M. *Introduction to Liquid Crystals. Chemistry and Physics*; Taylor & Francis: London, 1997.
(95) Wang, J. Y.; Yan, J.; Ding, L.; Ma, Y. G.; Pei, J. *Adv. Funct. Mater.* **2009**, *19*, 1746.
(96) Reczek, J. J.; Villazor, K. R.; Lynch, V.; Swager, T. M.; Iverson, B. L. *J. Am. Chem. Soc.* **2006**, *128*, 7995.
(97) Lozman, O. R.; Bushby, R. J.; Vinter, J. G. *J. Chem. Soc., Perkin Trans. 2* **2001**, 1446.
(98) Arikainen, E. O.; Boden, N.; Bushby, R. J.; Lozman, O. R.; Vinter, J. G.; Wood, A. *Angew. Chem., Int. Ed.* **2000**, *39*, 2333.
(99) Lehmann, M.; Köhn, C.; Meier, H.; Renker, S.; Oehlhof, A. *J. Mater. Chem.* **2006**, *16*, 441.
(100) Donnio, B.; Heinrich, B.; Allouchi, H.; Kain, J.; Diele, S.; Guillon, D.; Bruce, D. W. *J. Am. Chem. Soc.* **2004**, *126*, 15258.
(101) The theoretical surface of the PBI core was measured taking into account the modelled by AM1 core, which give diagonal values of 13.4 and 19.8 Å.
(102) Berova, N.; Nakanishi, K. *Circular Dichroism: Methods and Applications*; VCH: New York, 2000.
(103) Berova, N.; Di Bari, L.; Pescitelli, G. *Chem. Soc. Rev.* **2007**, *36*, 914-931.
(104) Buss, V.; Reichardt, C. *Chem. Commun.* **1992**, 1636-1638.
(105) UV/Vis spectra of (*rac*)-**1**, (*M*)-**1** and (*P*)-**1** are equal in solution and in thin film.
(106) Only (*M*)-**1** was investigated, as the morphology surfaces for the enantiomeric (*M*)-**1** and (*P*)-**1** should be the same.
(107) This value has been calculated from the average height of several layers in different points of the image.
(108) Huang, T. C.; Toraya, H.; Blanton, T. N.; Wu, Y. *J. Appl. Crystallogr.* **1993**, *26*, 180-184.

Chapter 5

Impact of Flexibility on Binding Strength and Self-Sorting of Chiral π-Surfaces

Abstract: In this chapter the successful synthesis of a series of conformationally stable chiral perylene bisimide (PBI) dyes is presented via introduction of different sized oligoethylene glycol (OEG) bridging units that shield one π-surface of the PBI aromatic core –allowing the exclusive formation of self-assembled dimers– and restrict the interconversion between *M* and *P* enantiomers. ^{1}H NMR and vapour pressure osmometry (VPO) studies offer valuable structural information of the dimeric self-assembled species. Circular dichroism (CD) investigations show the consequences of flexibility changes in the PBI naphthalene subunits –related to changes on the chiral surface of these macrocyclic PBIs– and the chiral supramolecular nature of the formed dimers. Concentration-dependent UV/Vis studies allow us to calculate the binding constants for the dimerization processes and quantify the ratio homo vs. heterochiral dimers of the different bridged PBIs illustrated in this work. Quantum mechanical calculations and experimental data revealed the differences between the relative energies of hetero vs. homodimers. Whilst in Chapter 3 the prevalence of self-recognition over self-discrimination in the dimerization process in solution and condensed state was demonstrated for a short bridged atropo-enantiomeric PBI, here it is revealed how a subtle change in the structure flexibility affects the chiral self-recognition efficiency and binding strength in the dimerization process and consequently the properties of these atropo-enantiomeric PBIs in solution and condensed state.

5.1. Introduction

A first example for *Chiral Self-Sorting* of perylene bisimide (PBI) dyes was introduced in Chapter 3 based on a stable atropo-enantiomeric macrocyclic PBI. Perylene bisimide (PBI) dyes are an outstanding class of chromophores which due to their optical and electronic properties[1] have been widely used for the development of functional organic materials such as organic light emitting diodes (OLEDs),[2-4] organic field effect transistors (OFETs)[5-8] and solar cells.[9-11] Moreover, by means of X-ray diffraction analysis of different bay-substituted PBIs it could be demonstrated that the introduction of substituents in the bay area leads to a twist of the two naphthalene units of the former planar perylene core caused by repulsive interactions of these substituents in the bay area.[8,12-19] The extent of this twisting is related to the bulkiness of the bay substituents varying from 4° for a 1,7-difluorosubstituted PBI[8,18] up to 37° for 1,6,7,12-tetrachloro derivatives.[16,20] A most interesting feature of the twisted perylene core is symmetry breaking leading to inherent chirality of the backbone. However, the isolation of single atropo-enantiomeric PBIs has been scarcely achieved as in most of the reported bay-substituted PBIs the two enantiomers are in a dynamic equilibrium.[21,22] To prevent racemization and thus, to achieve conformationally stable atropo-enantiomeric and diastereomeric PBIs our group has attached one or two bridging units shielding one or two of the PBI π-faces, respectively.[23-25] Similar approaches have been applied also for other dyes, e.g. porphyrins by Osuka[26-29] and coworkers and oligothiophenes by Takeuchi[30,31] and coworkers or for some special liquid crystalline substances by Swager[32-34] and coworkers to induce intriguing mesophase properties. In a recent communication we have shown by NMR and concentration-dependent UV/Vis studies the formation of π–π-stacked dimers with preferential self-recognition, i.e. *MM* and *PP* dimers for a derivative with a rather short bridging unit connected to the 1- and 7- bay positions (Chapter 3).[23] Other studies of self-sorting (chiral and general) of PBIs have been reported by Li and co-workers, however with conformationally unstable atropisomeric PBIs.[35] They provided strong evidence that the chiral self-recognition process was favored due to the better overlapping of the π-surfaces between the equal enantiomers. They also reported that the extent of twisting of the PBI cores caused by different sized bay substituents can be used as efficient molecular code leading to self-

recognition.[36] In our actual work we present the synthesis of a series of PBIs, bearing oligoethylene glycol (OEG) bridges of different length between the 1 and 7 bay positions. It has to be noted that the substituents directly attached at the 1,7-bay positions are in all cases phenoxy units which afford identical repulsive interactions between the bay substituents and thus an equal twist of the naphthalene entities. However, elongation of the OEG bridging units provides the molecules with greater flexibility, leading to a larger conformational space and a less "imprinted" inherent chirality (see Figure 1), which seriously affects two determinant features: chiral self-sorting of these molecules and binding strength in the dimerization process. We observed that the increase of flexibility in the PBI cores affects negatively the self-recognition process previously demonstrated for PBI **4a** (Chapter 3).[23] On the contrary, increase of the binding strength by this dimerization process upon elongation of the bridging units have been observed, which revealed that induced-fit [37,38] play a determinant role in our system. The induced-fit principle has been widely applied to explain the complexation process in various natural[37-41] and synthetic[42-47] host-guest systems, in which the flexibility of the structures allow undergoing structural changes to form more stable host-guest complexes or selective binding of specific guests. Similarly, our differently flexible macrocyclic PBIs can undergo structural changes in order to form more stable self-assembled structures optimizing the π–π-contact surfaces.

Figure 1. Schematic representation of novel strapped atropo-enantiomeric PBIs **4a–c** and variation of the naphthalene units twisting angle depending on the bridge length.

Moreover, the condensed and solid state properties of the new synthesized PBIs are deeply influenced by changes on the structure flexibility, reflected on significant differences between the racemates and their respective pure enantiomers –due to the different extent of

chiral self-sorting–, as well as between the different bridged PBIs –related to the different OEG units, which give different packing possibilities–.

5.2. Results and Discussion

5.2.1. Synthesis

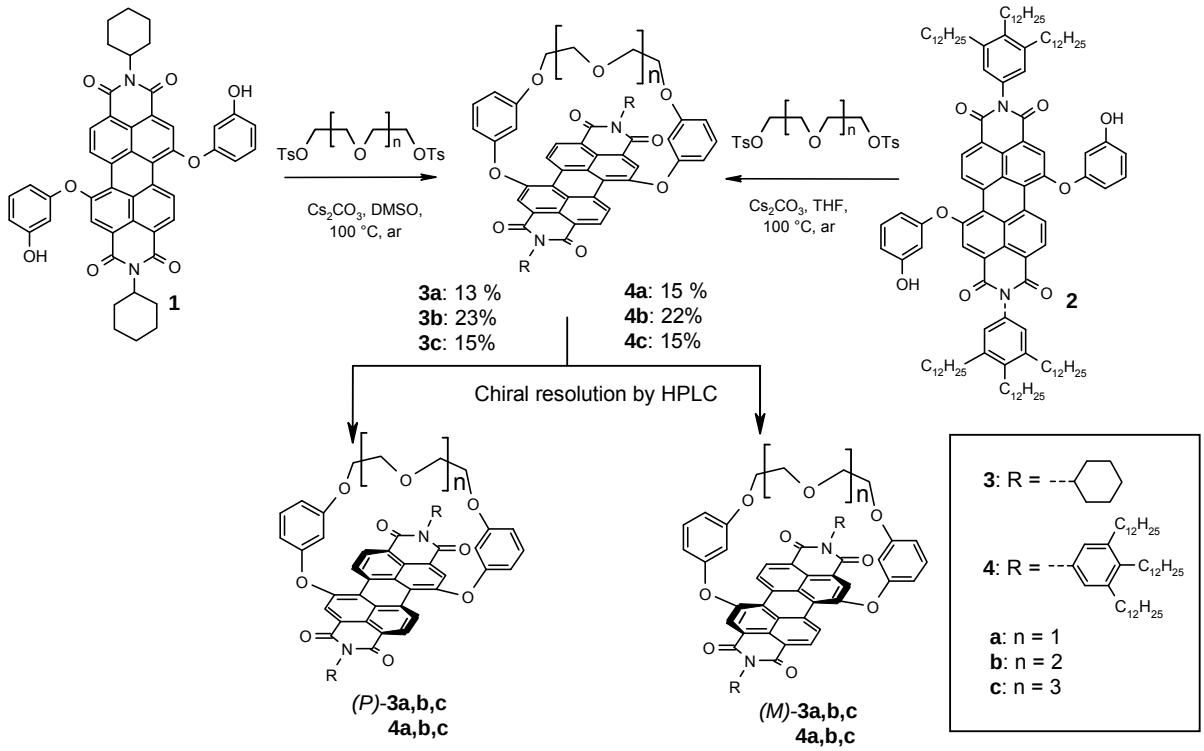

Scheme 1. Synthesis of macrocyclic PBIs **3** and **4**.

PBIs **3** and **4** were synthesized from previously reported precursors **1** and **2**, respectively (see Chapter 3). The 3,4,5-trisdodecylphenyl substituents in PBIs **4a–c** were introduced to provide the molecules with mesogenic properties and better solubility, while the cyclohexane substituents in PBIs **3a–c** facilitate the single crystal growth. The free OH groups of PBIs **1** and **2** are available for a two fold Williamson etherification with different sized ditosylates.[48] The macrocyclization reaction takes place in the presence of cesium carbonate, which is known to facilitate ring closures.[49] A solution of the respective ditosylate was slowly dropped over several hours using a syringe pump into a solution of the precursors **1** or **2** in DMSO or THF, respectively. After work up of the reaction mixtures the desired macrocycles **3a–c** and

4a–c could be isolated as racemates. The chiral resolution of those could be achieved by HPLC on a chiral column (Trentec Reprosil 100 chiral-NR) using different experimental conditions for each macrocycle in a purity of over 99% (see below for details).

5.2.2. Optical Properties of the Monomers

The optical properties of monomeric macrocycles **3** and **4** were investigated by UV/Vis, fluorescence and circular dichroism (CD) spectroscopy. The UV/Vis absorption of the racemates (no changes are observed in comparison with the UV/Vis spectra of the enantiomers) and CD spectra of their respective enantiomers in dichloromethane (DCM) are shown in Figure 2 and their optical data are summarized in Tables 1 and 2.

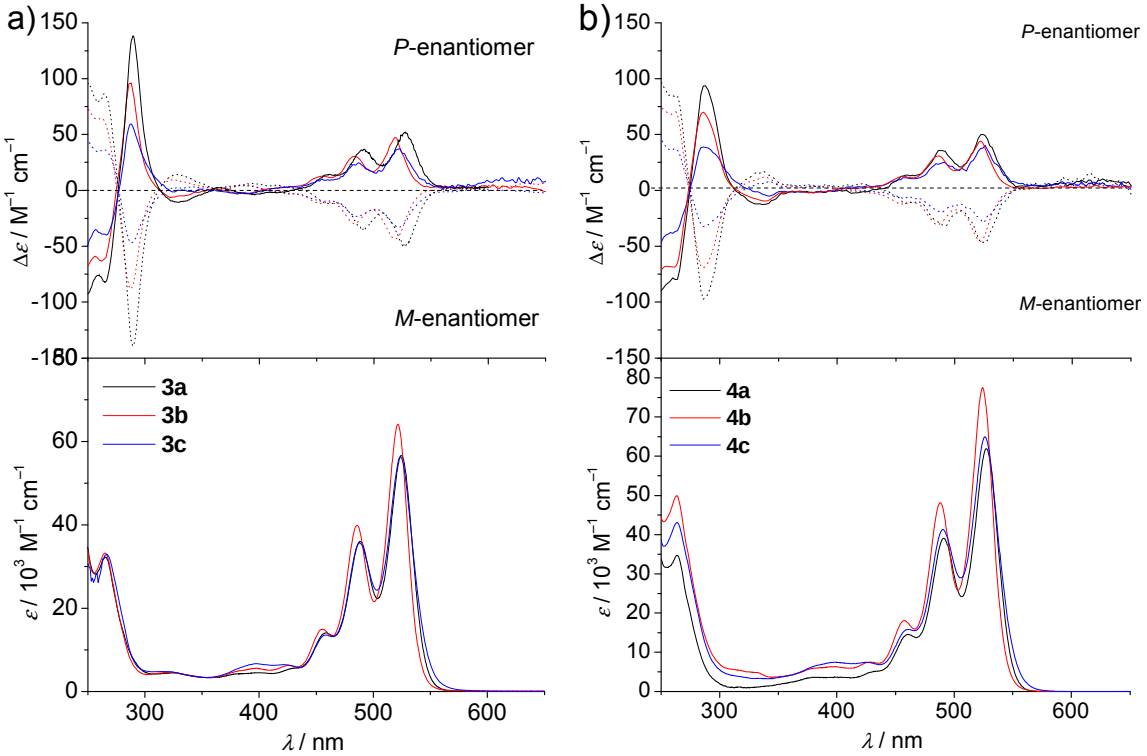

Figure 2. Bottom panel: UV/Vis absorption spectra of racemic solution in DCM at 5×10^{-6} M. Top panel: CD spectra of *P* enantiomer (solid lines) and *M* enantiomers (dashed lines) in DCM at 5×10^{-6} M. Figure (a) corresponds to macrocycles **3a–c** and Figure (b) to macrocycle **4a–c**.

The absorption spectra of macrocyclic PBIs **3a–c** and **4a–c** reveal S_0-S_1 transition with three vibronic progressions between 527–524 nm, 492–490 nm and 462–459 nm in DCM (Figure 2). The higher energetic S_0-S_2 transition has almost disappeared in the case of **3a** and **4a** while for **3c** and **4c** it is clearly visible. The absorption coefficients are lower for **3a–c**

derivatives than for the respective derivatives **4a–c** (Table 1 and 2). This appears to be a general absorption phenomenon and has been observed for other PBIs with alkyl and aromatic substituents in imide positions.[50] Some minor changes in the shape of the UV/Vis spectra are observed for **3**/**4a**, **3**/**4b** and **3**/**4c** that should be attributed to structural changes related to the different bridge lengths. The CD spectra of *M* and *P* enantiomers of **3a–c** and **4a–c** (top panels, Figure 2) are mirror images as expected for pure enantiomers. The stereochemical assignment of these enantiomers was achieved by comparison of the respective CD spectra with those of previously reported structurally similar epimerically pure *P*- and *M*-configured macrocyclic PBIs.[51]

Table 1. Optical properties of macrocyclic PBIs **3a–c** in DCM.

	$\lambda_{max(abs)}$ / nm	ε / $M^{-1}cm^{-1}$	$\lambda_{max(em)}$ / nm	ϕ_{FL}	$\Delta\varepsilon(P)^a$	$\Delta\varepsilon(M)^a$
3a	525	56000	538	27%	51	–49
3b	522	64000	533	33%	43	–44
3c	525	56000	550	57%	36	–33

[a] Determined for maximum emission of S_0-S_1 transition

Table 2. Optical properties of macrocyclic PBIs **4a–c** in DCM.

	$\lambda_{max(abs)}$ / nm	ε / $M^{-1}cm^{-1}$	$\lambda_{max(em)}$ / nm	ϕ_{FL}	$\Delta\varepsilon(P)^a$	$\Delta\varepsilon(M)^a$
4a	525	65000	545	9%	49	–47
4b	522	76000	534	14%	43	–45
4c	525	65000	553	25%	37	–33

[a] Determined for maximum emission of S_0-S_1 transition

Bisignate Cotton effects are not observed in the visible region. This observation supports the exclusive presence of monomeric species at this concentration ($c = 5 \times 10^{-6}$ M) in DCM and the absence of excitonic coupling in the S_0-S_1 transitions spectral range. The fact that the CD signal decreases in intensity upon increasing the bridge length (top panels, Figure 2, Table 1 and 2) is another evidence that this CD band solely originates from the twisted core. The drop of the signal intensity is about 33% from **3,4a** (shortest bridge) to **3,4c** (largest bridge) in the visible region. The latter effect is even more pronounced in the ultraviolet region with a descent in the intensity of about 58%. Here a distinct bisignate Cotton effect is observed that can be attributed to the chiral excitonic coupling between transition dipole moments that are

polarized perpendicular to the long molecular axis within the two naphthalene subunits in the PBI aromatic core. The magnitude of Δε for such excitonic coupling is directly related to the twist angle which is a consequence of repulsive interactions between the sterically encumbered bay substituents.[14-16,24] Although racemization via atropo-enantiomeric interconversion is not possible for PBIs **3** and **4** due to the bridging unit on one π-surface, the decrease of the intensity of the CD signal especially in this ultraviolet region is a clear indication that on average a less pronounced twisting angle is adopted upon increasing the bridge length, pointing to partial planarization or even temporary flip of the naphthalene units as suggested in Figure 1 for the most flexible PBIs **3c** and **4c**. For these two macrocyclic PBIs with the longest OEG chains a partial interconversion between *M* and *P* forms can be imagined based on molecular modeling studies. However, on average the total chirality is preserved as evidenced by the sign of the CD spectra. Therefore all these macrocyclic PBIs can be considered as conformationally stable chiral molecules.

The fluorescence spectra of **3** and **4** are the mirror images of their UV/Vis spectra, however, with less pronounced progression upon increasing bridge length. The detected emission maxima are between 532 and 553 nm (Figure 3). The emission maxima at longest wavelengths are concomitant with the largest Stockes shifts observed for **3c** and **4c** suggesting more pronounced structural relaxation processes of these more flexible molecules in the excited state. Similarly large or even larger Stokes shifts have been observed for tetraphenoxy substituted PBIs that were attributed to pronounced reorientation of those substituents.[52] Again, no significant spectral differences are found for the racemic mixtures and their respective pure enantiomers. The fluorescence quantum yields have been determined in DCM (Table 1 and 2) using *N′*-di(2,6-diisopropylphenyl)-3,4:9,10-tetracarboxylic acid bisimide as reference (Φ_{fl} = 1.00 in $CHCl_3$). It can be noticed that the quantum yield increases upon enlarging the bridging unit. This phenomenon has been already observed and explained for similar double bridged PBIs.[24]

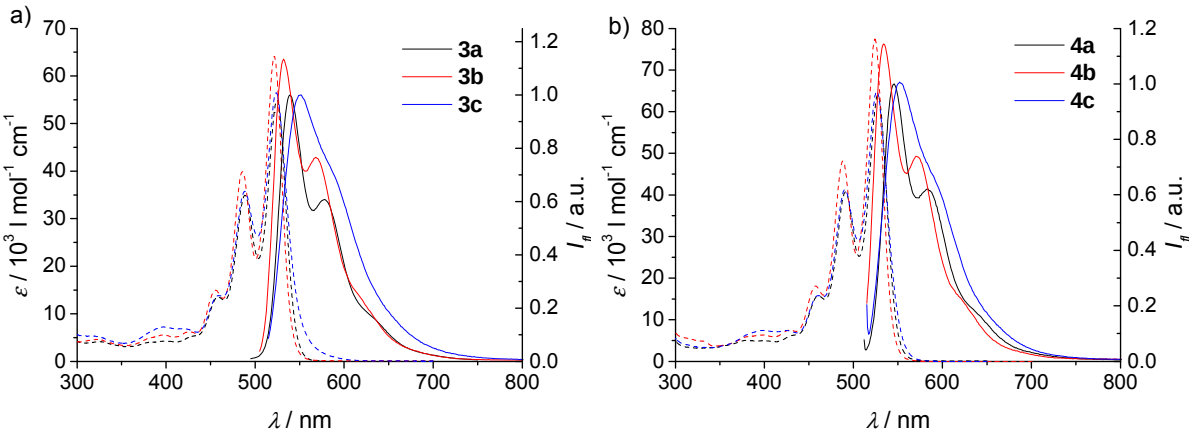

Figure 3. UV/Vis absorption (5×10^{-6} M, solid lines) and normalized emission fluorescence spectra (~10^{-7} M, dashed lines) in DCM of **3a–c** (a) and **4a–c** (b): **3**/**4a** (black line), **3**/**4b** (red line) and **3**/**4c** (blue line).

5.2.3. Dimer Formation in Solution

^{1}H NMR studies of **4b**,**c** (racemates and their respective pure enantiomers) in *n*-hexane-d_{14} at 331 K were performed. At the concentration of 10^{-3} M dimers are the major species, as indicated by vapor pressure osmometry (VPO) and concentration-dependent UV/Vis studies (about 80 % and 90 % of dimers are present in **4b** and **4c**, respectively, according to the data shown in Figures 9b and A1b–A5b in the appendix). VPO measurements of **4b** and **4c** (c = 1×10^{-3}–5×10^{-3} M) in *n*-hexane at 328 K using benzil for calibration gave aggregation numbers *N* of 1.81 and 2.05 respectively ($N = K_{cal}/K_{mean}$), confirming the exclusive presence of dimers in highly concentrated solutions of these dyes (Figure 4).

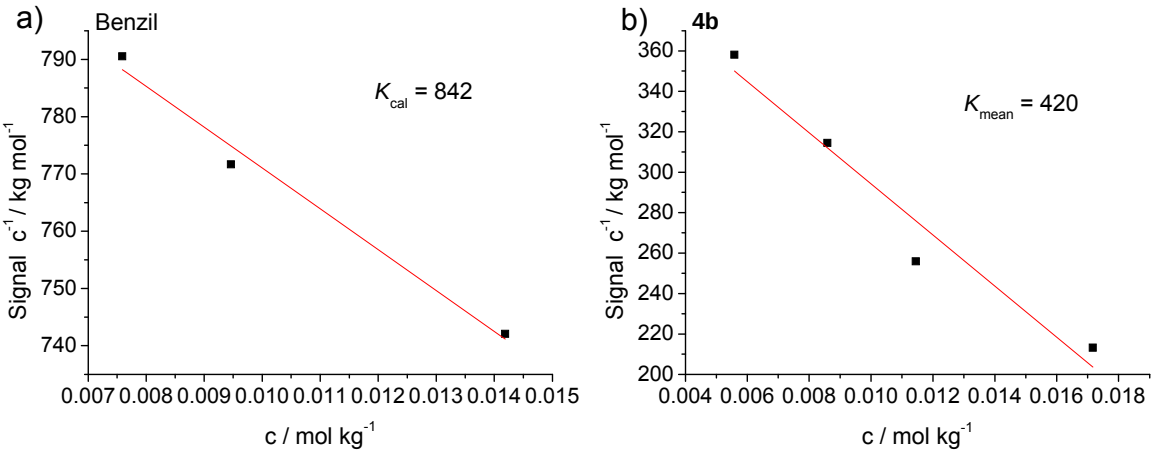

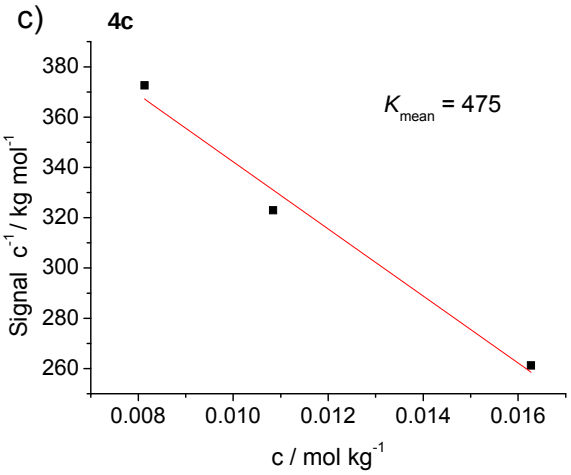

Figure 4. VPO measurements of a) benzil (calibration curve), b) **4b** and c) **4c** in *n*-hexane at 45 °C. The obtained signal divided into the measured concentration against the concentration in mol kg^{-1} is represented. The shown *K* values are in each case the extrapolated value of the y axis when x = 0.

In contrast to the spectra measured at RT, the ^{1}H NMR signals obtained at 331 K are sharp allowing a quantitative work-up of the NMR data. The superposed spectra of the racemates and their respective enantiomers revealed some differences in the shift of the aromatic protons, especially the ones corresponding to the protons of the PBI core. In Chapter 3 we have already demonstrated that the observed differences between the racemates and their respective pure enantiomers are related to the contemporaneous presence of homo and heterochiral dimers in the racemic solution.[23] For macrocycle **4a** it was found that for solutions with % *ee* not equaling 0 or 100 % at c = 2 x 10^{-3} M two sets of signals appear for each aromatic resonance of PBI core protons (H^a $H^{a'}$, H^b $H^{b'}$ and H^c $H^{c'}$) (Chapter 3). The signal splitting of these protons is related to the different chemical environments of H^x and $H^{x'}$ (being x = a, b or c) when they are in a homodimer or in a heterodimer, or what is the same, diastereomeric relationships between homo and heterodimers cause NMR non-equivalence between H^x and $H^{x'}$ protons. The relative intensities of the two signals related to one proton (H^x $H^{x'}$) of **4a** are directly proportional to the % *ee* and thus, the integration of the NMR signals can be used as direct measure of the % *ee*. Such correlation of the intensities of NMR signals and the *ee* indicates that the system is under fast exchange conditions.[53-58] Similarly, splitting of the signals at % *ee* different from 0 and 100% was found for **4b** and **4c**, pointing to diastereomeric relationships of the dimers (homo- and heterochiral) present in solution

(Figure 5).

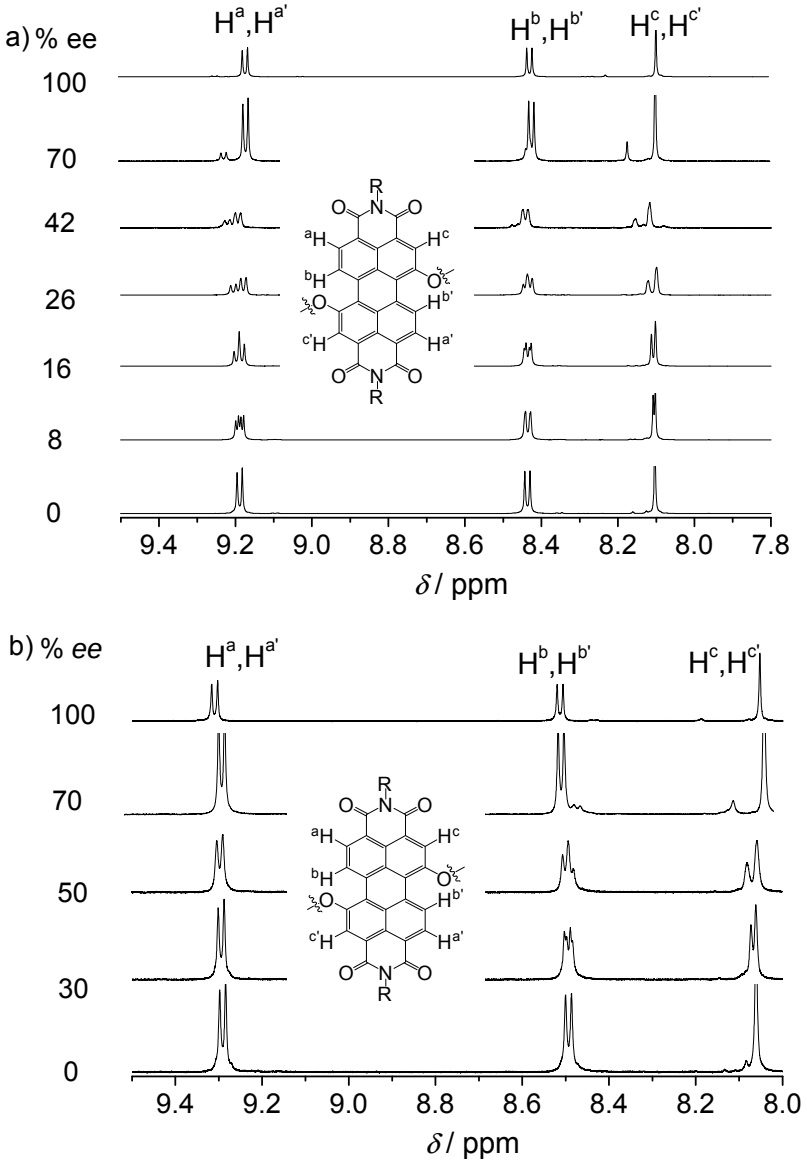

Figure 5. 600 MHz ^{1}H NMR spectra of solutions with different *ee* in *n*-hexane-$[D]_{14}$ at 331 K (c = 2 × 10^{-3} M^{-1}) (range of PBI protons) for **4b** (a) and **4c** (b).

However, for **4b** the splitting of the signals is less pronounced than for **4a**, and the splitting of **4c** is even less pronounced than for **4b** (Figure 5). This phenomenon indicates that upon increasing the bridge length and thus the flexibility of the molecules, the diastereomeric relationship between the homo and heterochiral dimers becomes less evident. Consequently, the observed splitting discovered in NMR is also less pronounced for the macrocyclic PBIs with larger bridging units (**4b** and **4c**) which prohibits a proper analysis of the data over the entire concentration range. Nevertheless, at least for **4b** the % *ee* can be determined from H^c, $H^{c'}$ between 100 and 26 % (Table 3).

Table 3. Comparison of the experimental *ee* values with those calculated from integral ratios of signal pairs of H^a,$H^{a\prime}$, H^b,$H^{b\prime}$ and H^c,$H^{c\prime}$ for **4b** (a) and **4c** (b).

a)

% *ee* experimental	% *ee* calculated		
	H^a,$H^{a\prime}$	H^b,$H^{b\prime}$	H^c,$H^{c\prime}$
70	[a]	70	70
44	[a]	[a]	46
26	[a]	[a]	25
16	[a]	[a]	[a]
8	[a]	[a]	[a]

[a] As the signals are superimposed, no accurate calculation of the % *ee* is possible.

b)

% *ee* experimental	% *ee* calculated		
	H^a,$H^{a\prime}$	H^b,$H^{b\prime}$	H^c,$H^{c\prime}$
70	[a]	[a]	70
50	[a]	[a]	[a]
30	[a]	[a]	[a]

[a] As the signals are superimposed, no accurate calculation of the % *ee* is possible.

ROESY and COSY NMR Spectroscopy

Several attempts to obtain proper ROESY spectra were performed with macrocycles (*P*)-**4a–c** (or (*M*)-**4a–c**) at 331 K and 298 K in *n*-hexane at a concentration of 2×10^{-3} M (at this concentration mostly dimeric aggregates are present in solution). The advantage of the measurements at high temperature (331 K) is the sharpening of the NMR signals. Unfortunately no intermolecular cross peaks at this temperature could be observed in any of the ROESY experiments performed for these pure enantiomeric PBIs. We attribute this fact to the fast exchange conditions at this temperature. To overcome this drawback experiments at 298 K were performed with (*P*)-**4a–c**. At this temperature the NMR signals of macrocyclic (*P*)-**4a** and (*P*)-**4c** are too broad especially in the aromatic region for ROESY measurements. Fortunately for (*P*)-**4b** signals which are sharp enough for recording a successful ROESY spectrum were found at RT (Figure 6a).

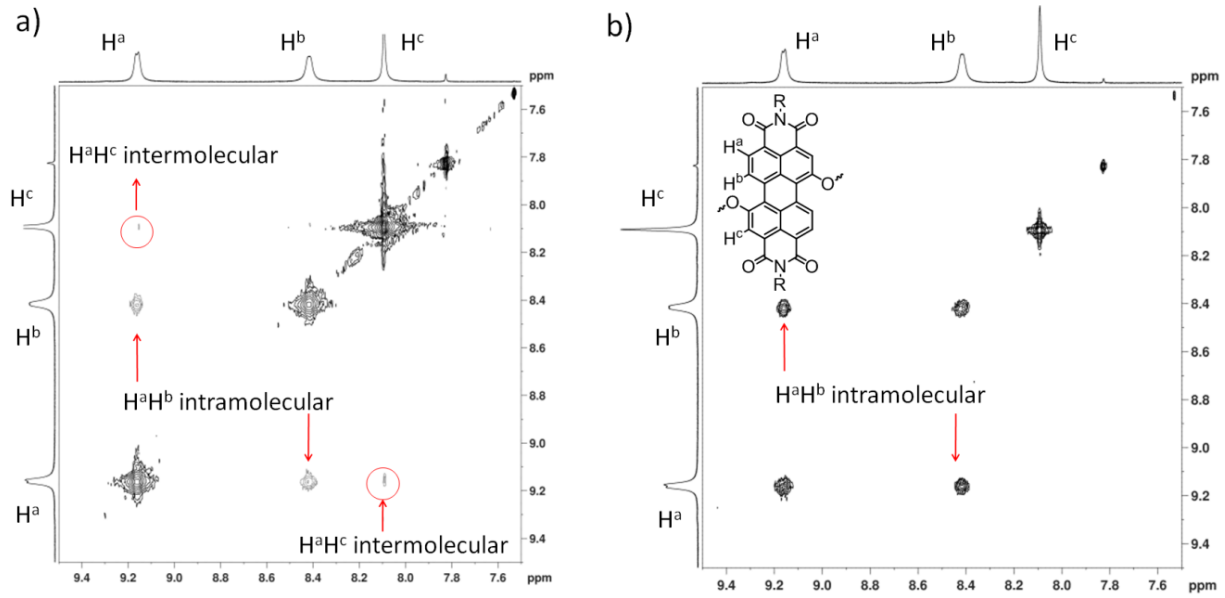

Figure 6. 600 MHz ROESY (a) and COSY (b) NMR experiments of (*P*)-**4b** in *n*-hexane-$[D]_{14}$ at 298 K ($c = 2 \times 10^{-3}\ M^{-1}$) (range of PBI protons).

As expected, intramolecular cross peaks between neighboring aromatic protons H^a and H^b can be observed in the ROESY spectrum. More interestingly, a much weaker cross peak appears between the distant aromatic protons H^a and H^c (Figure 6a). To rule out the possibility that this cross peak originates from the coupling between H^a and H^c protons through the aromatic naphthalene unit a COSY experiment was carried out under the same conditions as for the ROESY one. As can be appreciated in Figure 6b, expected intramolecular cross peaks between aromatic protons H^a and H^b can be observed. However, no trace of the cross peak resulting of the coupling between aromatic protons H^a and H^c is present. Accordingly this cross peak is attributed to an intermolecular contact in the homochiral dimer where these protons come into close proximity (see DFT calculations also).[a]

5.2.4. Optical Properties of the Dimers

The aggregation behaviour of PBIs **4a–c** (racemate and pure enantiomers) was investigated by concentration-dependent UV/Vis, CD and fluorescence spectroscopy in a concentration

[a] As COSY experiments are much more sensitive than ROESY ones, if the cross peak signal arises from an intramolecular coupling of the protons, it must be present in both ROESY and COSY spectra. As it is not the case, this cross peak between aromatic protons H^a and H^c can be exclusively attributed to intermolecular interactions between the PBIs in the homochiral dimers

range between 10^{-6} and 10^{-3} M in *n*-hexane (for CD and fluorescence) and *n*-heptane (for UV/Vis) at RT.[a]

Concentration-dependent UV/Vis studies of **4a–c** show pronounced spectral changes, including a hypsochromic shift of the absorption maxima upon increasing concentration (Figure 7, bottom panels). This clearly indicates the formation of H-type aggregated species in *n*-heptane.[59] Concentration-dependent UV/Vis spectra show no evident differences between racemates and pure enantiomers (for spectra of pure enantiomers see Figures A1–A2 in the Appendix). Spectral changes, however, are observed in the shape of the absorption bands for differently bridged PBIs **4a–c**, being most pronounced for the aggregate spectrum of **4c** (Figure 7c). Two clear isosbestic points are observed at about 470 and 525 nm (more or less shifted for **4a**, **4b** or **4c**), confirming the presence of two species in equilibrium.

CD spectra of **4a–c** *M* and *P* enantiomers were measured at 5×10^{-4} (strongly aggregated) and 5×10^{-6} M (not aggregated) in *n*-hexane at RT (see Figure 7, top panels). Hypsochromic shifts of the CD maxima are observed in accordance with the spectral changes recorded in UV/Vis spectra. Characteristic bisignate Cotton signals are present for all studied macrocyclic PBIs, indicating the helical nature of the formed dimers in solution, as it has been previously demonstrated for PBI **4a** (Chapter 3).[23] The negative sign of the exciton couplet for (*P*)-**4a–c** points to a left-handed helicity (the opposite for (*M*)-**4a–c**) of the respective dimeric aggregate according to exciton chirality method.[60-62] Interestingly, the intensity of the bisignate signal in the ultraviolet region corresponding to the chiral exciton coupling between the transition localized in the two naphthalene subunits of the PBI core is reduced in the case of the dimeric aggregates compared to the respective monomers forms **4a–c**. This result can be attributed to a decrease of the core twisting angle of these macrocyclic PBIs upon π–π-stacking after optimization of the contact surfaces of the interacting naphthalene subunits. It is reasonable that this special case of "induce-fit" mechanism is most pronounced for the less twisted PBI monomer **4c** (Figure 7c) in which the greater flexibility allows the largest changes in order to stabilize the self-assembled dimer, while less structural changes can be undergone by the

[a] Such studies are not possible for macrocycles **3a–c** due to solubility problems at the required concentrations in nonpolar solvents.

highest twisted PBI with the shortest bridge.

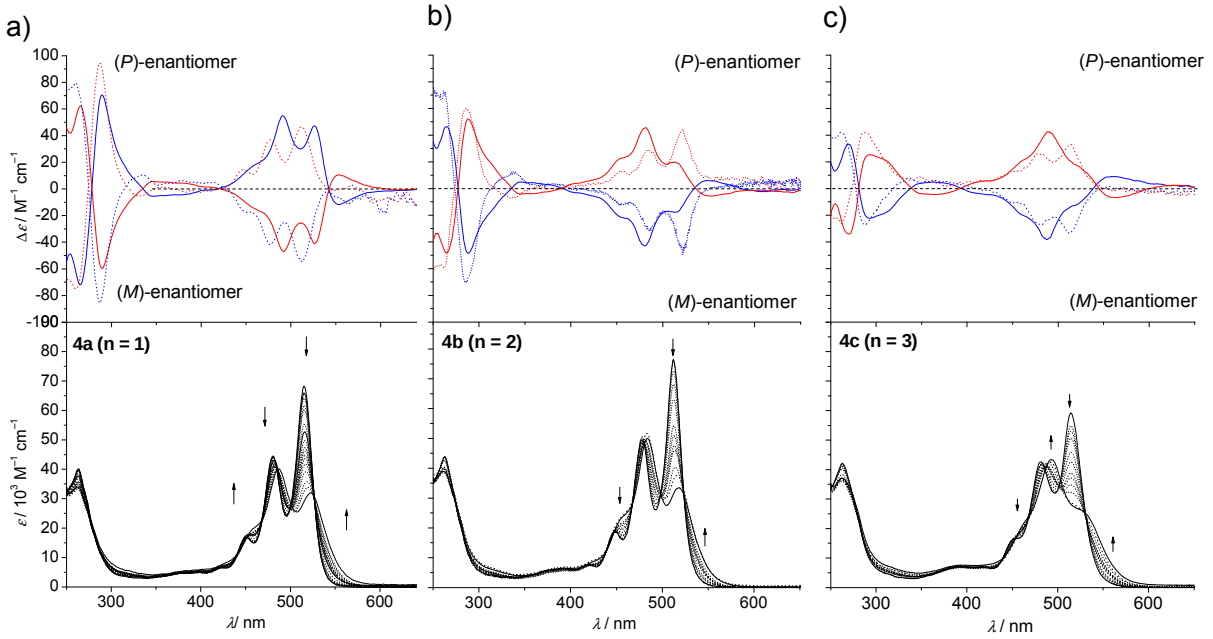

Figure 7. Concentration-dependent UV/Vis absorption (racemates, bottom panels) and CD spectra (*M*- and *P*- enantiomers top panels) of **4a–c** in *n*-heptane and *n*-hexane, respectively in the range from 5×10^{-6} M to 1×10^{-3} M (solid lines) at RT for **4a** (a), **4b** (b) and **4c** (c). Arrows indicate changes upon increasing concentration.

Concentration-dependent fluorescence spectra of **4a–c** are shown in Figure 8. The most remarkable feature is that fluorescence spectra of highly concentrated solutions (c = 5 x 10^{-4} M) show similar excimer-type emission characteristics as observed for extended π-stacks.[59,63-66] The pronounced concentration dependence indicated that this excimers are not formed from excited monomeric PBIs by diffusion but originated from photoexcited PBI dimers. To further elucidate the fluorescence properties of these macrocyclic PBIs **4a–c** lifetime experiments were carried out. The fluorescence decay times monitored at the monomer band (535 nm) and the aggregate band (610 nm) are collected in Table 4. Lifetime decay values of about 4 ns and 32 ns for the monomer and dimer bands, respectively, were found in all cases, in good accordance with values found for extended self-assembled π-stacks of PBIs[67,68] and covalently fixed dimeric π-stacks.[69] It is remarkable, that neither the shape of the fluorescence spectra nor the fluorescence decay values are strongly affected by the length of the bridge unit in **4a–c** which is in striking contrast to UV/Vis and CD spectra. The rationale behind these differences might be that all the dimer aggregates exhibit more similar structures in the relaxed excited state than in the ground state. Quantum mechanical calculations have

suggested that less crewed arrangement of PBI dimers in the excimer state due to excitonic coupling[70] which might indeed be quite similar for all three derivatives.

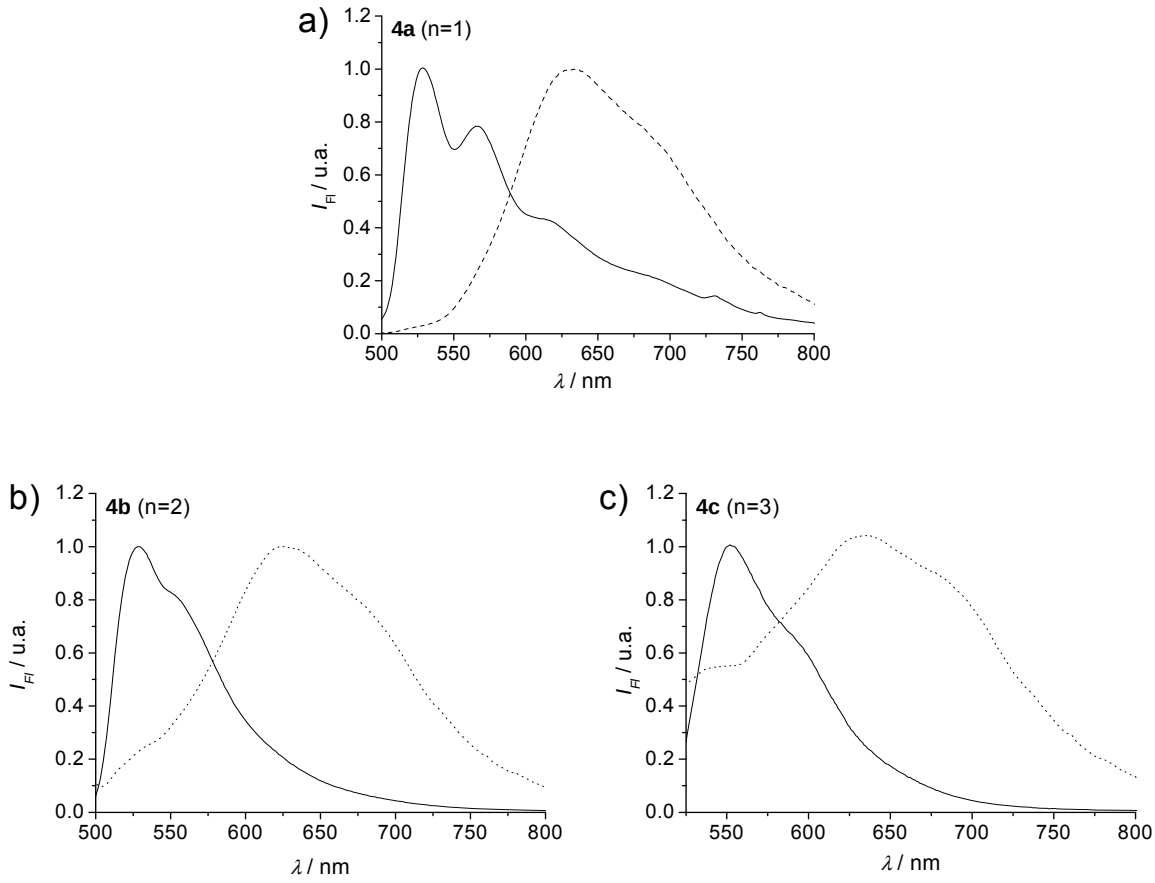

Figure 8. Normalized concentration-dependent fluorescence spectra of **4a** (a), **4b** (b) and **4c** (c) in *n*-hexane at 5×10^{-4} M (dashed line) to 5×10^{-6} M (solid line) at RT measured in a front face set up.

Table 4. Fluorescence lifetimes of **4a–c** measured at 610 and 535 nm (excitation wavelength 525 nm) at a concentration of 5×10^{-4} M in *n*-hexane at RT using front face set up.

		τ_f / ns		
		(*rac*)	(*M*)	(*P*)
4a	610 nm	33.16 ± 1.12	32.58 ± 1.77	32.68 ± 1.12
	535 nm	3.90 ± 0.05	3.65 ± 0.04	3.50 ± 0.0
4b	610 nm	29.61 ± 1.11	33.33 ± 2.06	33.93 ± 1.47
	535 nm	4.02 ± 0.05	3.66 ± 0.1	3.91 ± 0.15
4c	610 nm	32.43 ± 1.07	30.94 ± 1.39	30.31 ± 1.47
	535 nm	3.57 ± 0.05	3.90 ± 0.03	3.97 ± 0.01

5.2.5. Quantification of Chiral Self-Sorting and Effect of Temperature

The binding constants K_D for the dimerization of (*rac*)-**4a–c**, (*P*)-**4a–c** and (*M*)-**4a–c** were determined by concentration-dependent UV/Vis absorption 331 K (Figure 9 and A1–A5 in Appendix) in *n*-heptane. The concentration-dependent UV/Vis absorption spectra of the racemates and their respective pure enantiomers (all experiments were repeated twice) of these three macrocyclic compounds appear virtually identical, indicating similar aggregation behavior. The fitting of the experimental data obtained from the concentration-dependent UV/Vis absorption studies can be carried out by nonlinear regression analysis using the dimerization model[71,72] or applying a multilinear analysis of the data carried out by a custom made program.[73] Self-recognition at 331 K in *n*-heptane could recently be proven for compound **4a** using concentration-dependent UV/Vis studies.[23] Thus, similar studies on **4b** and **4c** will provide enough information to unravel the influence of the increasing flexibility of the PBI structures on the chiral self-sorting of PBIs. Moreover, all measurement were repeated at 298 K (see Figures A6–A14 in Appendix) to show the possible influence of temperature in the efficiency of chiral self-sorting events. The summarized data obtained at 298 K will be included together with the data at 331 K in the same Tables for better comparison of the data.

In Figures 9 and A1–A5 in the Appendix concentration-dependent UV/Vis studies of (*rac*)-**4b**,**c**, (*P*)-**4b**,**c** and (*M*)-**4b**,**c** at 331 K in *n*-heptane in a concentration range between 10^{-3} and 10^{-6} M are shown, as well as their fit by nonlinear regression analysis at selected wavelengths, and their multilinear fit. Analog to what was recently reported for **4a** (Chapter 3),[23] macrocyclic PBIs **4b** and **4c** show well defined isosbestic points at 465 and 525 nm for **4b** and at 469 and 531 nm for **4c**. Non-linear regression analysis of the data at selected wavelengths (506, 510, 514, 518, 522 and 539 nm for **4b** and 508, 512, 516, 520, 524 and 540 nm for **4c**) show coherence between the dimerization constants K_D obtained at each wavelength. Moreover, consistent results are obtained through multilinear analysis of the data, which is confirmed by the good accordance between the calculated and the experimental UV/Vis spectra at each measured concentration. Due to the larger amount of data processed in the multilinear analysis, we consider these results being more reliable in comparison to those

obtained by single wavelength fit of the data. Therefore, for further analysis only the K_D values obtained through multilinear routine will be considered.

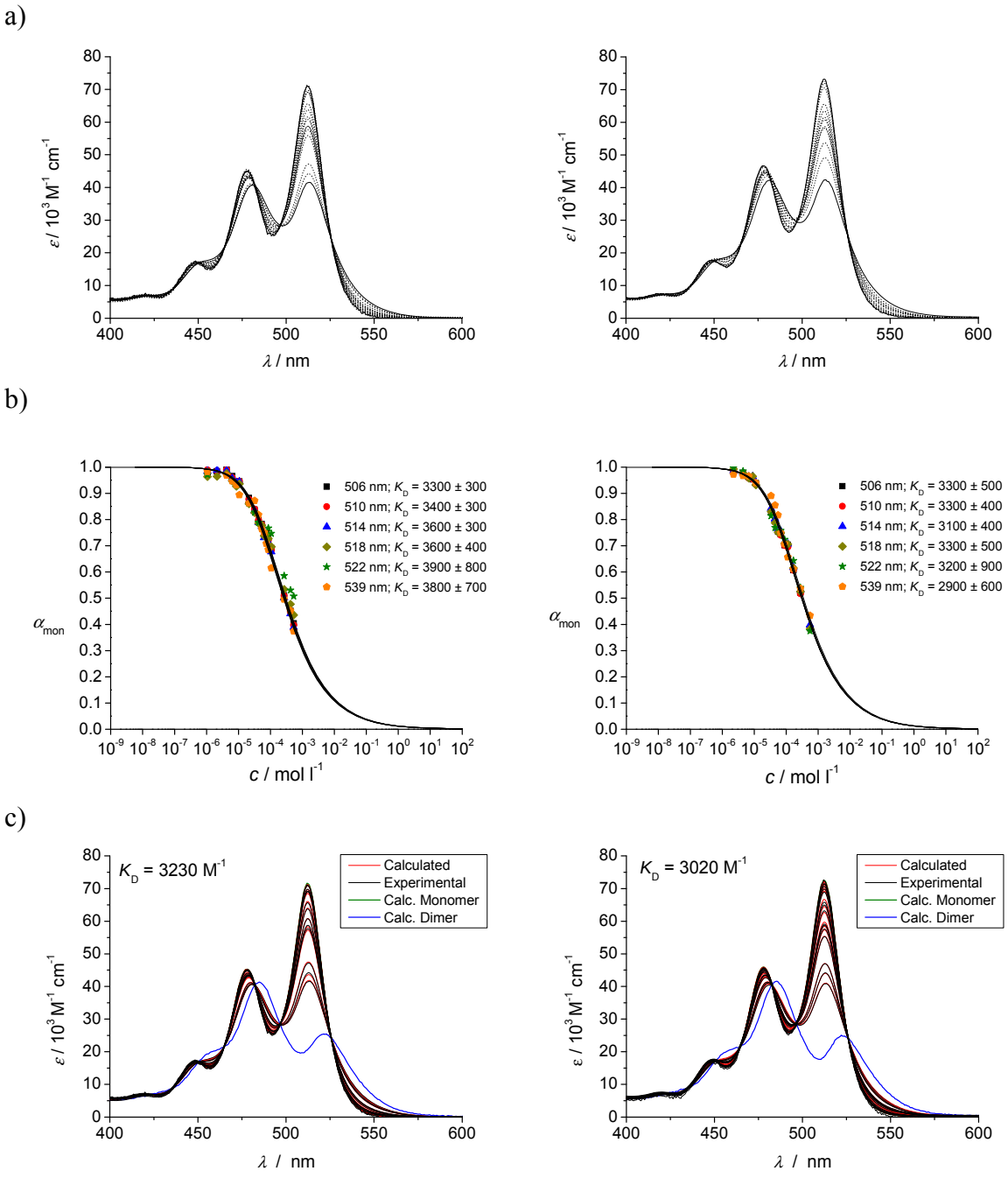

Figure 9. Illustration of the applied data acquisition and evaluation procedure based on two independent experiments (left and right). a) Concentration-dependent UV/Vis absorption spectra of (*rac*)-**4b** in *n*-heptane at 331 K ($[M]_0 = 4 \times 10^{-6}$ M to 5×10^{-4} M), b) molar fraction of monomer species and dimerization constants obtained from nonlinear regression analysis at selected wavelengths indicated in the inset, and c) results from the multilinear fit routine showing the comparison of experimental (black) and derived (red) spectra at respective concentrations as well as derived pure monomer (green) and dimer (blue) spectra.

Table 5. Dimerization constants K_D of racemate and pure enantiomers of PBI **4b** obtained from two independent studies by nonlinear regression analysis at selected wavelengths and multilinear fit of the data at 331K, respectively.

Sample	K_D [M^{-1}]						
	506 nm	510 nm	514 nm	518 nm	522 nm	539 nm	Multilinear fit (error ± 15 %)
(*rac*)-**4b**	3300 ± 300	3400 ± 300	3600 ± 300	3600 ± 400	3900 ± 800	3800 ± 700	3230
	3300 ± 500	3300 ± 400	3100 ± 400	3300 ± 500	3200 ± 900	2900 ± 600	3020
(*M*)-**4b**	5100 ± 600	5200 ± 500	5700 ± 600	6700 ± 1000	8000 ± 2800	4500 ± 600	5020
	4800 ± 500	5100 ± 400	5200 ± 400	6000 ± 700	8000 ± 2500	6600 ± 900	4990
(*P*)-**4b**	4600 ± 300	4700 ± 300	4700 ± 600	4900 ± 500	5000 ± 500	5000 ± 1200	5070
	5400 ± 600	5200 ± 400	5300 ± 500	5900 ± 800	8200 ± 1600	3600 ± 500	5400

Table 6. Dimerization constants K_D of racemate and pure enantiomers of PBI **4c** obtained from two independent studies by nonlinear regression analysis at selected wavelengths and multilinear fit of the data at 331 and 298 K, respectively.

Sample	K_D [M^{-1}]						
	508 nm	512 nm	516 nm	520 nm	524 nm	540 nm	Multilinear fit (error ± 15 %)
(*rac*)-**4c**	6100 ± 700	6500 ± 500	6500 ± 500	6300 ± 600	6400 ± 700	9100 ± 1300	7020
	7300 ± 600	7400 ± 400	7100 ± 4000	7100 ± 500	7000 ± 600	7700 ± 800	7010
(*M*)-**4c**	9900 ± 1400	12000 ± 1000	9800 ± 800	10000 ± 900	9600 ± 1300	14200 ± 2600	9500
	8900 ± 900	9400 ± 600	9400 ± 700	9300 ± 800	9300 ± 1100	7200 ± 4000	9000
(*P*)-**4c**	9900 ± 1300	10400 ± 900	10600 ± 900	9900 ± 900	9900 ± 1300	9500 ± 2000	9000
	7500 ± 700	8500 ± 600	8800 ± 600	8500 ± 600	7100 ± 700	19000 ± 180	9100

The results obtained from non-linear regression analysis at selected wavelength as well as from multilinear regression analysis (Figure 9 and A1-A5) are summarized in Tables 5 and 6.

The K_D values obtained after multilinear analysis of the concentration-dependent UV/Vis data of **4b** and **4c** at 331 K and 298 K in *n*-heptane for the quantitative analysis of chiral self-sorting are collected in Table 7 (some data of **4a** already presented in Chapter 3 are also included, for clarity in further discussion).

Table 7. Dimerization constants K_D determined for (*rac*)-**4a**–**c**, (*P*)-**4a**–**c** and (*M*)-**4a**–**c** in *n*-heptane at 331 and 298 K by multilinear fit of the concentration-dependent UV/Vis absorption.[a]

Sample	T / *K*	(*P*) / K_D [M^{-1}]	(*M*) / K_D [M^{-1}]	(*rac*) / K_D [M^{-1}]
4a	331 K	2800	2800	1500
	298 K	12100	12000	6100
4b	331 K	5200	5000	3100
	298 K	19700	18100	12000
4c	331 K	9100	9300	7000
	298 K	38400	39200	29900

[a] Values are averaged from two independent data sets

Applying Eq. 1[23] to the values collected in Table 7 quantitative information about the ratio of homo and heterochiral dimers in a racemic solution can be obtained (Table 8). As described in Chapter 3 the K_D of enantiopure (*P*)-**4a**–**c** (or (*M*)-**4a**–**c**) is related to the formation of homochiral dimers (i.e., $K_D = K_{D(homo)}$), while the obtained $K_{D(rac)}$ from (*rac*)-**4a**–**c** is the average value of homo- and hetero-dimerization processes.

$$K_{D(rac)} = \frac{K_{D(hetero)} + 2K_{D(homo)}}{4} \qquad (1)$$

The results in Table 8 clearly show that the increasing flexibility from PBIs **4a** to **4c** achieved by the introduction of more extended bridging units between 1 and 7 positions decreases the fidelity of chiral self-sorting in the dimerization process. Thus, upon increasing the bridge length the amount of heterochiral dimers present in the racemate increases from 1-7 % in **4a**, to 18-21% in **4b**, and to 34-35% in **4c**. Macrocyclic PBI **4a** with the shortest bridge shows the highest fidelity for chiral self-recognition, which must be directly related to the

higher rigidity of its twisted structure. The shortness of the bridge does not allow the twist angle of the PBI core to flip and hence no temporary planar conformation can be achieved, which restricts the stacking possibilities for the dimerization of PBIs **4a**.

Table 8. Dimerization constants $K_{D(hetero)}$ obtained from the values of Table 7 after applying Eq.1 determined for (*rac*)-**4a–c**, (*P*)-**4a–c** and (*M*)-**4a–c** in *n*-heptane at 331 and 298 K, the ratio of homo- *versus* heterodimers derived thereof, and corresponding percentage of homodimers present in each of the studied racemates.

Sample	T / K	$K_{D(homo)}$ / [M^{-1}]	$K_{D(hetero)}$ / [M^{-1}]	[homo]/[hetero] = $2K_{D(homo)}$ / $K_{D(hetero)}$	% Homo
4a	331	2800	400	14	93
	298	12100	200	121	99
4b	331	5100	2200	4.63	82
	298	18900	10200	3.70	79
4c	331	9200	9600	1.92	66
	298	38800	42000	1.84	65
2	331 K	55000 ± 5400[a]			

[a] See Figure 15A in the Appendix.

It has already been shown by CD studies that the twisting angle in the aromatic core region decreases on average upon increasing the length of the bridging unit, which can be explained by a partial planarization of the molecules resulting from the flipping of the naphthalene units, being more pronounced for larger bridges. The flipping process of molecules **4b** and **4c** (being more pronounced for **4c**, due to the larger bridging unit) provides the molecules with more stacking possibilities, some of them allowing a better overlapping of the aromatic surfaces in the heterochiral dimers (temporary planarization and/or flipped structures). These results point to a larger mixing rate upon increasing the bridge length and consequently the flexibility of the molecules, which is associated with a decreasing of the average twisting angle of the PBI core. Moreover, the quantity of homochiral dimers at both temperatures for the three studied racemic compounds is nearly the same. In the light of this data we can conclude that temperature has a very small effect in the fidelity of the chiral self-recognition of **4a–c**. This

is in good accordance with other reported systems, in which temperature only plays an important role when the thermodynamic equilibrium has not been achieved.[74,75]

It is also notable that the binding constants increase progressively for larger bridging units, being the largest value for the nonbridged precursor **2**. From **4a** to **4b** and from **4b** to **4c** the binding constants double upon increasing the OEG bridge, and this trend is lost for precursor **2**, which has a much higher binding constant than **4c** –about six times higher than $K_{D(homo)}$ and eight times higher than $K_{D(rac)}$–. This can be rationalized by the induced-fit effect, by which the PBIs go to an appreciable change in their threedimensional structure in their self-assembly process to form a more stable assembly. The induced fit is directly related to the flexibility of the molecules. The most flexible molecule, precursor **2**, is able to adopt the largest number of structural changes to fit other PBI molecule and self-assemble. The tremendous difference between the binding constants of **2** and (*rac*)-**4c** can be explained by two features of molecule **2**: i) the possibility of complete flipping of the naphthalene units from *M* to *P* atropo-enantiomers and ii) the possibility of the phenoxy groups attached to the 1,7-bay positions to freely rotate and adopt the most favorable conformation to stabilize the self-assemblies. The structural changes of these phenoxy units are considerably limited by the presence of the OEG bridges, thus, only the effect of the more or less restricted flipping of the naphthalene units will contribute to the induced fit process for the dimerization process of **4a**–**c**. Thus, the increasing flexibility in PBI aromatic cores has a positive influence on the induced-fit effects in the dimerization process as reflected in the calculated binding constants, whilst it clearly damages the quality of the chiral self-sorting process.

5.2.6. Equilibrium Constant *K′* for the Formation of Heterodimers from Homodimers

As indicated in Chapter 3, the equilibrium constant (K') and related Gibbs energy ($\Delta G'$) for the formation of heterodimers from a racemic mixture of homodimers can be calculated applying the values obtained for $K_{D(homo)}$ and $K_{D(hetero)}$ into equation 12, and the obtained K' into $\Delta G' = -RT \ln K'$ (where R is the ideal gas constant and T is the temperature in Kelvin). The calculated results for **4a**–**c** at 298 K and 331 K are summarized in Table 9.

$$4K' = \frac{K^2_{\mathrm{D(hetero)}}}{K^2_{\mathrm{D(homo)}}} \qquad (12)$$

The data in Table 9 indicate that $\Delta G'$ values stay positive for the whole series. Thus, the formation of heterodimers from the respective homodimers remains in all cases a disfavored process. The highest fidelity of chiral self-recognition, i.e. preference for homo- *versus* heterodimer formation, is found for the shortest bridging unit. Upon increasing the bridge length and hence the flexibility of the structures of **4a–c**, the formation of heterodimers becomes energetically less unfavorable, enabling an increasing amount of heterochiral dimers in the racemic solution. The tendency shown by these data anticipates that a long enough bridging unit could provide a system in which the formation of heterodimers is favored over the formation of homodimers, or at least equally favorable.

Table 9. Calculated equilibrium constant (K') and related Gibbs energies ($\Delta G'$) for the formation of heterodimers from a racemic mixture of homodimers of **4a–c** at 298 and 331 K.

	Sample	$K_{\mathrm{D(homo)}}$ [$\mathrm{M^{-1}}$]	$K_{\mathrm{D(hetero)}}$ [$\mathrm{M^{-1}}$]	K'	$\Delta G'$ [kJ $\mathrm{mol^{-1}}$]
	4a	12000	200	6.94×10^{-5}	23.40
298 K	**4b**	18900	10200	0.073	6.40
	4c	38800	42000	0.293	3.00
	4a	2800	400	0.005	14.58
331 K	**4b**	5100	2200	0.049	8.30
	4c	9200	9600	0.280	3.47

For a better understanding of the experimental results, structure optimization of homo and heterodimers formed by **4a** were performed at RI-BLYP-D/TZV(P)-level for the different diastereomers (*MM*, *PP* and *MP*).[a] Two different structure types with energetically similar minima could be found (Figure 10). One of the structures shows an ecliptic order, with the

[a] Calculations carried out by Manuel Renz and Prof. Martin Kaupp, Institut für Physikalische und Theoretische Chemie, Würzburg University.

PBIs almost superimposed and very small rotational displacement (Figure 10a). The second energetically favored structure presents two stacked PBIs with rotational displacement of about 30° (Figure 10b). This arrangement is in good accordance with previous experimental and theoretical results for unsubstituted PBIs [76] and our CD data at high concentrations in *n*-hexane whose bisignate Cotton effects indicate the presence of dimers with rotational displacements. Thus, only these dimeric species will be considered for further discussion.

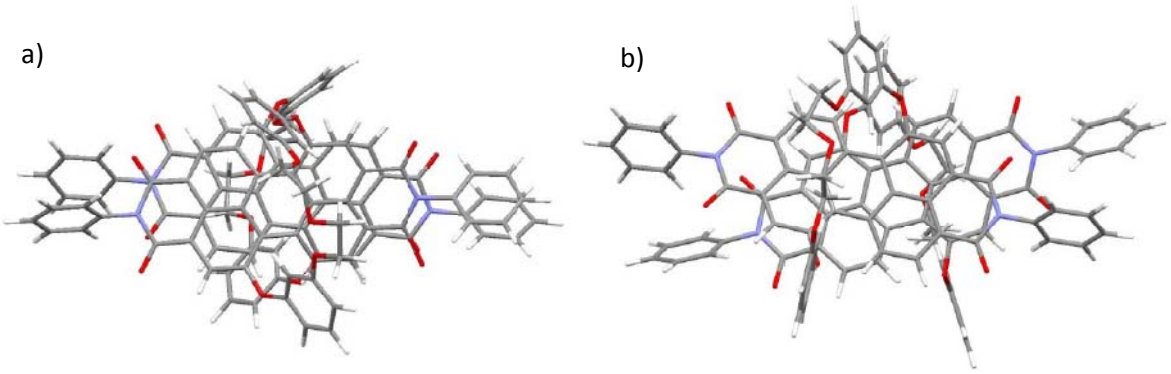

Figure 10. Two different structures found after energy minimization of the homodimer. a) Structure showing ecliptic order with slight rotational displacements and b) structure with a rotational displacement of about 30°.

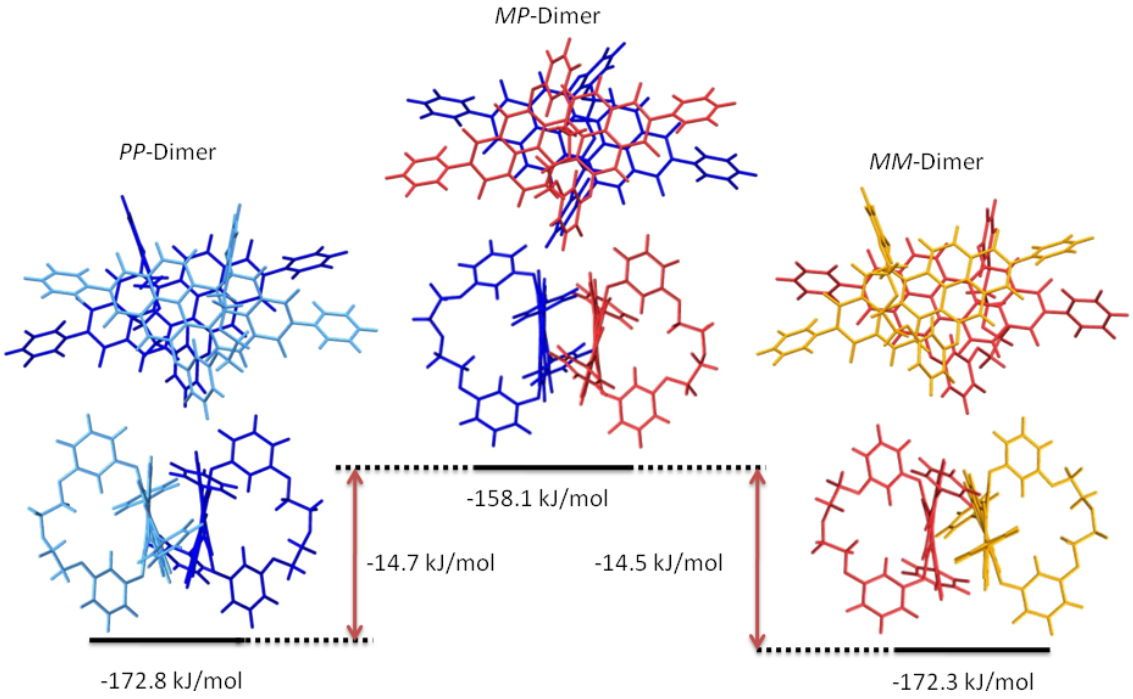

Figure 11. Energy diagram of the different supramolecular diastereomers of **4a**.

The energies obtained for both homochiral dimers are, as expected, equal in the range of error of the calculations (Figure 11). The heterochiral dimer was calculated to be 14.5 kJ

mol^{-1} less stable than the homodimers, which is in excellent accordance with the experimental values (Table 11), supporting the validity of the calculations. Thus, the higher stability of homochiral dimers over their heterochiral counterparts has been demonstrated both experimentally and theoretically. The reason of this extra stabilization in the case of the homodimers is clearly the better overlapping of the π-surfaces in comparison to the heterochiral dimers as can be appreciated in Figure 12. In Figure 12a the better fit between the aromatic surfaces is depicted, which in the case of the homodimer are self-complementary. This is not the case for the heterodimer which leads to less tight π–π-stacking and some distortion of the monomeric structures in the dimerization (Figure 12b). Such geometrical factors have been previously proven to be determinant in the efficiency of both chiral and "general" self-sorting processes.[28,36,77,78]

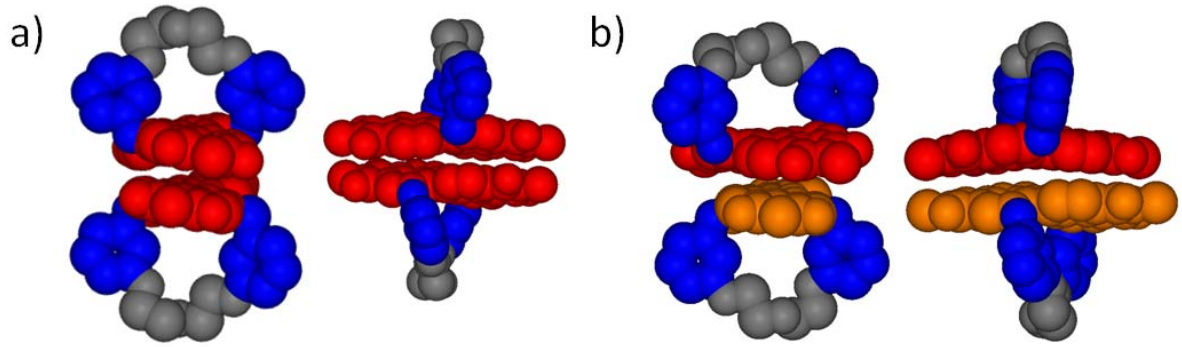

Figure 12. Energy minimized structures of a) *MM*-homodimer and b) *PP*-heterodimer of **4a**. Views through the long and short axis of the PBIs, respectively. The OEG are represented in grey, the phenoxy units in blue and the PBI core in red for *M*-enantiomer and orange for *P*-enantiomer.

5.2.7. Condensed State Properties

The liquid crystalline properties of racemic and enantiopure samples of macrocycle **4a** have been characterized in detail by differential scanning calorimetry (DSC), polarization optical microscopy (POM), atomic force microscopy (AFM) and X-Ray diffraction studies (Chapter 4). It is remarkable that important differences between (*rac*)-**4a** and (*P*)-**4a** (or (*M*)-**4a**) were found, showing the influence of chirality on the condensed properties of such macrocyclic mesogens.

Similarly, DSC and POM studies were carried out with macrocycles **4b** and **4c** (racemates and pure enantiomers) to determine their condensed state properties. DSC thermograms of

(*rac*)-**4b** and (*P*)-**4b** are shown in Figure 13. For (*rac*)-**4b** a phase transition at about 185 °C with a transition enthalpy of 18 kJ mol^{-1} is observed in the second heating cycle. Upon cooling two very close transitions are observed at 164 and 160 °C (Figure 13a). For (*P*)-**4b** a phase transition can be assigned at 109 °C with a very low transition enthalpy (~2 kJ mol^{-1}), typical for a transition from a liquid crystalline into the isotropic phase. Upon cooling down a slightly higher transition enthalpy is found at 100 °C (~5 kJ mol^{-1}) (Figure 13b). The transition to the isotropic phase occurs at much higher temperature and is energetically higher for (*rac*)-**4b** than for (*P*)-**4b** (or (*M*)-**4b**) (as it has been previously observed by **4a**). The transition enthalpy values point to a soft crystal in case of (*rac*)-**4b** while for (*P*)-**4b** (or (*M*)-**4b**) liquid crystallinity can be assumed.

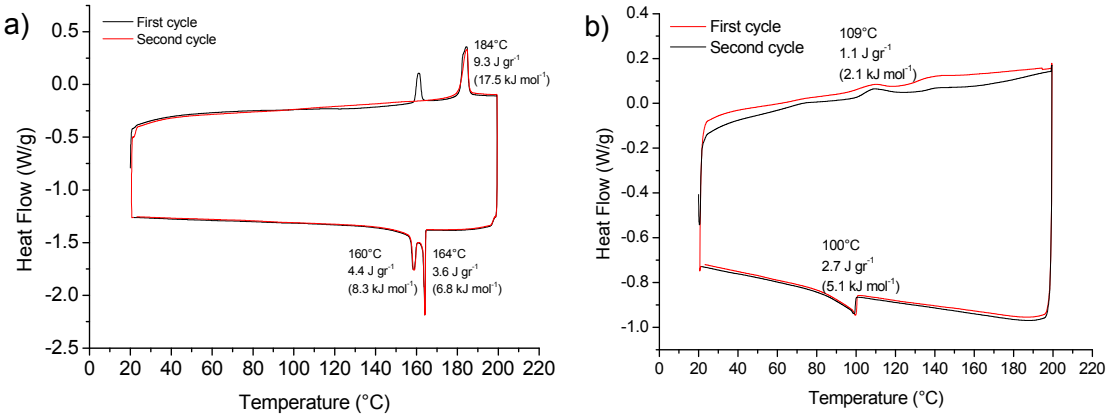

Figure 13. DSC profiles of a) (*rac*)-**4b** and b) (*P*)-**4b** with heating and cooling rates f 10 °C min^{-1}.

POM studies were performed for further insight into the condensed phase properties of compound **4b**. For (*rac*)-**4b** two different textures were observed (Figure 14). The first texture was observed after cooling down from the isotropic phase at a rate of 0.2 °C min^{-1} to 150 °C. Some radial-growing structures can be observed, however they do not correspond to any known liquid crystalline texture but are reminiscent to crystal growth (Figure 14a). The second texture (Figure 14b) was obtained after cooling down from the isotropic phase to 160 °C at a rate of 0.1 °C min^{-1}. Here some hardly shearable very large fan-shape-like structures appear pointing again to a soft crystalline structure of (*rac*)-**4b**.

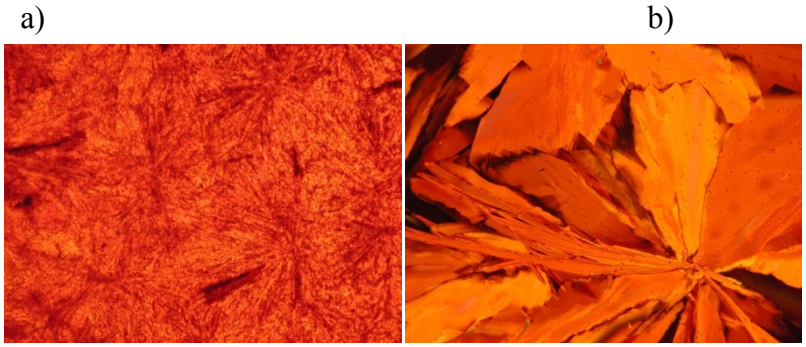

Figure 14. POM textures of (*rac*)-**4b**. a) Texture obtained after cooling down (0.2 °C min^{-1}) up to 150 °C. b) Texture obtained after cooling down (0.1 °C min^{-1}) up to 160 °C from the isotropic phase.

POM studies of (*P*)-**4b** show the formation of a fan-shape texture upon cooling down from the isotropic phase at a rate of 0.1 °C min^{-1} (Figure 15). Its shearability and the low transition enthalpy to the isotropic phase found for (*P*)-**4b** indicate the liquid crystalline nature of the material in accordance to DSC data.

Figure 15. POM textures of (*P*)-**4b** after cooling down (0.1 °C min^{-1}) up to 96 °C from the isotropic phase.

DSC and POM studies for macrocycles (*rac*)-**4c** and (*P*)-**4c** are shown in Figures 16 and 17, respectively. DSC chromatograms of (*rac*)-**4c** show a distinct phase transition at about 153 °C with a similar transition enthalpy of 23 kJ mol^{-1} whereas a less characteristic thermal behavior is found for (*P*)-**4c** with a very low transition enthalpy (~5 kJ mol^{-1}) around 109 °C (Figure 16). For (*rac*)-**4c** a transition at 121 °C upon cooling can be recorded (Figure 16a). The transition enthalpy observed for (*rac*)-**4c** is relatively high, but an unambiguous classification into liquid or plastic soft crystal phase cannot be carried out without further X-ray diffraction data. Remarkably, in the cooling cycles for (*P*)-**4c** or (*M*)-**4c** no phase transition from the isotropic phase can be observed, indicating that a glassy material is formed for these enantiomers upon cooling.

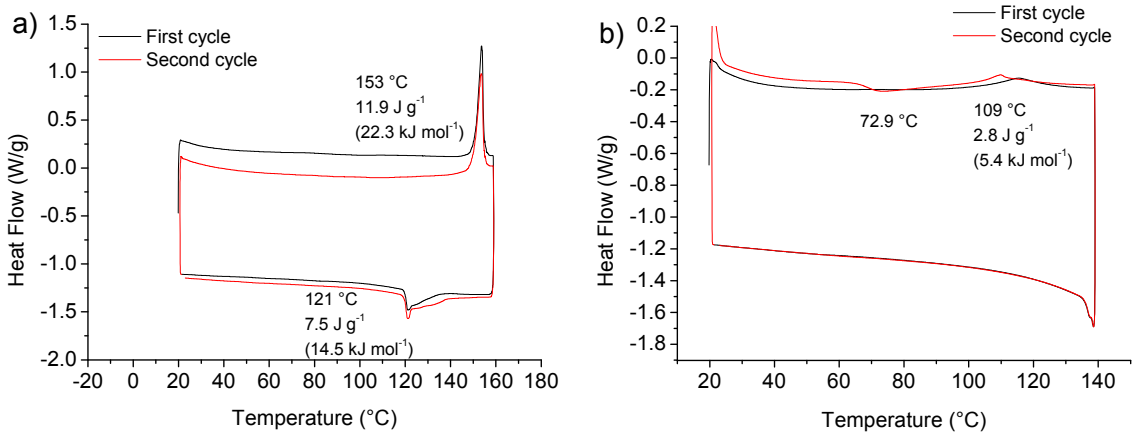

Figure 16. DSC profiles of (*rac*)-**4c** (a) and (*P*)-**4c** (or (*M*)-**4c**) (b) (10 °C min^{-1}).

To further elucidate the condensed state properties of macrocyclic PBI **4c** POM studies of (*rac*)-**4c** and (*P*)-**4c** (or (*M*)-**4c**) were performed (Figure 17). Different textures were obtained for (*rac*)-**4c** upon cooling down from the isotropic phase at a cooling rate of 0.1 °C min^{-1} depending on the thickness of the respective sample. For a thicker sample an unknown texture could be observed (Figure17a). In a thinner sample a texture could be observed at 143 ºC that seems to correspond to a nematic phase (Figure 17b). Both textures could be easily sheared supporting the liquid crystalline nature of (*rac*)-**4c**. (*P*)-**4c** (or (*M*)-**4c**) did not show formation of any textures in the POM in agreement with an amorphous state (see DSC).

a) b)

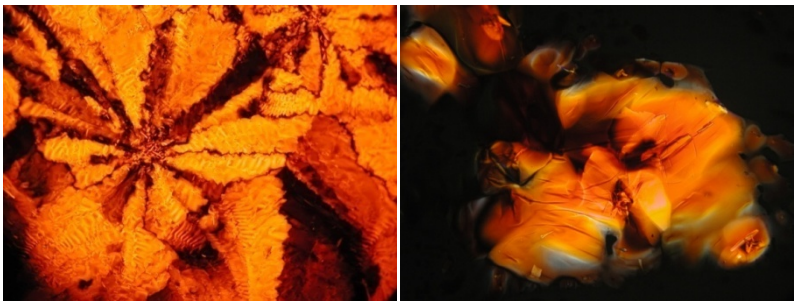

Figure 17. POM textures of (*rac*)-**4c**. a) Texture obtained after cooling down (0.1 °C min^{-1}) up to 110 °C in a thick sample. b) Texture obtained after cooling down (0.1 °C min^{-1}) from the isotropic phase up to 143 °C in a thin sample.

The obtained thermotropic parameters of macrocycles **4a–c** are collected in Table 10. It is remarkable that the transition temperature to the isotropic phase is progressively decreasing upon increasing the bridge length, in particular for the racemates. This indicates that the increasing flexibility and consequently the motional degrees of freedom of the macrocycles

have an important influence on the condensed state properties of PBIs **4a–c**. Another notable point are the higher transitions temperatures and enthalpies of all the racemates in comparison to their respective pure enantiomers. This can be related to the better three dimensional packing of the PBIs in the racemates than in the enantiopure samples. The impact of the bridging units for the packing of (*MM*)- and (*PP*)-dimers has been discussed in detail in Chapter 4 for compound **4a**.

Table 10. Thermal parameters of compounds **4a–c**.

	(*rac*)-**4**		(*M*)-**4** (or (*P*)-**4**)	
	Transition	ΔH (kJ mol^{-1})	Transition	ΔH (kJ mol^{-1})
a	245 °C	32.2	117 °C	4.3
b	184 °C	17.6	109 °C	2.1
c	153 °C	22.3	109 °C	5.4

5.2.8. Surface Morphology

The surface morphologies of **4b** and **4c** thin films (racemates and pure enantiomers) on glass surface were investigated by AFM in air using taping-mode (Figures 18–20). The measurement of pure enantiomeric **4c** could not be performed due to the low viscosity of the sample. For samples of (*rac*)-**4b** and (*M*)-**4b** similar homogeneous films can be observed at RT after drop-casting from a 10^{-3}M solution in *n*-hexane. After melting the samples and cooling down again some changes in the surface-structures can be observed, although no defined layer structure is present in any of the films (Figure 18b,c and Figure 19b–d). Similar studies were performed for (*rac*)-**4c** (Figure 20). After cooling down from the transition temperature multilayer structures with a step-height between 2.7 to 3.2 nm can be observed. This corresponds to the height of a PBI molecule if some interdigitation of the alkyl chains is taken into account. Accordingly this data point to a more defined surface structure than the ones observed for compounds (*rac*)-**4b** and (*M*)-**4b** (or (*P*)-**4b**).

Information about the viscosity of the samples could be obtained by measuring the elasticity module of the prepared thin films. The results obtained for compounds **4b** and **4c** and the previously recorded data for macrocycle **4a** are summarized in Table 11.

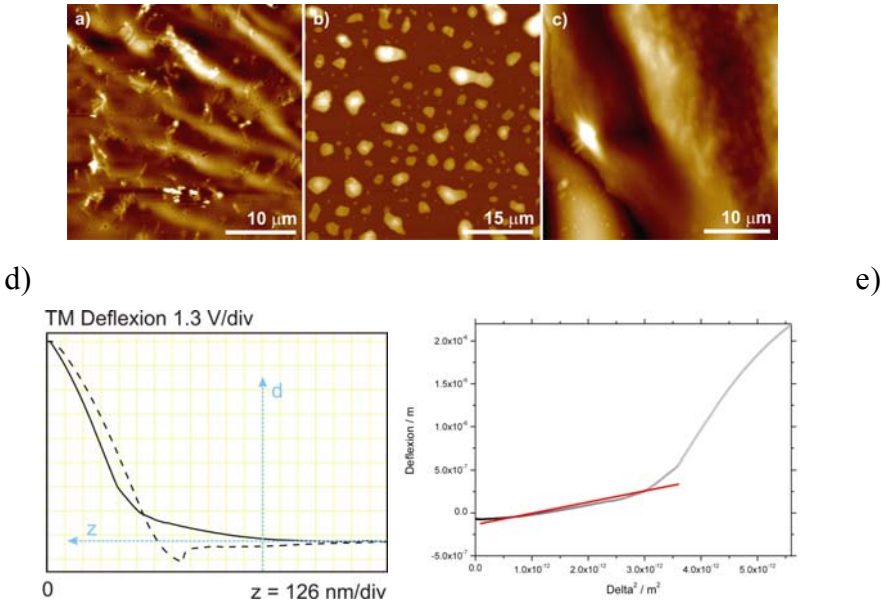

Figure 18. AFM height images of sample (*rac*)-**4b**: a) at 25 °C after drop-cast preparation from a 10^{-3}M solution in *n*-hexane; b,c) at 25 °C (after melting of sample at 190 °C); d) deflection of the tip as a function of its vertical displacement; e) deflection of the tip as a function of the square of the indentation depth δ.

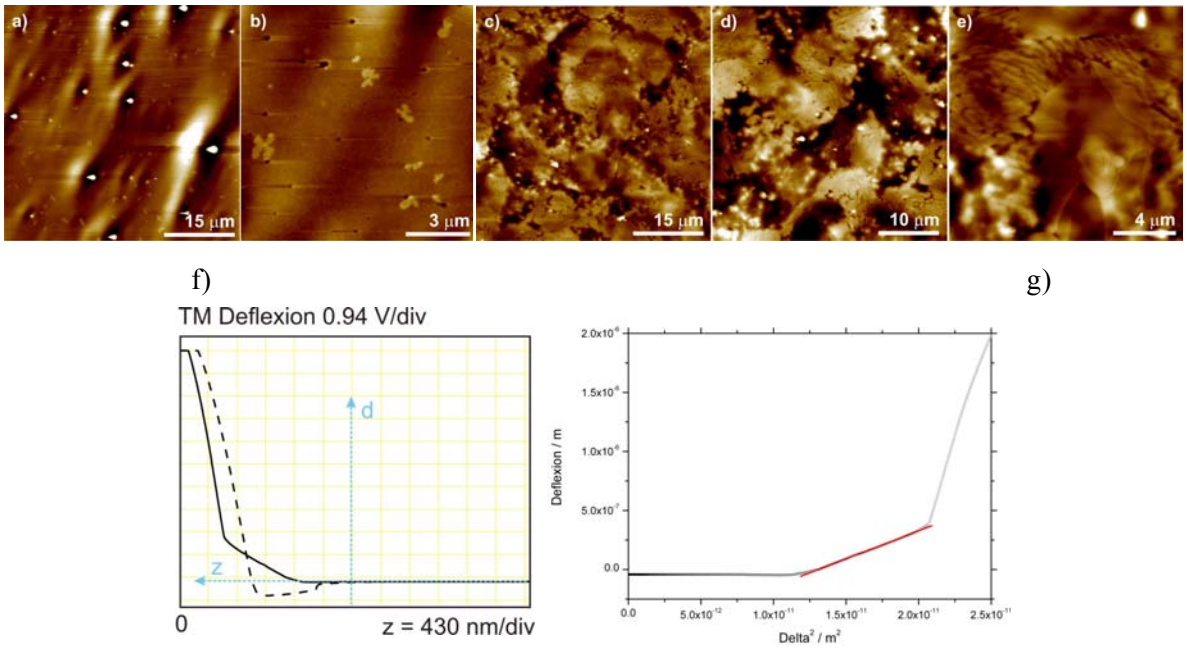

Figure 19. AFM height images of sample (*M*)-**4b**: a,b) at 25 °C after drop-cast preparation from a 10^{-3}M solution in *n*-hexane; c,d,e) at 25 °C (after melting of sample at 110 °C); f) deflection of the tip as a function of its vertical displacement; g) deflection of the tip as a function of the square of the indentation depth δ.

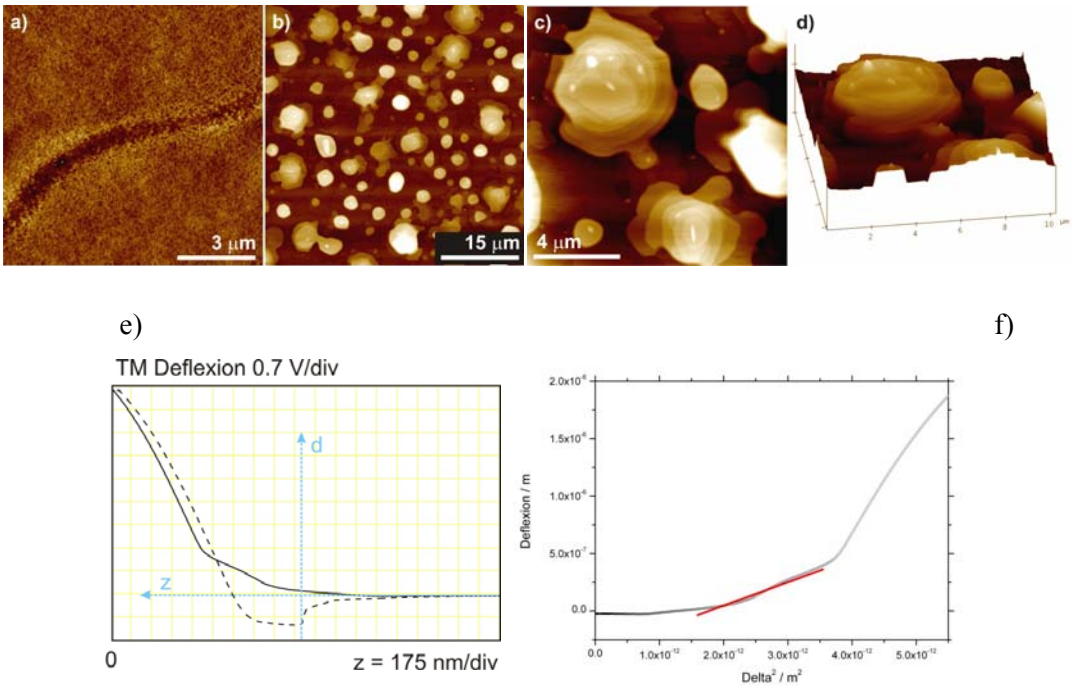

Figure 20. AFM height images of sample (*rac*)-**4c**: a) at 25 °C after drop-cast preparation from a 10^{-3}M solution in *n*-hexane; b,c,d) at 100 °C (after melting of sample at 146 °C); d) 3D surface plot showing steps of crystals (height of steps is 2.7–3.2 nm); e) deflection of the tip as a function of its vertical displacement; f) deflection of the tip as a function of the square of the indentation depth δ.

A larger value of the elasticity module implies a lower viscosity of the samples. Upon increasing the bridges the racemic samples gain in fluidity, in accordance with the decreasing transition temperatures observed by DSC. This can be explained by a looser packing of the PBIs due to a larger flexibility of the structures and bridging units combined with a greater extent of heterodimeric structures. In the case of the pure enantiomers only the measurement of **4b** was possible, while for **4a** and **4c** the structures were too fluid to be measured. Thus, in all cases lower viscosity is shown for the pure enantiomers than for the racemates, supporting the data obtained by DSC, in which the transition enthalpies were higher for racemic samples.

Table 11. Values of the elasticity module of macrocyclic PBIs **4a**–**c**.

E / [MPa]	**4a**	**4b**	**4c**
rac	0.052	0.68	0.99
M (or *P*)	[a]	0.25	[a]

[a] The viscosity of the sample was too low to aquire reliable data from the measurement.

5.3. Conclusions

We have successfully synthesized a series of conformationally restricted chiral 1,7-diaryloxy-substituted PBIs that are distinguished by different sized bridging units and resolved their atropo-enantiomers. The new chiral compounds have been fully characterized by HRMS spectrometry and UV/Vis, fluorescence, ^{1}H NMR and CD spectroscopy. Moreover, their condensed state properties have been investigated by DSC, POM and AFM techniques.

This series of core-twisted dyes enabled for the first time the elucidation of the conformational parameters (rigidity of a chiral π-scaffold) on binding constants for dimerization via π–π-stacking and selectivity of chiral recognition (homo- *versus* heterochiral dimerization). Already CD spectra of monomeric pure enantiomers revealed the greater flexibility of the PBI structures equipped with larger bridging units owing to a more pronounced *M*/*P* interconversion of the chiral PBI scaffold for the larger bridges. Spectroscopic studies of racemic and enantiopure PBI dyes **4a**–**c** provided unambiguous evidence for preferential chiral self-recognition over self-discrimination in π-stacking dimerization of these PBIs. However, the amount of heterochiral dimers present in the corresponding racemates increases for more extended bridging units. This demonstrates that the fidelity of chiral self-sorting in PBIs is compromised by an increasing flexibility of the structures. Less rigid scaffolds bearing longer bridging units were shown to enable more planarized π-scaffolds upon π–π-stacking (induced-fit) leading to higher binding strength but lower enantioselectivity for the recognition of the homo- or heterochiral partner molecule.

The relevance of chirality induced by the twisting of the aromatic core and the impact of the rigidity on the condensed state properties could also be elucidated for these macrocyclic atropo-enantiomeric PBIs **4a**–**c**. Increasing flexibility has been demonstrated to deteriorate the packing of the studied macrocycles, as higher fluidity and lower transition temperature have been found for larger bridged PBIs.

To conclude, we have revealed for the first time the impact of rigidity on chiral self-sorting processes for core-twisted π-scaffolds. Conformational flexibility was shown to improve the binding strength via induced-fit mechanism but to compromise the quality of chiral self-recognition between chiral π-surfaces.

5.4. Experimental Section

Cesium carbonate (99 %), and potassium carbonate (≥ 99 %), were obtained from Sigma-Aldrich and Merck. All chemicals and reagents were used as received, unless otherwise stated. Potassium carbonate was dried *in vacuo* at 100 °C for 24 h. Diethylene glycol ditosylates were prepared according to literature procedures.[79] Flash column chromatography was performed using silica gel (Si60, mesh size 40–63 μm) from Merck. ^{1}H NMR spectra were recorded with Bruker Avance 400 MHz and Bruker Advance DMX 600 MHz instruments. Chemical shifts are given in parts per million (ppm) and are referred to TMS as internal standard. ^{1}H coupling constants *J* are given in Hertz (Hz). High resolution mass spectra (HRMS) were recorded on a MicroTOF Focus from Bruker Daltonics. Analytical HPLC was carried out on a JASCO system (PU 2080 PLUS) with a diode array detector (MD 2015), equipped with a ternary gradient unit (DG-2080-533) and inline-degasser (LG 2080-02). Semi-preparative HPLC was performed on a JASCO system (PU 2080 PLUS) with an UV/Vis detector (UV 2077 PLUS). Preparative recycling GPC LC-9105, Japan Analytical Industry Co., Ltd. (JAI) was used in recycling mode for the separation of some of the racemates. Vapor pressure osmometry (VPO) measurements were performed on a KNAUER osmometer with a universal temperature measurement unit. Benzil was used as standard and a calibration curve in terms of *R* (ohm) vs. molal osmotic concentration (moles per kg *n*-hexane) was accomplished up to 0.016 molal. Differential scanning calorimetry (DSC) measurements were carried out using a TA Q1000 calorimeter with a heating/cooling rate of 10 °C min^{-1}. At least two heating–cooling cycles were performed for each compound. Optical textures of the liquid crystal phases at crossed polarizer were acquired with an Olympus BX-41 polarization microscope equipped with a Linkam THMS 600 hot stage and a temperature controller unit. The AFM images were recorded by using an E-scanner with a maximum scan area of 15 × 15 mm. Silicon cantilevers with a nominal spring constant of 34.0–71.0 N m^{-1} and with resonant frequency of 300 kHz, and a typical tip radius of 7 nm (OMCLAC160TS, Olympus) were employed.

UV/Vis Absorption and Fluorescence Spectroscopy, and Circular Dichroism (CD): For all spectroscopic measurements, spectroscopic grade solvents (Uvasol®) from Merck were used. UV/Vis spectra were recorded with a Perkin Elmer PE 950 equipped with a PTP-1 peltier element. CD spectra were measured with a JASCO J-810 spectrometer equipped with a CDF-242 peltier element. Fluorescence spectra were recorded with a PTI QM-4/2003 instrument. All fluorescence measurements were performed under ambient conditions and fluorescence spectra are corrected against photomultiplier and lamp intensity. The fluorescence quantum yields were determined as the average value for three different excitation wavelengths using *N,N'*-di(2,6-diisopropylphenyl)-3,4:9,10-tetracarboxylic acid bisimide as reference (Φ_{fl} = 1.00 in chloroform) by applying high dilution conditions (A < 0.05).[80,81]

For the measurements at high concentrations front-face set up with 30° light beam angle deviation and 1 mm cells were used. Fluorescence lifetimes were measured under ambient conditions by using a PTI LaserStrobe fluorescence lifetime spectrometer system containing a GL-3300 nitrogen laser (337.1 nm, pulse width 600 ps, pulse energy 1.45 mJ) coupled with a dye laser GL-302 (pulse width 500 ps, pulse energy 220 μJ at 550 nm) as an excitation source and a stroboscopic detector. Laser output was tuned within the emission curves of the laser dyes supplied by the manufacturer (PLD 421, 500, 579, 665, 735). The time resolution following deconvolution of experimental decays is 200 ps. The instrument response function was collected by scattering the exciting light of a dilute, aqueous suspension of Silica (LUDOX). Decay curves were evaluated using the software supplied with the instrument applying least square regression analysis. The quality of the fit was evaluated by analysis of $\chi 2$ (0.9 – 1.1), DW factor (> 1.75) and Z value (<−1.96, confidence level 0.95) as well as by inspection of residuals and autocorrelation function.

Synthesis of 3b,c (for the synthesis of the precursors 1 and 2 see Chapter 3) by *N,N'*-Dicyclohexyl-1,7-(3-hydroxyphenoxy)perylene-3,4:9,10-tetracarboxylic acid bisimide **1** (230 mg, 0.30 mmol for **3b** and 400 mg, 0.52 mmol for **3c**), and cesium carbonate (1.7 g, 5.21 mmol for **3b** and 3 g, 9.20 mmol for **3c**) were dissolved in DMSO (150 mL for **3b** and 500 mL for **3c**) and heated to 120 °C for 7 h. The addition of the correspondent tri or

tetra(ethylene glycol) distosylate (280 mg, 0.57 mmol and 520 mg, 1.00 mmol, respectively) dissolved in DMSO (20 mL) was carried out with a syringe pump over a period of 3 h. The reaction mixture was cooled to ambient temperature and dropped into 0.33 M hydrochloric acid (150 mL) under stirring. The resulting precipitate was collected by filtration and dried *in vacuo* (10 mbar). Silica gel column chromatography with DCM for **3b** and alox (neutral) with DCM for **3c** and precipitation with methanol from DCM afforded 0.069 mmol of **3b** (23% yield) as an orange solid and 0.078 mmol of **3c** (15% yield) as a red solid.

3b: Mp. 318–319 °C. ^{1}H NMR ($CDCl_3$): δ 9.42 (d, 2H, J = 8.2), 8.55 (d, 2H, J = 8.2), 8.38 (s, 2H), 7.32 (t, 2H, J = 8.3), 7.10 (m, 2H), 6.48 (m, 2H), 5.80 (s, 2H), 5.00 (m, 2H), 3.82–3.73 (m, 4H), 3.63–3.42 (m, 8H), 2.53 (m, 4H), 1.89 (bd, 4H), 1.74 (bd, 6H), 1.53–1.25 (m, 6H). HRMS (ESI-TOF, pos. mode, DCM:acetonitrile = 1:1): *m/z* calc. for $C_{54}H_{49}N_2O_{10}$ $[M+H]^+$: 885.3309, found: 885.3382. UV/Vis (CH_2Cl_2): λ_{max}/nm (ε_{max}/$M^{-1}cm^{-1}$) 522 (64000), 486 (39900), 454 (14800), 266 (33200). Fluorescence (CH_2Cl_2): λ_{max} = 532 nm, Φ_{fl} = 0.33.

3c: Mp. 210–211 °C. ^{1}H NMR ($CDCl_3$): δ 9. 53 (d, 2H, J = 8.5), 8.58 (d, 2H, J = 8.5), 8.34 (s, 2H), 7.38 (t, 2H, J = 8.2), 7.11 (m, 2H), 6.63 (m, 2H), 6.03 (t, J = 2.3 Hz, 2H), 5.00 (m, 2H), 3.88–3.78 (m, 4H), 3.65–3.61 (m, 4H), 3.51–3.44 (m, 8H), 2.53 (m, 4H), 1.89 (bd, 4H), 1.74 (bd, 6H), 1.53–1.25 (m, 6H). HRMS (ESI-TOF, pos. mode, DCM:acetonitrile = 1:1): *m/z* calc. for $C_{56}H_{52}N_2O_{11}Na$ $[M+Na]^+$: 951,3469, found: 951.3463, λ_{max}/nm (ε_{max}/$M^{-1}cm^{-1}$) 525 (55800), 488 (35500), 458 (13800), 265 (35200). Fluorescence (CH_2Cl_2): λ_{max} = 551 nm, Φ_{fl} = 0.57.

Separation of enantiomers *P*-(+)-3 and *M*-(-)-3 by HPLC

Separation of the enantiomers was achieved on a semi-preparative column (Trentec Reprosil 100 chiral-NR) using different mixtures of *n*-hexane and DCM.

3b: **3b** was eluted in a 3/2 mixture of DCM /*n*-hexane using a flow of 8 ml/min. The separation was done on a scale of 15 mg.

M-(–)-**3b**: Retention time (Trentec Reprosil 100 chiral-NR, DCM/*n*-hexane (3/2), flow: 8.0 mL min^{-1}; Ø = 2.5 cm): 22.0 min. λ_{max}/nm ($\Delta\varepsilon$/$M^{-1}cm^{-1}$) 518 (– 47), 484 (– 31), 454 (– 12), 286 (– 86), 262 (+ 64).

P-(+)-**3b**: Retention time (Trentec Reprosil 100 chiral-NR, DCM/*n*-hexane (3/2), flow: 8.0

mL min^{-1}; Ø = 2.5 cm): 32.0 min. CD (CH_2Cl_2): λ_{max}/nm ($\Delta\varepsilon$/M^{-1}cm^{-1}) 518 (+ 44), 484 (+ 30), 454 (+ 11), 286 (+ 86), 262 (– 64).

3c: **3c** was eluted in a 4/1 mixture of DCM/*n*-hexane using a flow of 8 ml/min. The separation was done on a scale of 15 mg.

M-(–)-**3c**: Retention time (Trentec Reprosil 100 chiral-NR, DCM/*n*-hexane (4/1), flow: 8.0 mL min^{-1}; Ø = 2.5 cm): 10.0 min. CD (CH_2Cl_2) λ_{max}/nm ($\Delta\varepsilon$/M^{-1}cm^{-1}) 522 (– 34), 486 (– 23), 458 (– 9), 287 (– 59), 264 (+ 36).

P-(+)-**3c**: Retention time (Trentec Reprosil 100 chiral-NR, DCM /*n*-hexane (4/1), flow: 8.0 mL min^{-1}; Ø = 2.5 cm): 12.0 min. CD (CH_2Cl_2): λ_{max}/nm ($\Delta\varepsilon$/M^{-1}cm^{-1}) 522 (+ 37), 486 (+ 24), 458 (+ 9), 287 (+ 47), 264 (– 39).

Macrocyclization of 2

N,N′-Di(3,4,5-tridodecylphenyl)-1,7-di(3-hydroxyphenoxy)perylene-3,4:9,10-tetracarboxylic acid bisimide **2** (300 mg, 0.17 mmol), and cesium carbonate (1 g, 3.06mmol) were dissolved in dry THF (400 mL) and heated to 120 °C for 7 h. The addition of the correspondent tri or tetra(ethylene glycol) distosylate (150 mg, 0.31 mmol and 170 mg, 0.32 mmol, respectively) dissolved in THF (20 mL) was carried out with a syringe pump over a period of 6 h. The reaction mixture was cooled to ambient temperature and dropped into 0.33 M hydrochloric acid (150 mL) under stirring. The resulting precipitate was collected by filtration and dried *in vacuo* (10 mbar). Silica gel (**b**: DCM /*n*-hexane, 1/1 **c**: DCM/*n*-hexane, 3/2) column chromatography and precipitation with methanol from DCM afforded 0.078 mmol of **4b** (22% yield) and 0.026 mmol of **4c** (15% yield) as an orange solid.

4b: Mp. 180–190 °C. ^{1}H NMR ($CDCl_3$): δ9.52 (d, 2H, J = 8.2), 8.64 (d, 2H, J = 8.2), 8.48 (s, 2H), 7.33 (t, 2H, J = 8.3), 7.10 (m, 2H), 6.93 (m, 2H), 6.50 (s, 2H), 5.87 (m, 2H), 3.90–3.62 (m, 4H), 3.55–3.48 (m, 8H), 2.64 (t, 12H), 1.59–1.55 (m, 12H), 1.32–1.18 (m, 108H), 0.83–0.78 (m, 18H). HRMS (ESI-TOF, pos. mode, DCM:acetonitrile = 1:1): *m/z* calc. for $C_{126}H_{181}N_2O_{10}$ $[M+H]^+$: 1882.3716, found: 1882.3711. UV/Vis (CH_2Cl_2): λ_{max}/nm (ε_{max}/M^{-1}cm^{-1}) 524 (77700), 488 (48100), 457 (18100), 263 (43000). Fluorescence (CH_2Cl_2): λ_{max} = 534 nm, Φ_{fl} = 0.14.

4c: Mp. 148 °C–155 °C. ^{1}H NMR ($CDCl_3$): δ9.62 (d, 2H, J = 8.3), 8.67 (d, 2H, J = 8.3), 8.44

(s, 2H), 7.37 (t, 2H, J = 8.2), 7.11 (m, 2H), 6.93 (m, 2H), 6.03 (t, J = 2.3 Hz, 2H), 6.10 (m, 2H), 3.92–3.82 (m, 4H), 3.67–3.65 (m, 4H), 3.55–3.48 (m, 8H), 2.64 (t, 12H), 1.59–1.55 (m, 12H), 1.32–1.18 (m, 108H), 0.83–0.78 (m, 18H). HRMS (ESI-TOF, pos. mode, DCM:acetonitrile = 1:1): *m/z* calc. for $C_{127}H_{182}N_2O_{11}$ $[M+H]^+$: 1926,39001, found: 1926.39729, λ_{max}/nm (ε_{max}/$M^{-1}cm^{-1}$) 526 (64900), 491 (41300), 461 (15800), 263 (43000). Fluorescence (CH_2Cl_2): λ_{max} = 551 nm, Φ_{fl} = 0.25.

Separation of enantiomers *P*-(+)-4 and *M*-(-)-4 by HPLC

Separation of the enantiomers was achieved on a semi-preparative column (Trentec Reprosil 100 chiral-NR) using different mixtures of *n*-hexane and DCM.

4b: **4b** was eluted in a 65/35 mixture of chloroform/*n*-hexane using a flow of 3.5 mL min^{-1}. The separation was done in the JAI recycling system, after 7 cycles and two iterations on a scale of 10 mg.

M-(–)-**4b**: CD (CH_2Cl_2):λ_{max}/nm ($\Delta\varepsilon$/$M^{-1}cm^{-1}$) 522 (– 43).

P-(+)-**4b**: CD (CH_2Cl_2): λ_{max}/nm ($\Delta\varepsilon$/$M^{-1}cm^{-1}$) 522 (+ 45).

4c: **4c** was eluted in a 7/3 mixture of chloroform/*n*-hexane using a flow of 10 mL min^{-1}. The separation was done in the JAI recycling system, after 7 cycles and several iterations on a scale of 5 mg.

M-(–)-**4c**: CD (CH_2Cl_2) λ_{max}/nm ($\Delta\varepsilon$/$M^{-1}cm^{-1}$) 525 (– 33).

P-(+)-**4c**: CD (CH_2Cl_2): λ_{max}/nm ($\Delta\varepsilon$/$M^{-1}cm^{-1}$) 525 (+ 37).

5.5. Notes and References

(1) Würthner, F. *Chem. Commun.* **2004**, 1564.
(2) Jaiser, F.; Neher, D.; Meisel, A.; Nothofer, H. G.; Miteva, T.; Herrmann, A.; Müllen, K.; Scherf, U. *J. Chem. Phys.* **2008**, *129*, 114901.
(3) Pandey, A. K.; Nunzi, J. M. *Appl. Phys. Lett.* **2007**, *90*, 263508.
(4) Ego, C.; Marsitzky, D.; Becker, S.; Zhang, J. Y.; Grimsdale, A. C.; Müllen, K.; MacKenzie, J. D.; Silva, C.; Friend, R. H. *J. Am. Chem. Soc.* **2003**, *125*, 437.
(5) Jones, B. A.; Facchetti, A.; Wasielewski, M. R.; Marks, T. J. *J. Am. Chem. Soc.* **2007**, *129*, 15259.
(6) Weitz, R. T.; Amsharov, K.; Zschieschang, U.; Villas, E. B.; Goswami, D. K.; Burghard, M.; Dosch, H.; Jansen, M.; Kern, K.; Klauk, H. *J. Am. Chem. Soc.* **2008**, *130*, 4637.
(7) Jones, B. A.; Facchetti, A.; Wasielewski, M. R.; Marks, T. J. *Adv. Funct. Mater.* **2008**,

18, 1329.

(8) Schmidt, R.; Oh, J. H.; Sun, Y. S.; Deppisch, M.; Krause, A. M.; Radacki, K.; Braunschweig, H.; Könemann, M.; Erk, P.; Bao, Z. A.; Würthner, F. *J. Am. Chem. Soc.* **2009**, *131*, 6215.

(9) Schmidt-Mende, L.; Fechtenkötter, A.; Müllen, K.; Moons, E.; Friend, R. H.; MacKenzie, J. D. *Science* **2001**, *293*, 1119.

(10) Peumans, P.; Uchida, S.; Forrest, S. R. *Nature* **2003**, *425*, 158.

(11) Lindner, S. M.; Huttner, S.; Chiche, A.; Thelakkat, M.; Krausch, G. *Angew. Chem., Int. Ed.* **2006**, *45*, 3364.

(12) Sautter, A.; Thalacker, C.; Würthner, F. *Angew. Chem., Int. Ed.* **2001**, *40*, 4425.

(13) Jones, B. A.; Ahrens, M. J.; Yoon, M. H.; Facchetti, A.; Marks, T. J.; Wasielewski, M. R. *Angew. Chem., Int. Ed.* **2004**, *43*, 6363.

(14) Chen, Z. J.; Debije, M. G.; Debaerdemaeker, T.; Osswald, P.; Würthner, F. *ChemPhysChem* **2004**, *5*, 137.

(15) Würthner, F.; Stepanenko, V.; Chen, Z. J.; Saha-Möller, C. R.; Kocher, N.; Stalke, D. *J. Org. Chem.* **2004**, *69*, 7933.

(16) Leroy-Lhez, S.; Baffreau, J.; Perrin, L.; Levillain, E.; Allain, M.; Blesa, M. J.; Hudhomme, P. *J. Org. Chem.* **2005**, *70*, 6313.

(17) Chao, C. C.; Leung, M. K.; Su, Y. O.; Chiu, K. Y.; Lin, T. H.; Shieh, S. J.; Lin, S. C. *J. Org. Chem.* **2005**, *70*, 4323.

(18) Würthner, F.; Osswald, P.; Schmidt, R.; Kaiser, T. E.; Mansikkamaki, H.; Könemann, M. *Org. Lett.* **2006**, *8*, 3765.

(19) Gsänger, M.; Oh, J. H.; Könemann, M.; Höffken, H. W.; Krause, A. M.; Bao, Z. N.; Würthner, F. *Angew. Chem., Int. Ed.* **2010**, *49*, 740.

(20) Gsänger, M.; Oh, J. H.; Könemann, M.; Hoffken, H. W.; Krause, A. M.; Bao, Z. N.; Würthner, F. *Angew. Chem., Int. Ed.*, *49*, 740.

(21) Xie, Z. Q.; Würthner, F. *Org. Lett.*, *12*, 3204.

(22) Osswald, P.; Würthner, F. *J. Am. Chem. Soc.* **2007**, *129*, 14319.

(23) Safont-Sempere, M. M.; Osswald, P.; Radacki, K.; Würthner, F. *Chem. Eur. J.* **2010**, *16*, 9366.

(24) Osswald, P.; Leusser, D.; Stalke, D.; Würthner, F. *Angew. Chem., Int. Ed.* **2005**, *44*, 250.

(25) Osswald, P.; Reichert, M.; Bringmann, G.; Würthner, F. *J. Org. Chem.* **2007**, *72*, 3403.

(26) Hwang, I. W.; Kamada, T.; Ahn, T. K.; Ko, D. M.; Nakamura, T.; Tsuda, A.; Osuka, A.; Kim, D. *J. Am. Chem. Soc.* **2004**, *126*, 16187.

(27) Kamada, T.; Aratani, N.; Ikeda, T.; Shibata, N.; Higuchi, Y.; Wakamiya, A.; Yamaguchi, S.; Kim, K. S.; Yoon, Z. S.; Kim, D.; Osuka, A. *J. Am. Chem. Soc.* **2006**, *128*, 7670.

(28) Mizumura, M.; Shinokubo, H.; Osuka, A. *Angew. Chem., Int. Ed.* **2008**, *47*, 5378.

(29) Maeda, C.; Kamada, T.; Aratani, N.; Sasamori, T.; Tokitoh, N.; Osuka, A. *Chem. Eur. J.* **2009**, *15*, 9681.

(30) Sugiyasu, K.; Honsho, Y.; Harrison, R. M.; Sato, A.; Yasuda, T.; Seki, S.; Takeuchi, M. *J. Am. Chem. Soc.*, *132*, 14754.

(31) Sugiyasu, K.; Takeuchi, M. *Chem. Eur. J.* **2009**, *15*, 6350.

(32) Long, T. M.; Swager, T. M. *J. Mater. Chem.* **2002**, *12*, 3407.
(33) Lohr, A.; Swager, T. M. *J. Mater. Chem.* **2010**, *20*, 8107.
(34) Lim, J.; Swager, T. M. *Angew. Chem., Int. Ed.* **2010**, *49*, 7486.
(35) Wang, W.; Shaller, A. D.; Li, A. D. Q. *J. Am. Chem. Soc.* **2008**, *130*, 8271.
(36) Shaller, A. D.; Wang, W.; Gan, H. Y.; Li, A. D. Q. *Angew. Chem., Int. Ed.* **2008**, *47*, 7705.
(37) Thoma, J. A.; Koshland, D. E., Jr *J. Am. Chem. Soc.* **1960**, *82*, 3329.
(38) Koshland, D. E. *Angew. Chem., Int. Ed.* **1995**, *33*, 2375.
(39) James, L. C.; Roversi, P.; Tawfik, D. S. *Science* **2003**, *299*, 1362.
(40) Martin Schmeing, T.; Huang, K. S.; Strobel, S. A.; Steitz, T. A. *Nature* **2005**, *438*, 520.
(41) Ringe, D.; Petsko, G. A. *Science* **2008**, *320*, 1428.
(42) Kasai, K.; Aoyagi, M.; Fujita, M. *J. Am. Chem. Soc.* **2000**, *122*, 2140.
(43) Gasparrini, F.; Pierini, M.; Villani, C.; Filippi, A.; Speranza, M. *J. Am. Chem. Soc.* **2007**, *130*, 522.
(44) Filby, M. H.; Dickson, S. J.; Zaccheroni, N.; Prodi, L.; Bonacchi, S.; Montalti, M.; Paterson, M. J.; Humphries, T. D.; Chiorboli, C.; Steed, J. W. *J. Am. Chem. Soc.* **2008**, *130*, 4105.
(45) Hiraoka, S.; Harano, K.; Nakamura, T.; Shiro, M.; Shionoya, M. *Angew. Chem., Int. Ed.* **2009**, *48*, 7006.
(46) Ménand, M.; Leroy, A.; Marrot, J.; Luhmer, M.; Jabin, I. *Angew. Chem., Int. Ed.* **2009**, *48*, 5509.
(47) Han, J.-M.; Pan, J.-L.; Lei, T.; Liu, C.; Pei, J. *Chem. Eur. J.* **2010**, *16*, 13850.
(48) Marquis, D.; Desvergne, J. P.; Bouaslaurent, H. *J. Org. Chem.* **1995**, *60*, 7984.
(49) Dijkstra, G.; Kruizinga, W. H.; Kellogg, R. M. *J. Org. Chem.* **1987**, *52*, 4230.
(50) Kaiser, H.; Lindner, J.; Langhals, H. *Chem. Ber.* **1991**, *124*, 529.
(51) Osswald, P.; Reichert, M.; Bringmann, G.; Würthner, F. *J. Org. Chem.* **2007**, *72*, 3403.
(52) Fron, E.; Schweitzer, G.; Osswald, P.; Würthner, F.; Marsal, P.; Beljonne, D.; Müllen, K.; De Schryver, F. C.; Van der Auweraer, M. *Photochemical & Photobiological Sciences* **2008**, *7*, 1509.
(53) Bergman, S. D.; Kol, M. *Inorg. Chem.* **2005**, *44*, 1647.
(54) Gut, D.; Rudi, A.; Kopilov, J.; Goldberg, I.; Kol, M. *J. Am. Chem. Soc.* **2002**, *124*, 5449.
(55) Giordano, C.; Restelli, A.; Villa, M.; Annunziata, R. *J. Org. Chem.* **1991**, *56*, 2270.
(56) Luchinat, C.; Roelens, S. *J. Am. Chem. Soc.* **1986**, *108*, 4873.
(57) Dobashi, A.; Saito, N.; Motoyama, Y.; Hara, S. *J. Am. Chem. Soc.* **1986**, *108*, 307.
(58) Harger, M. J. P. *J. Chem. Soc., Perkin Trans. 2* **1977**, 1882.
(59) Chen, Z. J.; Baumeister, U.; Tschierske, C.; Würthner, F. *Chem. Eur. J.* **2007**, *13*, 450.
(60) Berova, N.; Nakanishi, K. *Circular Dichroism: Principles and Applications*; Wiley-VCH: New York, 2000.
(61) Berova, N.; Di Bari, L.; Pescitelli, G. *Chem. Soc. Rev.* **2007**, *36*, 914.
(62) Buss, V.; Reichardt, C. *Chem. Commun.* **1992**, 1636.
(63) Rybtchinski, B.; Sinks, L. E.; Wasielewski, M. R. *J. Phys. Chem. A* **2004**, *108*, 7497.
(64) Ahrens, M. J.; Sinks, L. E.; Rybtchinski, B.; Liu, W. H.; Jones, B. A.; Giaimo, J. M.; Gusev, A. V.; Goshe, A. J.; Tiede, D. M.; Wasielewski, M. R. *J. Am. Chem. Soc.* **2004**,

126, 8284.
(65) van der Boom, T.; Hayes, R. T.; Zhao, Y. Y.; Bushard, P. J.; Weiss, E. A.; Wasielewski, M. R. *J. Am. Chem. Soc.* **2002**, *124*, 9582.
(66) Giaimo, J. M.; Gusev, A. V.; Wasielewski, M. R. *J. Am. Chem. Soc.* **2002**, *124*, 8530.
(67) Würthner, F.; Chen, Z.; Dehm, V.; Stepanenko, V. *Chem. Commun.* **2006**, 1188.
(68) Tolkki, A.; Vuorimaa, E.; Chukharev, V.; Lemmetyinen, H.; Ihalainen, P.; Peltonen, J.; Dehm, V.; Würthner, F. *Langmuir* **2009**, *26*, 6630.
(69) Yoo, H.; Yang, J.; Yousef, A.; Wasielewski, M. R.; Kim, D. *J. Am. Chem. Soc.*, *132*, 3939.
(70) Fink, R. F.; Seibt, J.; Engel, V.; Renz, M.; Kaupp, M.; Lochbrunner, S.; Zhao, H.-M.; Pfister, J.; Würthner, F.; Engels, B. *J. Am. Chem. Soc.* **2008**, *130*, 12858.
(71) Connors, K. A. *Binding Constants: The Measurement of Molecular Complex Stability*; Wiley: New York, 1987.
(72) Lagona, J.; Mukhopadhyay, P.; Chakrabarti, S.; Isaacs, L. *Angew. Chem., Int. Ed.* **2005**, *44*, 4844.
(73) Wortmann, R.; Rösch, U.; Redi-Abshiro, M.; Würthner, F. *Angew. Chem., Int. Ed.* **2003**, *42*, 2080.
(74) Zheng, Y. R.; Yang, H. B.; Ghosh, K.; Zhao, L.; Stang, P. J. *Chem. Eur. J.* **2009**, *15*, 7203.
(75) Wu, A. X.; Isaacs, L. *J. Am. Chem. Soc.* **2003**, *125*, 4831.
(76) Fink, R. F.; Seibt, J.; Engel, V.; Renz, M.; Kaupp, M.; Lochbrunner, S.; Zhao, H. M.; Pfister, J.; Würthner, F.; Engels, B. *J. Am. Chem. Soc.* **2008**, *130*, 12858.
(77) Amemiya, R.; Yamaguchi, M. *Org. Biomol. Chem.* **2008**, *6*, 26.
(78) Trzaska, S. T.; Hsu, H. F.; Swager, T. M. *J. Am. Chem. Soc.* **1999**, *121*, 4518.
(79) Marquis, D.; Desvergne, J. P.; Bouaslaurent, H. *J. Org. Chem.* **1995**, *60*, 7984.
(80) Gvishi, R.; Reisfeld, R.; Burshtein, Z. *Chem. Phys. Lett.* **1993**, *213*, 338.
(81) Sens, R.; Drexhage, K. H. *J. Lumin.* **1981**, *24-5*, 709.

Chapter 6

Summary

This thesis included the synthesis of conformationally stable chiral perylene bisimide (PBI) dyes, the study of their optical properties in solution and their chiral self-sorting behaviour in nonpolar solvents in which dimerization via π–π-stacking takes place. Furthermore, the influence of PBI core chirality on the properties of these dyes in the condensed state has been also studied.

In **Chapter 2** an overview of the work on general and chiral self-sorting carried out during the last ten years on synthetic supramolecular systems was given. Different definitions according to the pioneering authors were presented, as well as a classification of what we consider the main molecular codes which have been recognized to play a significant role directing self-sorting processes of molecules. We anticipate that, upon developing a better understanding of the variables influencing the efficiency of self-sorting, we will be able to act upon these variables to create supramolecular functional systems of high degree of complexity.

In **Chapter 3** the first successful synthesis of a conformationally restricted chiral macrocyclic 1,7-diaryloxy-substituted PBI and resolution of its atropo-enantiomers was presented (Figure 1a, n = 1). Concentration-dependent UV/Vis studies enabled the quantification of homo vs. heterochiral dimers, and thus the extent of self-recognition vs. self-discrimination in the racemate of this macrocyclic PBI. We showed for the first time that self-recognition prevails over self-discrimination in π-stacking dimerization of core twisted PBIs (Figure 1b) in an extent of 93% of homochiral dimers against only 7% heterochiral dimers at 331 K. Circular dichroism (CD) studies revealed the helical arrangement of the two PBIs within the formed dimers, in agreement with previous X-Ray diffraction studies on similar

macrocyclic PBIs.[i] It was demonstrated that the formation of minor amounts of heterochiral dimers allows the direct determination of the *ee* of chiral PBIs by ^{1}H NMR without using any extern chiral auxiliaries, due to the diastereomeric relationships arising between homo and heterochiral dimers.

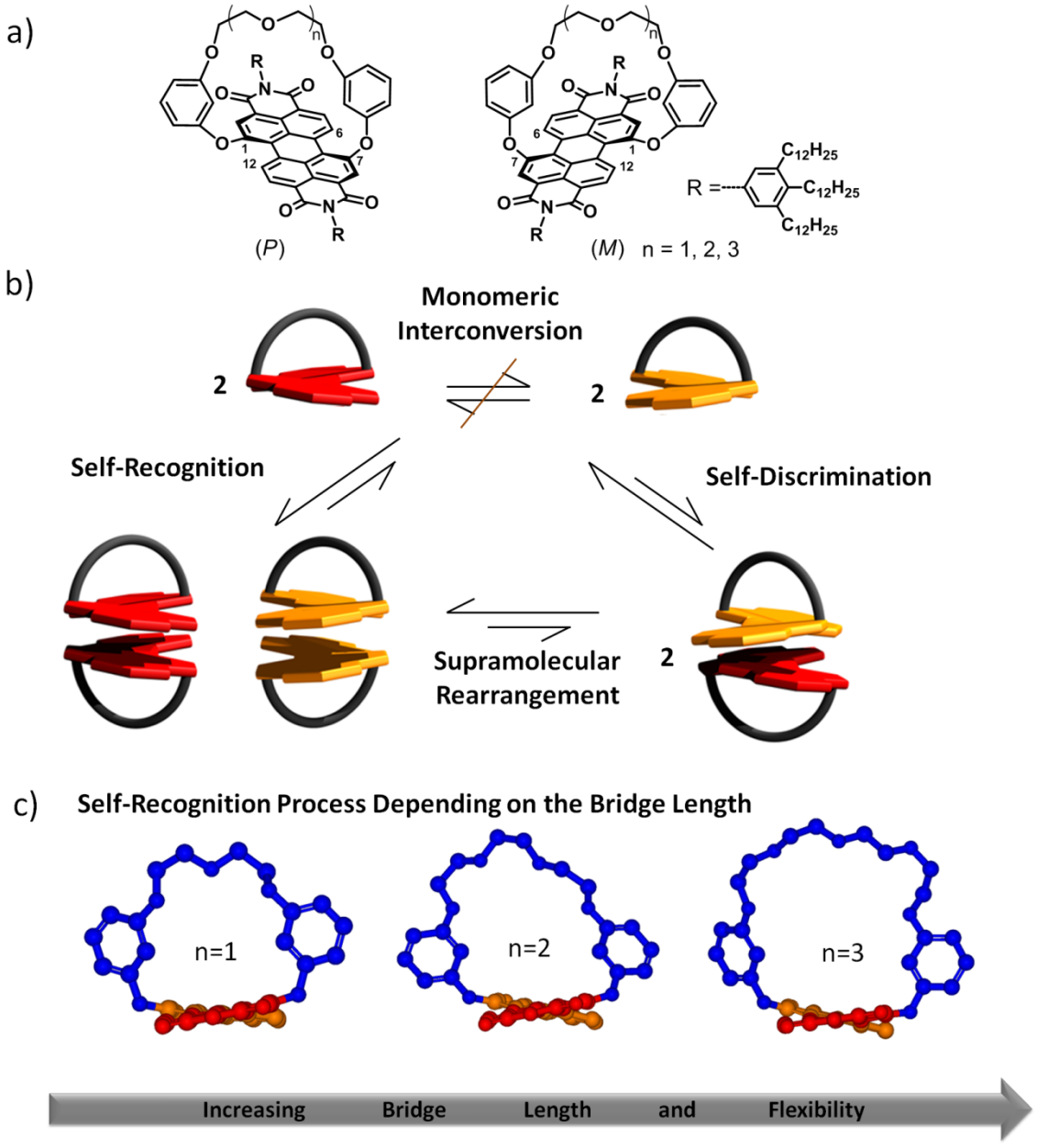

Figure 1. a) Chemical structures of newly synthesized conformationally stable chiral macrocyclic PBIs. b) Cartoon of the different possible equilibria present in a racemic mixture of chiral macrocyclic PBIs. c) Minimized structures of macrocyclic PBIs with increasing bridge length (n = 1–3). Imide substituents removed for clarity.

[i] Peter Osswald, PhD Thesis, University of Würzburg, (Germany), **2007**.

The presence of 3,4,5-tridodecylphenyl units in imide position provides these new chiral macrocyclic PBIs with intriguing liquid crystalline properties. In **Chapter 4** the detailed study on the influence of core-chirality on the mesophase properties of the PBIs with the shortest bridge (Figure 1a, n = 1) was presented. It was demonstrated using differential scanning calorimetry (DSC), polarization microscope (POM), atomic force microscopy (AFM) and X-ray diffraction that the simultaneous presence of equal amounts of each enantiomer in the racemate allows this material to self-organize in a highly organized soft columnar crystalline phase. On the contrary enantiopure (*M*) (or (*P*)) organizes in a less stable, highly fluid lamellar liquid crystalline phase. With the premise that exclusively homochiral π-stacking dimers are formed in the racemate (demonstrated in Chapter 3) a model of alternating *MM* and *PP* homochiral dimers in the condensed phase of the racemate, which allows for excellent nanosegregation and dense packing in columns, was proposed. This model was supported by calculations of the condensed state packing with the force field COMPASS in the module Forcite Plus. In contrast, for pure enantiomers (*M*) (or (*P*)) the bridging units act as sterically shielding entities preventing nanosegregation into columns, which leads to a lamellar organization of the chromophores. Thus, we found strong evidence that π-dimer formation, nanosegregation and optimized packing of the bridging units are the crucial parameters for the differences in the condensed state properties of the racemate and the pure enantiomers.

Finally, the synthesis of conformationally restricted chiral 1,7-diaryloxy-substituted PBIs with different oligoethylene glycol (OEG) bridging units and the resolution of their atropo-enantiomers were discussed in **Chapter 5** (Figure 1c). CD studies of the monomers and dimeric species provided strong evidence that the structures increase in flexibility upon elongation of the OEG bridging units. Similarly as in Chapter 3, the quantification of the extent of chiral self-recognition was carried out after analyzing the concentration-dependent UV/Vis data applying the dimer model. It was found that the presence of homochiral dimers in the racemates was about 95 % for n = 1, 80 % for n = 2 and 65 % for n = 3 at 298 K and 331 K (Figure 1a). Thus, the fidelity of chiral self-sorting in PBIs is compromised by the increasing flexibility of the structures, which was attributed to a partial planarization process and/or a flipping of the naphthalene core units. Less restricted conformations enable more packing possibilities, some of them obviously favoring the formation of heterochiral dimers.

It was proven that temperature does not play a role in the efficiency of chiral self-sorting. Quantum mechanical calculations confirmed the preference of homodimers in comparison to the less energetically favored heterodimers (Figure 1b), which is in accordance with the experimental data. ^{1}H NMR studies demonstrated that all aggregates of macrocyclic PBIs (n = 1−3) self-assemble under fast exchange conditions and ROESY studies show intermolecular crossing peaks corresponding to π-stacked dimers. The investigations carried out by DSC, POM and AFM proved that the condense state properties of this series of macrocyclic PBIs is strongly affected by the elongation of the EOG bridging units, which is both related to the chirality of the PBI cores and the increasing flexibility of the structures.

In conclusion, we have demonstrated and quantified the prevalence of chiral self-recognition over self-discrimination in π-stacking dimerization of PBIs. It has been shown that this self-recognition event is compromised by the increasing flexibility of the structures related to the size of the OEG bridging units. Moreover, the inherent chirality of these PBIs has been proven to strongly influence their condensed state properties, for which large differences between the pure enantiomers and the racemates were revealed, as well as between the different bridged macrocyclic PBIs.

Zusammenfassung

Das Ziel der vorliegenden Arbeit war die Synthese von konformationsstabilen chiralen Perylenbisimidfarbstoffen (PBI), die Bestimmung ihrer optischen Eigenschaften in Lösung und ihrer chiralen Selbstsortierung in unpolaren Lösungsmitteln, in denen Dimerisierung durch π- π Stapelung stattfindet. Des Weiteren wurde noch der Einfluss der PBI Kernchiralität auf die flüssigkristallinen Eigenschaften untersucht.

In **Kapitel 2** wurde zunächst ein Überblick über die aktuellen Arbeiten der letzten zehn Jahre im Bereich der allgemeinen und chiralen Selbstsortierung supramolekularer Komplexe gegeben. Es wurden sowohl verschiedene Definitionen der Pioniere dieses Gebietes als auch die Klassifizierungen der molekularen Codes, welche die molekulare Selbstsortierung maßgeblich beeinflussen, vorgestellt. Durch das vollständige Verständnis der molekularen Eigenschaften, die die Effizienz der Selbstsortierung beeinflussen, sollen zukünftig funktionale supramolekulare Systeme von sehr hoher Komplexität zugänglich werden.

Kapitel 3 beschreibt die erfolgreiche Synthese der ersten konformationsfixierten chiralen makrozyklischen 1,7-diaryloxy-substituierten PBIs und die Trennung ihrer Atropo-Enantiomere (Figure 1a, n=1). Konzentrationsabhängige UV/Vis-Studien ermöglichten die Quantifizierung von homo- gegenüber heterochiralen Dimeren und dadurch die Bestimmung des Verhältnisses von Selbsterkennung und Selbstdiskriminierung im Racemat dieses makrozyklischen Farbstoffes. Es konnte zum ersten Mal gezeigt werden, dass die Selbsterkennung gegenüber der Selbstdiskriminierung bei der π-Dimerisierung von kernverdillten PBIs mit einem Verhältnis von 93% homochiralen Dimeren gegenüber nur 7% heterochiralen Dimeren bevorzugt wird (Figure 1b). Mit Hilfe von CD-Untersuchungen konnte außerdem die supramolekulare Natur der gebildeten Dimere belegt werden, in Einklang mit kristallographischen Ergebnissen für ähnliche makrozyklische PBIs.[j] Es wurde ferner gezeigt, dass die Bildung kleiner Anteile von heterochiralen Dimeren die direkte Bestimmung der *ee*-Werte der chiralen PBIs mit Hilfe von ^{1}H NMR gestattet. Dies ist

[j] Peter Osswald, Doktorarbeit, Würzburg Universität, (Deutschland), **2007**.

aufgrund der diastereomeren Beziehung zwischen homo- und heterochiralen Dimeren ohne die Verwendung von externen chiralen Hilfsreagenzien möglich.

Die Verwendung von 3,4,5-Tridodecylphenyl-Einheiten in den Imidpositionen führte zu interessanten flüssigkristallinen Eigenschaften für diese neuen chiralen makrozyklischen PBIs. In **Kapitel 4** wird der Einfluss der Chiralität des π-Systems auf die Mesophase der PBIs mit der kürzesten Brücke (Figure 1a, n=1) beschrieben. Mit Hilfe von Pulverröntgenbeugung, DSC-, POM-, und AFM-Messungen konnte bewiesen werden, dass bei Anwesenheit gleicher Anteile beider Enantiomere im Racemat eine Selbstsortierung unter Ausbildung kolumnarer soft-kristalliner Phasen stattfindet. Im Gegensatz dazu bildet das enantiomerenreine Material eine lamellare flüssigkristalline Phase aus. Unter der Voraussetzung, dass nur homochirale π-gestapelte Dimere im Racemat gebildet werden (gezeigt in Kapitel 3), wird ein Model von wechselnden *MM* und *PP* homochiralen Dimeren in der Mesophase des Racemats vorgestellt. Dieses führt zu einer Nanosegregation und ermöglicht eine dichte Packung in den Kolumnen. Das Model wird durch Berechnungen für die verdichtete Phase mit dem Kraftfeld COMPASS Forcite Plus unterstützt. Für reine Enantiomere (*M*) (oder (*P*)) agiert die Brückeneinheit dagegen als sterische Abschirmung, welche die Nanosegregation in den Kolumnen verhindert. Dies führt zu einer lamellaren Anordnung der Chromophore. Auf diese Weise konnte überzeugend gezeigt werden, dass die Nanosegregation und die Optimierung der Packung der Brückeneinheiten die entscheidenden Parameter für die Unterschiede in den kondensierten Phasen des Racemats und des reinen Enantiomeren sind.

Im letzten **Kapitel 5** wird die Synthese von konformationsbeschränkten chiralen 1,7 diaryloxy-substituierten PBIs mit verschieden langen Oligoethyleneglykol-Brückeneinheiten und ihre Auftrennung in ihre atropo-Enantiomere beschrieben (Figure 1c). Die durch längere Brückeneinheiten gegebene erhöhte Flexibilität zeigte sich in den CD-Spektren der Monomer- und Dimereinheiten. Vergleichbar zu Kapitel 3 konnte der Überschuss von chiraler Selbsterkennung gebildeter Homodimere durch Analyse der konzentrationsabhängigen UV/Vis Daten erfolgen. Im Racemat konnten sowohl bei 298 als auch bei 331 K 95 % (für n=1), 80 % (für n=2) bzw. 65 % (für n=3) homochirale Dimere nachgewiesen werden. Die Präferenz für die chirale Selbstanordnung der PBIs wird somit durch die größer werdende Flexibilität der Strukturen verringert. Dies kann mit einem erleichterten

Planarisierungsprozess bei Vorliegen weniger rigider Naphthalineinheiten erklärt werden. Ein möglicher Temperatureinfluss wurde untersucht und ausgeschlossen. Quantenmechanische Berechnungen unterstützen die experimentellen Daten für die Bevorzugung von Homodimeren im Vergleich zu energetisch weniger begünstigten Heterodimeren. ^{1}H NMR Messungen bewiesen des Weiteren, dass alle Aggregate einem schnellen molekularem Austausch unterliegen. Zusätzlich konnten intermolekulare Kreuzsignale der ROESY Messungen den entsprechenden π-gestapelten Dimeren zugeordnet werden. DSC-, POM- und AFM-Messungen zeigten auch, dass die Festkörpereigenschaften dieser Reihe von makrozyklischen PBIs stark durch die Brückeneinheiten geprägt werden, da diese direkt die Chiralität der PBI Kerne und ihre strukturelle Flexibilität beeinflussen.

Zusammenfassend konnte im Rahmen dieser Arbeit die Bevorzugung der chiralen Selbst-Erkennung gegenüber der Selbst-Diskriminierung in π-gestapelten dimerisierten PBIs quantifiziert und bewiesen werden. Eine erhöhte Flexibilität der Moleküle durch Verlängerung der OEG Brückeneinheiten verringert jedoch die Qualität dieses Selbsterkennungsvorgangs. Des Weiteren hat die Chiralität dieser PBIs einem sehr starken Einfluss auf die Eigenschaften der kondensierten Materie, in welcher große Unterschiede für reine Enantiomere und das Racemat sowie zwischen PBIs mit unterschiedlichen Brückeneinheiten gefunden wurden.

Resumen

Esta tesis trata de la síntesis de perileno-bisimidas (PBI) quirales conformacionalmente estables, el estudio de sus propiedades ópticas en disolución y su comportamiento de auto-selección quiral en disolventes apolares en los que tiene lugar un proceso de dimerizacion a traves de apilamiento π–π . Por ultimo desvelamos la influencia de la chiralidad del centro aromatico del PBI en las propiedades de cristal líquido de este tipo de moleculas.

En el **Capítulo 2** se ofrece una visión general sobre el trabajo llevado a cabo en los últimos años en comportamiento auto-selectivo ordinario y quiral. Diferentes definiciones de acuerdo con los autores pioneros en este tema son presentadas asi como una selección en lo que nosotros consideramos los codigos moleculares que se han manisfestado como más relevantes y fructíferos en los procesos de auto-selección. Adelantamos que la comprensión de las variables que influyen en la eficiencia de procesos de auto-selección nos llevará a poder actuar sobre estas variables para crear sistemas supramoleculares que muestren la complejidad de sus contrapartes naturales.

En el **Capítulo 3** se muestra la síntesis de PBIs macrocíclicas quirales 1,7-diaryloxy-sustituidas con la conformación restringida ademas de la la resolución de sus atropo-enantiómeros (Figure 1a, n = 1). Estudios de UV/Vis dependientes de la concentración han permitido la cuantificación de la relación homo vs. heterodímeros chirales, y por lo tanto el grado de auto-reconocimiento vs. auto-discriminación en el racemato de estas PBI macrocíclicas. Hemos podido demostrar por primera vez que el auto-reconocimiento prevalece sobre la auto-discriminación a traves de apilamiento π en la dimerización de PBIs (Figure 1b) en una extensión del 93% de homodímeros frente a sólo el 7% de heterodímeros a 331K. Estudios de dicroísmo circular (CD) han revelado la naturaleza quiral de estos dímeros supramoleculares, apoyada por anteriores estudios de difracción de rayos X en PBIs macrocíclicas similares.[k] Se expone que la formación de pequeñas cantidades de dímeros heterochirales permite la determinación directa del *ee* de PBIs quirales usando ^{1}H RMN sin utilizar ningún auxiliar quiral externo, debido a las relaciones diastereoméricas que surgen

[k] Peter Osswald, Thesis Doctoral, Universidad de Wurzburgo (Alemania), 2007.

entre homo y heterodímeros quirales.

La presencia de unidades de 3,4,5- tridodecanofenol en las posiciones imida proporcionana interesantes propiedades de cristal líquido a estas nuevas PBIs quirales. En el **Capítulo 4** se presenta un estudio detallado sobre la influencia del núcleo quiral en las propiedades de la mesofase de las PBIs con el menor puente (Figura 1a, n = 1). Se pudo demostrar mediante calorimetría diferencial de barrido (DSC), microscopio de polarización (POM), microscopía de fuerza atómica (AFM) y difracción de rayos X que la presencia simultánea de cantidades iguales de cada uno de los enantiómeros en el racemato de este material permite la auto-organización en una fase cristalina columnar suave con una mayor estabilidad en comparación con los enantiómeros puros (*M*) (o (*P*)), que se organizan en fase laminar líquido cristalina. Con la premisa de que en el racemato se forman casi exclusívamente homodímeros por apilamiento π (demostrado en el Capítulo 3) se ha propuesto un modelo en el que los dímeros homochirales *MM* y *PP* se apilan alternativamente en la fase condensada del racemato permitiendo una nanosegregación excelente y una alta densidad del material. Este modelo se apoya en los calculos del empaquetamiento del racemato realizado con el programa de campo de fuerza COMPASS en el módulo Forcite Plus del estado condensado. En cambio, para los enantiómeros puros (*M*) (o (*P*)), las unidades-puente actuan como blindajes estéricos que impiden a las entidades la nanosegregación en columnas, que conduce a una organización laminar de los cromóforos. Así, encontramos una fuerte evidencia de que la nanosegregación y la optimización del empaquetamiento de las unidades-puente son los parámetros fundamentales para la diferencia en las propiedades de estado condensado del racemato y los enantiómeros puros. En consecuencia, podemos afirmar que la quiralidad del núcleo aromático del PBI juega un papel crucial en el auto-ensamblaje de estos PBIs en el estado condensado.

Por último, en el **Capítulo 5** se muestra la síntesis de PBIs 1,7-diaryloxy-sustituidos de conformación quiral restringida con diferentes tamaños de unidades-puente ademas de la resolución de sus atropo-enantiómeros (Figure 1c). Estudios de CD de los monómeros y dímeros de estas nuevas especies proporcionan una fuerte evidencia de que la flexibilidad de estas estructuras aumenta con el alargamiento de las unidades-puente. Del mismo modo que en el Capítulo 3, la cuantificación de la magnitud de auto-reconocimiento quiral ha podido

llevarse a cabo después del procesamiento de los datos UV/Vis dependientes de la concentración. Se encontró que la presencia de dímeros homoquirales en el racemato es alrededor del 95 % para n = 1, 80 % para n = 2 y el 65 % para n = 3 a 298 K y 331 K. Por lo tanto, la fidelidad de auto-selección quiral en PBIs se ve comprometida por la creciente flexibilidad de las estructuras, lo que se atribuye al proceso planarización parcial que tiene lugar por interconvesión de las unidades básicas de naftaleno. Se ha demostrado que la temperatura no tiene ninguna influencia en la eficiencia del proceso de auto-selección quiral. Cálculos de mecánica cuántica han confirmado la prevalencia de homodímeros en comparación con los heterodímeros –menos energéticamente favorecidos– (Figura 1b), de acuerdo con los datos experimentales previos. Estudios de ^{1}H RMN han demostrado que todos los sistemas están en condiciones de intercambio rápido y los estudios de ROESY muestran señales correspondientes al apilamiento π intermolecular de dímeros. Las investigaciones por DSC, POM y AFM muestran que las propiedades de cristal líquido de esta serie de PBIs macrocíclicas se ven afectadas en gran medida por el alargamiento de las unidades-puente y a su vez por la quiralidad en los núcleos aromáticos de estas PBIs y el aumento de la flexibilidad de las estructuras.

En conclusión, hemos probado y cuantificado la prevalencia del auto-reconocimiento sobre la auto-discriminación quiral en la dimerización de apilamiento π de PBIs. Se ha demostrado que el auto-reconocimiento se ve comprometido por la creciente flexibilidad de las estructuras, lo que esta relacionado con el tamaño de las unidades-puente. Por otra parte, la quiralidad inherente en estas PBIs ha demostrado tener una fuerte influencia sobre sus propiedades en la mesofase, en la que se ha observado grandes diferencias entre los enantiómeros puros y racematos, así como entre las diferentes PBIs macrocíclicas.

Appendix

Supplement to Chapter 5

a)

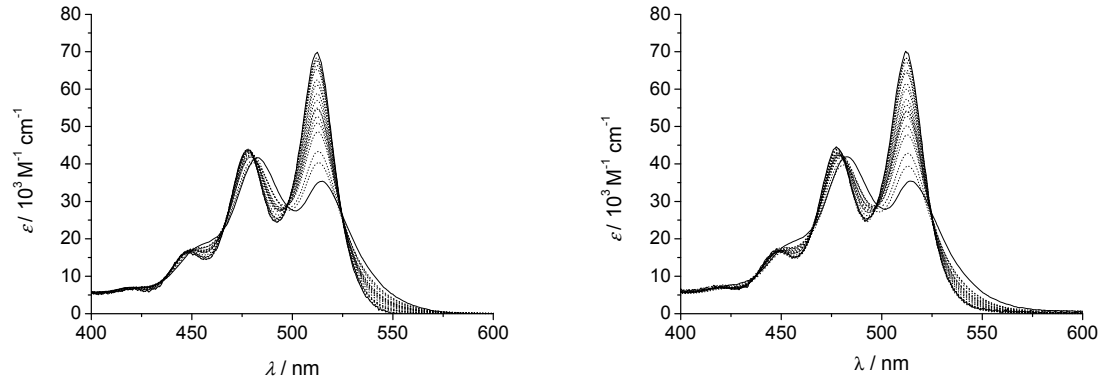

b)

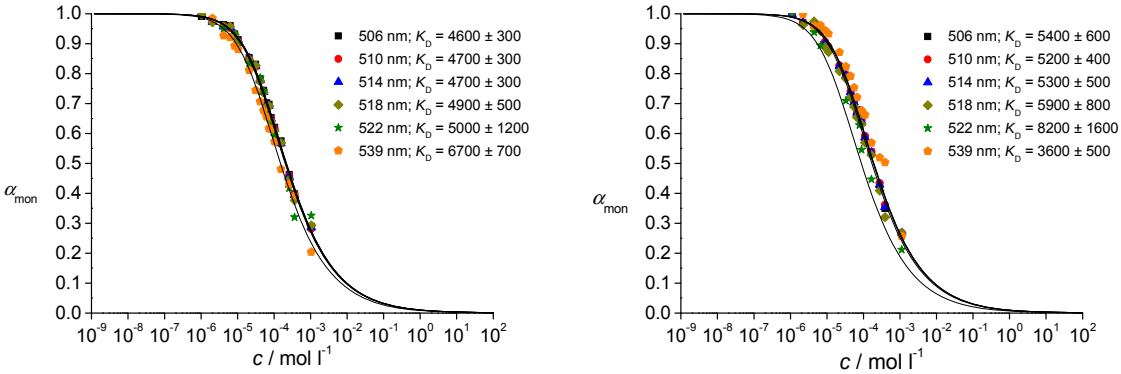

c)

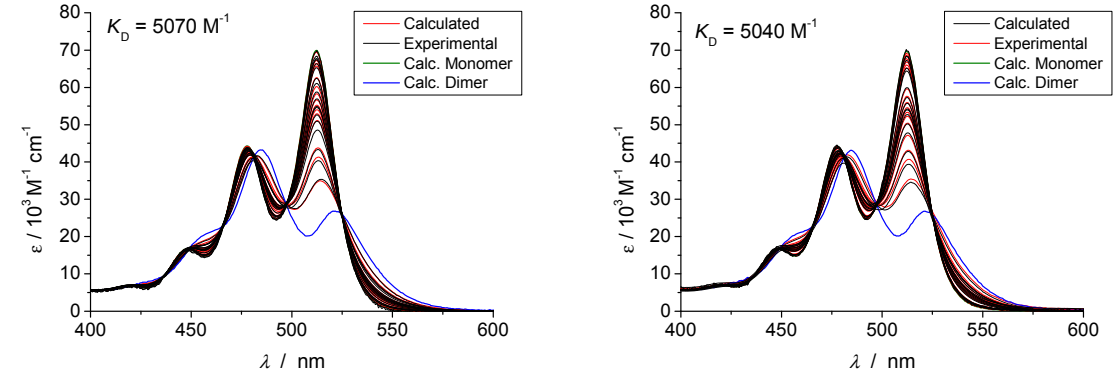

Figure A1. Illustration of the applied data acquisition and evaluation procedure based on two independent experiments (left and right). a) Concentration-dependent UV/Vis absorption spectra of (*P*)-**4b** in *n*-heptane at 331 K ($[M]_0 = 4 \times 10^{-6}$ M to 1×10^{-3} M), b) molar fraction of monomer species and dimerization constants obtained from nonlinear regression analysis at selected wavelengths indicated in the inset, and c) results from the multilinear fit routine showing the comparison of experimental (black) and derived (red) spectra at respective concentrations as well as derived pure monomer (green) and dimer (blue) spectra.

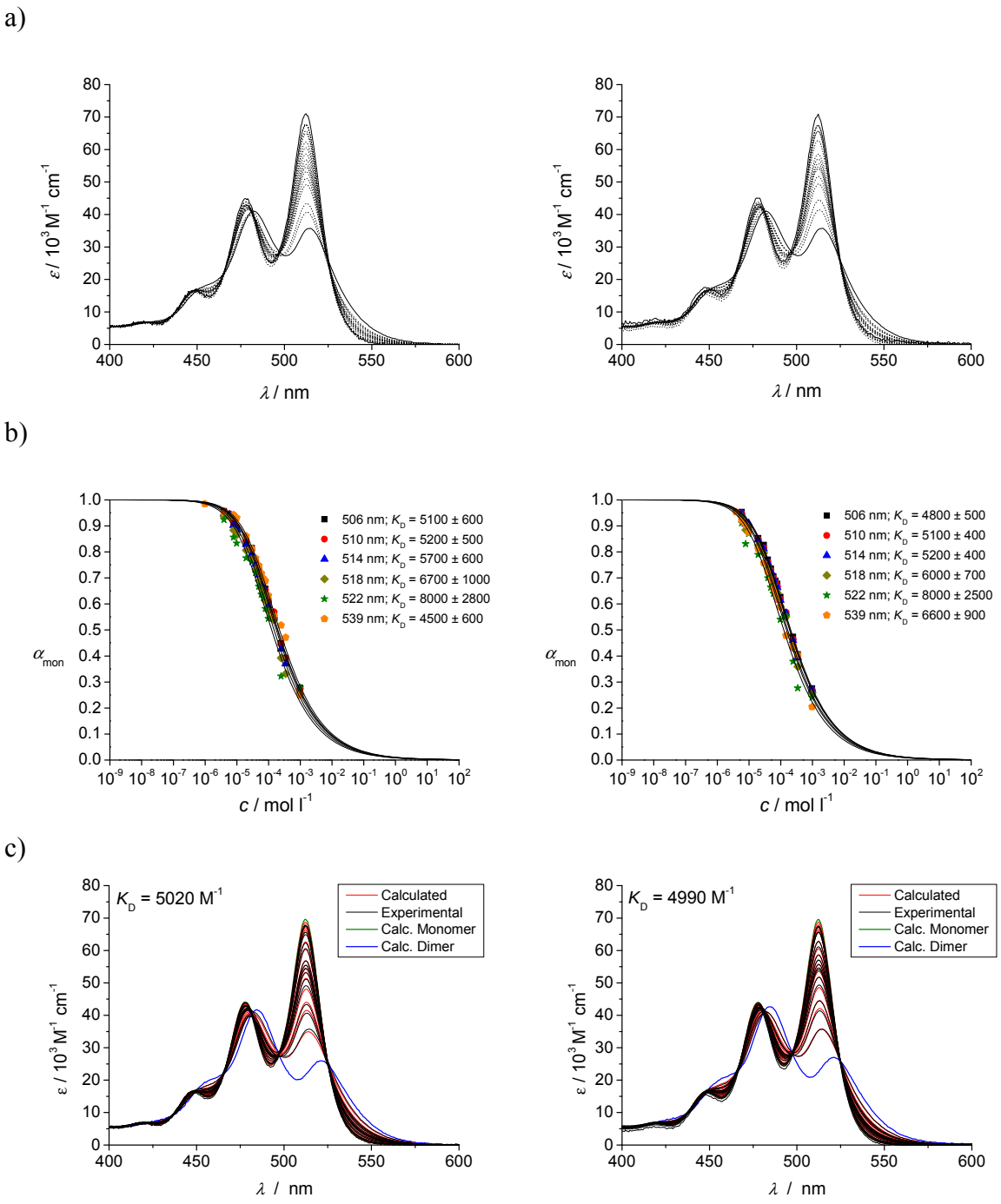

Figure A2. Illustration of the applied data acquisition and evaluation procedure based on two independent experiments (left and right). a) Concentration-dependent UV/Vis absorption spectra of (*M*)-**4b** in *n*-heptane at 331 K ($[M]_0 = 4 \times 10^{-6}$ M to 1×10^{-3} M), b) molar fraction of monomer species and dimerization constants obtained from nonlinear regression analysis at selected wavelengths indicated in the inset, and c) results from the multilinear fit routine showing the comparison of experimental (black) and derived (red) spectra at respective concentrations as well as derived pure monomer (green) and dimer (blue) spectra.

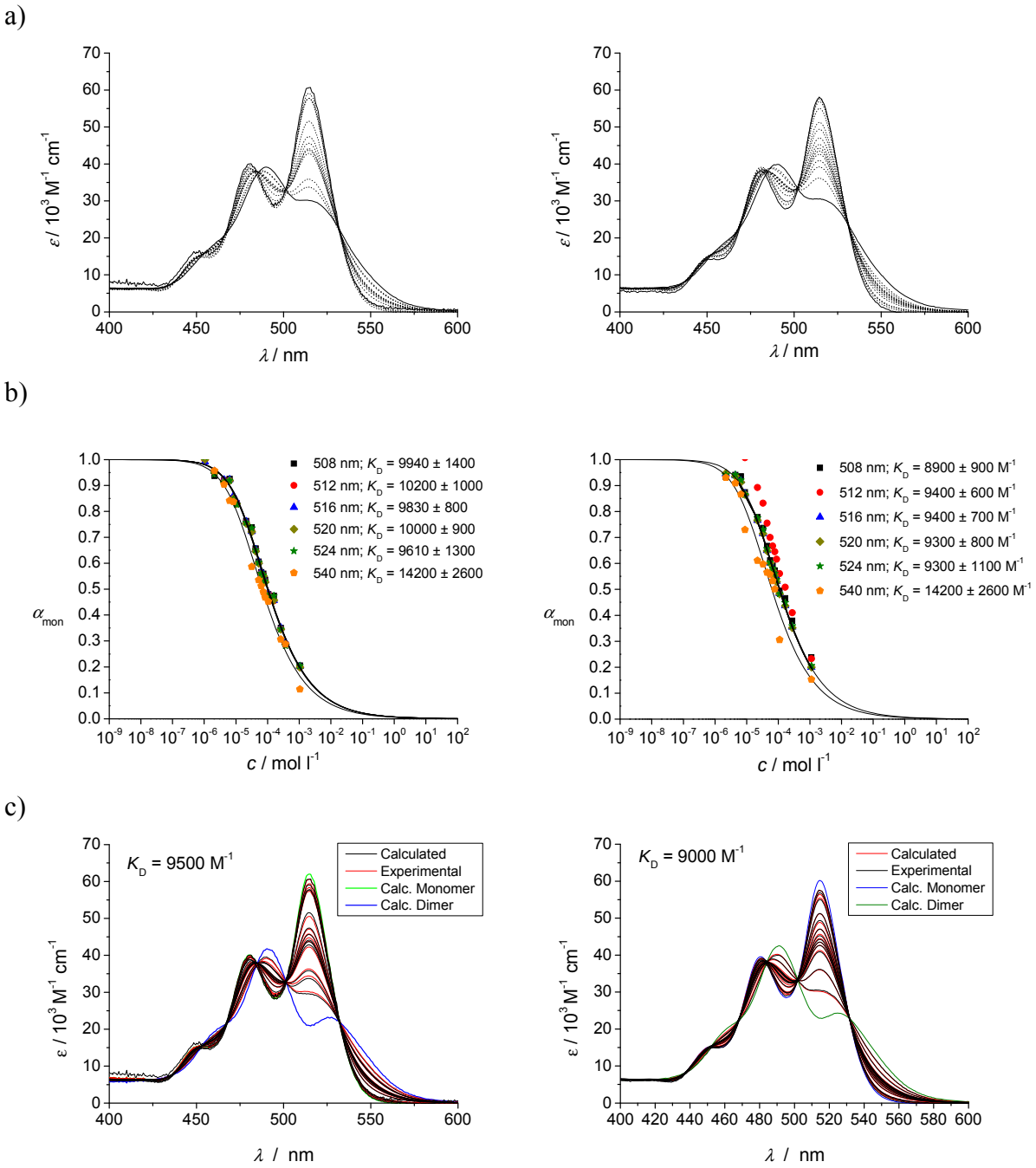

Figure A3. Illustration of the applied data acquisition and evaluation procedure based on two independent experiments (left and right). a) Concentration-dependent UV/Vis absorption spectra of (*M*)-**4c** in *n*-heptane at 331 K ($[M]_0 = 4 \times 10^{-6}$ M to 1×10^{-3} M), b) molar fraction of monomer species and dimerization constants obtained from nonlinear regression analysis at selected wavelengths indicated in the inset, and c) results from the multilinear fit routine showing the comparison of experimental (black) and derived (red) spectra at respective concentrations as well as derived pure monomer (green) and dimer (blue) spectra.

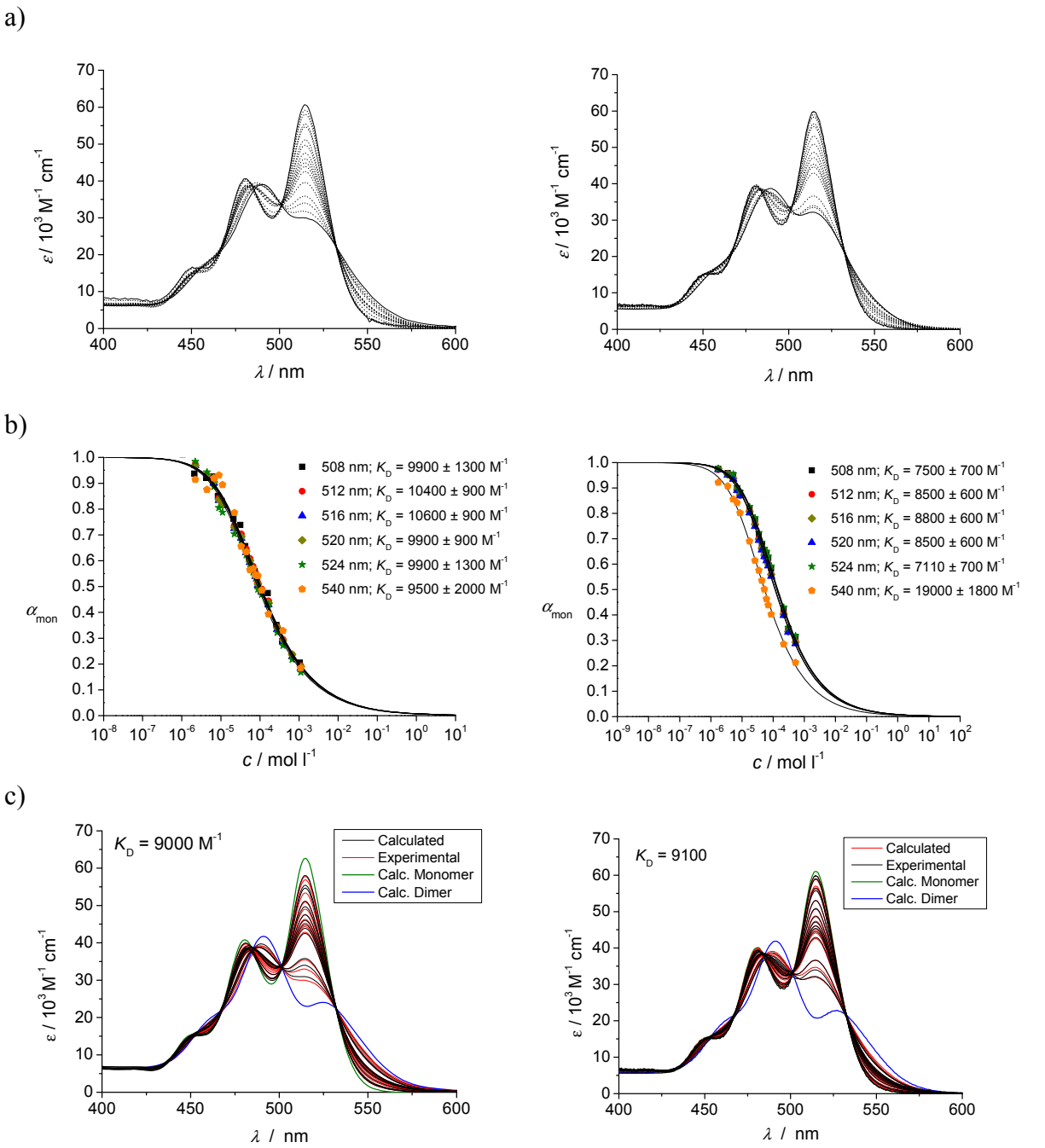

Figure A4. Illustration of the applied data acquisition and evaluation procedure based on two independent experiments (left and right). a) Concentration-dependent UV/Vis absorption spectra of (*P*)-**4c** in *n*-heptane at 331 K ($[M]_0 = 4 \times 10^{-6}$ M to 1×10^{-3} M), b) molar fraction of monomer species and dimerization constants obtained from nonlinear regression analysis at selected wavelengths indicated in the inset, and c) results from the multilinear fit routine showing the comparison of experimental (black) and derived (red) spectra at respective concentrations as well as derived pure monomer (green) and dimer (blue) spectra.

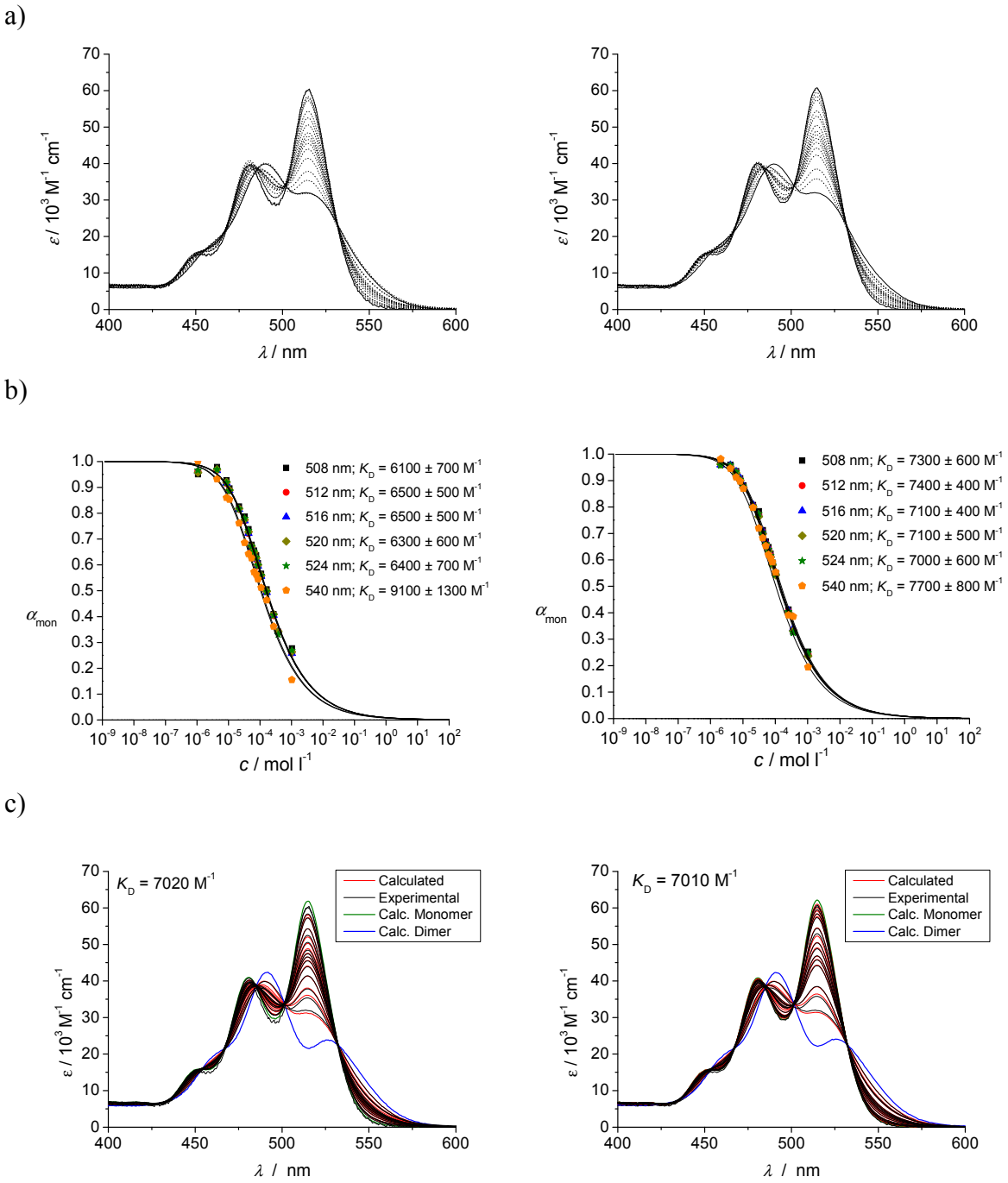

Figure A5. Illustration of the applied data acquisition and evaluation procedure based on two independent experiments (left and right). a) Concentration-dependent UV/Vis absorption spectra of (*rac*)-**4c** in *n*-heptane at 331 K ($[M]_0 = 4 \times 10^{-6}$ M to 1×10^{-3} M), b) molar fraction of monomer species and dimerization constants obtained from nonlinear regression analysis at selected wavelengths indicated in the inset, and c) results from the multilinear fit routine showing the comparison of experimental (black) and derived (red) spectra at respective concentrations as well as derived pure monomer (green) and dimer (blue) spectra.

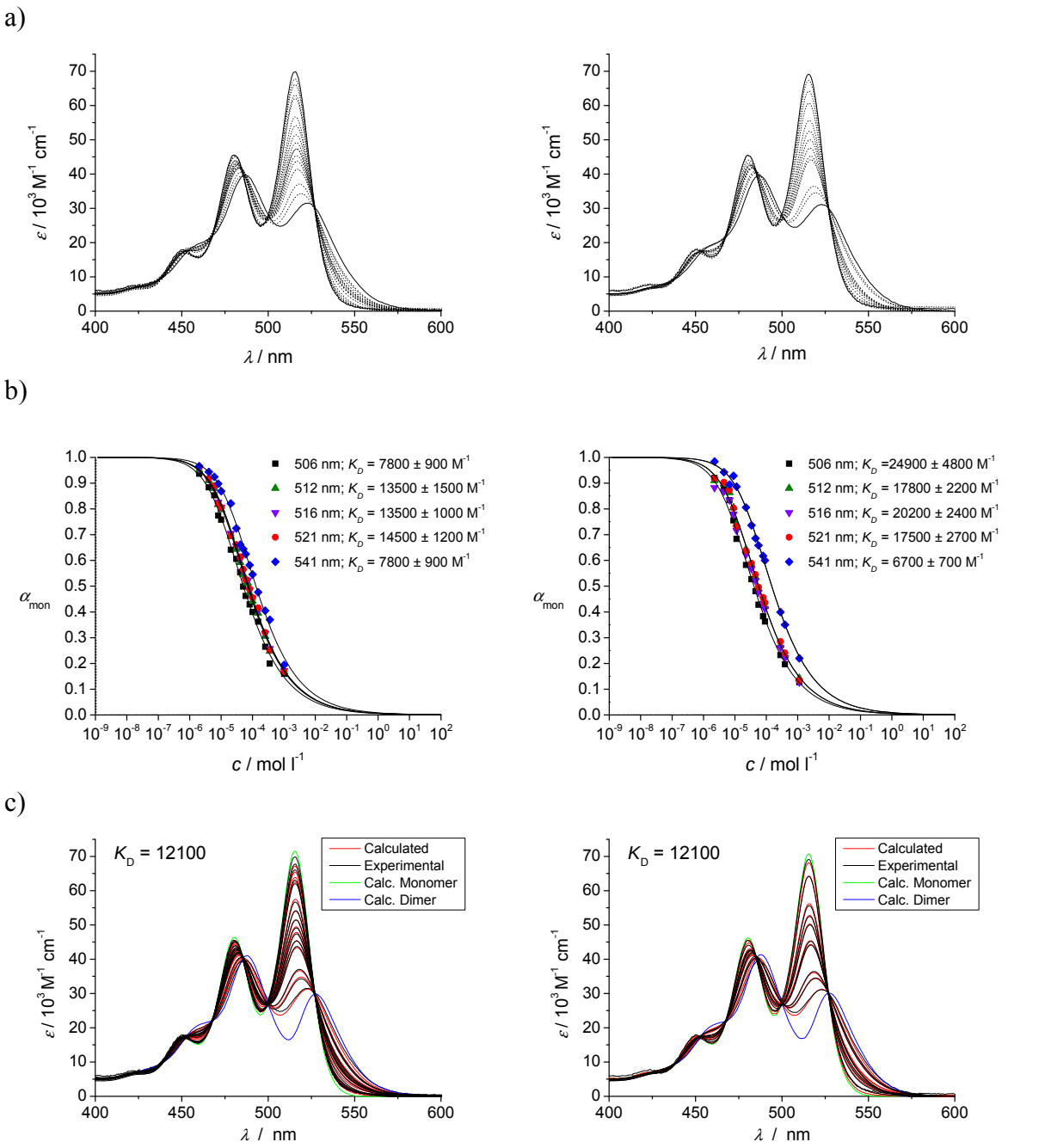

Figure A6. Illustration of the applied data acquisition and evaluation procedure based on two independent experiments (left and right). a) Concentration-dependent UV/Vis absorption spectra of (*P*)-**4a** in *n*-heptane at 298 K ($[M]_0 = 4 \times 10^{-6}$ M to 1×10^{-3} M), b) molar fraction of monomer species and dimerization constants obtained from nonlinear regression analysis at selected wavelengths indicated in the inset, and c) results from the multilinear fit routine showing the comparison of experimental (black) and derived (red) spectra at respective concentrations as well as derived pure monomer (green) and dimer (blue) spectra.

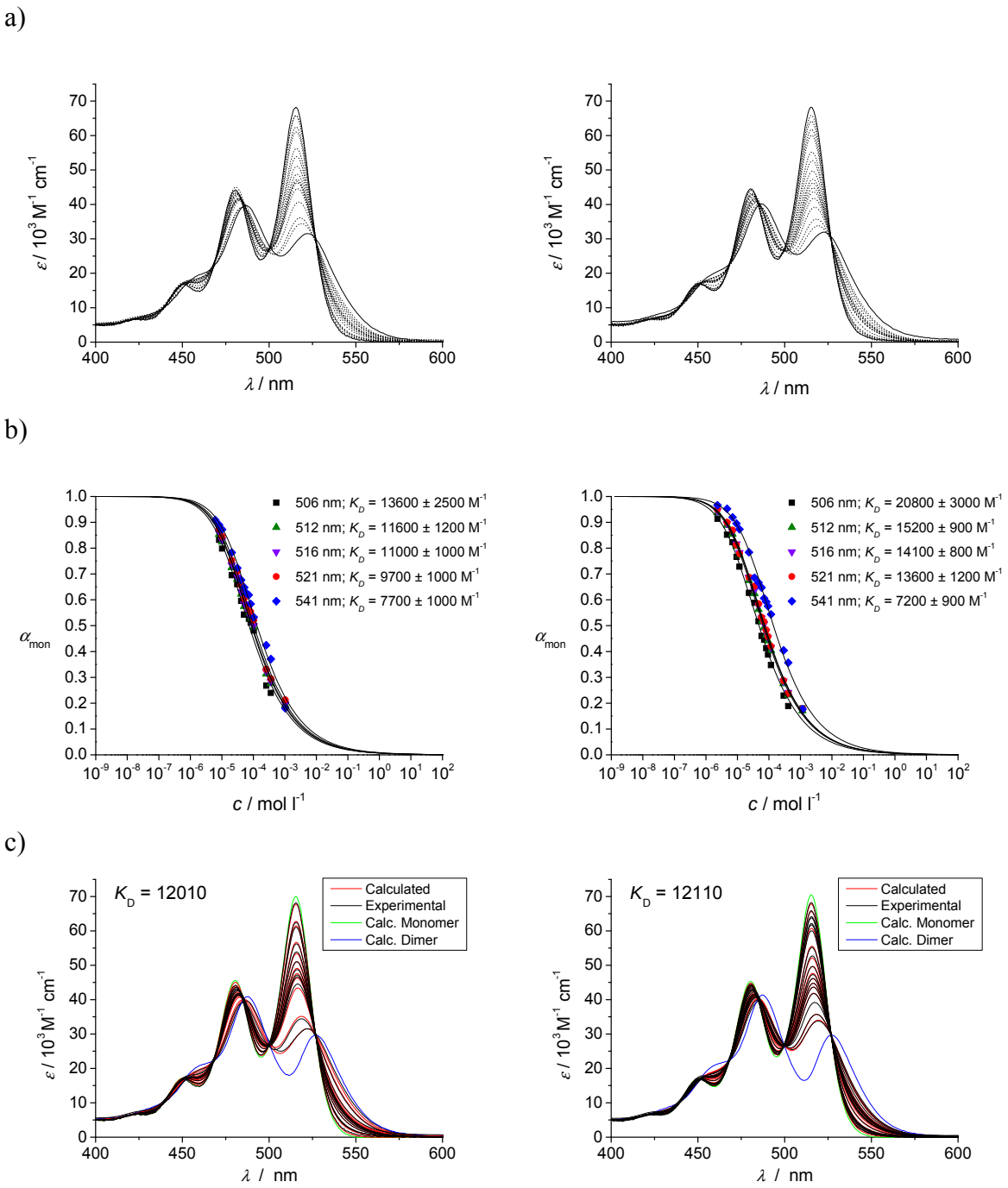

Figure A7. Illustration of the applied data acquisition and evaluation procedure based on two independent experiments (left and right). a) Concentration-dependent UV/Vis absorption spectra of (*M*)-**4a** in *n*-heptane at 298 K ($[M]_0 = 4 \times 10^{-6}$ M to 1×10^{-3} M), b) molar fraction of monomer species and dimerization constants obtained from nonlinear regression analysis at selected wavelengths indicated in the inset, and c) results from the multilinear fit routine showing the comparison of experimental (black) and derived (red) spectra at respective concentrations as well as derived pure monomer (green) and dimer (blue) spectra.

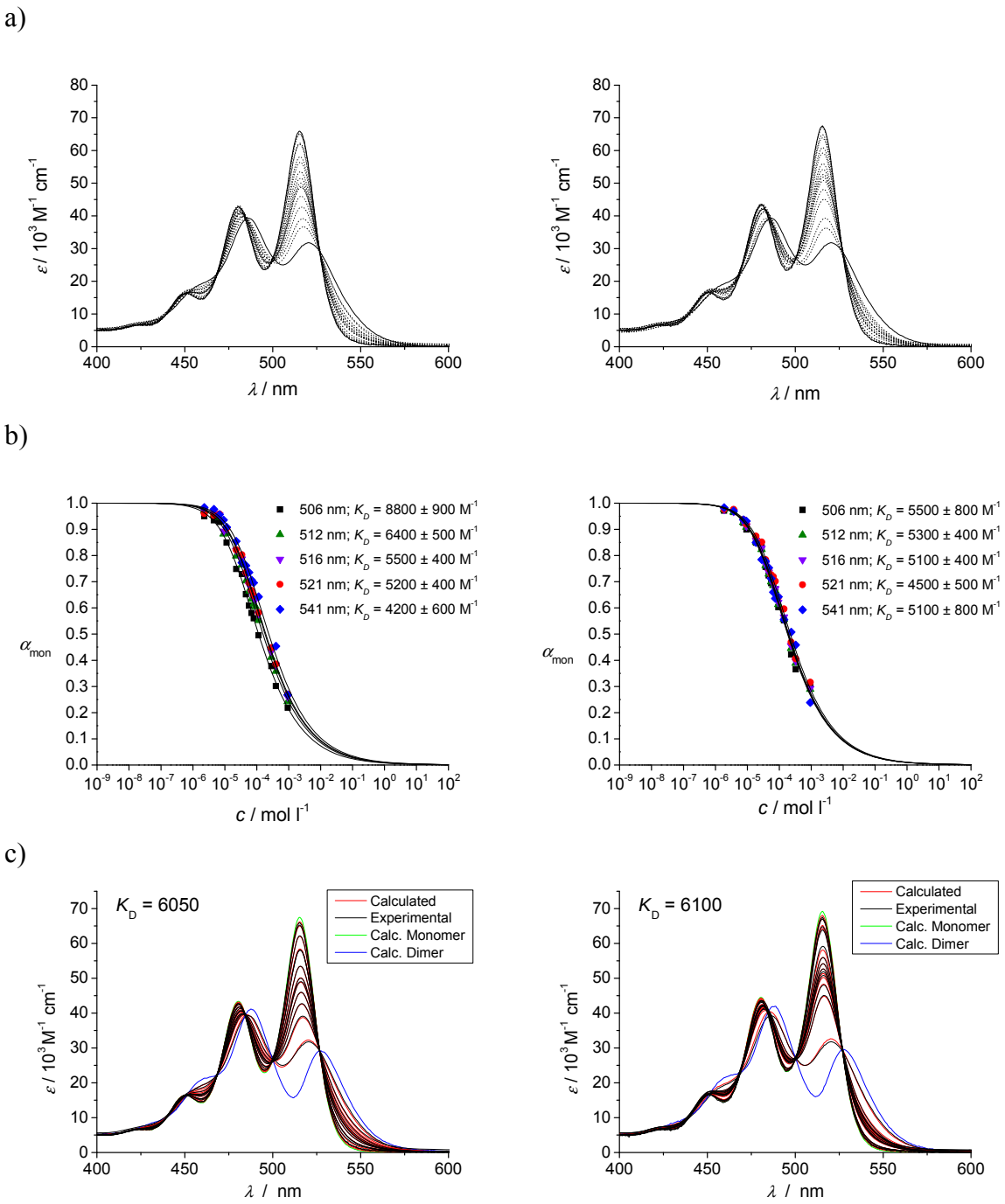

Figure A8. Illustration of the applied data acquisition and evaluation procedure based on two independent experiments (left and right). a) Concentration-dependent UV/Vis absorption spectra of (*rac*)-**4a** in *n*-heptane at 298 K ($[M]_0 = 4 \times 10^{-6}$ M to 1×10^{-3} M), b) molar fraction of monomer species and dimerization constants obtained from nonlinear regression analysis at selected wavelengths indicated in the inset, and c) results from the multilinear fit routine showing the comparison of experimental (black) and derived (red) spectra at respective concentrations as well as derived pure monomer (green) and dimer (blue) spectra.

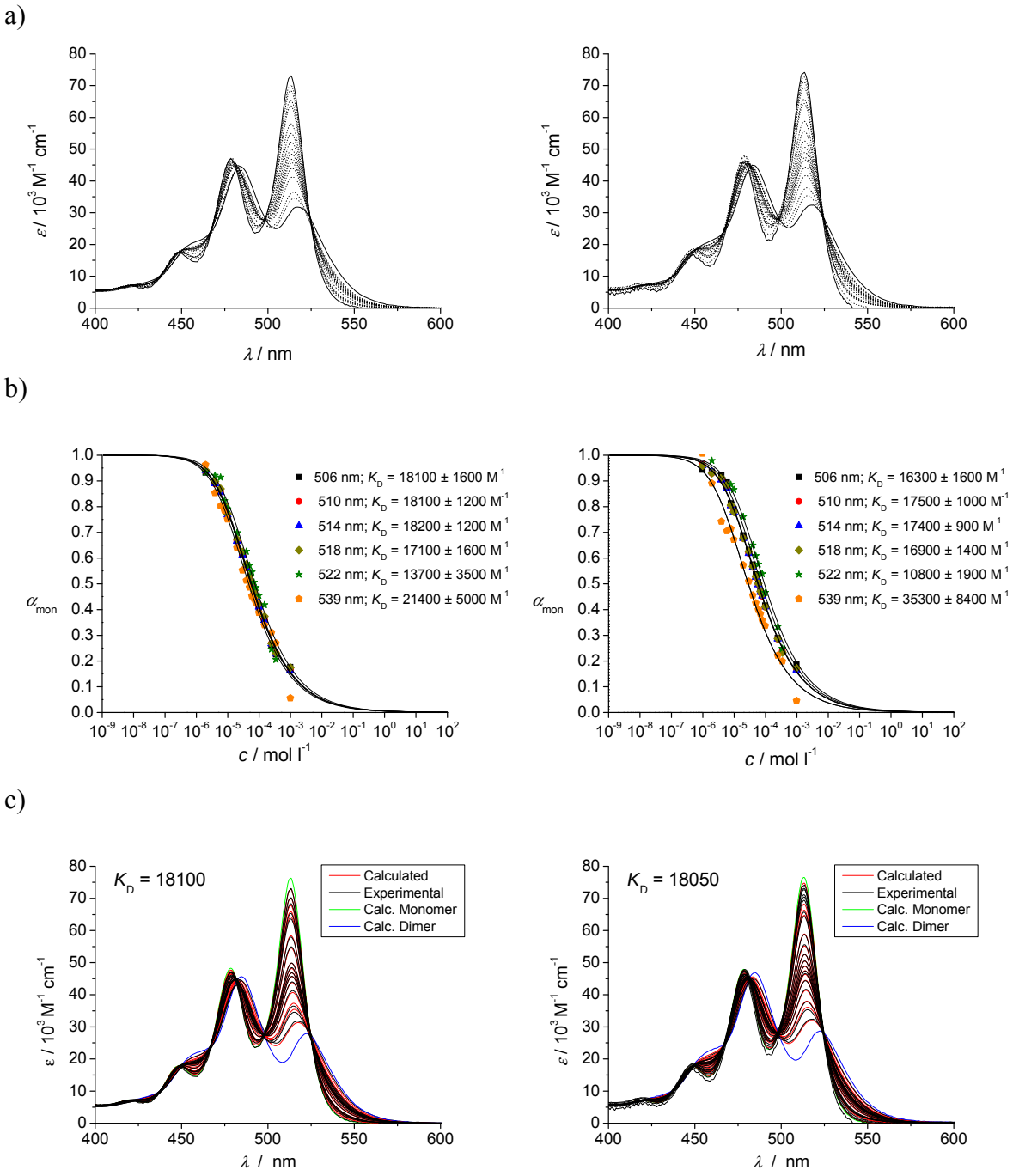

Figure A9. Illustration of the applied data acquisition and evaluation procedure based on two independent experiments (left and right). a) Concentration-dependent UV/Vis absorption spectra of (*P*)-**4b** in *n*-heptane at 298 K ($[M]_0 = 4 \times 10^{-6}$ M to 1×10^{-3} M), b) molar fraction of monomer species and dimerization constants obtained from nonlinear regression analysis at selected wavelengths indicated in the inset, and c) results from the multilinear fit routine showing the comparison of experimental (black) and derived (red) spectra at respective concentrations as well as derived pure monomer (green) and dimer (blue) spectra.

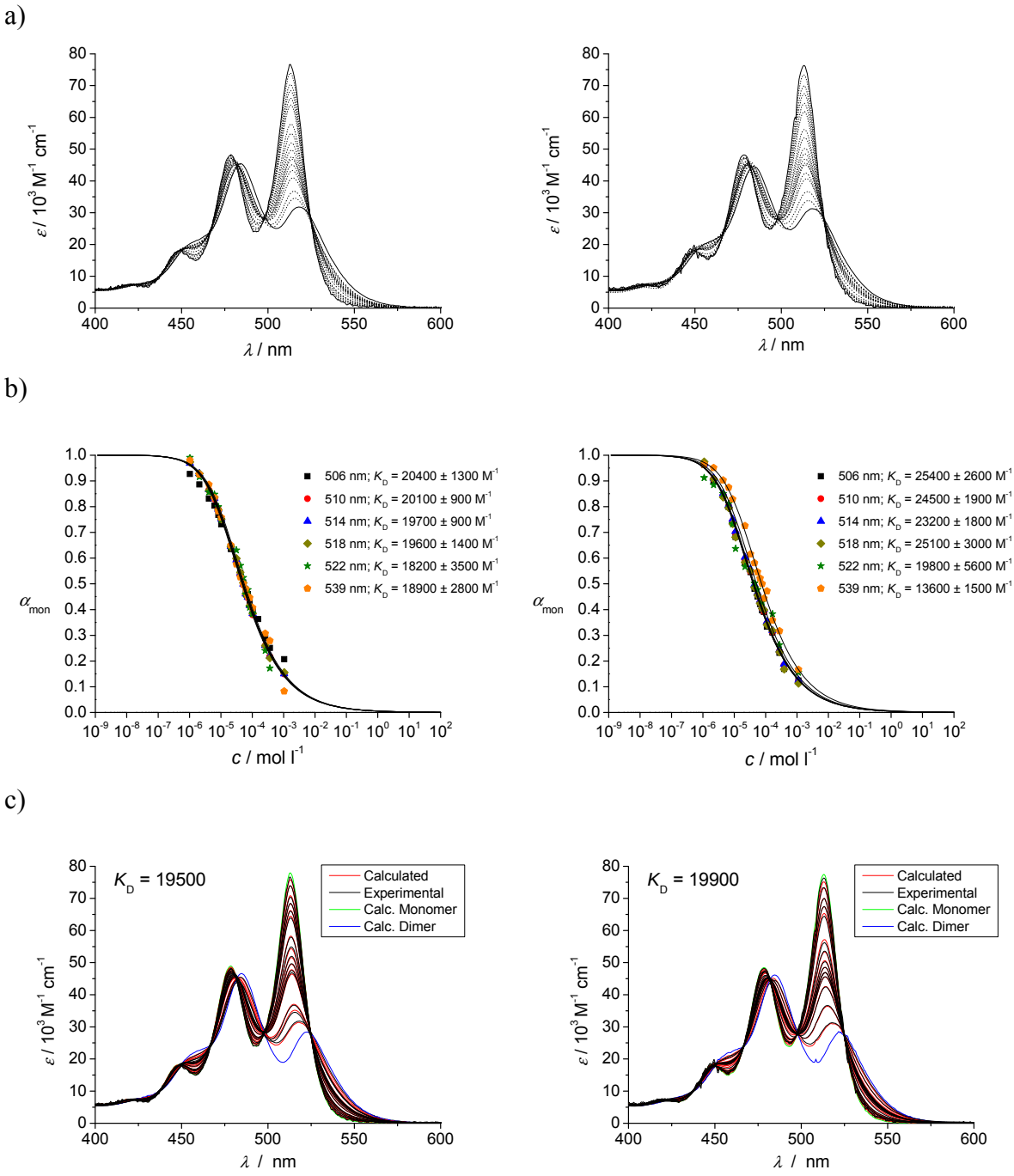

Figure A10. Illustration of the applied data acquisition and evaluation procedure based on two independent experiments (left and right). a) Concentration-dependent UV/Vis absorption spectra of (*M*)-**4b** in *n*-heptane at 298 K ($[M]_0 = 4 \times 10^{-6}$ M to 1×10^{-3} M), b) molar fraction of monomer species and dimerization constants obtained from nonlinear regression analysis at selected wavelengths indicated in the inset, and c) results from the multilinear fit routine showing the comparison of experimental (black) and derived (red) spectra at respective concentrations as well as derived pure monomer (green) and dimer (blue) spectra.

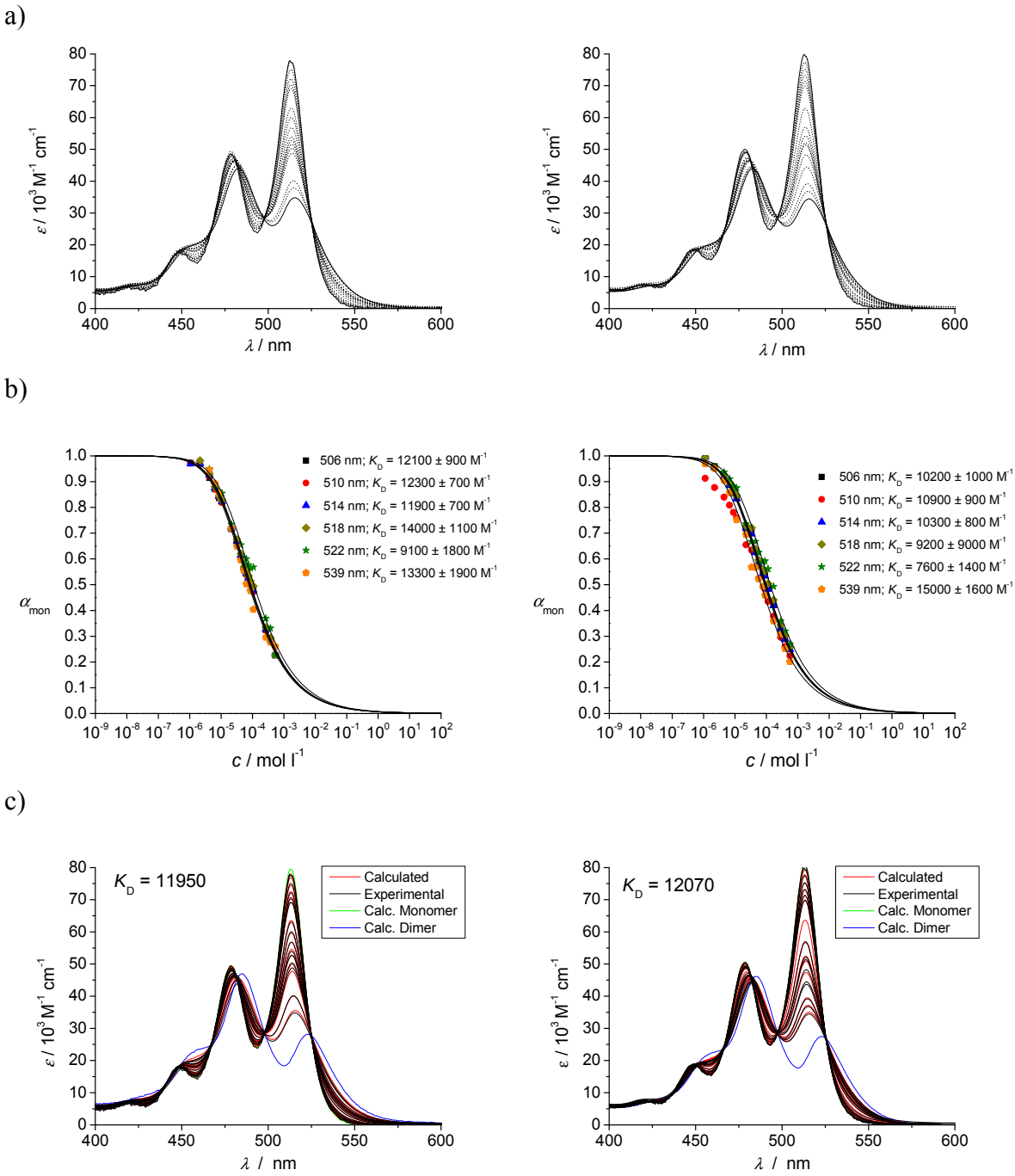

Figure A11. Illustration of the applied data acquisition and evaluation procedure based on two independent experiments (left and right). a) Concentration-dependent UV/Vis absorption spectra of (*rac*)-**4b** in *n*-heptane at 298 K ($[M]_0 = 4 \times 10^{-6}$ M to 1×10^{-3} M), b) molar fraction of monomer species and dimerization constants obtained from nonlinear regression analysis at selected wavelengths indicated in the inset, and c) results from the multilinear fit routine showing the comparison of experimental (black) and derived (red) spectra at respective concentrations as well as derived pure monomer (green) and dimer (blue) spectra.

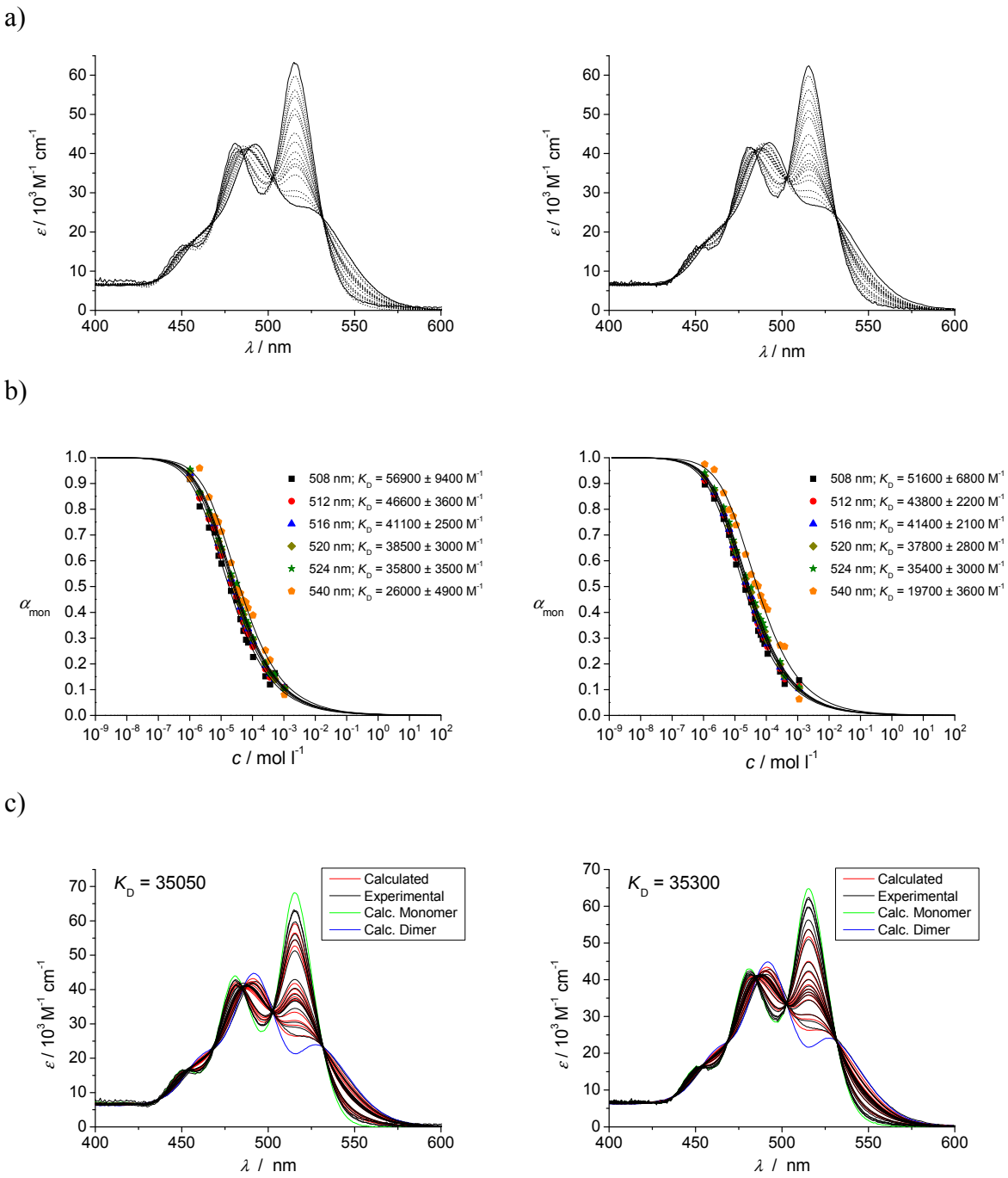

Figure A12. Illustration of the applied data acquisition and evaluation procedure based on two independent experiments (left and right). a) Concentration-dependent UV/Vis absorption spectra of (*P*)-**4c** in *n*-heptane at 298 K ($[M]_0 = 4 \times 10^{-6}$ M to 1×10^{-3} M), b) molar fraction of monomer species and dimerization constants obtained from nonlinear regression analysis at selected wavelengths indicated in the inset, and c) results from the multilinear fit routine showing the comparison of experimental (black) and derived (red) spectra at respective concentrations as well as derived pure monomer (green) and dimer (blue) spectra.

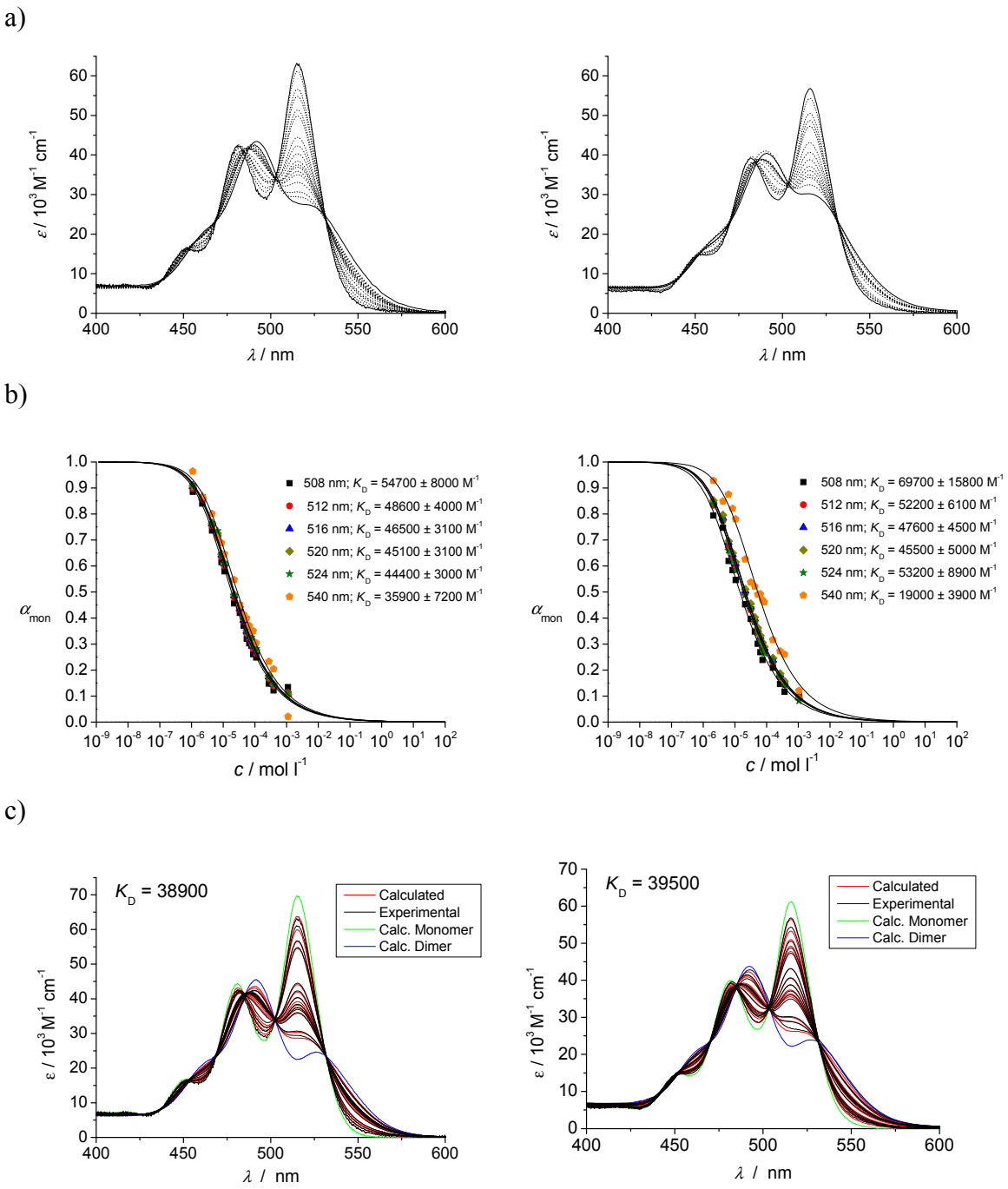

Figure A13. Illustration of the applied data acquisition and evaluation procedure based on two independent experiments (left and right). a) Concentration-dependent UV/Vis absorption spectra of (*M*)-**4c** in *n*-heptane at 298 K ($[M]_0 = 4 \times 10^{-6}$ M to 1×10^{-3} M), b) molar fraction of monomer species and dimerization constants obtained from nonlinear regression analysis at selected wavelengths indicated in the inset, and c) results from the multilinear fit routine showing the comparison of experimental (black) and derived (red) spectra at respective concentrations as well as derived pure monomer (green) and dimer (blue) spectra.

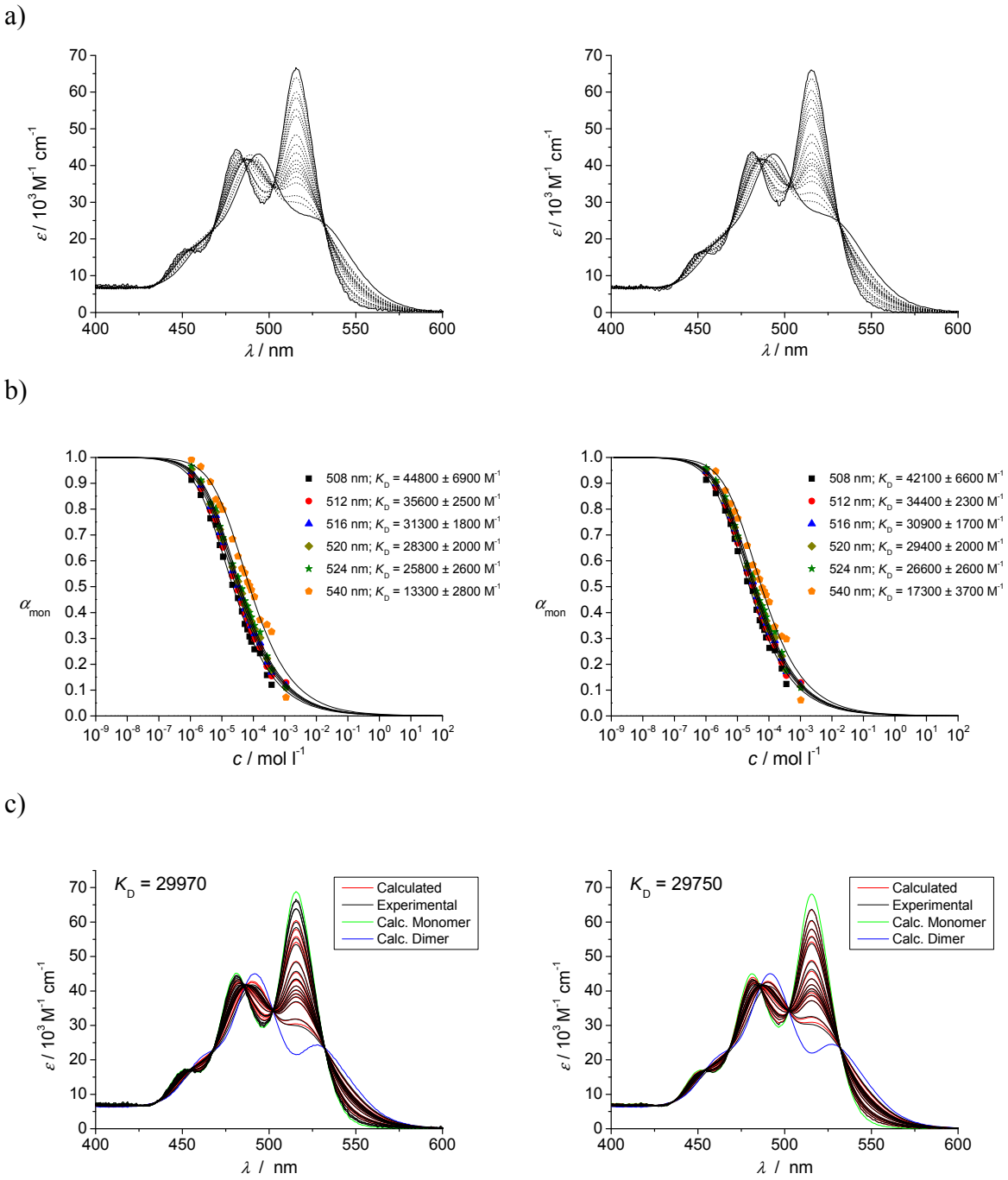

Figure A14. Illustration of the applied data acquisition and evaluation procedure based on two independent experiments (left and right). a) Concentration-dependent UV/Vis absorption spectra of (*rac*)-**4c** in *n*-heptane at 298 K ($[M]_0 = 4 \times 10^{-6}$ M to 1×10^{-3} M), b) molar fraction of monomer species and dimerization constants obtained from nonlinear regression analysis at selected wavelengths indicated in the inset, and c) results from the multilinear fit routine showing the comparison of experimental (black) and derived (red) spectra at respective concentrations as well as derived pure monomer (green) and dimer (blue) spectra.

Table A1. Dimerization binding constants K_D of racemate and pure enantiomers of PBI **4a** as obtained from two independent studies by nonlinear regression analysis at selected wavelengths and multilinear fit of the data at 298K, respectively.

Sample	K_D [M^{-1}]					
	506 nm	512 nm	516 nm	521 nm	541 nm	Multilinear fit (error ± 15 %)
(*rac*)-**4a**	8800 ± 900	6400 ± 500	5500 ± 400	5200 ± 400	4200 ± 600	6050
	5500 ± 800	5300 ± 400	5100 ± 400	4500 ± 500	5100 ± 800	6100
(*M*)-**4a**	13600 ± 2500	11600 ± 1200	9700 ± 1000	9700 ± 1000	7700 ± 1000	12010
	20800 ± 3000	15200 ± 900	14100 ± 800	13600 ± 1200	7200 ± 900	12110
(*P*)-**4a**	7800 ± 900	13500 ± 1500	13500 ± 950	14500 ± 1200	7800 ± 900	12100
	24900 ± 4800	17800 ± 2200	20200 ± 2400	17500 ± 2700	6700 ± 700	11900

Table A2. Dimerization binding constants K_D of racemate and pure enantiomers of PBI **4b** as obtained from two independent studies by nonlinear regression analysis at selected wavelengths and multilinear fit of the data at 298K, respectively.

Sample	K_D [M^{-1}]						
	506 nm	510 nm	514 nm	518 nm	522 nm	539 nm	Multilinear fit (error ± 15 %)
(*rac*)-**4b**	12100 ± 900	12300 ± 700	11900 ± 700	1400 ± 1100	9100 ± 1800	13300 ± 1900	11950
	10200 ± 1000	10900 ± 900	10300 ± 800	9200 ± 900	7600 ± 1400	15000 ± 1600	12070
(*M*)-**4b**	20400 ± 1300	20100 ± 900	19700 ± 900	19600 ± 1400	18200 ± 3500	18900 ± 2800	19500
	25400 ± 2600	24500 ± 1900	23200 ± 1800	25100 ± 3000	19800 ± 5600	13600 ± 1500	19900
(*P*)-**4b**	18100 ± 1600	18100 ± 1200	18200 ± 1200	17100 ± 1600	13700 ± 3500	21400 ± 5000	18100
	16300 ± 1600	17500 ± 1000	17400 ± 900	16900 ± 1400	10800 ± 1900	35300 ± 8400	18050

Table A3. Dimerization binding constants K_D of racemate and pure enantiomers of PBI **4c** as obtained from two independent studies by nonlinear regression analysis at selected wavelengths and multilinear fit of the data, respectively, at 298 K.

Sample	K_D [M^{-1}]						
	508 nm	512 nm	516 nm	520 nm	524 nm	540 nm	Multilinear fit (error ± 15 %)
(*rac*)-**4c**	44800 ± 6900	35600 ± 2500	31300 ± 1800	28300 ± 2000	25800 ± 2600	13300 ± 2800	29970
	42100 ± 6600	34400 ± 2300	30900 ± 1700	29400 ± 2000	26600 ± 2600	17300 ± 3700	29750
(*M*)-**4c**	54700 ± 8000	48600 ± 4000	46500 ± 3100	45100 ± 3100	44400 ± 3000	35900 ± 7200	38900
	19000 ± 3900	52200± 6100	47600 ± 4500	45500 ± 5000	53200 ± 8900	19000 ± 3900	39500
(*P*)-**4c**	56900 ± 9400	46600 ± 3600	41100 ± 2500	38500 ± 3000	35800 ± 3500	26000 ± 4900	37400
	51600 ± 6800	43800 ± 2200	41400 ± 2100	37800 ± 2800	35400 ± 3000	19700 ± 3600	39400

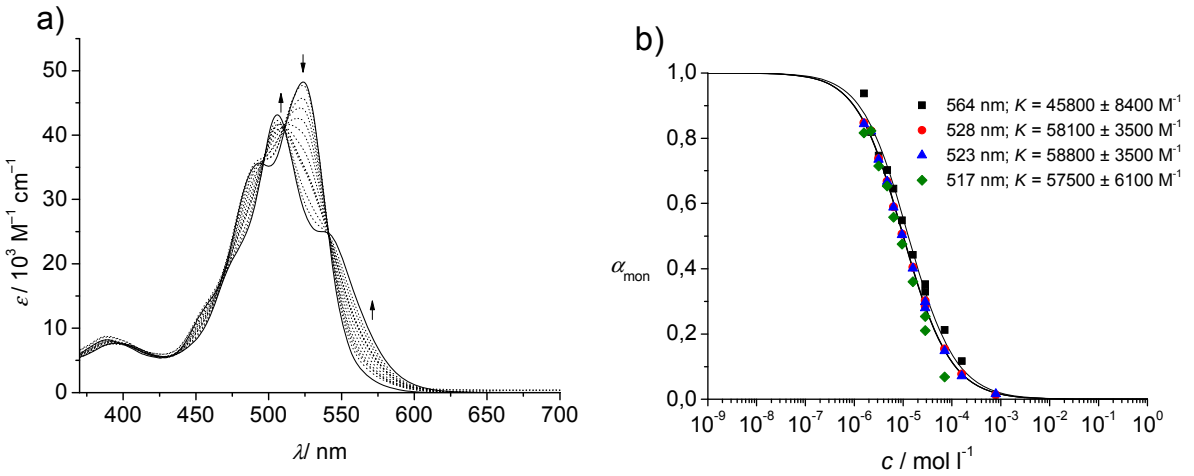

Figure A15. a) Concentration-dependent UV/Vis absorption spectra of **2** in *n*-heptane at 331 K ($[M]_0$ = 1×10^{-6} M to 8×10^{-4} M) and b) molar fraction of monomer species and dimerization constants obtained from nonlinear regression analysis at selected wavelengths indicated in the inset applying the equal K model. Arrows indicate changes upon increasing concentration.

Publications

2009 X. Zhang, S. Rehm, M. M. Safont-Sempere, F. Würthner, *Nature Chemistry,* **2009**, *1*, 623–629

"Vesicular perylene dye nanocapsules as supramolecular fluorescent pH sensor systems"

2010 M. M. Safont-Sempere, P. Osswald, K. Radacki, F. Würthner, *Chem. Eur. J.*, **2010**, *16*, 7380–7384

"Chiral self-recognition and self-discrimination of strapped perylene bisimides by π-stacking dimerization"

M. M. Safont-Sempere, V. Stepanenko, M. Lehmann, F. Würthner, *J. Mater. Chem.*, **2010** submitted

"Impact of core chirality on mesophase properties of atropo-enantiomeric perylene bisimides"

M. M. Safont-Sempere, G. Fernández, F. Würthner, *Chem. Rev.*, **2010** submitted

"Self-sorting phenomena in complex supramolecular systems"

Acknowledgments / Agradecimientos

Mi profundo agradecimiento a mi supervisor el Profesor Dr. Frank Würthner por haberme dado la oportunidad de llevar a cabo mi doctorado en su grupo de trabajo. Gracias por las criticas y discusiones que paso a paso me han ayudado a superarme y lograr mi objetivo final, ademas de obligarme a poner en práctica valores tan necesarios para el futuro como trabajo duro e independiente, espiritu de lucha y superación personal.

Al Dr. Chantu Saha-Möller quisiera agracerle su paciencia en la corrección de artículos científicos. Por su indispensable ayuda en mejorar mi trabajo, y la horas de discusión, todo el tiempo invertido, y el haber podido aprender del "perfecto perfeccionista". Porque las formalidades si importan, como muy bien he podido aprender de Chantu.

Al programa GRK1221 de la DFG le agradezco el apoyo financiero aportado durante mis estudios de doctorado y la oportunidad de participar el múltiples conferencias y work-shops.

Muchas gracias al Profesor Matthias Lehmann, con el que ha sido un placer trabajar y aprender sobre los entresijos de los cristales líquidos. Gracias por una fructífera y más que agradable cooperación.

Gracias a los compañeros del departamento de química inorgánica, el Profesor Martin Kaupp y su estudiante de doctorado Manuel Renz por su aportación a mi trabajo con cálculos teóricos que ha ayudado al esclarecimiento de algunas de las preguntas clave de mi doctorado.

Al equipo analítico de la Universidad de Würzburg, Dr. Matthias Grüne y Elfriede Rückdeschel, además de Dr. Michael Büchner und Fritz Dadrich, me gustaria agradecerle el impecable trabajo realizado en la caracterización de mis compuestos via RMN y espectroscopía de masas, ademas de la grata atmósfera de trabajo que he podido disfrutar con ellos. Al Dipl.-Ing Bernd Brunner por haber resucitado mi ordenador en múltiples ocasiones y por su paciencia a cada nuevo problema que le presentaba.

A nuestro equipo técnico Ana Maria Krause y Dr. Vladimir Stepanenko, les gradezco su aportacion a mi trabajo en medidas de calorimetría diferencial de barrido y microscopía de fuerza atómica, respectivamente, además de por su complaciente compañía.

Gracias a Joachin Bialas y Manuela Kaiser por su ayuda en la síntesis de algunos de mis compuestos y por las risas y buen humor que he podido disfrutar en estos años de trabajo a su lado.

A Peter Osswald debo agradecerle los continuos consejos e ideas aportadas a lo largo de todo mi doctorado, gracias por su supervisión continua y amistad, a pesar de la distancia.

A Christian Simon le agradezco el intachable trabajo realizado en la síntesis de mis compuestos durante su periodo de aprendizaje bajo mi supervisión.

Muchas gracias a Christiana por toda la ayuda administrativa y también por su buen humor y alegría, que por suerte he podido disfrutas cada medio día, amenizándome todas las comidas.

Mi profundo agradecimiento a Christina Rest, por su esfuerzo y entusiamo en la realización de su trabajo de diploma. No sólo el trabajo realizado fue impecable, sino la atmósfera de trabajo y amistad que pude disfrutar con ella hicieron del día a día en ese periodo de tiempo uno de los mejores momentos de mi doctorado.

A Ralf me gustaria agradecerle su ayuda y disposición durante todo el doctorado. Por fructíferas discusiones científicas ademas del tiempo y creatividad invertidos en la realización de figuras con el Strata, que han provisto mis artículos y trabajo de doctorado con un toque de color que no hubiera conseguido sin su irremplazable aportación.

A Gustavo quisiera agradecerle su apoyo incondicional, su ayuda en el ámbito científico y personal. Por acercarme un trocito de patria y de mi querido humor español cada día. Por que estos dos últimos años con Gustavo han traido alegría a mi día a día.

Por innumerables discusiones y quedadas quisiera agradecer a Volker, Thomas, Matthias, Felix, Ralf, Gustavo, Sanchita, Daniel y Charlotte. Nos lo hemos pasado muy bien juntos, y la diversión y las risas es el motor que mueve muchas cosas.

A toda la gente del grupo de trabajo con la que me he cruzado en mi camino, gracias a cada uno por vuestras aportaciones personales y profesionales.

Gracias al Dr. Xin Zhang por su amabilidad, su ayuda profesional, su gentileza y sencillez, ha sido un auténtico placer trabajar a su lado.

A mis amigos alemanes Conny, Kristina, Fabian, Stefanie, Thomas, Volker, Ralf, Felix, Matthias, Peter, Andreas, Valerie y Christian que siempre han estado ahí para animarme en los momentos malos y alegrarse conmigo en los buenos, sobre todo Christian que ha sido mi terapia semanal durante muchas muchas semanas, gracias por estar ahí.

Desde aquí les mando las gracias a mis amigas españolas Bea, Yovi, Laurica, Cris y mi hermanica Bar, que han estado en todo momento a mi lado a pesar de la distancia y el contacto limitado, ayudándome a seguir aquí sintiendo el calor de casa. Amenizando con sus e-mails y haciendo siempre un esfuerzo por verme cuando he estado en España.

Muchas gracias a toda la gente que desde España ha estado atenta a cada movimiento, siempre preparados para darme unas palabras de aliento cuando ha sido necesario, y acogiéndome como antes de irme cada vez que he vuelto a casa.

Gracias a Michael, Margret y Heike, mi familia Alemana, que me han acogido y apoyado desde el primer día que entré en su casa como a una más de la familia, ademas de darme valiosos consejos y cuidados.

El agradecimiento más profundo va dedicado a mi familia y a mi marido, que han sudado cada paso conmigo sufriendo cada momento, y disfrutando todos los logros tanto o más que yo. Por que sin su apoyo incondicional en todos los aspectos nunca hubiera podido llegar tan lejos, por prestarme fuerzas cuando las he necesitado, mil gracias.